

SYNTHESIS AND APPLICATIONS OF ELECTRON DEFICIENT
CONJUGATED POLYMERS

BY

YOUNGMI KIM

B.S., Chemistry
Kyungpook National University, Daegu, Korea, 1992

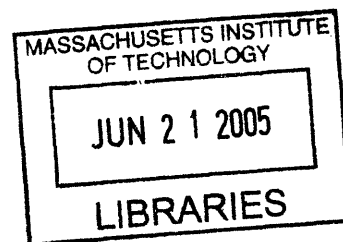
Submitted to the Department of Chemistry
in Partial Fulfillment of the Requirements for the Degree of

DOCTOR OF PHILOSOPHY

at the

MASSACHUSETTS INSTITUTE OF TECHNOLOGY

May 2005 [June 2005]



© Massachusetts Institute of Technology, 2005. All rights reserved.

Signature of Author: _____

Department of Chemistry
May 24, 2005

Certified by: _____

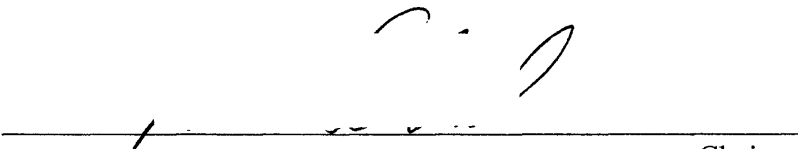
Timothy M. Swager
Thesis Supervisor

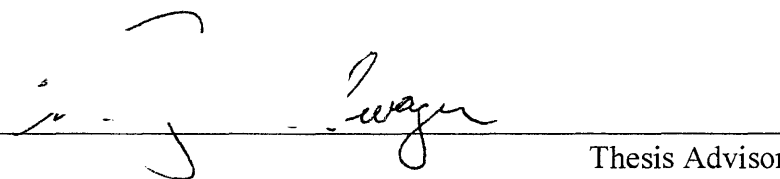
Accepted by: _____

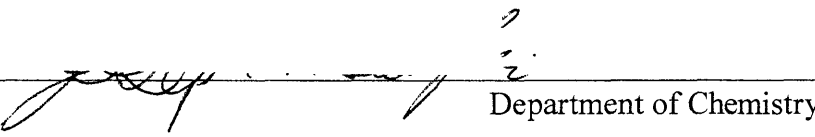
Robert W. Field
Chairman, Departmental Committee on Graduate Studies

ARCHIVES

This doctoral thesis has been examined by a Committee of the Department of Chemistry as follows:

Professor Richard R. Schrock:  _____ Chairman

Professor Timothy M. Swager:  _____ Thesis Advisor

Professor Joseph P. Sadighi:  _____ Department of Chemistry

*Dedicated to my son and my husband:
Their support and love have been a constant
source of making me move forward.*

Synthesis and Applications of Electron Deficient Conjugated Polymers

by

Youngmi Kim

Submitted to the Department of Chemistry, May, 2005
In partial fulfillment of the requirements for the degree of
Doctor of Philosophy in Chemistry

ABSTRACT

Chapter 1.

In this introductory chapter, we present the general properties of conjugated polymers for sensory and electronic applications, with a special emphasis placed on electron-deficient materials.

Chapter 2.

In this chapter is presented the synthesis, characterization, and applications of a series of electron-deficient poly(*p*-phenylene vinylene)s (PPVs) homopolymers and copolymers. Poly(*p*-phenylenevinylene)s containing trifluoromethyl substituted aromatic rings (CF₃-PPVs) exhibited high photooxidative stability to give robust materials suitable for molecular electronic device applications.

Chapter 3. Hyperconjugative and Inductive Perturbations in Poly(*p*-phenylene vinylenes)

New approaches that produce high fluorescence quantum yields and also tune electron affinity of conjugated polymers are presented. Novel three-dimensional poly(phenylene vinylenes) having [2.2.2] bicyclic ring system were synthesized to give highly efficient solid-state fluorescence and hyperconjugative and inductive electronic perturbations. The ability of hyperconjugative and inductive perturbation to tune the polymers' sensory applications was determined by investigating the fluorescence quenching responses to electron-rich and electron-deficient analytes in solution and solid thin films.

Chapter 4. High Ionization Potential Conjugated Polymers

In this chapter is presented a series of poly(*p*-phenylene ethynylenes) (PPEs) with high ionization potentials. Their photophysical properties were investigated using steady-state and time-resolved fluorescence techniques. The ionization potentials of the polymer thin films were determined using ultraviolet photoelectron spectroscopy (UPS), and those with the highest ionization potentials displayed high sensitivity for the detection of electron-donating aromatic compounds. The effects of sterics and electronic properties on the polymers' sensory responses were investigated by fluorescence quenching experiments in both solution and solid thin films. In addition, in some cases the excited state charge-transfer complexes

(exciplexes) of the PPEs with analytes were observed. These effects provide promising opportunities for the formation of sensitive and selective chemical sensors.

Chapter 5. Highly Emissive Conjugated Polymer Excimers

Conjugated polymers often display a decrease of fluorescence efficiency upon aggregation due in large part to enhanced interpolymer interactions that produce weakly emissive species generally described as having excimer character. We have found that poly(phenylene ethynylene)s with fused pendant [2.2.2] ring structures having alkene bridges substituted with two ester groups function to give highly emissive, broad, and red-shifted emission spectra in the solid state. To best understand the origin of this new solid-state emissive species, we have performed photophysical studies of a series of different materials in solution, spin-coated thin films, solid solutions, and Langmuir films. We conclude that the new, red-shifted, emissive species originate from excimers produced by interchain interactions being mediated by the particular [2.2.2] ring system employed. The ability to predictably produce highly emissive excimers from conjugated polymers is important for the understanding how solid-state structures can control emissive behaviors.

Chapter 6. Electron-Deficient Polyelectrolytes For Biosensory Applications

In this chapter is described a novel photo-oxidizing water-soluble fluorescent polymer that was designed for the detection of electron-rich biological analytes. The polymer fluorescence is strongly quenched through an efficient photoinduced electron transfer from electron-donating aromatic moieties in amino acids, neurotransmitters, and proteins to the photo-oxidizing polymer. These efficient fluorescence quenching responses may be further enhanced by rapid exciton migration in the polymer backbone and further facilitated by ion-pairing between the polymer and quencher.

Thesis Supervisor: Timothy M. Swager
Title: Professor of Chemistry

Table of Contents

| | |
|------------------------|----|
| Dedication..... | 3 |
| Abstract..... | 4 |
| Table of Contents..... | 6 |
| List of Figures..... | 10 |
| List of Schemes..... | 14 |
| List of Tables..... | 15 |

CHAPTER 1: INTRODUCTION OF CONJUGATED POLYMERS FOR SENSORY AND MOLECULAR ELECTRONICS APPLICATIONS.....17

| | |
|--|----|
| A brief introduction of conjugated polymers..... | 18 |
| Fluorescent conjugated polymers for sensory applications..... | 19 |
| One-dimensional signal amplification: solution study..... | 19 |
| Two- or three-dimensional signal amplification: solid-state sensors..... | 21 |
| Sensory mechanisms..... | 24 |
| Conjugated polymer for biological sensory application..... | 27 |
| Conjugated polymers as molecular electronic materials..... | 30 |
| n-Type materials..... | 30 |
| Stability of materials..... | 33 |
| Thesis overview..... | 34 |
| References..... | 35 |

CHAPTER 2: SYNTHESIS AND STABILITY OF PERFLUORINATED POLY(*P*-PHENYLENE VINYLENE) DERIVATIVES.....39

| | |
|---|----|
| Introduction..... | 40 |
| Results and Discussion..... | 43 |
| Synthesis and photophysical properties of CF ₃ -PPV homopolymers..... | 44 |
| Synthesis and photophysical properties of PPV homopolymers with longer perfluoroalkyl groups..... | 50 |
| Synthesis and photophysical properties of CF ₃ -PPV copolymers..... | 52 |
| Stability studies..... | 55 |

| | |
|-----------------------------|----|
| Potential applications..... | 58 |
| Conclusions..... | 59 |
| Experimental Section..... | 59 |
| References..... | 70 |

CHAPTER 3: HYPERCONJUGATIVE AND INDUCTIVE PERTURBATIONS IN

| | |
|--|-----------|
| POLY(<i>P</i>-PHENYLENE VINYLENES)..... | 73 |
| Introduction..... | 74 |
| Results and Discussion..... | 75 |
| Synthesis..... | 75 |
| Photophysical Studies..... | 77 |
| Hyperconjugative and inductive effect on PPVs..... | 78 |
| Acid-base response..... | 82 |
| Photobleaching studies..... | 84 |
| Electrostatic layer-by-layer film assembly..... | 86 |
| Conclusions..... | 88 |
| Experimental Section..... | 88 |
| References..... | 94 |

CHAPTER 4: HIGH IONIZATION POTENTIAL CONJUGATED POLYMERS.....96

| | |
|---|-----|
| Introduction..... | 97 |
| Results and Discussion..... | 99 |
| Synthesis..... | 99 |
| Photophysical studies..... | 101 |
| Ionization potential determination..... | 105 |
| Photobleaching studies..... | 107 |
| Steady-state and time-resolved fluorescence quenching studies in solution.. | 108 |
| Fluorescence quenching study in polymer films..... | 110 |
| Conclusions..... | 115 |
| Experimental Section..... | 115 |

| | |
|--|------------|
| References..... | 136 |
| CHAPTER 5: HIGHLY EMISSIVE CONJUGATED POLYMER EXCIMERS..... | 139 |
| Introduction..... | 140 |
| Results and Discussion..... | 142 |
| Synthesis..... | 142 |
| Photophysical studies..... | 144 |
| Time-resolved photoluminescence decay dynamics..... | 151 |
| X-ray diffraction studies..... | 154 |
| Computer modeling of model compounds..... | 156 |
| Study of interchain interaction on Langmuir-Blodgett monolayer..... | 157 |
| Conclusions..... | 159 |
| Experimental Section..... | 160 |
| References..... | 164 |
| | |
| CHAPTER 6: ELECTRON-DEFICIENT POLYELECTROLYTES FOR BIOSENSORY APPLICATIONS..... | 166 |
| Introduction..... | 167 |
| Results and Discussion..... | 168 |
| Synthesis..... | 168 |
| Photophysical properties..... | 169 |
| Fluorescence quenching in solution..... | 171 |
| Conclusions..... | 177 |
| Experimental Section..... | 178 |
| References..... | 179 |
| | |
| <i>Curriculum Vitae</i> | 181 |
| | |
| Acknowledgements..... | 184 |

| | |
|---|------------|
| APPENDIX A: NMR SPECTRA FOR CHAPTER 2..... | 186 |
| APPENDIX B: NMR SPECTRA FOR CHAPTER 3..... | 204 |
| APPENDIX C: NMR SPECTRA FOR CHAPTER 4..... | 212 |
| APPENDIX D: NMR SPECTRA FOR CHAPTER 5..... | 229 |
| APPENDIX E: NMR SPECTRA FOR CHAPTER 6..... | 234 |

List of Figures

Chapter 1.

| | |
|---|----|
| Figure 1.1. Structures of conjugated polymers (top) and band structure in an electronically conjugated polymer. | 18 |
| Figure 1.2. Conjugated “molecular wire” polymer-based sensor: signal amplification due to a collective system response. | 20 |
| Figure 1.3. Traditional molecule-based chemosensor: sensitivity determined by the association constant of the receptor-analyte complex. | 20 |
| Figure 1.4. Fluorescent CPs and quenchers for sensory application. | 21 |
| Figure 1.5. Conceptual and idealized model of porous pentiptycene-derived PPE 3 film. | 23 |
| Figure 1.6. Energy level diagram depicting fluorescence quenching mechanism in CPs with electron acceptor analytes. | 24 |
| Figure 1.7. Energy level diagram depicting fluorescence enhancement or a shift to new emission in CPs. | 26 |
| Figure 1.8. Fluoride sensor based on the fluorescence enhancement and wavelength shift in emission spectra. | 27 |
| Figure 1.9. Molecular structure of CP (left) and dicationic viologen quencher containing boronic acid groups become neutral in the presence of sugar (in box)... | 28 |
| Figure 1.10. Fluorescence quenched PPE-based substrate as protease sensors. | 29 |
| Figure 1.11. A typical structure of single LED with ITO/PPV/Al, Mg or Ca (left) and schematic energy level diagram of same LED. | 31 |
| Figure 1.12. Examples of electron-transporting (n-type) organic semiconductors. | 32 |
| Figure 1.13. Photooxidation reaction of PPV with singlet oxygen. | 33 |
| Figure 1.14. Perfluorinated-PPVs and PPEs. | 34 |

Chapter 2.

| | |
|---|----|
| Figure 2.1. Perfluorinated-PPV homopolymers and copolymers. | 42 |
| Figure 2.2. The absorption and emission spectra of CF ₃ -PPV in THF. | 45 |

| | |
|---|----|
| Figure 2.3. The emission spectra of CF3-PPV thin films prepared by chemical (Gilch) and electrochemical polymerizations. | 49 |
| Figure 2.4. The absorption and emission spectra of <i>alt-co</i> -PPV (solid line) and MEH-PPV (dotted line) in chloroform. | 53 |
| Figure 2.5. The structure of polymers used for stability studies. | 55 |
| Figure 2.6. The time dependence of fluorescence intensity of CF3-PPV, <i>alt-co</i> -CF3-PPV, MEH-PPV and PF thin films under UV irradiation. | 56 |
| Figure 2.7. The time dependence of fluorescence intensity of CF3-PPV prepared electrochemically on ITO. | 57 |
| Figure 2.8. TGA of CF3-PPV (left) and MEH-PPV (right). | 58 |
| Chapter 3. | |
| Figure 3.1. The Stern-Volmer plots of polymers 4a (■), 4b (●) and 4d (X) in spin-cast films with DMT (A) and DNT (B) vapor. | 79 |
| Figure 3.2. The pictures of sensory response of polymer 4b and 4d in thin films with DMT (A) and DNT (B) vapor. | 80 |
| Figure 3.3. The Stern-Volmer plots (left) and the lifetime measurements (right) of polymers 4a (■), 4b (●) and 4d (X) with <i>N,N</i> -dimethyl <i>p</i> -toluidine (DMT) in THF. | 81 |
| Figure 3.4. The Stern-Volmer plots (left) and the lifetime measurements (right) of polymers 4a (■), 4b (●) and 4d (X) with 2,4-dinitrotoluene (DNT) in THF. | 81 |
| Figure 3.5. The emission spectra of polymer 4b on the treatment with TFA. | 83 |
| Figure 3.6. The picture (left) of polymer 4a on the treatment with TFA and then pyridine and (right) their emission spectra change. | 84 |
| Figure 3.7. The time dependent of fluorescence intensity of polymers 4a , 4b and MEH-PPV thin films under UV irradiation. The polymers 4a and 4b were excited at 400 nm and MEH-PPV was excited at 500 nm in air. | 86 |
| Figure 3.8. The Layer-by-Layer thin film prepared with anionic polymer 4f | 87 |

Figure 3.9. The growth of optical density of as a function of layer number deposited.87

Figure 3.10. The Stern-Volmer plots of polymer **4a**, **4b** and **4d** with DMT (upper row) and DNT (lower row) in THF.94

Chapter 4.

Figure 4.1. Single-crystal X-ray ORTEP structures of (left) **3-a** (50% probability) and (right) **3-b** (30% probability).101

Figure 4.2. The absorption and emission spectra of (a) **P-1** and (b) **P-3** in chloroform (dotted line) and solid film (solid line).104

Figure 4.3. (a) He I ultraviolet photoelectron spectra of **P-1**, **P-3** and **P-10** polymer films spin-coated on gold substrates and (b) expanded graph of the HOMO threshold region.107

Figure 4.4. The fluorescence intensity of polymer thin films after UV irradiation for 30 min.108

Figure 4.5. (a) The fluorescence spectra ($\lambda_{ex} = 380$ nm) of **P-10** as a function of added indole in THF. (b) The Stern-Volmer plot and lifetime measurements of **P-10** as a function of added indole in THF.110

Figure 4.6. The Stern-Volmer plots of **P-1**, **P-3**, **P-5** and **P-10** in spin-cast films as function of exposure time to indole vapor.112

Figure 4.7. The time-dependent fluorescence spectra of (a) **P-10** film before (dotted line) and after exposure to indole vapor (solid line) at 1 s, 1, 2, 3, 4, 5, 6, 7, and 10 min (top to bottom). (b) The normalized fluorescence spectra of **P-10** films blended with indole, dimethyl aniline (DMA), 1,4-dimethoxybenzene (DMB), and *N,N*-dimethyl *p*-toluidine (DMT).113

Figure 4.8. Plot of changes in fluorescence intensity of (a) **P-1** and (b) **P-10** film exposed to indole (blue solid) and 2,4-DNT (red dot) vapors for the indicated time.115

Chapter 5.

Figure 5.1. Normalized absorption and emission spectra of polymers (A) **1**, (B) **2**, (C) **3**, (D) **4**, (E) **5**, (F) **6**, and (G) **7** in chloroform (dotted line) and solid films (solid line).

| | |
|--|-----|
| | 145 |
| Figure 5.2. The emission spectra of polymer 1 films as a function of film thickness (top) and normalized emission spectra of polymer 1 in THF and as spin-cast films in PMMA (O.D: 0.05 for 0.03/1 and 0.3 for 0.06/1) (bottom). | 147 |
| Figure 5.3. The emission spectra of polymer 5 (top) and polymer 7 (bottom) films as a function of film thickness. | 150 |
| Figure 5.4. The emission spectra of polymer 3 films as a function of film thickness. | 151 |
| Figure 5.5. Time-resolved emission decays of polymer films (a) 1 and (b) 2 | 153 |
| Figure 5.6. A perspective view of crystal packing of monomers 8 (top) and 9 (bottom). | 155 |
| Figure 5.7. Semi-empirical simulations (PM3) of model compounds with energy minimization. The structure is shown in inset. (Hydrogens are omitted in images for clarity.) | 156 |
| Figure 5.8. Normalized fluorescence excitation and emission spectra of Langmuir monolayers of polymer 7 of during cycles of compressions and expansions. Inset: Pressure-area (P-A) isotherms of polymer 7 , first (solid line) and second (dashed line) compression cycles. | 159 |
| Chapter 6. | |
| Figure 6.1. Normalized absorption and emission spectra of polymer A as a function of the solution pH. | 170 |
| Figure 6.2. The changes in emission spectra (top) and S-V plot (bottom) of polymer A upon addition of tryptophan in phosphate buffer (pH 7.4). | 173 |
| Figure 6.3. The S-V plots of anionic polymer A upon titration with neurotransmitters in phosphate buffer solution (pH 7.4). | 176 |
| Figure 6.4. The changes in emission spectra (left) and S-V plot (right) of anionic polymer A upon addition of lysozyme in phosphate buffer (pH 7.4). | 176 |

List of Schemes

Chapter 2.

| | |
|--|----|
| Scheme 2.1. Several routes for perfluorinated-PPV homopolymers. | 43 |
| Scheme 2.2. Perfluorinated-PPV copolymers prepared by Wittig/Horner-Emmons polymerization. | 43 |
| Scheme 2.3. Synthesis of CF ₃ -PPV. | 44 |
| Scheme 2.4. The preparation of CF ₃ -PPV by sulfonium precursor route. | 46 |
| Scheme 2.5. The preparation of CF ₃ -PPV by Stille polymerization. | 47 |
| Scheme 2.6. The preparation of trimer 10 | 48 |
| Scheme 2.7. Synthesis of monomer 12 with perfluorobutyl groups. | 51 |
| Scheme 2.8. Synthesis of monomer 14 with perfluorodecyl groups. | 51 |
| Scheme 2.9. Synthesis of monomer 19 with perfluorooctyl group. | 51 |
| Scheme 2.10. Synthesis of perfluorinated-PPV. | 52 |
| Scheme 2.11. Synthesis of <i>alt-co</i> -CF ₃ -PPV. | 53 |
| Scheme 2.12. The preparation of random copolymers. | 54 |

Chapter 3.

| | |
|--|----|
| Scheme 3.1. | 75 |
| Scheme 3.2. Synthesis of monomers and polymers. | 76 |
| Scheme 3.3. Synthesis of monomer and polymer. | 77 |
| Scheme 3.4. Synthesis of anionic polymer 4f | 87 |

Chapter 4.

| | |
|---|-----|
| Scheme 4.1. Synthetic Route to Monomers 3-a and 3-b | 100 |
| Scheme 4.2. Synthetic Route to Monomer 4 | 100 |
| Scheme 4.3. Synthetic Route to Monomer 6 | 101 |

Chapter 5.

| | |
|---|-----|
| Scheme 5.1. Synthesis of polymers 5 and 6 | 143 |
| Scheme 5.2. Synthesis of polymer 7 | 143 |

Chapter 6.

| | |
|---|-----|
| Scheme 6.1. Synthesis of polymer A | 169 |
|---|-----|

List of Tables

Chapter 2.

| | |
|--|----|
| Table 2.1. Summary of molecular weight and photophysical properties. | 54 |
|--|----|

Chapter 3.

| | |
|--|----|
| Table 3.1. Summary of molecular weight and photophysical data. | 78 |
|--|----|

| | |
|--|----|
| Table 3.2. The quenching constants of polymers 4a , 4b and 4d | 82 |
|--|----|

Chapter 4.

| | |
|--|-----|
| Table 4.1. Photophysical Data of Polymers. | 102 |
|--|-----|

| | |
|---|-----|
| Table 4.2. He I Ultraviolet Photoelectron Spectroscopy Results. | 106 |
|---|-----|

| | |
|---|-----|
| Table 4.3. Stern-Volmer Quenching Constants of Polymers with Indole in THF. | 110 |
|---|-----|

| | |
|---|-----|
| Table 4.4. Crystal data and structure refinement for Compound 3-a and 3-b | 125 |
|---|-----|

| | |
|---|-----|
| Table 4.5. Selected bond lengths [\AA] and angles [$^\circ$] for compound 3-a | 126 |
|---|-----|

| | |
|---|-----|
| Table 4.6. Selected bond lengths [\AA] and angles [$^\circ$] for compound 3-b | 128 |
|---|-----|

| | |
|--|-----|
| Table 4.7. Atomic coordinates ($\times 10^4$) and equivalent isotropic displacement parameters ($\text{\AA}^2 \times 10^3$) for compound 3-a . $U(\text{eq})$ is defined as one third of the trace of the orthogonalized U_{ij} tensor. | 131 |
|--|-----|

| | |
|---|-----|
| Table 4.8. Anisotropic displacement parameters ($\text{\AA}^2 \times 10^3$) for compound 3-a . The anisotropic displacement factor exponent takes the form: $-2\pi^2 [h^2 a^{*2} U^{11} + \dots + 2 h k a^* b^* U^{12}]$ | 132 |
|---|-----|

| | |
|--|-----|
| Table 4.9. Hydrogen coordinates ($\times 10^4$) and isotropic displacement parameters ($\text{\AA}^2 \times 10^3$) for compound 3-a | 133 |
|--|-----|

| | |
|---|-----|
| Table 4.10. Atomic coordinates ($\times 10^4$) and equivalent isotropic displacement parameters ($\text{\AA}^2 \times 10^3$) for compound 3-b . $U(\text{eq})$ is defined as one third of the trace of the orthogonalized U_{ij} tensor. | 134 |
|---|-----|

| | |
|--|-----|
| Table 4.11. Anisotropic displacement parameters ($\text{\AA}^2 \times 10^3$) for compound 3-b . The anisotropic displacement factor exponent takes the form: $-2\pi^2 [h^2 a^{*2} U^{11} + \dots + 2 h k a^* b^* U^{12}]$ | 135 |
|--|-----|

Table 4.12. Hydrogen coordinates ($\times 10^4$) and isotropic displacement parameters ($\text{\AA}^2 \times 10^3$) for compound **3-b**.136

Chapter 6.

Table 6.1. Stern-Volmer quenching constants (M^{-1}) of polymer **A** with given analytes in aqueous media at 25°C172

Chapter 1:

Introduction of Conjugated Polymers for Sensory and Molecular Electronic Applications

A brief introduction of conjugated polymers

Since the discovery of metallic conductivities in polyacetylene doped with various electron acceptors or electron donors in 1977,¹ the field of conducting polymers has developed very rapidly. Conjugated polymers (CPs), also known as conducting polymers, are polyunsaturated compounds in which a continuous π -electron path extends along the entire backbone. The mixing of interacting molecular orbitals of the constituent monomer units creates a delocalized band-like electronic structure (Figure 1.1). The extensive delocalization of π -electrons along polymer chain is well known to be responsible for the array of remarkable optical and optoelectronic properties that these polymers exhibit. As a result, CPs have been the object of academic and industrial interests as useful components in many applications, including field-effect transistors, optical and electronic sensors, light-emitting devices, nonlinear optical materials.²

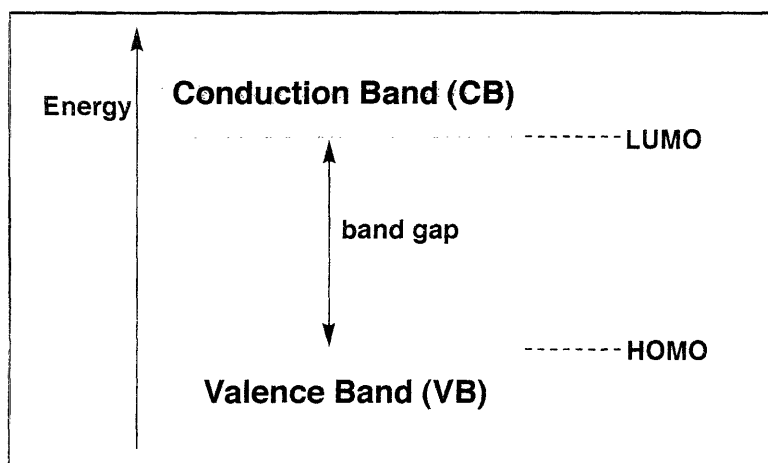
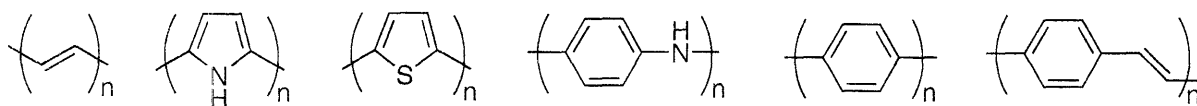


Figure 1.1. Structures of conjugated polymers (top) and band structure in an electronically conjugated polymer. (For semiconducting polymers, the valence band (VB) is filled with electrons and the conduction band (CB) is devoid of electrons. The band gap, E_g , represents the amount of energy required to promote an electron into the conduction band.)

This introduction will not attempt to give a comprehensive survey of CP-based applications since many review articles have appeared in the literature.³ Instead, we will focus herein the precedents either from the Swager group or elsewhere to provide the motivations and objectives behind this thesis work. We are particularly interested in the development of electron-deficient fluorescent CPs for sensory and molecular electronics applications. This introduction begins with sensory application of CPs, including their signal amplification properties and sensory mechanism. Then, we will discuss CPs for molecular electronic applications with special interest in electron-deficient materials.

Fluorescent conjugated polymers for sensory applications

One-dimensional signal amplification: solution study

The design of highly sensitive and selective sensory materials having easily detectable recognition events is of critical interest for the detection of chemical and biological species. To this end, fluorescence-based sensors have received a great deal of attention due to their highly sensitive optical transduction modes including attenuation, enhancement, or wavelength shifts in the emission spectra upon analyte binding event. During the past decade, the Swager group has been focused on the development of fluorescent CP-based sensory materials utilizing a variety of different detection mechanisms. CPs for fluorescent sensors are superbly attractive because they provide extended electronic communication and transport properties of excited states (excitons), which lead to signal amplification. That is, in CP-based sensors, polyreceptors interconnected within a polymer backbone induce a fluorescence change of the entire polymer chain with a small percentage of analyte binding events (Figure

1.2) whereas sensitivity in a traditional chemosensor is from the collection of individual receptor-analyte interactions (Figure 1.3).⁴

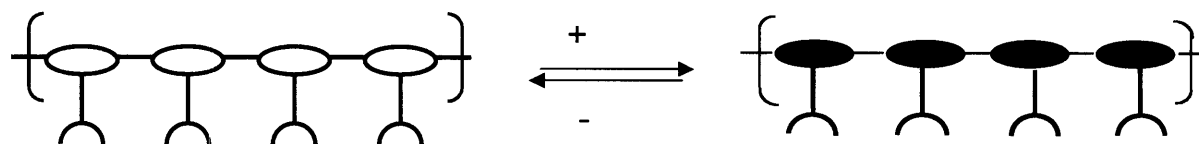


Figure 1.2. Conjugated “molecular wire” polymer-based sensor: signal amplification due to a collective system response.

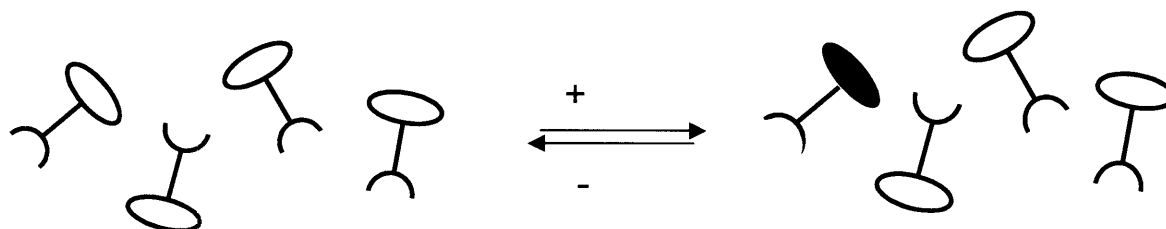


Figure 1.3. Traditional molecule-based chemosensor: sensitivity determined by the association constant of the receptor-analyte complex.

This amplifying ability of a CP-based sensor was first demonstrated by Zhou and Swager via amplified fluorescence quenching using poly(*p*-phenylene ethylene) containing a cyclophane-based receptor (**1**, Figure 1.4) with quencher, paraquat (PQ²⁺, **2**).⁵ A 65-fold increase in fluorescence quenching response is observed in the conjugated polymer (polyreceptor) as compared with monomeric analogue containing only one cyclophane receptor per molecule.

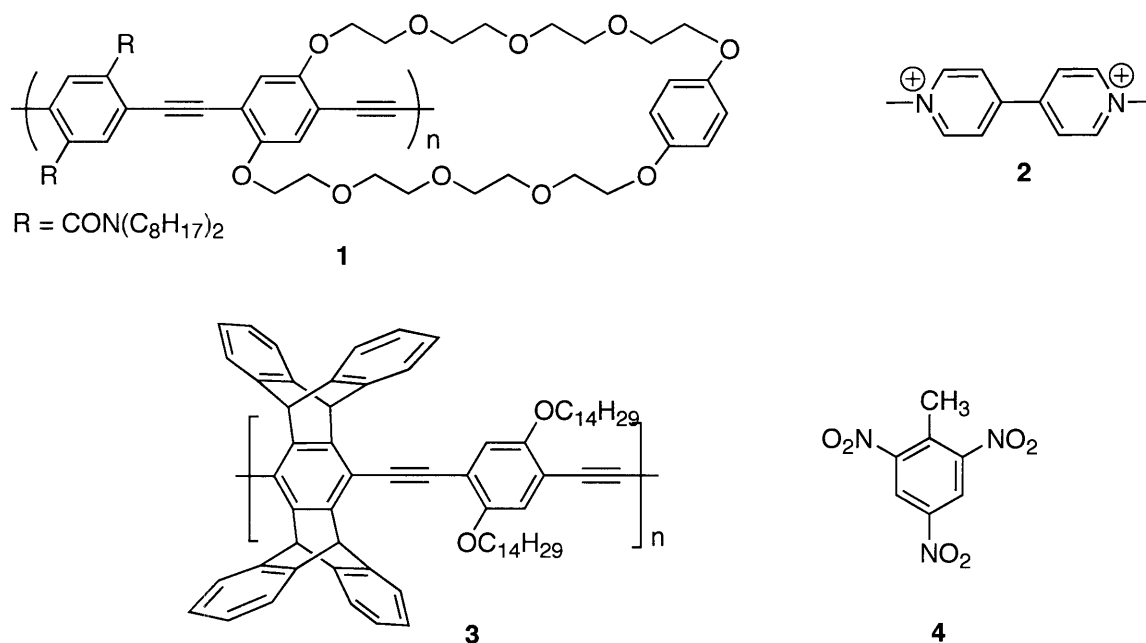


Figure 1.4. Fluorescent CPs and quenchers for sensory application.

This study also demonstrated that the degree of amplification had a molecular weight dependence (length of polymer chain) up to $M_n = 65,000$ (about 130 phenylene ethylene units), indicating that exciton can sample about 130 phenylene ethylene units during its excited state lifetime (6.4×10^{-10} s). In this case, analyte sampling by excitons was confined to an isolated single polymer chain in dilute solution.

Two- or three-dimensional signal amplification: solid-state sensors

The efficiency of signal amplification exploited in a one-dimensional configuration was extended to the solid state, in which interpolymer electronic communication could be further extended into two- or three-dimensional structures. Moreover, since many sensory applications require the use of thin films, the added amplification by two- or three-dimensional exciton transport would have a significant impact on the realization of sensory

materials. However, it is common that thin films exhibit enhanced intermolecular interactions, which often induce non-radiative deactivation processes,⁶ typically resulting in the quenching and bathochromic shift of fluorescence emission with a few exceptional cases.⁷ Therefore, mitigation of non-radiative decay channels for CPs in the solid state has been an important research topic to maximize sensitivity and improve the reproducibility of analytical results. Many attempts to reduce such interchain interactions have been made, for example, through the incorporation of three-dimensional structures, dendrimer frameworks,⁸ or derivatization with long side chains.⁹

The Swager group has been exploiting sterically hindered monomers to increase the dimensionality of polymer structure. The rigid three-dimensional pentaptycene moiety was incorporated into polymer backbone to prevent π - π stacking or excimer formation.⁶ As a result, thin films of pentaptycene-derived PPE **3** exhibited the same absorption and emission characteristics as observed in solution, indicating minimal interpolymer electronic coupling in solid state. The electron-rich backbone of this polymer displayed dramatic and reversible fluorescence quenching within seconds upon exposure to 2,4,6-trinitrotoluene (TNT, **4**) vapor, which is the primary constituent of landmine explosives. In this three-dimensional system, the exciton mobility increased while suppressing electronic coupling between polymer chains. Moreover, the highly porous internal structure provided a cavity for analyte binding and facilitated rapid diffusion of the analyte as shown in Figure 1.5. Therefore, the influence of the solid-state organization (conformations) of the polymers will likely play a role in determining the efficiency of exciton migration. Levitsky and Swager also found that thin films displaying two- and three-dimensional exciton diffusion exhibited more favorable transporting properties.¹⁰ It was attributed to the benefit from the improved energy-transfer

process between polymer chains as compared with energy migration in one-dimensional exciton diffusion, suggesting a clear sensory advantage of three-dimensional structures over isolated polymer chains.

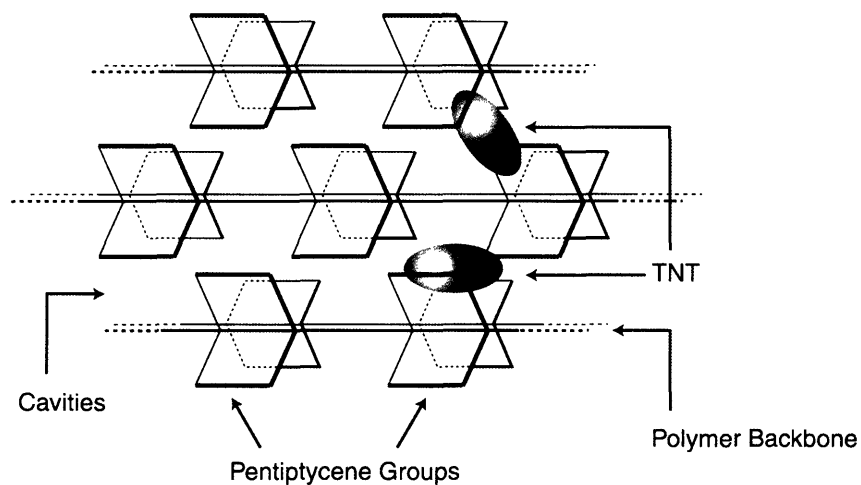


Figure 1.5. Conceptual and idealized model of porous pentiptycene-derived PPE 3 film.

Sensory mechanisms

In both cases (solution and solid state), the transduction scheme is based on fluorescence quenching of polymers **1** and **3** in presence of analyte. That is, electron-deficient species (paraquat or TNT) interact with electron-rich polymer backbone, inducing non-radiative decay. The mechanism of fluorescence quenching as well as sensitivity enhancement can be illustrated by an exciton migration scheme using the band diagram as shown in Figure 1.6.

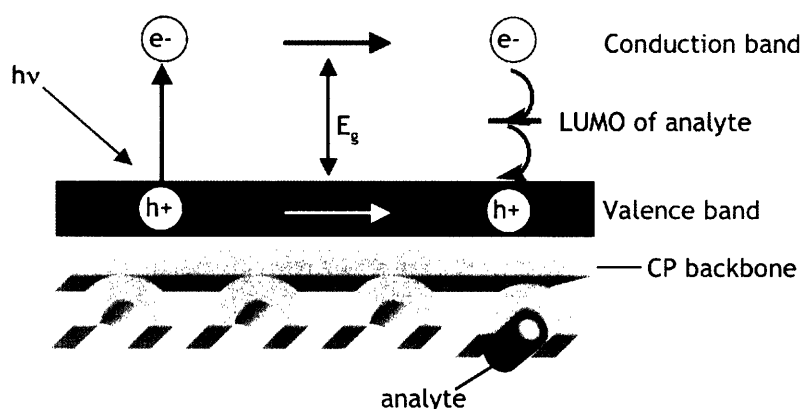


Figure 1.6. Energy level diagram depicting fluorescence quenching mechanism in CPs with electron acceptor analytes. E_g is the bandgap energy, $h\nu$ is a photon.

Upon photoexcitation of a conjugated polymer, the electrons from the valence band are excited to the conducting band, thus generating excitons (electron-hole pairs). The excitons can efficiently migrate along the polymer's backbone. This transport allows excitons to visit many potential binding sites that may be occupied by an analyte molecule that is capable of inducing a fluorescence change. In the absence of analyte, the fluorescence of a CP comes from the radiative decay that results from recombination of the excitons. In presence of analyte, an electron transfer process occurs from the excited polymer to the low-lying LUMO of the analyte, inducing significant fluorescence attenuation.

In consideration of the above mentioned processes the rational design of photoinduced electron transfer (PET)-based sensor must meet certain criteria. Firstly, the PET process should occur with a time constant at least 10- to 100-fold shorter than the lifetime of the excited state. Secondly, there has to be a strong electronic interaction between the donor and acceptor. Finally, the overall free energy change (ΔG°) for an electron-transfer reaction should be exergonic. Estimations of the efficiency of PET process, ΔG° , can be obtained by using Weller's Equation (1).¹¹

$$\Delta G_{\text{PET}}^\circ = E_{\text{ox}}(\text{D}) - E_{\text{red}}(\text{A}) - E_{0-0} - C \quad (1)$$

In the case of oxidative quenching, where $E_{\text{ox}}(\text{D})$, $E_{\text{red}}(\text{A})$, and E_{0-0} are the oxidation potential of electron-donating polymer, the reduction potential of electron-accepting analyte and the lowest singlet 0-0 excitation energy of the polymer. C ($e^2/\epsilon r$) is the solvent dependent Coulombic attraction energy and in moderately polar environment it is sufficiently small that it can often be neglected. The redox potential can be measured by using cyclic voltammetry and the excitation energy (E_{0-0}) is estimated by using wavelength of the emission (λ_{em}). If $\Delta G_{\text{PET}}^\circ < 0$, electron transfer can occur between the photoexcited electron donor and ground state electron acceptor. In case of the fluorescence quenching of polymer **3** with TNT ($E_{\text{red}}(\text{A}) = -0.7$ eV versus SCE), the values of $E_{\text{ox}}(\text{D})$, and E_{0-0} for polymer **3** are 1.22 V (vs SCE) and 2.74 eV, respectively. Therefore, photoinduced electron transfer from polymer **3** to TNT is energetically favorable process. In fluorescence quenching (FQ) of polymer thin films, several other factors need to be considered, including vapor pressure (VP) of analytes, and the binding strength (K_b) as well as the exergonicity ($-\Delta G^\circ$) of electron transfer, as shown in Equation 2.

$$\text{FQ} \propto (\text{VP})[\exp(-\Delta G^\circ)^2](K_b) \quad (2)$$

In addition to detection schemes based on electron-transfer amplified fluorescence quenching, variations on this scheme have been used to create a number of chemical and biological sensory methods: fluorescence enhancement and/or wavelength shift in emission spectra. If an analyte binding event can produce local minimum in the band gap, this leads to the selective recombination of excitons at that site, and produces fluorescence enhancement and/or a new emission of light (turn-on sensor) (Figure 1.7).

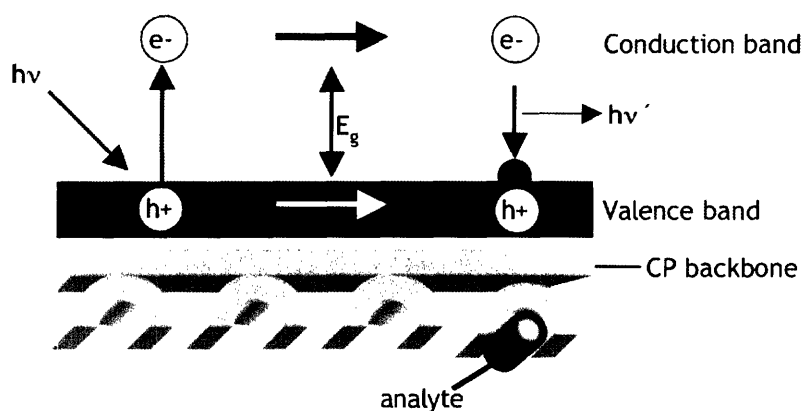


Figure 1.7. Energy level diagram depicting fluorescence enhancement or a shift to new emission in CPs.

For instance, Kim and Swager have demonstrated fluoride-selective sensors utilizing fluoride-induced lactonization to generate a highly fluorescent coumarin derivative (Figure 1.8).¹² In this system, the unique chemical reactivity of fluoride with silicon results in Si-O cleavage, and leads to the formation of a highly fluorescent compound. Due to the electronic perturbation from the appended indicator, strong changes in photophysical properties of PPEs were observed. These include red-shifted absorbance and emission spectra and increased quantum yield of the coumarin-containing form **6** in dichloromethane solution compared to those of its precursor **5**. Moreover, polymer **5** exhibited a 100-fold larger sensitivity to fluoride than that of a small molecule-based counterpart. Overall, fluorescence sensory

schemes involving a new emission at a different wavelength would be preferable to the modulation of changes in the emission intensities.

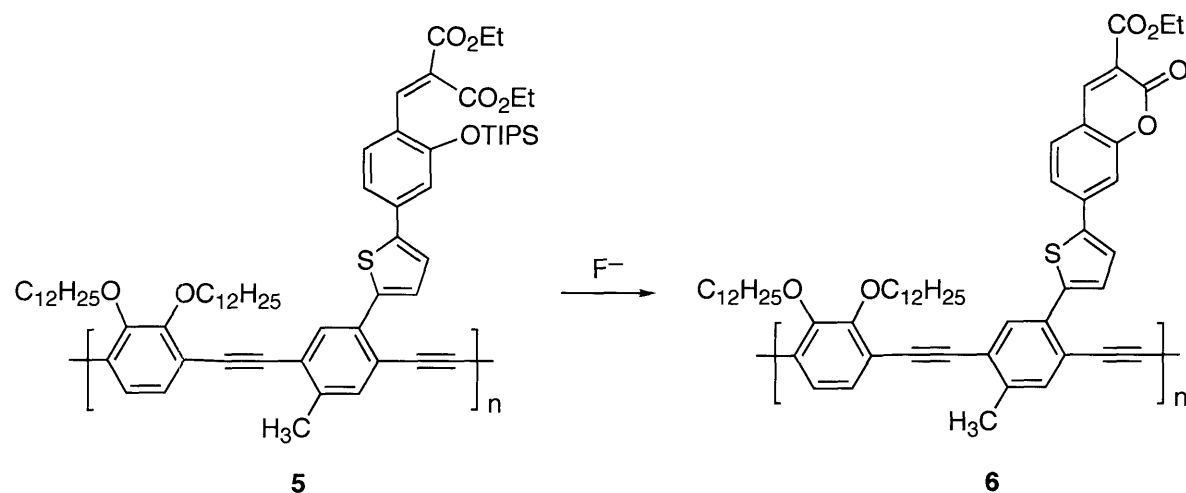


Figure 1.8. Fluoride sensor based on the fluorescence enhancement and wavelength shift in emission spectra.

Conjugated polymer for biological sensory application

For the past several years, fluorescent conjugated polymers have been exploited with great interest for the detection of biological related species such as sugars,¹³ bacteria,¹⁴ proteins,¹⁵ and DNA.¹⁶ Chen *et al.* reported the fluorescence of water-soluble polymer methoxypropyloxysulfonate-phenylenevinylene (MPS-PPV) can be quenched by using low concentration of methyl viologen (MV²⁺).¹⁷ The quenching mechanism was based on ultrafast electron transfer from the polymer to the acceptor. They proposed that this anionic polymer was used as a “turn-on” sensor using strong binding interaction between biotin and avidin: fluorescence of polymer is first quenched by biotinylated viologen derivative, but high association constant of biotin and avidin allow restoration of polymer fluorescence upon addition of avidin. However recent research by Bazan have cast serious doubts on the validity of the conclusions of mechanism.¹⁸ Nevertheless since then, a variety of different water-

soluble conjugated polymers (cationic, anionic, neutral) and detection mechanisms have been intensively investigated by our group and others. In general, such signal transduction schemes are based on facile energy transfer from a polymer to a dye acceptor (i.e. fluorescence resonance energy transfer, FRET) or photoinduced electron transfer (PET) from a polymer to an analyte, resulting in the change of fluorescence properties of materials.¹⁹ DNA detection has been demonstrated by electrostatically binding with cationic poly(thiophene) or poly(fluorene-*co*-phenylene) derivatives using colorimetric detection method based on conformational change or FRET-based system where long range dipole-dipole interaction occurs.²⁰ As example of biosensory application based on PET process, the fluorescence detection of sugar has been reported by the amplified fluorescence quenching of anionic PPE **7** by cationic quencher **8** that consists of a boronic acid functionalized benzyl viologen.²¹ Dicationic boronic acid-viologen species quenches the fluorescence of PPE by electrostatic interaction. However, upon the addition of a sugar, the boronic acid-viologen species becomes a neutral zwitterionic species and does not have an affinity for the anionic polymer chain. (Figure 1.9).

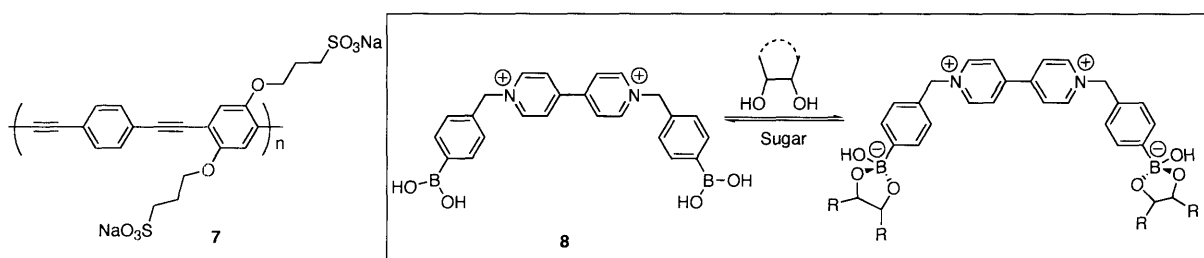


Figure 1.9. Molecular structure of CP (left) and dicationic viologen quencher containing boronic acid groups become neutral in the presence of sugar (in box).

More recently, another example of turn-on sensor was demonstrated by Wosnick and Swager for the selective detection of a protease.²² A PPE **9** containing carboxylic acid

terminated oligo(ethylene glycol) side chains is functionalized with quencher-modified peptide (Figure 1.10), so that initially, fluorescence of polymer is quenched by efficient PET process. A proteolytic cleavage by trypsin releases the quencher into solution and fluorescence is restored (Figure 1.10). In this manner, turn-on fluorescence sensing can monitor protease activity. The use of conjugated polymer allows three-fold amplification in the sensory scheme over fluorescence enhancement of small molecule mimic.

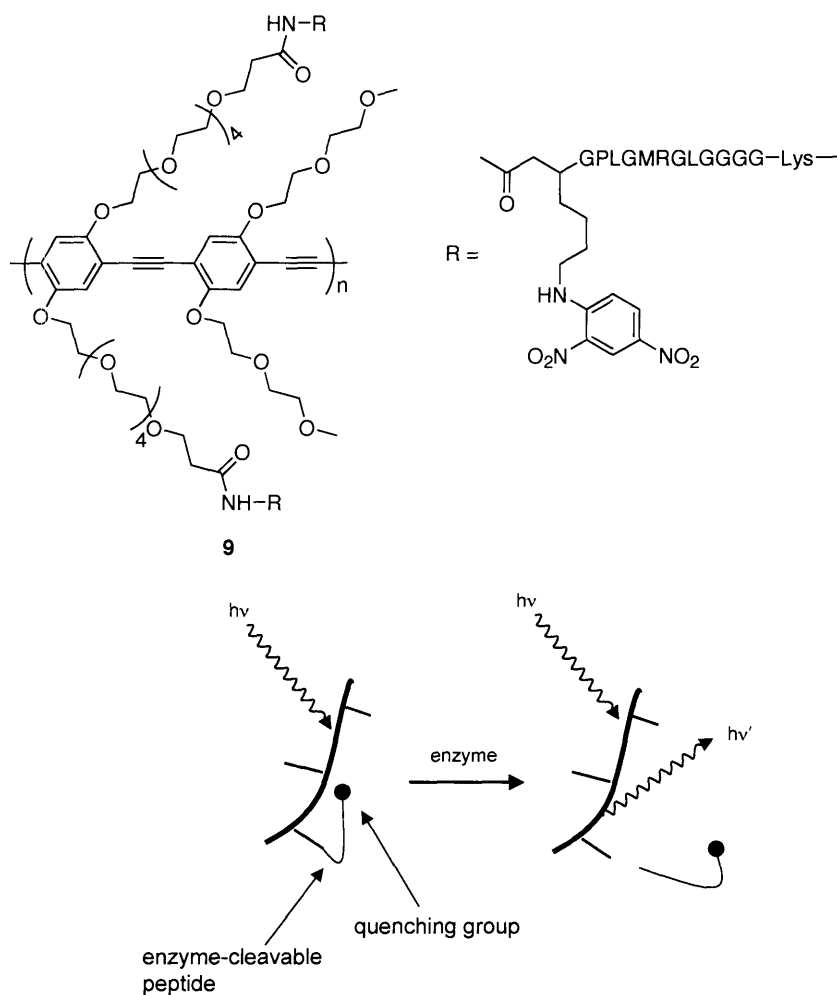


Figure 1.10. Fluorescence quenched PPE-based substrate as protease sensors.

Conjugated polymers as molecular electronic materials

Ignited by the discovery of electroluminescence (EL) in a conjugated polymer in 1990 by the Holmes and Friend groups,²³ a wide range of polymers such as poly(*p*-phenylenevinylene) (PPV), polythiophene (PT), poly(*p*-phenylene) (PPP), polyfluorene (PF), and their derivatives have been extensively investigated because of their potential application as active layers in organic electronics such as thin film transistors (TFTs), organic light-emitting diodes (OLEDs), and photovoltaics. Compared with traditional inorganic counterparts (e.g., GaAs), conjugated polymers are very attractive due to their low cost, convenient processability, and flexibility. Moreover, their key redox and optical properties can be readily fine-tuned by synthetic manipulations of their chemical structures. These modifications lead to effective control of energy levels of molecular orbitals (HOMO and LUMO) of the polymer, resulting in affecting the charge transport characteristics of materials and emission efficiency for particular applications.

n-Type materials

Most of the current highly fluorescent conjugated polymers used as organic electronics are p-type (hole-transport) materials that have generally small electron affinities and poor electron-transport properties. Therefore, one of the current broad needs in the field is the development of n-type (electron-transport) conjugated polymer semiconductors for improving the performance of LEDs, solar cells, and n-channel thin film transistors.

Organic light-emitting diodes (LEDs), in which the device consists of PPV sandwiched between two electrode layers (Figure 1.11) elegantly illustrate the need for performant n-type semiconducting CPs. The energy barrier for electron injection (ΔE_e) from

cathodes such as Al, Mg, or Ca is larger than the barrier for hole injection (ΔE_h) from anodes such as indium/tin oxide (ITO). A balanced and efficient injection of charge carriers at both interfaces is necessary to enhance quantum efficiency. Although the use of metals having a low work function, such as calcium (2.9-3.0 eV), may facilitate electron injection, the high susceptibility of these metals toward atmospheric degradation significantly diminishes their utility.²⁴ The use of a more stable, higher work function metal such as aluminum (4.1-4.4 eV) is highly desirable especially for commercial applications, but the quantum efficiency of ITO/PPV/Al device is very low ($< 10^{-2}$ %) due to high LUMO energy of PPV.³

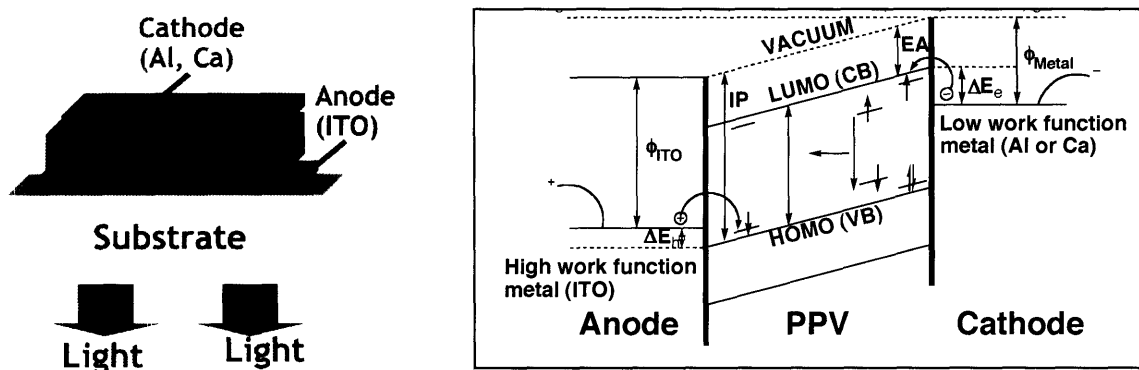


Figure 1.11. A typical structure of single LED with ITO/PPV/Al, Mg or Ca (left) and schematic energy level diagram of same LED under a forward bias showing work functions of ITO and Al (Φ_{ITO} and Φ_{metal}), energy barrier to injection of electrons and hole (ΔE_e and ΔE_h) and band gap (E_g) (right).

In order to provide acceptable efficiencies by polymer LED using an aluminum electrode, it is important to lower the energy of conduction band of the polymer by the chemical modification of polymer structure. Quantum chemical calculations²⁵ and studies reported elsewhere have demonstrated that the introduction of electron-withdrawing substituents such as cyano, halide or trifluoromethyl group onto either the aryl ring or vinyl linkage of PPV increases electron affinity and lowers the HOMO and LUMO energies of the

polymer,²⁶ affording high efficiency devices with easier electron injection from environmentally stable cathodes such as Al. Holmes *et al.*²⁷ have demonstrated the improved device efficiency using poly(cyanoterephthalylidene) **10** (CN-PPV), a dialkoxy-substituted PPV derivative with cyano groups on vinylene, in LED application. This improved efficiency is attributed to better electron injection facilitated by electron-withdrawing cyano groups. As shown several examples of n-type materials in Figure 1.12, fluorine-substituted PPVs **11** by Karasz *et al.*²⁸ and pyridine-based PPV **12** by Swager *et al.*²⁹ showed interesting spectral properties.

Other possible applications of CPs with high electron affinity are as the electron-accepting material in photodiodes or photovoltaic devices, or n-type thin film transistors (TFT). PPV with pyridopyrazine heterocycle **13** was reported by Andersson *et al.* as electron-accepting material in photovoltaic device.³⁰ Marks *et al.* recently reported polyfluoroarene-modified oligothiophene semiconductors **14** as TFT n-type materials.³¹

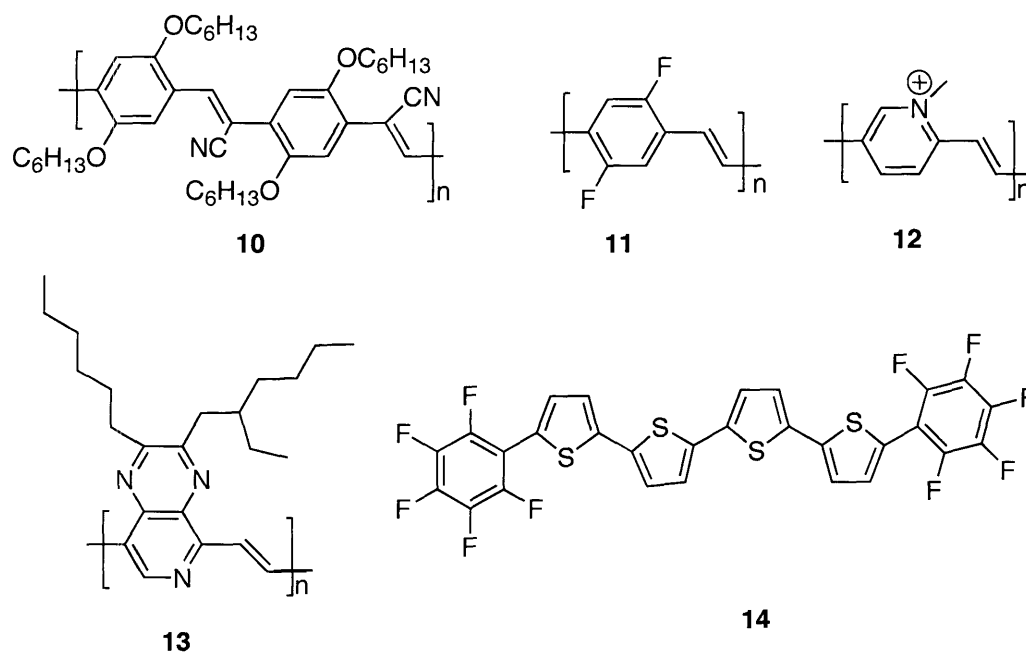


Figure 1.12. Examples of electron-transporting (n-type) organic semiconductors.

Stability of materials

Thermally robust and photochemically stable conjugated polymers are particularly attractive for electronic device applications. Photooxidation in the presence of water or oxygen has been demonstrated to be at the origin of performance degradation and breakdown in both polymer and single-molecule based devices. Singlet oxygen has been reported as a reactive intermediate in the photodegradation of materials as shown in proposed mechanism (Figure 1.13).³²

This reaction yields a dioxetane, which cleaves, resulting in macromolecular chain scission and shortening of π -conjugation in PPV and the formation of carbonyl fragment. Although stilbene, the potential monomeric analogue for these PPV systems, does not react with singlet oxygen, electron-rich olefins are known to readily yield dioxetane upon reaction with singlet oxygen. Thus, the withdrawal of electron density is expected to result in a significant reactivity decrease of the double bond toward the electrophilic singlet oxygen. It was also demonstrated that the substitution of highly electron-withdrawing groups directly onto the vinyl moiety could be very effective in improving the oxidative stability of the polymers.³³

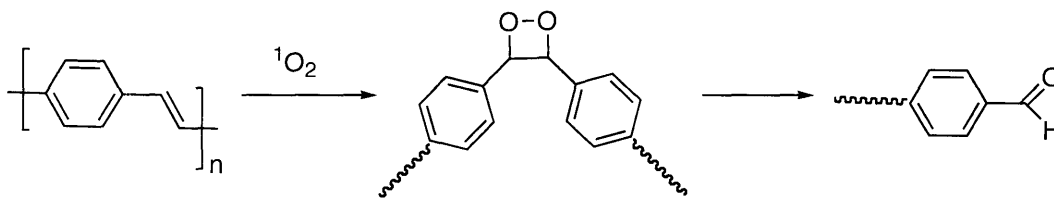


Figure 1.13. Photooxidation reaction of PPV with singlet oxygen.

Thesis overview

Our current research interest is focused on the design of electron deficient PPVs and PPEs, especially perfluorinated polymers, for molecular electronic devices and sensory application (Figure 1.14). In this work, we present the synthesis and characterization of a new PPV-based conjugated polymer, in which the electron-withdrawing groups are either directly attached on PPV backbone (Chapter 2), or they are also in electronic communication with the conjugated backbone via hyperconjugative and inductive interactions (Chapter 3). Electron deficient PPEs will be investigated to extend the scope of analytes in amplified sensory schemes (Chapter 4). Studies aimed at a deeper understanding of the interchain interactions in such polymers are detailed. (Chapter 5). Finally, these materials will be investigated for the detection of the analytes of biological interest (Chapter 6).

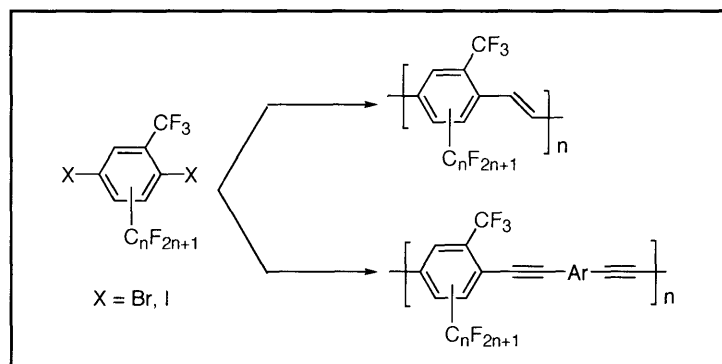


Figure 1.14. Perfluorinated-PPVs and PPEs.

References

- (1) Shirakawa, H.; Louis, E. J.; MacDiarmid, A. G.; Chiang, C. K.; Heeger, A. J. *J. Chem. Soc., Chem. Commun.* **1977**, *16*, 578–580.
- (2) (a) Heeger, A. J.; Díaz-García, M. A. *Curr. Opin. Solid. Phys. Mater. Sci.* **1998**, *3*, 16–22.
(b) Saricifti, N. S. *Curr. Opin. Solid. Phys. Mater. Sci.* **1999**, *4*, 373–378.
- (3) (a) *Handbook of Conducting Polymer* 2nd ed; Skotheim, T. A.; Elsenbaumer, R. L.; Reynolds, J. R.; Marcel Dekker; New York, **1998**. (b) Wosnick, J. H.; Swager, T. M. *Curr. Opin. Chem. Biol.* **2000**, *4*, 715–720. (c) Kraft, A.; Grimsdale, A. C.; Holmes, A. B. *Angew. Chem. Int. Ed.* **1998**, *37*, 402–428.
- (4) Swager, T. M. *Acc. Chem. Res.* **1998**, *31*, 201–207.
- (5) (a) Zhou, Q.; Swager, T. M. *J. Am. Chem. Soc.* **1995**, *117*, 7017–7018. (b) Zhou, Q.; Swager, T. M. *J. Am. Chem. Soc.* **1995**, *117*, 12593–12602.
- (6) (a) Cornil, J.; dos Santos, D. A.; Crispin, X.; Silbey, R.; Brédas, J.-L. *J. Am. Chem. Soc.* **1998**, *120*, 1289–1299. (b) Jenekhe, S. A.; Osaheni, J. A. *Science*, **1994**, *265*, 765–768.
- (7) (a) Yang, J.-S.; Swager, T. M. *J. Am. Chem. Soc.* **1998**, *120*, 11864–11873. (b) Deans, R.; Kim, J.; Machacek, M. R.; Swager, T. M. *J. Am. Chem. Soc.* **2002**, *122*, 8565–8566. (c) An, B.-K.; Kwon, S.-K.; Jung, S.-D.; Park, S. Y. *J. Am. Chem. Soc.* **2002**, *124*, 14410–14415. (d) Levitus, M.; Schmieder, K.; Ricks, H.; Schimizu, K. D.; Bunz, U. H. F.; Garcia-Garibay, M. A. *J. Am. Chem. Soc.* **2001**, *123*, 4259–4256.
- (8) (a) Bao, Z.; Amundson, K. R.; Lovinger, A. J. *Macromolecules* **1998**, *31*, 8467–8469. (b) Malenfant, P. R. L.; Groenendaal, L.; Fréchet, J. M. J. *J. Am. Chem. Soc.* **1998**, *120*, 10990–10991.

- (9) (a) Rodriquiz-Prada, J. M.; Duran, R.; Wegner, G. *Macromolecules* **1989**, *22*, 2507–2516.
(b) Weder, C.; Wrighton, M. S.; *Macromolecules* **1996**, *29*, 5157–5165.
- (10) Levitsky, I. A.; Kim, J.; Swager, T. M. *J. Am. Chem. Soc.* **1999**, *121*, 1466–1472.
- (11) (a) Weller, A. *Pure. Appl. Chem.* **1968**, *16*, 115. (b) Yanagidate, M.; Takayama, K.; Takeuchi, M.; Nishimura, J.; Shizuka, H. *J. Phys. Chem.* **1993**, *97*, 8881–8888.
- (12) Kim, T.-H.; Swager, T. M. *Angew. Chem. Int. Ed.* **2001**, *40*, 4803–4806.
- (13) DiCesare, N.; Pinto, M.; Schanze, K. S.; Lakowicz, J. R. *Langmuir* **2002**, *18*, 7785–7787.
- (14) Disney, M. D.; Zheng, J.; Swager, T. M.; Seeberger, P. H. *J. Am. Chem. Soc.* **2004**, *126*, 13343–13346.
- (15) Fan, C.; Plaxco, K. W.; Heeger, A. J. *J. Am. Chem. Soc.* **2002**, *124*, 5642–5643.
- (16) (a) Ho, H. A.; Boissinot, M.; Bergeron, M. G.; Corbeil, G.; Dore, K.; Boudreau, D.; Leclerc, M. *Angew. Chem. Int. Ed.* **2002**, *41*, 1548–1551. (b) Nilsson, K. P. R.; Inganäs, O. *Nat. Mater.* **2003**, *2*, 419–410. (c) Liu, B.; Bazan, G. C. *J. Am. Chem. Soc.* **2004**, *126*, 1942–1943.
- (17) Chen, L.; McBranch, D. W.; Wang, H.-L.; Helgeson, R.; Wudl, F.; Whitten, D. G. *Proc. Natl. Acad. Sci. U.S.A.* **1999**, *96*, 12287–12292.
- (18) Dwight, S. J.; Gaylord, B. S.; Hong, J. W.; Bazan, G. C. *J. Am. Chem. Soc.* **2004**, *126*, 16850–16859.
- (19) (a) McQuade, D. T.; Hegedus, A. H.; Swager, T. M. *J. Am. Chem. Soc.* **2000**, *122*, 12389–12390. (b) Murphy, C. B.; Zhang, Y.; Troxler, T.; Ferry, V.; Martin, J. J.; Jones, W. E., Jr. *J. Phys. Chem. B* **2004**, *108*, 1537–1543.
- (20) Liu, B.; Bazan, G. *Chem. Mater.* **2004**, *16*, 4467–4476.
- (21) DiCesare, N.; Pinto, M.; Schanze, K. S.; Lakowicz, J. R. *Langmuir* **2002**, *18*, 7785–7787.

- (22) Wosnick, J. H.; Mello, C. M.; Swager, T. M. *J. Am. Chem. Soc.* **2005**, *127*, 3400–3405.
- (23) Burroughes, J. H.; Bradley, D. D. C.; Brown, A. R.; Marks, R. N.; Mackay, K.; Friend, R. H.; Burns P. L.; Holmes A. B. *Nature* **1990**, *347*, 539–541.
- (24) (a) Friend, R. H.; Gymer, R. W.; Holmes, A. B.; Burroughes, J. H.; Marks, R. N.; Taliani, C.; Bradley, D. D. C.; Dos Santos, D. A.; Brédas, J. L.; Logdlund, M.; Salaneck, W. R. *Nature* **1999**, *397*, 121–128. (b) Dai, L.; Winkler, B.; Dong, L; Tong, L.; Mau, A. W. H. *Adv. Mater.* **2001**, *13*, 915–925. (c) Halls, J. J.; Walsh, C. A.; Greenham, N. C.; Marseglla, E. A.; Friend, R. H.; Moratti, S. C.; Holmes A. B. *Nature* **1995**, *376*, 498–500.
- (25) Brédas, J. L.; Heeger, A. J. *Chem. Phys. Lett.* **1994**, *217*, 507–511.
- (26) (a) Riehn, R.; Morgado, J.; Iqbal, R.; Moratti, S. C.; Holmes, A. B.; Volta, S.; Cacialli, F. *Synth. Met.* **2001**, *124*, 67–69. (b) Xiao, Y.; Yu, W.-L.; Pei, J.; Chen, Z.; Huang, W.; Heeger, A. J. *Synth. Met.* **1999**, *106*, 165–170. (c) Greenham, N. C.; Moratti, S. C.; Bradley, D. D. C.; Friend, R. H.; Holmes, A. B. *Nature* **1993**, *365*, 628–630. (d) Shim, H.-K.; Zyung, T. *Chem. Mater.* **1997**, *9*, 746–749. (e) Benjamin, I.; Faraggi, E. Z.; Avny, Y.; Davidov, D.; Nenmann, R.; *Chem. Mater.* **1996**, *8*, 352–355.
- (27) Greenham, N. C.; Moratti, S. C.; Bradley, D. D. C.; Friend, R. H.; Holmes A. B. *Science* **1993**, *365*, 628–630.
- (28) Gurge, R. M.; Sarker, A. M.; Lahti, P. M.; Bin Hu, B.; Karasz, F. E. *Macromolecules* **1997**, *30*, 8286–8292.
- (29) Marsella, M. J.; Fu, D.-K.; Swager, T. M. *Adv. Mater.* **1995**, *7*, 145–147.
- (30) Jonforsen, M.; Ahmad, I.; Johansson, T.; Larsson, J.; Roman, L. S.; Svensson, M.; Inganäs, O.; Andersson, M. R. *Synth. Met.* **2001**, *119*, 185–186.

- (31) (a) Facchetti, A.; Yoon, M.-H.; Stern, C. L.; Katz, H. E.; Marks, T. J. *Angew. Chem. Int. Ed.* **2003**, *42*, 3900–3903. (b) Facchetti, A.; Yoon, M.-H.; Stern, C. L.; Hutchison, G. R.; Ratner, M. A.; Marks, T. J. *J. Am. Chem. Soc.* **2004**, *126*, 13480–13501.
- (32) (a) MacManus-Spencer, L. A.; Latch, D. E.; Kroncke, K. M.; McNeill, K. *Anal. Chem.* **2005**, *77*, 1200–1205. (b) Scurlock, R. D.; Wang, B.; Ogilby, P. R.; Sheats, J. R.; Clough, R. L. *J. Am. Chem. Soc.* **1995**, *117*, 10194–10202.
- (33) Cumpston, B. H.; Jensen, K. F. *J. Appl. Poly. Sci.* **1998**, *69*, 2451–2468.

Chapter 2:

Synthesis and Stability Studies of Perfluorinated Poly(*p*-phenylene vinylenes) Derivatives

Adapted from:

Kim, Y.; Swager, T. M.
Chem. Commun. **2005**, 126, 372-374.

Swager, T. M.; Kim, Y.
U.S. Patent Application Serial No.: 60/526,886.

Introduction

Since the discovery of electroluminescence in a conjugated polymer in 1990,¹ luminescent conjugated polymers (CPs), especially poly(*p*-phenylenevinylene) (PPV) based polymers, have been intensively investigated in a wide range of electronic and optoelectronic applications including light-emitting diodes (LEDs),² photovoltaic cells,³ thin film transistors (TFT),⁴ and optically pumped lasers.⁵ Among their advantageous attributes are their low cost, easily tunable optical and electrical properties, and facile processibility.⁶ Despite significant progress in this field, there are still some challenges associated with organic conjugated polymer based-electronic materials. For example, most of the current highly fluorescent conjugated polymers used as emissive materials in LEDs, are good p-type (hole transport) materials, but they have generally small electron affinities and poor electron transport properties. The resulting devices show low level of efficiency and limited durability and stability. In FET devices, a variety of organic structures have been demonstrated to be active p-channel materials between source and drain electrode.⁷ Therefore, one of the current broad needs in the field is the development of n-type (electron transport) conjugated polymer for improving the performance of LEDs, solar cells, and n-channel thin film transistors.

In addition, dramatic improvements in the durability and stability of CPs are necessary for many applications. The design of organic electronic polymers having enhanced photooxidative stability and charge transport properties is of particular importance for application in solar cells,⁸ since stability to UV light is necessary for long-term use in exterior applications. Efforts to increase the stability of conjugated polymers include encapsulation to protect them from oxygen and moisture⁹ and the incorporation of electron-withdrawing groups such as cyano or trifluoromethyl on the vinylene units of PPV to decrease

photooxidation.¹⁰ Although PPV derivatives containing electron-withdrawing substituents at vinylene units have shown improved photooxidation stability, undesirable conformational changes arise from this substitution as a result of increased steric hindrance.¹¹ The resulting nonplanarity can disturb the transport properties and result in a strong reduction of fluorescence yields due to torsion-induced nonradiative deactivation.¹²

As new n-type materials having high device efficiency and stability for electronics and optoelectronics, we are particularly focused on perfluorinated-PPVs in which perfluoroalkyl groups are directly attached to the phenyl rings. Our motivation for incorporating perfluoroalkyl groups as electron-withdrawing substituents onto a polymer backbone originates from the unique behavior of perfluorinated compounds.¹³ The high electronegativity of fluorine (4.0 on Pauling's electronegativity scale) combined with strong C-F bond, and high electron-withdrawing effect of perfluoroalkyl groups, leads to increased oxidative, chemical, and thermal stability. Whereas most polymers are p-type, which can be easily oxidized, polymers with high electron withdrawing groups such as perfluoroalkyl groups could be used for stable n-type materials in organic semiconductor device.

In addition, we expect that substitution with perfluoroalkyl groups can give rise to unique interactions at interfaces between metal and polymer in conjugated polymer-based devices. Perfluoroalkyls may provide thermodynamically favorable interactions with the reactive metal interfaces. It is anticipated that the evaporation of metal onto these materials will generate highly stable metal fluorides and new perfluorinated alkyl groups bound to the metal ions.¹⁴ This is based on the fact that metals bound to perfluorinated alkyl groups are known to be more stable than their hydrocarbon analogs; hence, these structures can give rise to very stable interfaces between the metals and polymers. This is important because many

OLED technologies suffer from degradation of the cathode interface, and these materials may offer a general solution for stabilizing such interfaces.

In this chapter, we report the synthesis and characterization of a series of perfluorinated PPV homopolymers and copolymers (Figure 2.1) and the dramatic improvement in their stability against photooxidation.

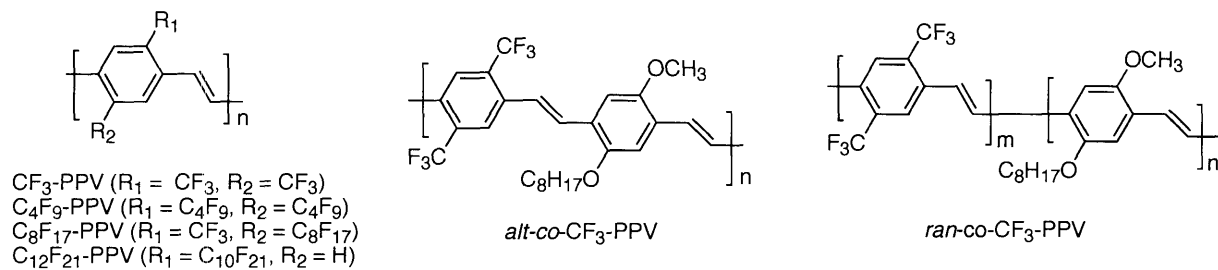
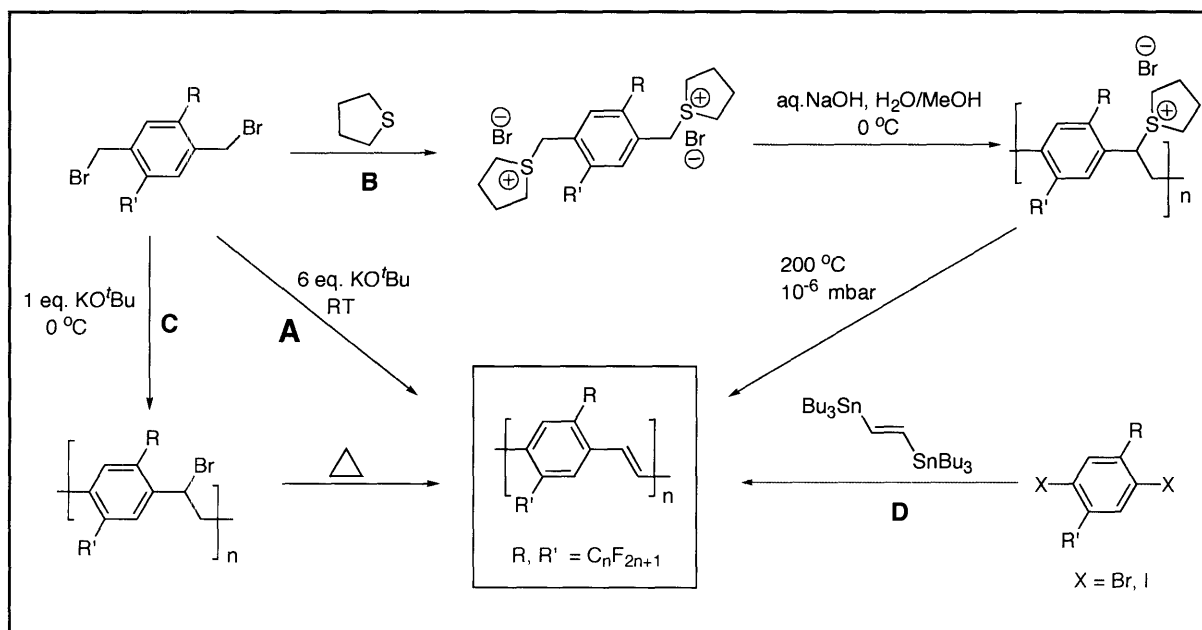


Figure 2.1. Perfluorinated-PPV homopolymers and copolymers.

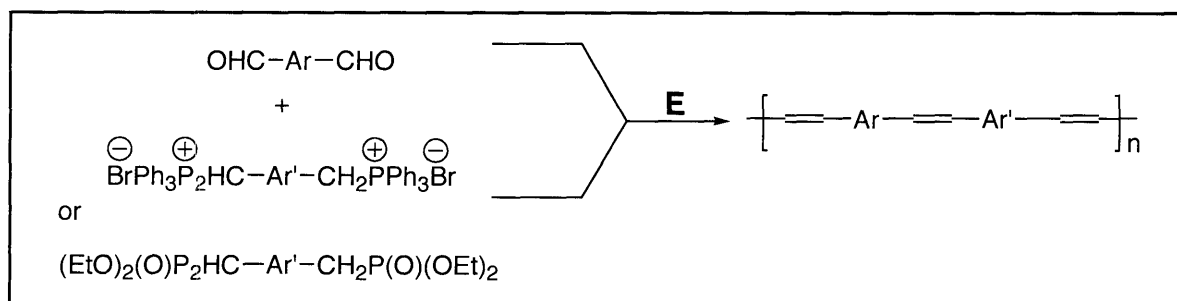
Results and Discussions

The overall synthetic methodology used for perfluorinated-PPV homopolymers and copolymers and their thin films is summarized in Scheme 2.1 and 2.2. These routes include the Gilch method (dehydrohalogenation route **A**),¹⁵ the Wessling method (sulfonium precursor route **B**),¹⁶ a halogen precursor route (**C**),¹⁷ a metal-catalyzed polycondensation (**D**)¹⁸ and a Wittig/Horner-Emmons-Wittig polymerization (**E**).¹⁹ Electropolymerization was also explored as an alternate route for the preparation of PPV.

Scheme 2.1. Several routes for perfluorinated-PPV homopolymers.



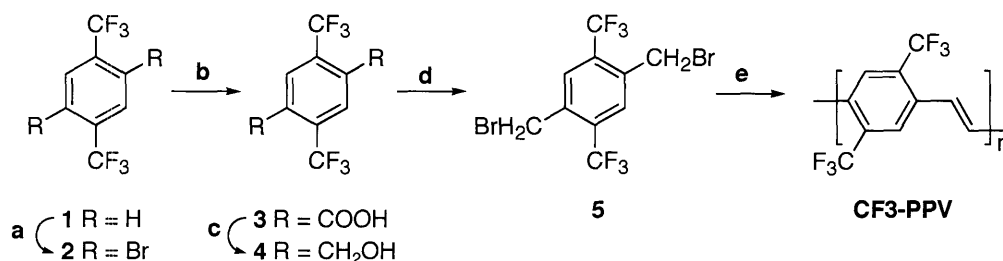
Scheme 2.2. Perfluorinated-PPV copolymers prepared by Wittig/Horner-Emmons polymerization.



Synthesis and photophysical properties of CF₃-PPV homopolymers

As shown in Scheme 2.3, the synthesis of monomer **5**, 1,4-bis(trifluoromethyl)-2,5-dibromomethylbenzene involves bromination of 1,4-bis(trifluoromethyl)benzene (**1**) in the presence of NBS/CF₃COOH and H₂SO₄ to obtain **2**. Lithiation of **2** with *n*-butyllithium in THF followed by addition of CO₂ gives 2,5-bis(trifluoromethyl)-terephthalic acid (**3**), and reduction leads to the corresponding diol (**4**). Monomer **5** is prepared from bromination of **4** and is polymerized via dehydrohalogenation route, including the treatment with excess of KO^tBu in THF at room temperature for 1 day. The reaction mixture was poured into methanol, and the resulting precipitate was filtered and washed with methanol, hexane, and acetone. The solid was dried to give poly-[2,5-bis(trifluoromethyl)-*p*-phenylenevinylene] (CF₃-PPV) as a green fluorescent solid.

Scheme 2.3. Synthesis of CF₃-PPV.^a



^a(a) NBS, CF₃CO₂H, H₂SO₄, 60 °C. (b) (i) *n*-BuLi, THF, -78 °C. (ii) CO₂. (c) BH₃-THF, RT. (d) PBr₃, THF. (e) KO^tBu, THF, RT.

The photophysical properties and molecular weights of the resulting polymer are summarized in Table 2.1. The relative number average molecular weights (*M_n*) of CF₃-PPV estimated by gel permeation chromatography (GPC) relative to polystyrene standards (THF solvent) was 25,000 with a polydispersity index (*M_w*/*M_n*) of 1.25. CF₃-PPV showed strong

green fluorescence but poor solubility in CH_2Cl_2 , or CHCl_3 and partial solubility in THF and DMF. The latter solvents allowed solution photoluminescence studies and the spin coating of thin films. As shown in Figure 2.2, the UV-visible absorption spectrum of the CF3-PPV in THF has a maximum at 361 nm and the emission spectrum displays a large Stokes-shift with a peak maximum at 489 nm and a shoulder at 514 nm. The magnitude of the Stokes shift suggests large differences in the conformation of the polymer's ground state and the excited states and energy migration to minority segments having greater conjugation lengths.²⁰

CF3-PPV showed relatively high fluorescence quantum yields in both THF solution (0.63) and in thin films (0.25). In contrast we find that poly[(2-methoxy-5-ethylhexyloxy)-1,4-phenylene vinylene] (MEH-PPV), which is the most widely used materials in electronic application, has lower fluorescence quantum yields in solution (0.08) and in thin films (0.03).

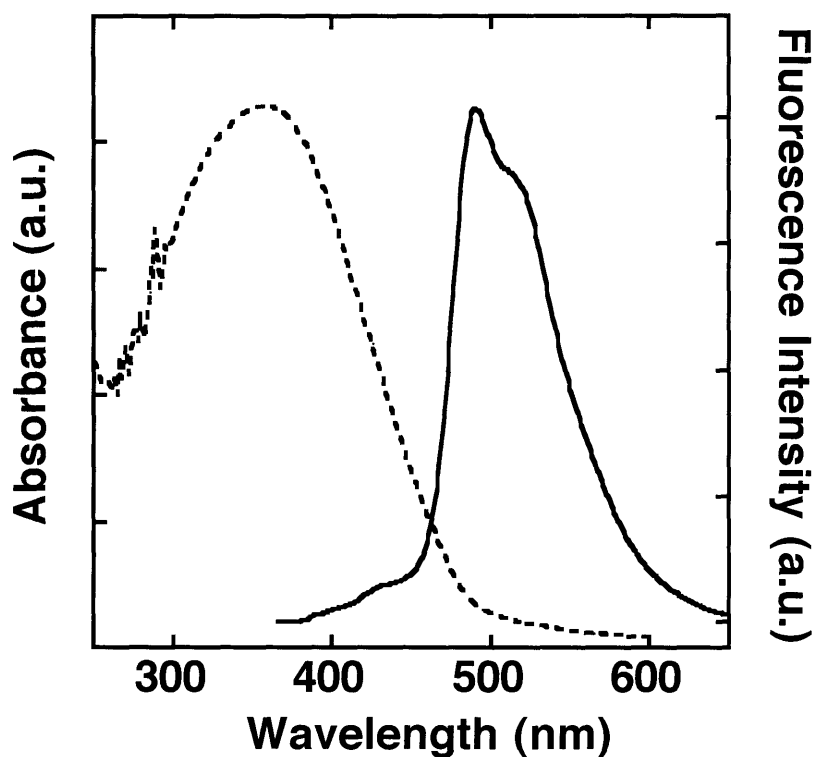
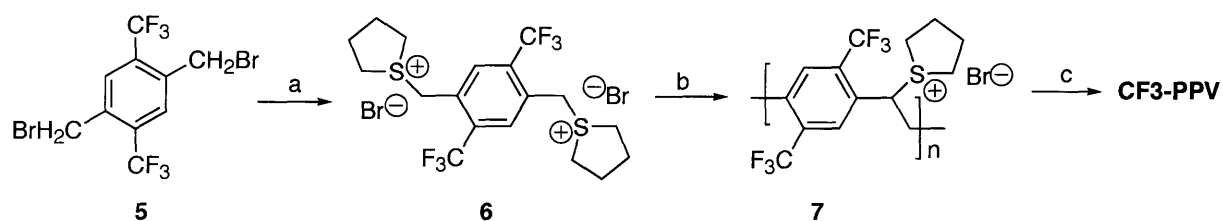


Figure 2.2. The absorption and emission spectra of CF3-PPV in THF.

Although the Gilch polycondensation is an especially convenient synthetic method, the low solubility of CF₃-PPV required dramatic enhancements to be applicable to thin film device applications. To this aim, various soluble precursor approaches for the preparation of CF₃-PPV thin film were screened. The sulfonium precursor route, the most popular method to prepare PPV thin films, is a base-induced polymerization of arylsulfonium salt monomer in aqueous solution (Scheme 2.4). The polymerization reaction is terminated with dilute HCl aqueous solution and the solution is then dialysed against deionized water for several days. The dialyzed solution of sulfonium precursor polymer **7** was spin-coated on a glass substrate and then thermally converted at 200 °C for 5 h to give fully conjugated CF₃-PPV thin film. The film exhibited emission peaks at 485 and 513 nm, which are identical to ones obtained by dehydrohalogenation route.

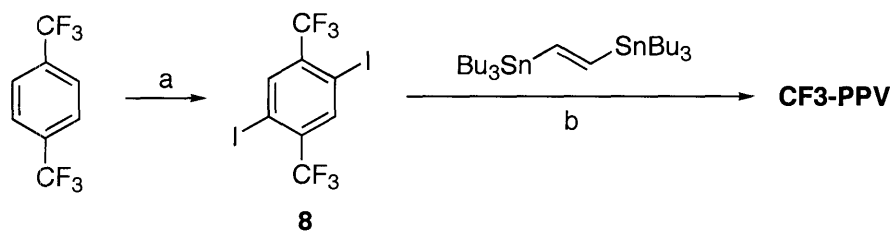
Scheme 2.4. The preparation of CF₃-PPV by sulfonium precursor route.^a



^a(a) tetrahydrothiophene, MeOH, 50 °C, 24 h. (b) (i) aq. NaOH/MeOH 0 °C (ii) HCl (iii) dialysis. (iii) 200 °C, 10⁻⁶ mbar, 5 h.

Preparation of CF₃-PPV by a Stille cross-coupling polymerization (Scheme 2.5) gave materials of low molecular weights ($M_n \sim 3,000$, PDI = 1.05), as corroborated by the absorption and emission spectra in chloroform, which showed blue shifted ($\lambda_{\max, \text{abs}} = 339 \text{ nm}$, $\lambda_{\max, \text{emi}} = 406, 423 \text{ nm}$) relative to polymers obtained from Gilch or Wessling polymerizations. These hypsochromic shifts are indicative of short conjugation length, as confirmed by model compound studies.

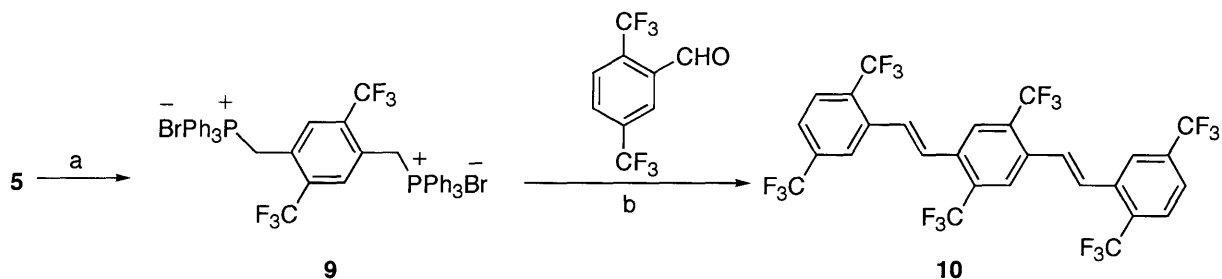
Scheme 2.5. The preparation of CF₃-PPV by Stille polymerization.^a



^a(a) Periodic acid/KI, H₂SO₄, 70 °C, 5 h. (b) 1.5% Pd₂(dba)₃, 6% P^tBu₃, LiCl, NMP, 80-100 °C, 2 d.

As the model for CF₃-PPV, trimer **10** was synthesized by Wittig/Horner-Emmons-Wittig condensation of aldehyde and p-xylene-bis-(triphenylphosphonium bromide) **9** in the presence of base (Scheme 2.6). The compound **10** displayed λ_{\max} at 313 nm for absorption and at 393 and 413 nm for emission in CHCl₃.

Scheme 2.6. The preparation of trimer **10**.^a



^a(a) PPh₃, DMF, reflux, 24 h. (b) NaOEt, CHCl₃/Ethanol, RT, overnight.

Chang *et al.*²¹ reported that poly(*p*-phenylene vinylene) (PPV) have been prepared electrochemically from *p*-xylylenebis(triphenylphosphonium bromide). In this process, the ionic monomer *p*-xylylenebis(triphenylphosphonium bromide) also acts as an electrolyte and undergoes an electrochemical polymerization on a cathode (indium-tin oxide) (ITO). Following the modified procedure, CF₃-PPV film on ITO was prepared via a simple and convenient electrochemical polymerization reaction from the ionic monomer **9** in acetonitrile solution with an applied potential of 5.5 V. The resultant CF₃-PPV film deposited on ITO was transparent and emitted green light with an emission peak maximum at 487 nm and a shoulder at 516 nm. As shown in Figure 2.7, the spectra of the electropolymerized CF₃-PPV film on ITO exhibited similar emission peaks, compared with the CF₃-PPV films on glass slide prepared from chemical polymerization.

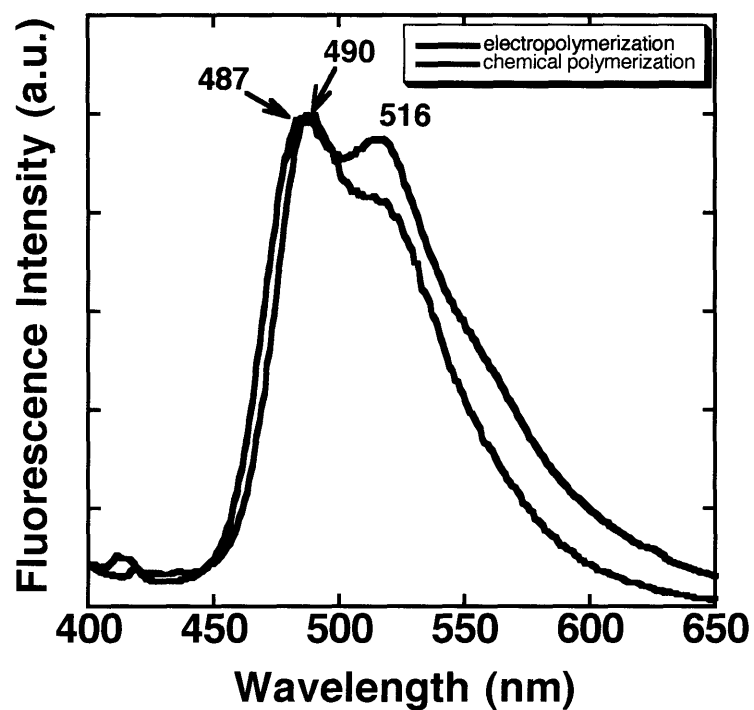
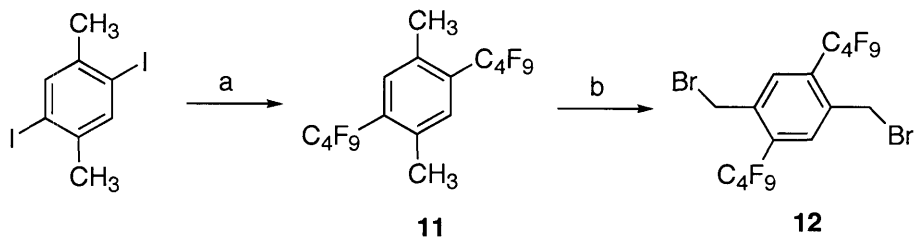


Figure 2.3. The emission spectra of CF3-PPV thin films prepared by chemical (Gilch) and electrochemical polymerizations.

Synthesis and photophysical properties of PPV homopolymers with longer perfluoroalkyl groups

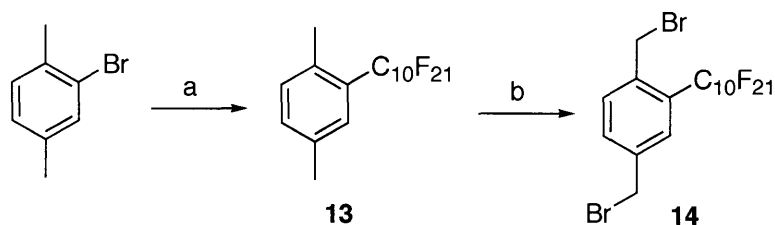
Longer perfluoroalkyl groups were introduced into the phenyl ring in order to produce more soluble fluorinated materials. Monomers with longer perfluoroalkyl chains such as perfluorobutyl (C₄F₉), perfluorooctyl (C₈F₁₇) and perfluorodecyl (C₁₀F₂₁) groups were prepared as shown in Schemes 2.7 - 2.9. These perfluoroalkyl groups were incorporated by Cu-mediated coupling reaction²² with aryl halides and followed by the bromination to give monomers **12** and **14**. Monomer **19**, which asymmetrically incorporates one trifluoromethyl group and one perfluorooctyl group, was similarly prepared. As shown in Scheme 10, perfluorinated polymers (C₄F₉-, C₈F₁₇-, C₁₀F₂₁-PPV) were prepared by the Gilch dehydrohalogenation route. C₈F₁₇-PPV showed good solubility in common organic solvents but the number average molecular weight (*M_n*) of C₈F₁₇-PPV, as estimated by gel permeation chromatography (GPC) relative to polystyrene standards (THF solvent), was only 3,000 (*M_w*/*M_n* = 1.16). This low molecular weight leads to blue shifted absorption and emission spectra of C₈F₁₇-PPV relative to CF₃-PPV. The UV-visible absorption spectrum of the C₈F₁₇-PPV in THF has a maximum at 354 nm and the emission spectrum displays a large Stokes-shift with a peak maximum at 470 nm and a shoulder at 495 nm. C₁₀F₂₁-PPV, which is substituted with a single long perfluoroalkyl side-chain, was found to be sparingly soluble in THF but highly soluble in DMF. The absorption ($\lambda_{\text{max}} = 375$ nm) and emission spectra ($\lambda_{\text{max}} = 498$ nm) of C₁₀F₂₁-PPV in DMF exhibited similar characteristics to those of CF₃-PPV.

Scheme 2.7. Synthesis of monomer **12** with perfluorobutyl groups.^a



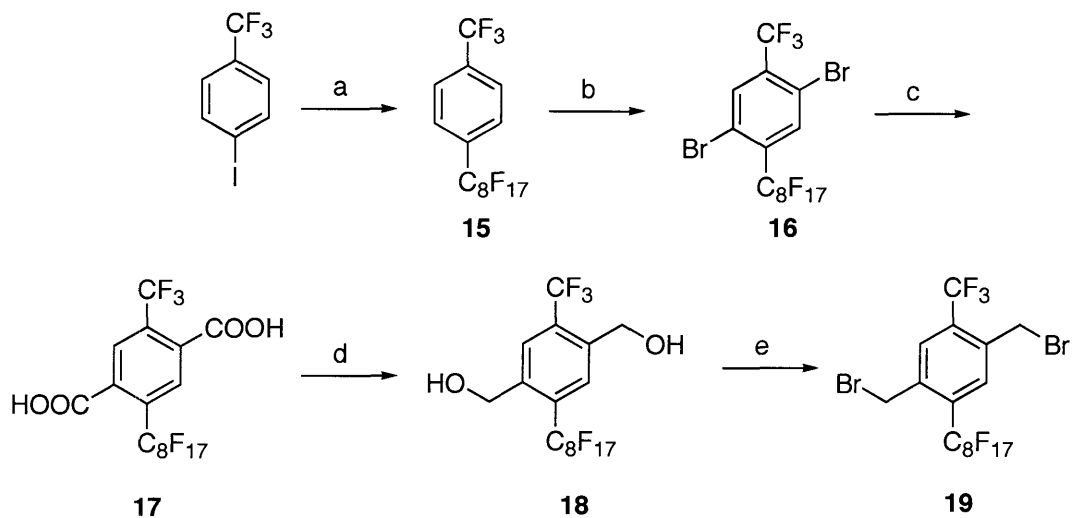
^a(a) perfluorobutyl iodide, Cu, DMSO, 130 °C, 2 d. (b) NBS, AIBN, CCl₄, 24 h.

Scheme 2.8. Synthesis of monomer **14** with perfluorodecyl group.^a



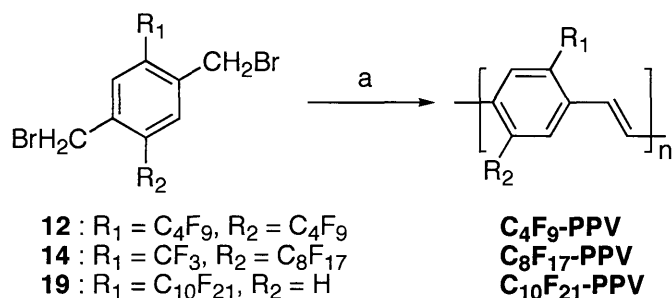
^a(a) perfluorodecyl iodide, Cu, DMSO, 130 °C, 2 d. (b) NBS, AIBN, CCl₄, 24 h.

Scheme 2.9. Synthesis of monomer **19** with perfluorooctyl group.



^a(a) CF₃(CF₂)₇I, Cu, DMSO, 2,2'-bipyridine, 70 °C, 3 d. (b) H₂SO₄/TFA (0.3 v/v), NBS, 60 °C, 2 d. (c) (i) *n*-BuLi, THF/-78 °C (ii) CO₂. (d) BH₃-THF, RT, 2 d. (e) PBr₃/THF, 0 °C to RT, 40 h.

Scheme 2.10. Synthesis of perfluorinated-PPV.^a

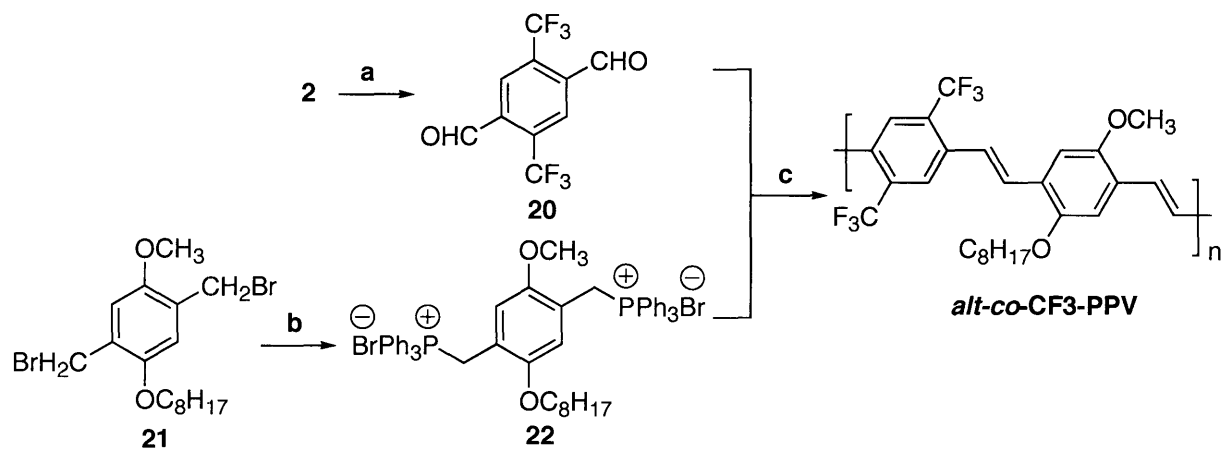


^a(a) KO^tBu, THF, RT.

Synthesis and photophysical properties of CF₃-PPV copolymers

Alternating copolymer containing CF₃-PV and MEH-PV units were also synthesized. MEH-PPV was used as one component of the copolymer because MEH-PPV had been widely used in LEDs owing to its efficient hole injection from ITO and high solubility. Poly-[(2-methoxy-5-(2'-ethylhexyloxy)-1,4-phenylenevinylene-*alt*-2,5-bis(trifluoromethyl)-1,4-phenylenevinylene] (*alt-co*-PPV) was prepared by Wittig condensation of 2,5-bis(trifluoromethyl)-1,4-benzenedicarboxyaldehyde (**20**) with 2-methoxy-5-(2'-ethylhexyloxy)-1,4-xylenebis(triphenylphosphoniumbromide) (**22**) as shown in Scheme 2.11. The mixture was quenched with 2% HCl solution and then poured into methanol. The polymer was isolated by filtration, dried, and purified by reprecipitation from MeOH to give an orange solid with a yield of *ca* 55%. The *alt-co*-PPV (M_n 5,500, PDI = 1.35, THF) consisting of alternate p- and n-type moieties for balanced properties of conducting holes and electrons, was highly soluble in common organic solvent. As expected with CF₃ substitution, the absorption and emission spectra of *alt-co*-PPV are blue shifted relative to MEH-PPV (Figure 2.4).

Scheme 2.11. Synthesis of *alt-co*-CF₃-PPV.^a



^a(a) (i) *n*-BuLi, THF, -78 °C, (ii) DMF. (b) PPh₃, DMF, reflux. (c) NaOEt, CHCl₃/Ethanol, RT.

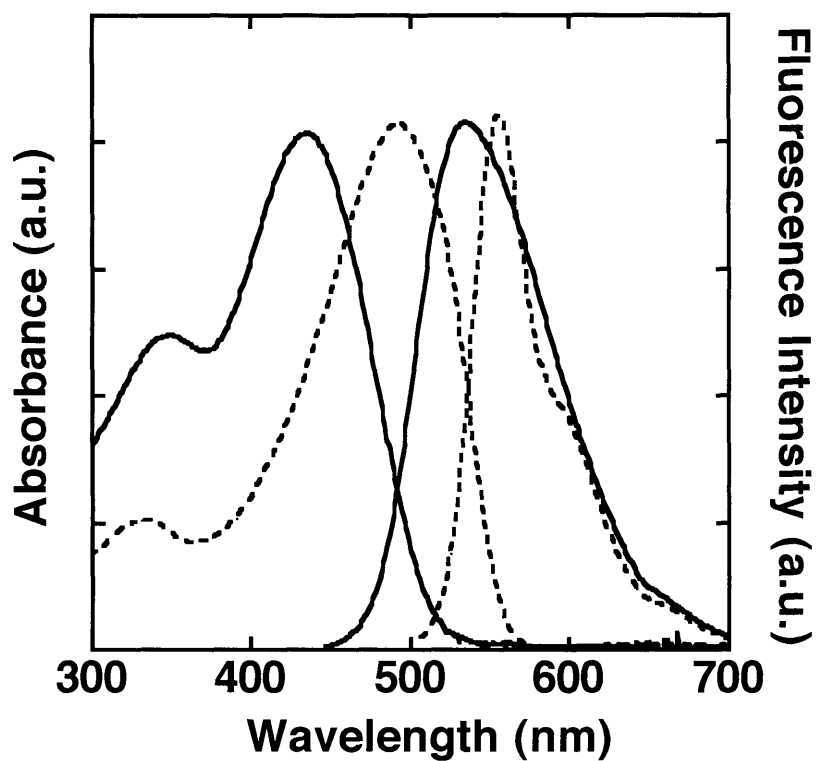
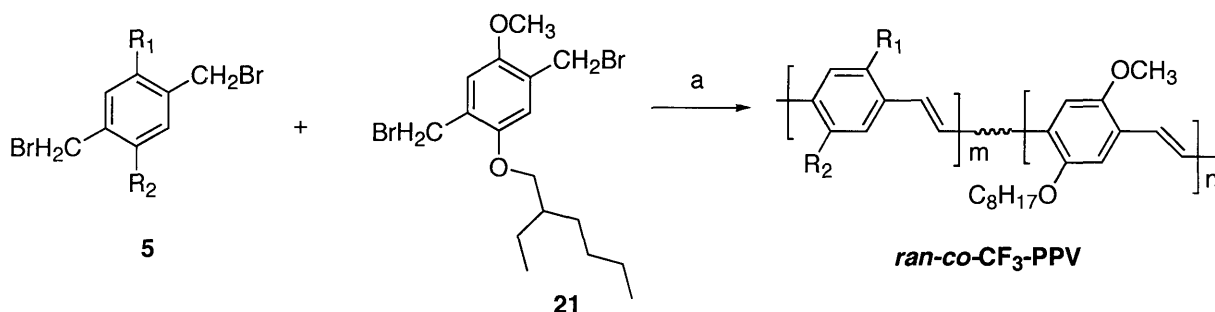


Figure 2.4. The absorption and emission spectra of *alt-co*-PPV (solid line) and MEH-PPV (dotted line) in chloroform.

Random copolymers of the CF₃-PPV with MEH-PPV were also prepared by the dehydrohalogenation route. Regardless of the feed ratios of each monomer (1:4, 1:1, 0:1 CF₃-PV: MEH-PV), materials exhibiting essentially identical absorption and emission maxima were obtained. As the ratio of CF₃-PV was increased, decrease in the solubility was observed for the materials obtained (Scheme 2.12).

Scheme 2.12. The preparation of random copolymers.^a



^a(a) KO^tBu, THF, RT.

Table 2.1. Summary of molecular weight and photophysical properties.

| Polymer | <i>M</i> _n (PDI) | $\lambda_{\text{max, abs}}$ (nm) | $\lambda_{\text{max, em}}$ (nm) |
|---|-----------------------------|----------------------------------|---------------------------------|
| CF₃-PPV | 25,000 (1.25) | 374 (THF) | 489, 519 (THF) |
| C4F9-PPV | 5,000 (1.04) | 320 (THF) | 440 (THF) |
| C8F17-PPV | 3,040 (1.16) | 354 (THF) | 470, 496 (THF) |
| C10F21-PPV | 1,800 (1.40) | 345 (THF) 378 (DMF) | 421, 478 (THF) 488 (DMF) |
| <i>alt-co-CF₃-PPV</i> | 5,522 (1.32) | 483 (THF) | 531, 564 (THF) |
| <i>ran-co-CF₃-PPV</i> (1:1) | 19,000 (2.14) | 488 (CHCl ₃) | 548 (CHCl ₃) |

Stability studies

Trifluoromethyl groups provide for a strong inductive perturbation of polymer's electronic structure, thereby significantly increasing their ionization potential. Such substitution renders the polymers very resistant to oxidation and creates extremely durable materials for electronic device applications or highly robust CP-based sensors. In order to investigate photo- and thermal stability of perfluorinated-PPVs, photobleaching study and thermogravimetric analysis (TGA) were carried out.

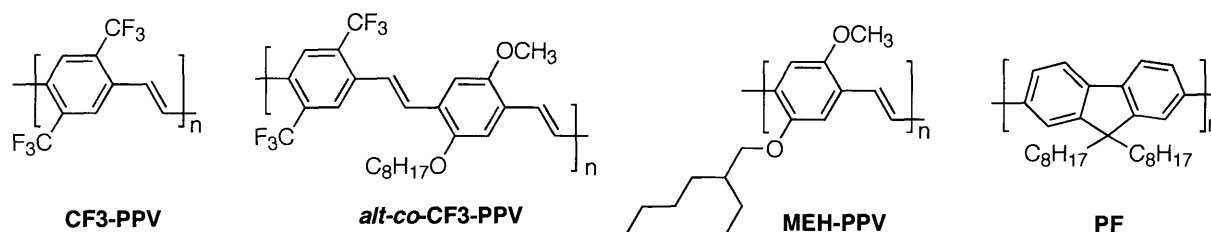


Figure 2.5. The structure of polymers used for stability studies.

Upon exposure to light, organic chromophores typically degrade or decompose by inducing a decrease in the absorbance intensity and/or, in the case of fluorescent materials, a decrease in emission intensity. This phenomenon is known as photobleaching. We have investigated photostabilities of CF₃-PPV, *alt-co*-CF₃-PPV, MEH-PPV, and PF²³ thin films (Figure. 2.5). The photooxidation studies were performed by continuous UV irradiation of polymer thin films using a 450 W steady-state Xe lamp as the irradiation source (slit width = 10 nm) under aerobic conditions. Polymer films having similar optical density (0.05 ± 0.01) were irradiated at their absorption maxima (CF₃-PPV = 370 nm; *alt-co*-CF₃-PPV and PF = 380 nm, MEH-PPV = 505 nm), and photoinduced degradation was quantified by monitoring the decrease of fluorescence intensity as a function of elapsed photolysis time (Figure. 2.6).

The fluorescence intensity of CF3-PPV did not show any decrease after 2 hours of irradiation despite the fact that it was excited at a higher energy excitation, whereas fluorescence intensity of MEH-PPV and PF decreased rapidly as indicated by the fact that only 10% fluorescence intensity remained after irradiation of 2 hours. As indicated by photolysis experiments with *alt-co*-CF3-PPV, the incorporation of the electron-withdrawing substituents contributes to the decrease of the rate of photobleaching. However, only the homopolymer CF3-PPV demonstrated extraordinary photostability and emission spectra that are unchanged for hours of UV irradiation.

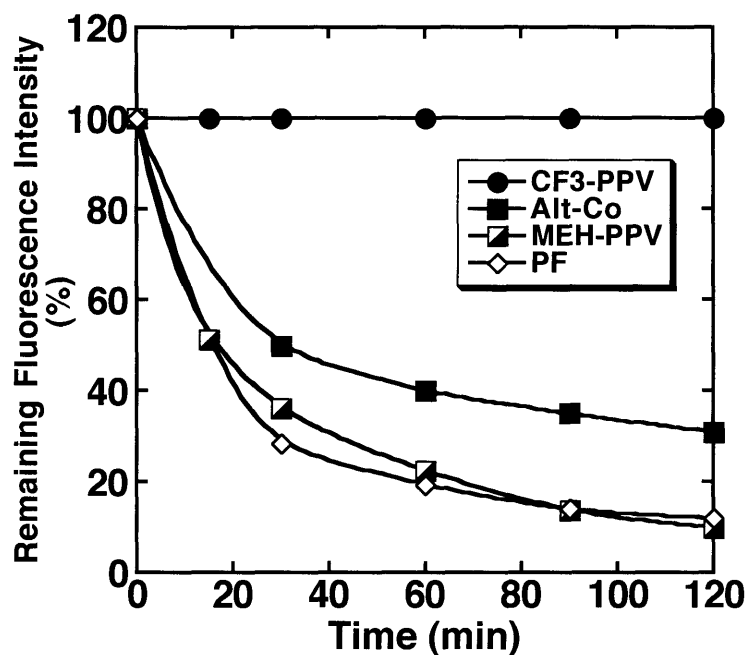


Figure 2.6. The time dependence of fluorescence intensity of CF3-PPV, *alt-co*-CF3-PPV, MEH-PPV and PF thin films under UV irradiation.

Meanwhile, CF3-PPV thin film deposited on ITO electrochemically showed some signs of photodegradation under the same photolysis conditions. This might be attributed to defects such as residual P-C bond on the electropolymerized PPV chain. The level of stability of CF3-PPV thin film prepared either chemically or electrochemically is unprecedented for a semiconductive conjugated organic polymer. It indicates that these materials may be promising materials for many sensors, photovoltaic, display, and electronic technologies.

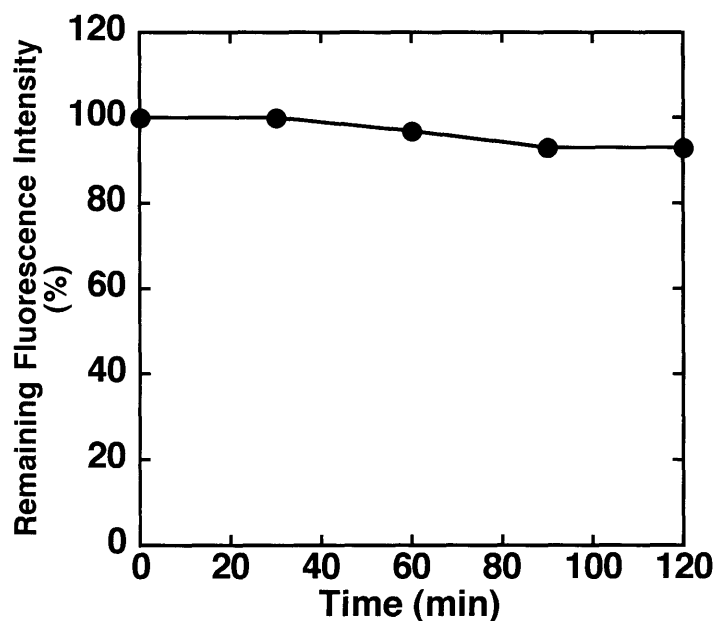


Figure 2.7. The time dependence of fluorescence intensity of CF3-PPV prepared electrochemically on ITO.

The thermal stabilities of CF3-PPV and MEH-PPV were investigated by thermogravimetric analysis (TGA) under nitrogen atmosphere with heating rate of 25 °C/min. Both polymers showed good thermal stability up to 300 °C. CF3-PPV showed the onset of decomposition at 288 °C, 10% weight loss at 400 °C, less than 50% weight loss by 600 °C, whereas MEH-PPV showed the onset of decomposition at 295 °C, 40% weight loss at 400 °C, and 70% weight loss by 600 °C (Figure. 2.9).

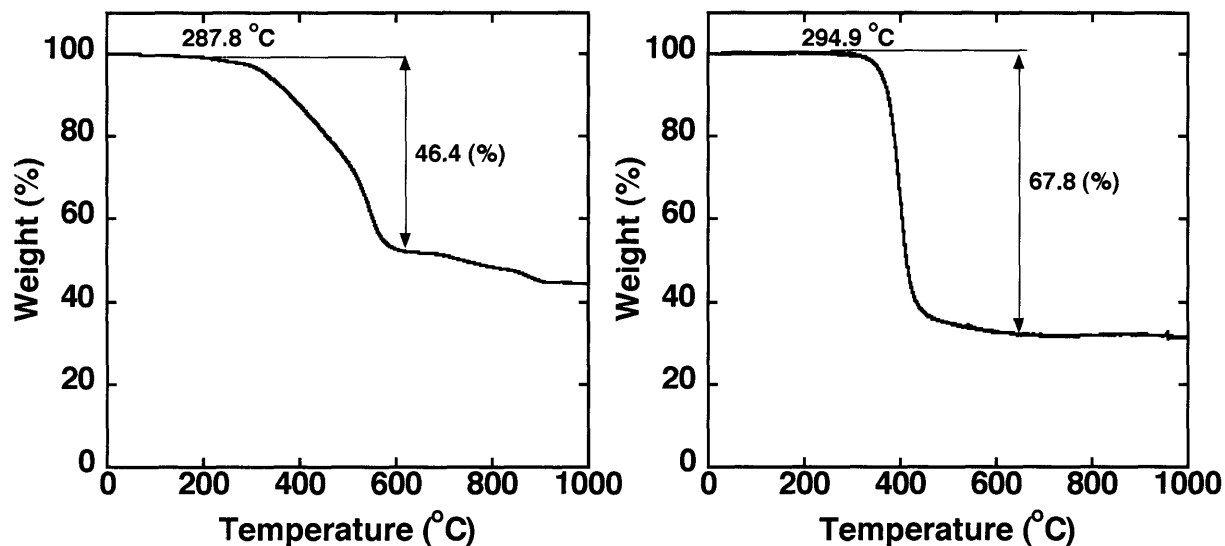


Figure 2.8. TGA of CF3-PPV (left) and MEH-PPV (right).

Potential applications

Thin films of CF3-PPV showed large fluorescence quenching responses with several electron-donating analytes (aromatic amine compounds), indicating its high electron affinity. However, the preliminary studies directed at the fabrication of n-type field effect transistors, based on a Ag/CF3-PPV/ITO structure, were inconclusive with regards to n-type conductivity in these materials. It is proposed that optimization of the device configuration may solve these problems. Nevertheless these novel conjugated fluorinated polymers are remarkably well suited for a wide range of other optoelectronic applications. The observation of fluorescence quenching in polymer blend composed of MEH-PPV and CF₃-PPV in THF solution is especially relevant for the development of photovoltaics, as it implicates a strong interaction of the two components in the excited state. CF3-PPV may be used as electron-accepting materials in photovoltaic devices, in which photoinduced energy transfer occurs

from excited MEH-PPV to CF3-PPV. The high durability of these perfluorinated materials will be useful since stability to UV light is necessary for long-term use in exterior applications.

Conclusions

In summary, PPV homopolymers and copolymers containing perfluoroalkyl groups directly attached onto phenyl ring were synthesized, resulting in materials with high electron affinity where photooxidative degradation is prevented. Their superior photostability revealed by photobleaching studies endows these materials with critical stability needed for optoelectronic devices and sensory applications. These polymers and model compounds require further investigation for surface interaction using XPS as well as n-type materials in polymer electronic devices.

Experimental Section

General Methods. NMR (^1H , ^{13}C , and ^{19}F) spectra were recorded on a Varian Mercury-300 MHz or Bruker Advance 400 MHz spectrometers. The ^1H and ^{13}C chemical shifts are given in parts per million relative to tetramethylsilane (TMS), and referenced to the residual solvent. ^{19}F -NMR chemical shifts are reported in units of δ (ppm) or Hz relative to trichlorofluoromethane as the reference. Melting point determinations were performed using a Laboratory Devices MEL-TEMP instrument (open capillaries used) and are reported uncorrected. High-resolution mass spectra were obtained with a Finnigan MAT 8200 system using sector double focus and an electron impact source with an ionizing voltage of 70 V. The molecular weights of polymers were determined by using three PLgel 5 μm (300 x 7.5

mm) columns in series and a diode detector at 254 nm at a flow rate of 1.0 ml/min in THF. The molecular weights are reported relative to polystyrene standards purchased from Polysciences, Inc. Polymer thin films deposited on a cover glass (18 mm x 18 mm) were prepared by spin casting using an EC101DT photo resist spinner (Headway Research, Inc.) from solutions of the polymers. UV-vis spectra were obtained from Hewlett-Packard 8452A diode array or Cary 50 UV-Visible Spectrophotometers. Fluorescence studies were conducted with a SPEX Fluorolog- τ 2 fluorometer (model FL112, 450 W xenon lamp) equipped with a model 1935B polarization kit. The spectra in solution were obtained at 25 °C using a quartz cuvette with a path length of 1 cm. Polymer thin film spectra were recorded by front-face (22.5°) detection. The quantum yield measurement was performed in a self-consistent fashion for all of the samples. Quinine sulfate (in 0.1 N sulfuric acid) and (fluorescein in 0.1 N NaOH) were used as standard for the solution quantum yield of CF3-PPV and fluorescein, respectively because their emission spectra have the best overlap to minimize variations in the detector response. The solid state quantum yields were obtained relative to 10^{-3} M 9,10-diphenylanthracene in poly(methyl methacrylate) (PMMA) ($\Phi_F = 0.83$) as a reference.

Materials. All solvents were spectral grade unless otherwise noted. Anhydrous THF, CCl₄, DMSO, and ethanol were purchased from Aldrich Chemical Co., Inc. All other compounds were purchased from Aldrich and used as received. Compound **8**, **15**, **16**, and **21** are reported elsewhere. All air and moisture-sensitive synthetic manipulations were performed under an argon atmosphere using standard Schlenk techniques. Silica gel (40 μ m) was obtained from J. T. Baker.

2,5-dibromo-1,4-bis(trifluoromethyl)benzene (2). Into a 1000 mL round-bottomed flask were placed 250 mL trifluoroacetic acid, 1,4-bis(trifluoromethyl)benzene **1** (19 g, 88.7 mmol), and 60 mL sulfuric acid (98%). The mixture was stirred vigorously and NBS (47.4 g, 267 mmol) was added in portions at 60 °C over 5-hour period. After stirring at the temperature for 2 d, the mixture was poured into 500 mL of ice-water. The precipitates were filtered and purification by sublimation gave a white solid (30 g, 91%): m.p. 64-65 °C; ¹H NMR (300 MHz, CDCl₃): 8.01 (2H, s); ¹³C NMR (75 MHz, CDCl₃): 134.3, 123.4, 119.7, 119.3; ¹⁹F NMR (282 MHz, CDCl₃): -64.4; HR-MS (EI) calcd. for C₈H₂F₆Br₂ (M⁺): 369.8422, found: 369.8529.

2,5-bis(trifluoromethyl)terephthalic acid (3). At -78 °C, precooled tetrahydrofuran (80 mL) and compound **2** (12.5 g, 33.6 mmol) dissolved in THF (60 mL) were consecutively added to *n*-butyllithium (2.5 M solution in hexane, 30 mL, 75 mmol). A white precipitate formed instantaneously. After 30 min of vigorous stirring at -78 °C, the mixture was poured on freshly crushed dry ice. The reaction mixture was diluted with diethyl ether (150 mL) and the organic layer was extracted with 2 M NaOH (3 X 50 mL). The acid was collected as a white powder after acidification with 2 M HCl of the aqueous phase and recrystallized from hexane to give a white solid (7 g, 70%): m.p. > 230 °C; ¹H NMR (300 MHz, Acetone-*d*₆): 8.34 (2 H, s), 2.06 (2H, s); ¹³C NMR (75 MHz, Acetone-*d*₆): 165.1, 134.7, 131.8, 129.1, 124.5; ¹⁹F NMR (282 MHz, Acetone-*d*₆): -61.5; HR-MS (ESI) calcd. for C₁₀H₄F₆O₄ ([M-H]⁻): 300.99, found: 300.99.

1,4-bis(trifluoromethyl)-2,5-di(hydroxymethyl)benzene (4). Compound **3** (10 g, 33 mmol) was placed into Schlenk flask and followed by the addition of THF (150 mL). Into the resulting solution was added BH₃-THF (1 M solution in THF, 86.1 mL) dropwise at 0 °C.

After stirring at room temperature for 48 h, a mixture of diethyl ether (100 mL) and water (100 mL) was added to the reaction mixture. The organic layer was separated, washed with water (3 X 50 mL) and dried over MgSO₄. The solid was purified by column chromatography (5 : 1 hexane/ethyl acetate as eluant) to afford compound **4** as a white solid (7.1 g, 79%): m.p. 120-122 °C; ¹H NMR (300 MHz, Acetone-*d*₆): 8.14 (2H, s), 4.87 (4H, s), 2.83 (2H, s); ¹⁹F NMR (282 MHz, Acetone-*d*₆): -62.1; HR-MS (EI) calcd. for C₁₀H₈F₆O₂ (M⁺): 274.0423, found: 274.0412.

1,4-bis(trifluoromethyl)-2,5-di(bromomethyl)benzene (5). At 0 °C, PBr₃ (10.4 mL, 109 mmol) was slowly added to compound **4** (5 g, 18 mmol) dissolved in THF (125 mL). The reaction mixture was stirred for 30 min at 0 °C and then stirred for 40 h at room temperature. After the addition of water (20 mL) to quench the reaction under ice-bath, organic layer was diluted with diethyl ether (100 mL). The organic layer was washed with water (3 X 100 mL), dried over anhydrous MgSO₄, evaporated, and sublimed to give compound **5** as a white solid (4.6 g, 65%): m.p. 80-81 °C; ¹H NMR (300 MHz, CDCl₃): 7.89 (2H, s), 4.65 (4H, s); ¹³C NMR (75 MHz, CDCl₃): 137.1, 130.8, 124.9, 121.3, 27.1; ¹⁹F NMR (282 MHz, CDCl₃): -61.2; HR-MS (EI) calcd. for C₁₀H₆F₆Br₂ (M⁺): 397.8735, found: 397.8744.

2,5-bis(trifluoromethyl)-1,4-xylene-bis(triphenylphosphoniumbromide) (9). Triphenylphosphine (730 mg, 2.75 mmol) was added to compound **5** (500 mg, 1.25 mmol) dissolved in DMF (5 mL) at room temperature. The reaction mixture was stirred and heated to reflux for 24 h. After cooling to room temperature, this solution was poured into 150 mL anhydrous ethyl acetate. The precipitate was then filtered, washed with diethyl ether and dried *in vacuo* to give a white solid **9** (786 mg, 95%): m.p. > 270 °C; ¹H NMR (300 MHz, CDCl₃): 7.90(2H, s), 7.88-7.58 (30H, m), 4.81 (4H, m).

trimer (10). A solution of sodium ethoxide (30.6 mg, 0.45 mmol) dissolved in abs. ethanol (2 mL) was added dropwise to a solution of compound **9** (60 mg, 0.09 mmol) dissolved in chloroform (2 mL) with stirring at room temperature. 2,5-Bis(trifluoromethyl)benzaldehyde (43.9 mg, 0.18 mmol) was then added to the reaction mixture. After stirring at room temperature overnight, the reaction was quenched by the addition of water. The solvent was removed *in vacuo*, the residue was dissolved in dichloromethane (30 mL), and the organic layer was washed with water (3 X 20 mL), dried over MgSO₄, and concentrated *in vacuo* again. The crude product was purified by silica column chromatography (hexane as eluant) to afford compound **10** as a white solid (34 mg, 56%): m.p. 115-117 °C ¹H NMR (300 MHz, CDCl₃): 7.86 (2H, d, *J* = 8.4 Hz), 7.63 (2H, d, *J* = 7.8 Hz), 7.16 (4H, s), 7.13 (1H, d, *J* = 2.1 Hz), 7.09 (1H, d, *J* = 2.1 Hz), 7.02 (1H, d, *J* = 1.8 Hz), 6.99 (1H, d, *J* = 1.8 Hz); ¹⁹F NMR (282 MHz, CDCl₃): -61.9, -62.4, -64.5; HR-MS (EI) calcd. for C₂₈H₁₂F₁₈(M⁺):690.0646, found:690.0670; λ_{max}(abs, CHCl₃) = 313 nm, λ_{max}(emi, CHCl₃) = 393, 413 nm.

2,5-bis(perfluorobutyl)-p-xylene (11). Perfluorobutyl iodide (0.96 mL, 5.6 mmol) was added dropwise over 10 min to a stirred mixture of 2,5-diiodo-*p*-xylene (0.5 g, 1.4 mmol), copper powder (1.4 g, 22.4 mmol) in DMSO (10 mL) at 130 °C. The reaction mixture was subsequently stirred for a further 24 h at this temperature. After cooling to room temperature, it was poured into a beaker containing dichloromethane (30 mL) and water (30 mL). After filtering, the organic layer was separated, washed with water (3 X 30 mL) and dried over MgSO₄. The residue was purified by silica column chromatography (hexane as eluant) to give the product **11** as a white solid (553 mg, 73%): m.p. 39-40 °C; ¹H NMR (300 MHz, CDCl₃): 7.43 (2H, s), 2.51 (6H, t); ¹⁹F NMR (282 MHz, CDCl₃): -81.3, -107.7, -122.1, -126.2; HR-MS (EI) calcd. for C₁₆H₈F₁₈ ([M]⁺): 542.0333, found ([M]⁺): 542.0346.

2,5-bis(perfluorobutyl)-1,4-di(bromomethyl)benzene (12). A mixture of compound **11** (200 mg, 0.37 mmol), N-bromosuccinimide (138 mg, 0.78 mmol) and AIBN (2 mg, 0.01 mmol) in carbon tetrachloride (5 mL) was stirred under reflux for 24 h. The mixture was cooled to room temperature and filtered to remove salts. The filtrate was washed with CCl₄ and the solution was evaporated to give a crude product. This was purified by recrystallization from hexane to give **12** as a white solid (100 mg, 39%): m.p. 120-122 °C; ¹H NMR (300 MHz, CDCl₃): 7.82 (2H, s), 4.62 (4H, s); ¹⁹F NMR (282 MHz, CDCl₃): -81.6, -107.6, -121.9, -125.9; HR-MS (EI) calcd. for C₁₆H₆F₁₈Br₂ ([M]⁺): 697.85, found ([M]⁺): 697.87.

2-(perfluorodecyl)-p-xylene (13). Perfluorodecyl iodide (4.2 g, 6.5 mmol) was added dropwise over 10 min to a stirred mixture of 2-bromo-*p*-xylene (1 g, 5.4 mmol), copper powder (1.9 g, 29.7 mmol), DMSO (80 mL) at 130 °C. The reaction mixture was subsequently stirred for a further 2 d at this temperature. After cooling to room temperature, it was poured into a beaker containing dichloromethane (50 mL) and saturated potassium iodide solution (50 mL). After filtering, the organic layer was separated, washed with water (3 X 30 mL) and dried over MgSO₄. Recrystallization from hexane gave the product **13** as a white solid (2.7 g, 82%): ¹H NMR (300 MHz, CDCl₃): 7.31 (1H, s), 7.24 (1H, d, *J*=8.1 Hz), 7.17 (1H, d, *J*=8.1 Hz), 2.46 (3H, t, *J*=3.0 Hz), 2.39 (3H, s); ¹⁹F NMR (282 MHz, CDCl₃): -81.4, -106.7, -121.1, -121.8, -122.0, -122.9, -126.3; HR-MS (EI) calcd. for C₁₈H₉F₂₁ (M⁺): 624.0363, found: 624.0353.

2-(perfluorodecyl)-1,4-di(bromomethyl)benzene (14). A mixture of compound **13** (648 mg, 1.04 mmol), N-bromosuccinimide (406 mg, 2.28 mmol) and AIBN (5.1 mg, 0.03 mmol) in carbon tetrachloride (15 mL) was stirred under reflux for 24 h. The mixture was cooled to room temperature and filtered to remove salts. The filtrate was washed with CCl₄ and the

solution was evaporated to give a crude product. This was purified by recrystallization from hexane to give **14** as a white powder (550 mg, 68%): m.p. 96-97 °C; ¹H NMR (300 MHz, CDCl₃): 7.71 (1H, d, *J*=8.1 Hz), 7.68 (1H, s), 7.57 (1H, s), 4.61 (2H, s), 4.51 (2H, s); ¹⁹F NMR (282 MHz, CDCl₃): -81.3, -106.5, -120.8, -121.5, -121.9, -122.9, -126.3; HR-MS (EI) calcd. for C₁₈H₇F₂₁Br₂ ([M-H]⁺): 778.8495, found ([M-H]⁺): 778.8518.

2-perfluorooctyl-5-trifluoromethyl-terephthalic acid (17). At -78 °C, precooled tetrahydrofuran (20 mL) and compound **16** (3 g, 4.16 mmol) dissolved in THF (20 mL) were consecutively added to n-butyllithium (2.5 M solution in hexane, 3.66 mL, 9.14 mmol). After stirring at -78 °C for 60 min, the mixture was poured into freshly crushed dry ice. The reaction mixture was diluted with diethyl ether (100 mL) and the organic layer was extracted with 2 M NaOH (3 X 30 mL). The acid was collected as a white powder after acidification with 2 M HCl of the aqueous phase and recrystallized from hexane to give a white solid **17** (1.65 g, 61%): ¹H NMR (300 MHz, CDCl₃): 8.27 (1H, s), 8.26 (1H, s), 2.07 (2H, s); ¹⁹F NMR (282 MHz, CDCl₃): -61.5, -82.3, -106.2, -119.4, -121.5, -122.6, -123.5, -126.9.

1-perfluorooctyl-4-trifluoromethyl-2,5-di(hydroxymethyl)benzene (18). Compound **17** (294 mg, 0.45 mmol) was placed into Schlenk flask and followed by the addition of THF (5 mL). Into the resulting solution was added BH₃-THF (1 M solution in THF, 1.17 mL) dropwise at 0 °C. After stirring at room temperature for 48 h, a mixture of diethyl ether (10 mL) and water (10 mL) was added to the reaction mixture. The organic layer was separated, washed with water (3 X 10 mL) and dried over MgSO₄. The solid was purified by silica column chromatography (5 : 1 hexane/ethyl acetate as eluant) to afford compound **18** as a white solid (284 mg, 51%): m.p. 108-110 °C; ¹H NMR (300 MHz, Acetone-*d*₆): 8.26 (1H, s),

8.26 (1H, s), 4.92 (2H, s), 4.90 (2H, s), 2.86 (2H, s); ^{19}F NMR (282 MHz, Acetone- d_6): -62.6, -82.3, -106.7, -121.5, -122.2, 122.6, -123.5, -126.9.

1-perfluorooctyl-4-trifluoromethyl-2,5-dibromomethylbenzene (19). At 0 °C, PBr_3 (0.24 mL, 2.54 mmol) was slowly added to compound **14** (317 mg, 0.51 mmol) dissolved in THF (10 mL). The reaction mixture was cooled to 0 °C in an ice-water bath, and then quenched with the addition of water (2 mL). The organic layer was diluted with diethyl ether (20 mL), washed with water (3 x 10 mL), dried over anhydrous MgSO_4 , evaporated, and sublimed to give compound **19** as a white solid (240 mg, 63%): m.p. 89-90 °C; ^1H NMR (300 MHz, CDCl_3): 7.90 (1H, s), 7.79 (1H, s), 4.64 (2H, s), 4.62 (2H, s); ^{19}F NMR (282 MHz, CDCl_3): -61.3, -81.3, -107.1, -120.8, -121.5, 122.0, -122.9 -126.3; HR-MS (ESI) calcd. for $\text{C}_{17}\text{H}_6\text{F}_{20}\text{Br}_2$ ($[\text{M}-\text{H}]^-$): 746.8433, found ($[\text{M}-\text{HBr}+\text{CH}_3]^-$): 682.92.

2,5-bis(trifluoromethyl)-1,4-benzenedicarboxyaldehyde (20). At -78 °C, precooled tetrahydrofuran (10 mL) and compound **2** (2 g, 5.4 mmol) dissolved in THF (10 mL) were consecutively added to *n*-butyllithium (1.6 M solution in hexane, 7.4 mL, 11.8 mmol). A white precipitate formed instaneously. After 30 min of vigorous stirring at -78 °C, *N,N*-dimethylformamide (3 mL, 38.8 mmol) was slowly added to the reaction mixture and then stirred for 1 h at -40 °C. The dialdehyde was isolated after neutralization with 2 M HCl, ethereal extraction, and recrystallization from hexane to give a white solid **20** (539 mg, 37%): m.p. 56-57 °C; ^1H NMR (300 MHz, CDCl_3): 10.47 (2H, s), 8.55 (2H, s); ^{13}C NMR (75 MHz, CDCl_3): 186.7, 164.6, 136.9, 127.6, 119.0; ^{19}F NMR (282 MHz, CDCl_3): -56.8; HR-MS (EI) calcd. for $\text{C}_{10}\text{H}_4\text{F}_6\text{O}_2$ (M^+): 270.0110, found: 270.0111.

2-methoxy-5-(2'-ethylhexyloxy)-1,4-xylene-bis(triphenylphosphonium bromide) (22).

Triphenylphosphine (1.38 g, 5.24 mmol) was added to 1,4-bis(bromomethyl)-2((2-ethylhexyl)oxy)-5-methoxybenzene **21** (1 g, 2.38 mmol) dissolved in DMF (10 mL) at room temperature. The reaction mixture was stirred and heated to reflux for 24 h. After cooling to room temperature, this solution was poured into 300 mL ethyl acetate. The precipitate was then filtered, washed with diethyl ether and dried *in vacuo* to give a white solid **22** (1.4 g, 93%): m.p. 176-178 °C; ¹H NMR (300 MHz, CDCl₃): 7.78-7.64 (30H, m), 6.83 (1H, s), 6.72 (1H, s), 5.32 (4H, m), 2.92 (3H, s), 1.78 (2H, s), 1.21 (2H, m), 1.05 (7H, m), 0.88 (3H, t), 0.68 (3H, t).

CF3-PPV, **C4F9-PPV**, **C8F17-PPV**, and **C12F21-PPV** via Gilch polymerization: A general procedure is illustrated by the synthesis of **CF3-PPV**. The complete characterization of some of the resulting polymers (e.g.: NMR) was made impossible due to their limited solubility in organic solvents.

poly-[2,5-bis(trifluoromethyl)-p-phenylene vinylene] (CF3-PPV). Compound **5** (360 mg, 0.9 mmol) was placed in a 50 mL Schlenk flask with a stir bar. The flask was evacuated and back-filled with argon three times, followed by the addition of dry THF (15 mL). Under an atmosphere of argon, an excess of potassium *t*-butoxide (1 M solution in THF, 2.7 mL) was added to the reaction mixture and this was left to stir for 24 h at room temperature. The resulting solution was then poured into a mixture of methanol and water (10/1, 250 mL). **CF3-PPV** (150 mg, 71%) was collected by filtration as a sparingly soluble yellow-orange solid: ¹H NMR (400 MHz, THF-*d*₈): 8.5-8.3 (1H, br), 8.0-7.8 (1H, br), 5.7-5.5 (2H, br).

CF3-PPV via Sulfonium precursor route

1,1'-[2,5-bis (trifluoromethyl)-1,4-phenylene-bis(methylene)]-bis[tetrahydrothiophenium]dibromide (6). Tetrahydrothiophene (0.27 mL, 3 mmol) was added to a suspension of

compound **5** (200 mg, 0.5 mmol) in dry methanol (5 mL). The solid was dissolved to form a clear solution within 10 min. This solution was filtered via 0.45 μm membrane filter and then heated to 50 $^{\circ}\text{C}$ with stirring for 24 h. After cooling down to room temperature, the solvent was completely removed *in vacuo* and cold acetone (10 mL) was added to the residue. The precipitate was then filtered and dried to give compound **6** as a colorless, hygroscopic solid (192 mg, 67%): m.p. 128-130 $^{\circ}\text{C}$; ^1H NMR (300 MHz, D_2O): 8.17 (2H, s), 4.76 (4H, s), 3.52-3.62 (8H, m), 2.34-2.47 (8H, m); ^{19}F NMR (282 MHz, D_2O): -60.2; HR-MS (EI) calcd. for $\text{C}_{18}\text{H}_{22}\text{F}_6\text{S}_2\text{Br}_2$ (M^+): 573.94, found ($[\text{M}-\text{Br}]^+$): 495.04.

poly-[2,5-bis(trifluoromethyl)-1,4-phenylene vinylene] (7). To a deoxygenated solution of compound **6** (267 mg, 0.46 mmol) in a mixture of water (2 mL) and methanol (1 mL) cooled in an ice bath was added dropwise an ice-cold aqueous sodium hydroxide solution (1 M, 0.46 mL) over 10 min. The reaction mixture was stirred at 0 $^{\circ}\text{C}$ for 8 h under Ar and then neutralized with 0.5 M HCl (0.5 mL). The solution was then dialyzed against water over 3 days (3 X 500 mL), after which the solvent was completely removed.

CF3-PPV thin film was obtained by spin-coating the CF3-PPV precursor solution **7** on glass slide and then thermal conversion at 200 $^{\circ}\text{C}$ and 10^{-6} mbar for 5 h.

CF3-PPV via Stille polymerization

A mixture of compound **8** (30 mg, 0.06 mmol), bis(tributylstannyl)ethylene (36.4 mg, 0.06 mmol), tri(*t*-butylphosphine) (0.73 mg, 0.004 mmol), tri(dibenzylideneacetone)dipalladium (0.82 mg, 0.001 mmol), and LiCl (5.1 mg, 0.12 mmol) dissolved in NMP was stirred at 80-100 $^{\circ}\text{C}$ for 48 h. The reaction mixture was cooled to room temperature and then extracted with chloroform and water. The organic layer was evaporated and the collected precipitate was washed with methanol to give sparingly soluble polymer **CF3-PPV**.

alt-co-CF3-PPV. Into a mixture of compound **20** (10 mg, 0.037 mmol) and **22** (24.6 mg, 0.037 mmol) dissolved in chloroform (1.5 mL) was added sodium ethoxide (12.6 mg, 0.19 mmol) dissolved in ethanol (1.5 mL). The reaction mixture was stirred at room temperature overnight. The reaction was quenched with 2% HCl solution and the solution was poured into 100 mL of methanol to give orange polymer. The polymer ***alt-co-CF3-PPV*** was isolated by filtration, dried, and reprecipitated in methanol: ¹H NMR (300 MHz, CDCl₃): 8.05-7.75 (2 H, br), 7.55-7.20 (2 H, br), 6.96-6.55 (4 H, br), 3.85-3.65 (3 H, br), 1.45-0.45 (17 H, br).

ran-co-CF3-PPV (1:1). A solution of potassium *tert*-butoxide (1 M solution in THF, 0.45 mL) was added dropwise to a mixture of compound **5** (21 mg, 0.05 mmol) and compound **21** (20 mg, 0.05 mmol) in tetrahydrofuran (4.5 mL) at room temperature. After stirring at the temperature for 24 h, the resulting mixture was poured into methanol (125 mL). The precipitate was filtered out and reprecipitated from tetrahydrofuran/methanol to afford polymer ***ran-co-CF3-PPV***. ¹H NMR (300 MHz, CDCl₃): 7.6-7.5 (2H, br), 7.4-7.2 (6H, br), 3.96 (5H, br), 2.0-1.7 (2H, br), 1.7-1.4 (6H, br), 1.1-0.8 (7H, br).

Preparation of electropolymerized CF3-PPV

The solution for the electropolymerization was obtained by dissolving 0.05 g *p*-xylylenebis(triphenylphosphonium bromide) **9** in 50ml acetonitrile. A precleaned ITO (area 3.5 x 2.5 cm²) conductive glass was used as a working electrode at the cathode, and a platinum plate (area 1.0 x 1.0 cm²) was employed as a counter electrode at the anode. The two electrodes were separated by 1.5 cm. The electropolymerization reaction was carried out by a current with a fixed voltage level under ambient conditions. After the electropolymerization reaction, transparent PPV was obtained by heating the electropolymerized film under a high vacuum (10⁻⁶ mbar) oven at 220°C for 2 h.

References

- (1) Burroughes, J. H.; Bradley, D. D. C.; Brown, A. R.; Marks, R. N.; Mackay, K.; Friend, R. H.; Burns P. L.; Holmes A. B. *Nature* **1990**, *347*, 539–541.
- (2) (a) Friend, R. H.; Gymer, R. W.; Holmes, A. B.; Burroughes, J. H.; Marks, R. N.; Taliani, C.; Bradley, D. D. C.; Dos Santos, D. A.; Bredas, J. L.; Logdlund, M.; Salaneck, W. R. *Nature* **1999**, *397*, 121–128. (b) Dai, L.; Winkler, B.; Dong, L; Tong, L.; Mau, A. W. H. *Adv. Mater.* **2001**, *13*, 915–925.
- (3) Halls, J. J.; Walsh, C. A.; Greenham, N. C.; Marseglla, E. A.; Friend, R. H.; Moratti, S. C.; Holmes, A. B. *Nature* **1995**, *376*, 498–500.
- (4) (a) Li, W.; Katz, H. E.; Lovinger, A. J.; Laquindanum, J. G. *Chem. Mater.* **1999**, *11*, 458–465. (b) Horowitz, G. *Adv. Mater.* **1998**, *10*, 365–377.
- (5) (a) Tessler, N.; Denton, G. J.; Friend, R. H. *Nature* **1996**, *382*, 695–697. (b) Díaz-García, M. A.; Hide, F.; Schwartz, B. J.; Andersson, M. R.; Pei, Q.; Heeger, A. J. *Synth. Met.* **1997**, *84*, 455–462.
- (6) Kraft, A.; Grimsdale, A. C.; Holmes, A. B. *Angew. Chem. Int. Ed. Engl.* **1998**, *37*, 402–428.
- (7) Dodabalapur, A.; Torsi, L.; Katz, H. E. *Science* **1995**, *268*, 270–271.
- (8) Nelson, J. *Curr. Opin. Solid. Phys. Mater. Sci.* **2002**, *6*, 87–95.
- (9) Cardin, D. J. *Adv. Mater.* **2002**, *14*, 553–563.
- (10) Scurlock, R. D.; Wang, B.; Ogilby, P. R.; Sheats, J. R.; Clough, R. L. *J. Am. Chem. Soc.* **1995**, *117*, 10194–10202.

- (11) (a) Lux, A.; Holmes, A. B.; Cervini, R.; Davies, J. E.; Moratti, S. C.; Grüner, J.; Cacialli, F.; Friend, R. H. *Synth. Met.* **1997**, *84*, 293–294. (b) Cumpston, B. H.; Jensen, K. F. *J. Appl. Poly. Sci.* **1998**, *69*, 2451–2468.
- (12) (a) Oelkrug, D.; Tompert, A.; Gierschner, J.; Egelhaaf, H.-J.; Hanack, M.; Hohloch, M.; Steinhuber, E. *J. Phys. Chem. B* **1998**, *102*, 1902–1907. (b) Fahlman, M.; Brédas, J. L. *Synth. Met.* **1996**, *78*, 39–46.
- (13) *Organofluorine Compounds. Chemistry and Applications*; Hiyama, T. Eds; Springer Press: Heidelberg, 2000.
- (14) Albéniz, A. C.; Espinet, P.; Martín-Ruiz, B.; Milstein, D. *J. Am. Chem. Soc.* **2001**, *123*, 11504–11505.
- (15) Gilch, H. G.; Wheelwright, W. L. *J. Polym. Sci., Part A* **1966**, *4*, 1337–1349.
- (16) Wessling, R. A. *J. Polym. Sci., Polym. Symp.* **1985**, *72*, 55–66.
- (17) Wan, W. C.; Antoniadis, H.; Choong, V. E.; Razafitrimo, H.; Gao, Y.; Feld, W. A.; Hsieh, B. R. *Macromolecules* **1997**, *30*, 6567–6574.
- (18) (a) Lère-Porte, J.-P., Moreau, J. J. E., Torreilles, C. *Eur. J. Org. Chem.* **2001**, 1249–1258. (b) Dhanabalan, A.; van Dongen, J. L. J.; van Duren, J. K. J.; Janssen, H. M.; van Hal, P. A.; Janssen, R. A. J. *Macromolecules* **2001**, *34*, 2495–2501.
- (19) McDonald, R. N.; Campbell, T. W. *J. Org. Chem.* **1960**, *82*, 4669–4671.
- (20) (a) Li, L.; Counts, K. E.; Kurosawa, S.; Teja, A. S.; Collard, D. M. *Adv. Mater.* **2004**, *16*, 180–183. (b) Nguyen, T.-Q.; Doan V.; Schwartz, B. J. *J. Chem. Phys.* **1999**, *110*, 4068–4078.
- (21) Chang, W.-P.; Whang, W.-T.; Lin, P.-W. *Polymer* **1996**, *37*, 1513–1518.
- (22) Krebs, F. C.; Spanggaard, H. *J. Org. Chem.* **2002**, *67*, 7185–7192.

(23) Scherf, U.; List, E. J. W. *Adv. Mater.* **2002**, *14*, 477–487. Poly(9,9-dioctylfluorene-2,7-diyl) (PF, M_n 64,000, PDI = 2.9) was purchased from H.W. SANDS Corp.

Chapter 3:

Hyperconjugative and Inductive Perturbations in Poly(*p*-phenylene vinylenes)

Adapted from:

Kim, Y.; Zhu, Z.; Swager, T. M.
J. Am. Chem. Soc. **2004**, *126*, 452-453.

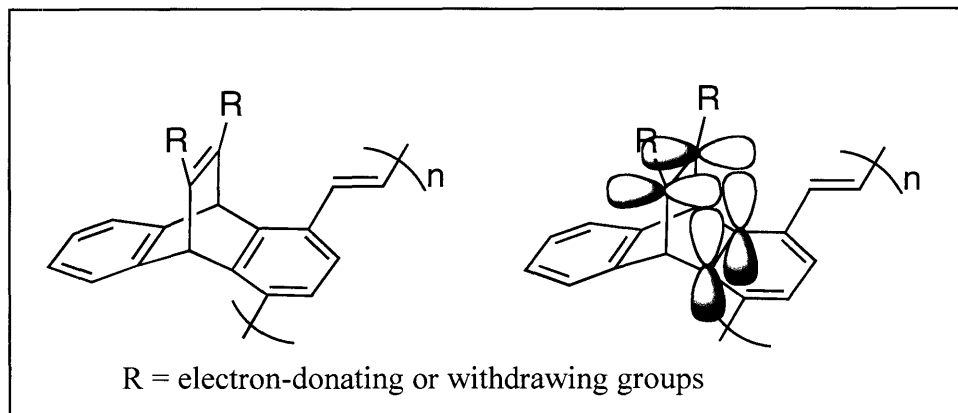
Introduction

Poly(*p*-phenylene vinylene) (PPV) and its derivatives are among the most extensively studied organic semiconductive polymers. In spite of their processability, high luminescence, and structural diversity, several challenges remain for further applications. As in many conjugated polymers (CPs), the fluorescence quantum yields of PPVs are substantially lower in the solid state due to interchain interactions.¹ Successful approaches to enhance the solid state emission efficiency of CPs include the incorporation of bulky side chains or rigid three-dimensional moieties.² Another key issue to be addressed is the tuning of the electron affinity of CPs in order to control their work functions and charge transport properties.³ Traditionally, electron donating or electron withdrawing groups connected directly to the π -system have been utilized to modify their electron affinity. Although direct attachment of such groups can produce large effects, steric repulsion of bulky substituents at the phenylene or vinylene subunits often induces deviations from planarity and decrease conjugation.⁴

We are interested in developing new generations of CPs that produce high fluorescence quantum yields and permit the fine-tuning of their electron affinity. Simultaneously, we seek architectures for the covalent attachment of the CPs to peptides, nucleic acids or antibodies for biosensor applications that avoid potentially deleterious barriers or traps⁵ in the electronic structure caused by conformational disorder. To perturb the electronic structure of CPs without interrupting conjugation by adding steric bulk in the plane of polymer backbone, we designed a new [2.2.2] bicyclic ring system that contains an electron deficient double bond that can interact with the polymer backbone in a hyperconjugative fashion (Scheme 3.1).⁶ Herein, we report novel CPs having three-dimensional structures that

display highly efficient solid-state fluorescence and demonstrate how groups with hyperconjugation and inductive interactions can be used to tune their electron affinity.

Scheme 3.1.

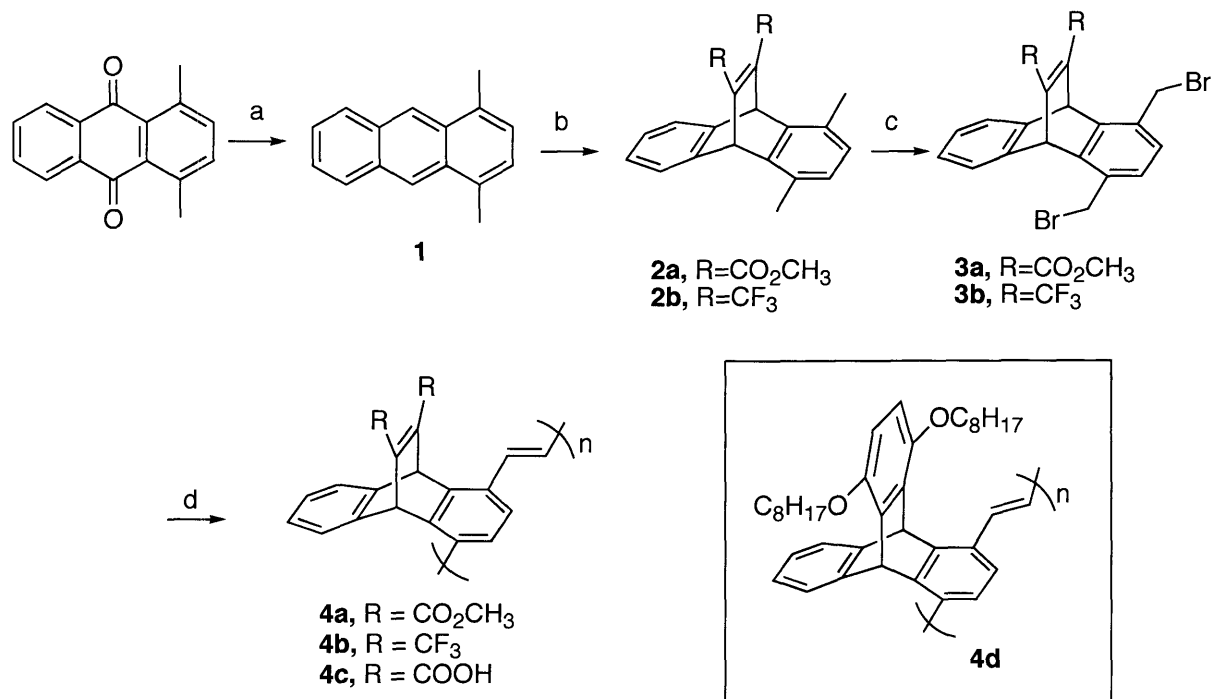


Results and Discussions

Synthesis

Compounds **3a** and **3b**, which have ester or trifluoromethyl groups appended to the alkene of the bicyclic ring system, were synthesized and then polymerized by reaction with excess KO^tBu to give polymers **4a** and **4b** (Scheme 3.2). Ester groups in polymer **4a** included both methyl and (30 %) *tert*-butyl groups, with the latter being produced by transesterification under the polymerization conditions. The triptycene polymer **4d** represents an electron-rich model polymer for the comparison with relative electron-poor polymers **4a** and **4b**.

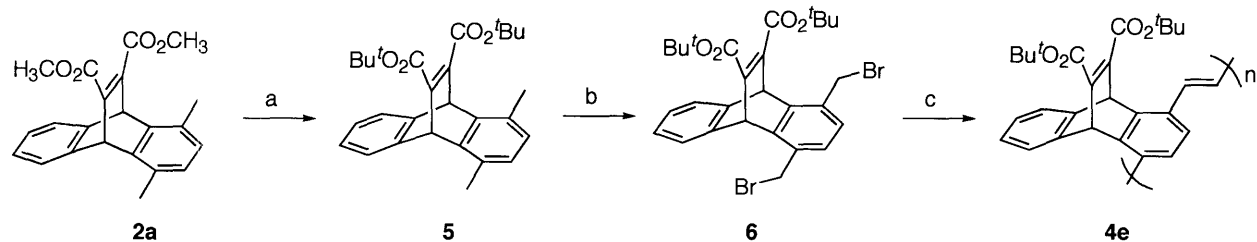
Scheme 3.2. Synthesis of monomers and polymers.^a



^a(a) NaBH₄, 2-propanol, reflux. (b) dimethylacetylenedicarboxylate or hexafluorobutyne, xylene, 140 °C. (c) NBS, AIBN, CCl₄, reflux. (d) KO^tBu, THF, RT.

To increase the solubility of methyl ester polymer **4a** and give the polymer which can be readily acid-hydrolyzed, monomer **6** with *tert*-butyl ester was synthesized by transesterification followed by bromination as shown in Scheme 3.3. A more convergent synthesis based on the Diels-Alder reaction of 1,4-dimethylantracene with di-*tert*-butylacetylene dicarboxylate was not successful. Polymer **4e** was obtained by reaction with excess KO^tBu.

Scheme 3.3. Synthesis of monomer and polymer.^a



^a(a) KO^tBu, diethyl ether, 3 h, RT. (b) NBS, AIBN, CCl₄, reflux, 24 h. (c) KO^tBu, THF, RT.

Molecular weights of the resulting polymers are summarized in Table 1. The relative number average molecular weights (M_n) were estimated by gel permeation chromatography (GPC) relative to polystyrene standards (THF solvent) and ranged from 68,000 to 790,000 g/mol with polydispersity indices (M_w/M_n) from 2.1 to 2.6.

Photophysical Studies

The absorption and emission maxima of polymers **4a** and **4b** are extremely similar (Table 3.1). The spectra of polymer **4a**, which has partial transesterification with *t*-butyloxy groups, was also similar to that of polymer **4e** with 100% *t*-butyloxy groups. This insensitivity of **4a**'s spectra confirms that the [2.2.2] system tolerates the functionalization at these positions with bulky groups without reducing conjugation length. High fluorescence quantum yields were observed for all of the polymers in THF solution and in thin films. The latter feature is attributed to the greatly reduced interchain interactions enforced by the three-dimensional frameworks.¹

Table 3.1. Summary of molecular weight and photophysical data.

| Polymer | GPC (M_n) | PDI | Abs λ_{\max} (nm) ($\log \epsilon$) | em λ_{\max} (nm) | Φ_F^a | τ (ns) |
|------------------|-------------------|-----|--|-----------------------------|------------|-------------|
| 4a (THF) | 1.2×10^5 | 2.5 | 401 (3.83) | 473, 498 | 0.58 | 1.16 |
| 4a (Film) | | | 401 | 507 | 0.42 | |
| 4b (THF) | 6.8×10^4 | 2.6 | 403 (3.48) | 471, 497 | 0.86 | 0.75 |
| 4b (Film) | | | 405 | 506 | 0.43 | |
| 4d (THF) | 7.9×10^5 | 2.1 | 413 (4.32) | 469, 499 | 0.76 | 0.62 |
| 4d (Film) | | | 414 | 477, 511 | 0.61 | |
| 4e (THF) | 1.8×10^5 | 2.4 | 401 (4.02) | 471, 499 | | |

^aFluorescence quantum yields in THF solution were determined relative to quinine sulfate ($\Phi_F = 0.53$) in 0.1 N sulfuric acid as the fluorescence standard. The quantum yields for solid-state thin films were obtained relative to 0.01 mol% 9,10-diphenylanthracene in PMMA ($\Phi_F = 0.83$) as a reference.

Hyperconjugative and inductive effects on PPVs

The effect of hyperconjugative and inductive perturbations on the sensory properties was determined by investigating fluorescence quenching responses of thin films with exposure to vapors of electron-rich (*N,N*-dimethyl *p*-toluidine (DMT)) and electron-deficient (2,4-dinitrotoluene (DNT)) aromatic compounds. All of the thin films displayed the largest quenching response (Figure 3.1) to DNT despite the fact that it has lower vapor pressure (1.47×10^{-4} mmHg) than DMT (1.78×10^{-1} mmHg). This result is likely due to the former's strong π -acid character that favors association with electron-donating π -electron systems.² As shown in Figure 3.1, the relative quenching response of **4a**, **4b** and **4d** reflects the expected hyperconjugative and inductive effects with **4b** being the most oxidizing and **4d** being the

most reducing.⁷ Hence, **4b** gives the strongest relative response to DMT and the weakest relative response to DNT. Correspondingly, **4d** displays the opposite behavior having a larger response relative to the other polymers to DNT and a weaker relative response to DMT. Polymer **4a** exhibits responses intermediate to those of **4b** and **4d**. The sensory response is also shown in picture of thin films upon the exposure to DMT or DNT vapor: the acceptor polymer film (**4b**) was quenched by aromatic amine donor and donor polymer film (**4d**) was quenched by nitro aromatic acceptor (Figure 3.2).

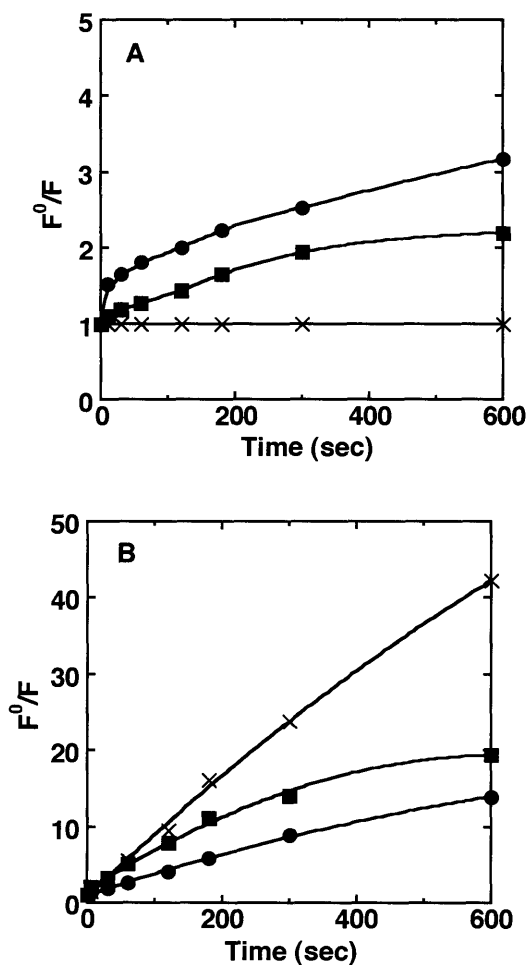


Figure 3.1. The Stern-Volmer plots of polymers **4a** (■), **4b** (●) and **4d** (X) in spin-cast films with DMT (A) and DNT (B) vapor.

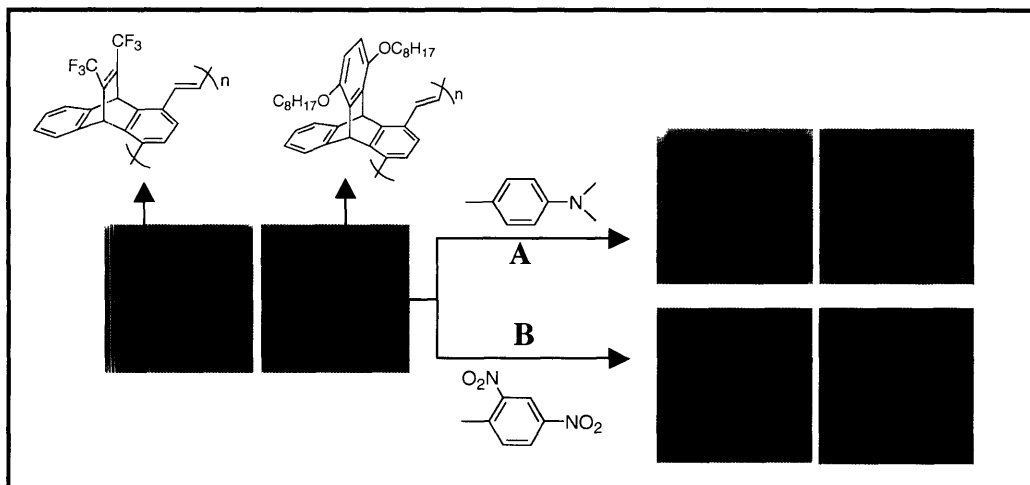


Figure 3.2. The pictures of sensory response of polymer **4b** and **4d** in thin films with DMT (**A**) and DNT (**B**) vapor.

To further investigate the quenching behavior, we conducted solution Stern-Volmer quenching studies and determined the rates of static and dynamic quenching by performing steady-state and time-resolved experiments.⁸ Static quenching, involving a preformed complex, does not reduce the excited state lifetime whereas dynamic quenching, resulting from diffusion, lowers the lifetime. The trends in the solution Stern-Volmer rate constants, summarized in Table 3.2, contrast markedly to those from our thin film studies. As expected, the electron-poor polymer **4b** exhibits the largest quenching (both static and dynamic) with DMT (Figure 3.3). However, we find that polymer **4d**, the most electron-rich polymer, has a much higher diffusive quenching rate than diester containing **4a** and shorter excited state lifetime. The deviations from thin film behaviors are even more pronounced with DNT quenching as shown in Figure 3.4. In this case **4d** exhibits the lowest static quenching (K_S) even though it has the best sensitivity in thin films. These results underscore the fact that the sensory behaviors of conjugated polymers in solution can be very different than their

responses in devices that often employ thin films. There are multiple origins for these differences including different hydrodynamic volumes for each polymer that can be influenced by the analyte, steric effects that restrict the close approach of quenchers, and the degree of amplification by energy migration. For **4d**, its lower solution sensitivity to DNT than expected is likely due to the steric bulk of alkyl side-chains and as a result it exhibits smaller static quenching than **4a** and **4b** even though it should be a better π -base.²

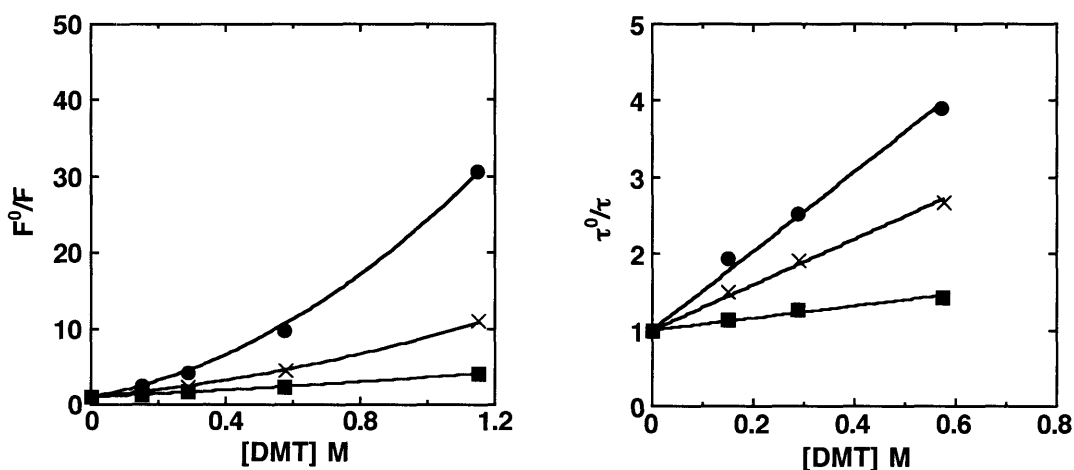


Figure 3.3. The Stern-Volmer plots (left) and the lifetime measurements (right) of polymers **4a** (■), **4b** (●) and **4d** (X) with *N,N*-dimethyl *p*-toluidine (DMT) in THF.

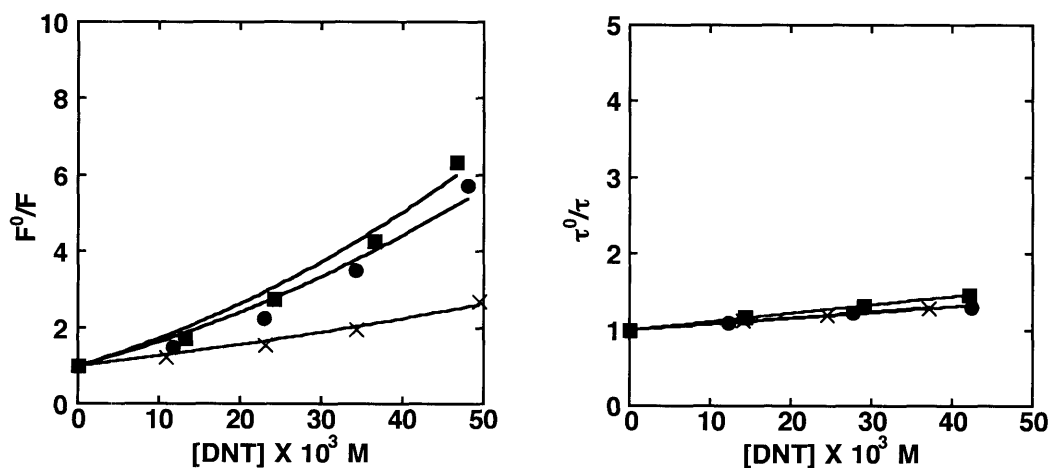


Figure 3.4. The Stern-Volmer plots (left) and the lifetime measurements (right) of polymers **4a** (■), **4b** (●) and **4d** (X) with 2,4-dinitrotoluene (DNT) in THF.

Table 3.2. The quenching constants of polymers **4a**, **4b** and **4d**.^a

| Polymer | Quencher | K_D (M ⁻¹) | K_S (M ⁻¹) | k_q (M ⁻¹ s ⁻¹) |
|-----------|------------|--------------------------|--------------------------|--|
| 4a | DMT | 0.80 | 0.92 ± 0.58 | 6.9 X 10 ⁸ |
| 4b | DMT | 5.19 | 2.49 ± 0.60 | 7.0 X 10 ⁹ |
| 4d | DMT | 2.99 | 0.94 ± 0.67 | 4.8 X 10 ⁹ |
| 4a | DNT | 11.00 | 86 ± 65 | 9.4 X 10 ⁹ |
| 4b | DNT | 7.60 | 108 ± 93 | 1.0 X 10 ¹⁰ |
| 4d | DNT | 8.00 | 25 ± 15 | 1.3 X 10 ¹⁰ |

^aSee experimental section for conditions. (K_D , K_S , and k_q : dynamic quenching, static quenching and bimolecular quenching constant, respectively)

Acid-base response

Emerging sensor applications of CPs require conjugation to biorecognition elements,⁹ and to this end we have tested the acid stability of polymers **4a**, **4b** and **4d** to conditions associated with solid-phase peptide synthesis. Polymers linked to peptides for biosensor application should be stable to acidic conditions during peptide synthesis containing the acid cleavage of protecting groups. In addition, polymer **4c**, which allows for an expeditive bioconjugation of molecules of biological relevance such as peptides, is prepared from **4a** or **4d** by treatment with aqueous acid and THF. Conjugated polymers often exhibit reactivity with strong electrophiles such as trifluoroacetic acid (TFA) as a result of the electron-donating properties of polymers. In fact, we find that electron-rich semiconductive organic polymers are in general quenched by the presence of acid, and electron-rich PPEs tend to undergo irreversible decomposition. This high acid lability of many polymers can be the limitation in

the development of biosensory applications.

However, treatment of **4b** and **4d** with TFA in CH_2Cl_2 solutions or immersion of solids in neat TFA results in no apparent reduction/modification of its emission (Figure 3.5). As shown in Figure 3.6, methylene chloride solutions of polymer **4a** (or **4e**) are quenched with the addition of TFA, however its fluorescence was immediately and completely recovered without any spectral shift after neutralization with pyridine. As a result, the fluorescence quenching of ester polymer **4a** solutions by strong acid can be interpreted in terms of the ester protonation without any degradation of polymer backbone. Polymer **4d** is completely insensitive to acid deprotection conditions typical of solid-phase peptide synthesis.

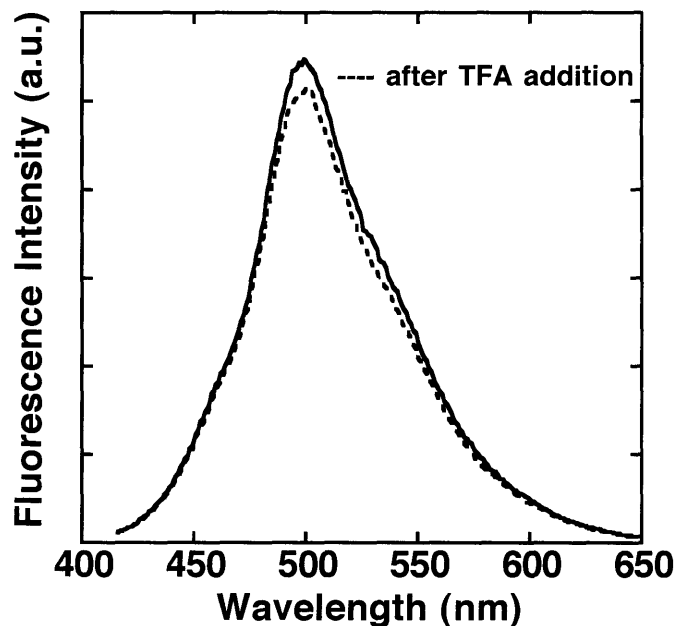


Figure 3.5. The emission spectra of polymer **4b** on the treatment with TFA.

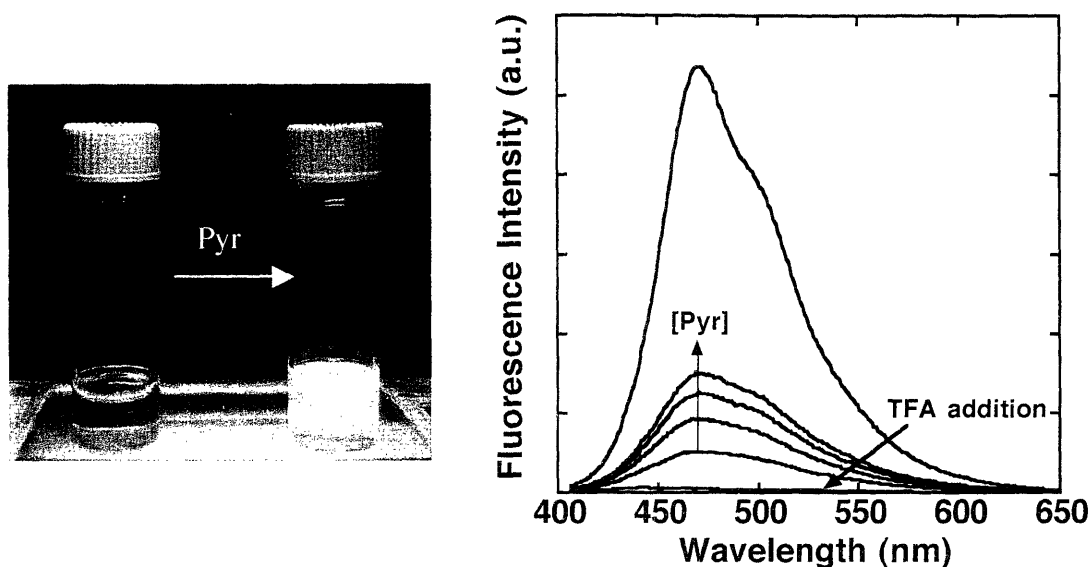


Figure 3.6. The picture (left) of polymer **4a** on the treatment with TFA and then pyridine and (right) their emission spectra change.

Non-fluorescent small polymer aggregate particles, formed by the addition of TFA to polymer **4a** in methylene chloride solution, were spotted on a TLC plate and then exposed to pyridine, triethylamine vapor or air. The small particles on the TLC plate turned to green fluorescent particles immediately when exposed to pyridine or triethylamine vapor. If simply exposed to ambient atmosphere without added base, the particle's fluorescence was not recovered.

Photobleaching studies

A second motivation for the study of hyperconjugative effects lie in the modification of polymers' band structure to prevent photodegradation by oxidation, which usually results in photobleaching. The photostability is important for the development of various optical devices that require more stable polymers. The photobleaching of polymers **4a** and **4b** in thin films was investigated and compared with that of poly[(2-methoxy-5-ethylhexyloxy)-1,4,-

phenylene vinylene] (MEH-PPV) thin film. MEH-PPV is selected as a relevant standard for its photophysical properties that have been extensively studied in the context of both fundamental studies and device applications.

Figure 3.7 compares the photobleaching of polymer thin films with the same optical density, as monitored by fluorescence spectroscopy. The photooxidation studies were performed by continuous UV irradiation of polymer thin films using a 450 W Xe lamp as the irradiation source (slit width = 10 nm) under aerobic conditions. The percent of photobleaching was calculated from the loss in fluorescence intensity at their maximum emission wavelength. As shown in Figure 3.7, in case of polymer **4b** film, 43% of emission intensity is conserved after excitation for 2 hours, whereas only 33% and 10% of fluorescence intensity remained in polymer **4a** and MEH-PPV thin films, respectively. This result also clearly reflects the expected hyperconjugative and inductive perturbations on conjugated polymer backbone as observed with sensory responses of the polymer thin films. In addition, the most electron-deficient polymer **4b** containing perfluoroalkyl groups are the most photostable against photooxidation.

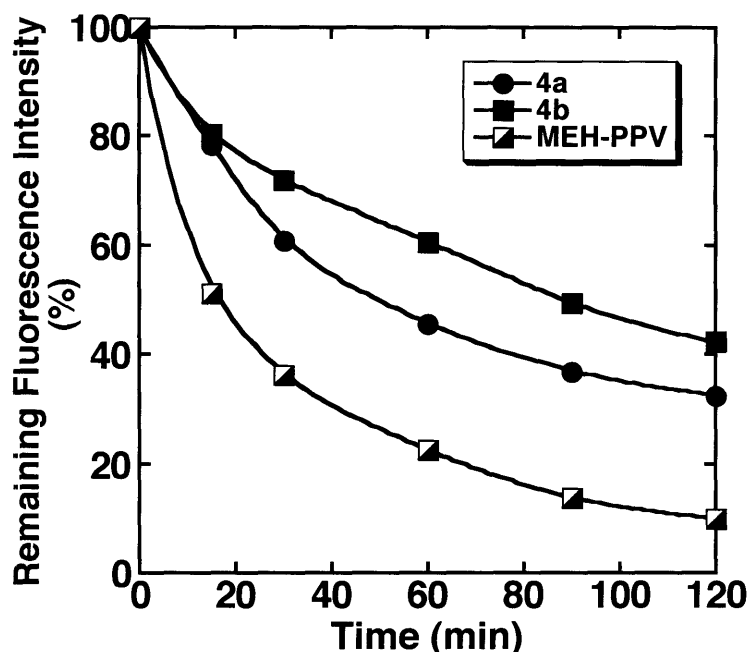


Figure 3.7. The time dependent of fluorescence intensity of polymers **4a**, **4b** and MEH-PPV thin films under UV irradiation. The polymers **4a** and **4b** were excited at 400 nm and MEH-PPV was excited at 500 nm in air.

Electrostatic layer-by-layer film assembly

Layer-by-layer (LBL) self-assembly process is powerful approach to create a well-defined polymer film which may provide new platforms for sensory materials or electronic materials.¹⁰ Electrostatic self-assembled LBL films can be successfully fabricated by sequential dipping pretreated glass substrates into cationic and anionic polymer solutions.

The carboxylate side chains in polymer **4f** provide polyanionic character for layer-by-layer deposition. As a test application, we carried out LBL deposition of this polymer onto a base-treated glass slide. The multilayer film was assembled by means of electrostatic alternating adsorption of anionic carboxylate polymer **4f**, which was prepared by base hydrolysis of polymer **4a** (LiOH/THF and H₂O) (Scheme 3.4), with poly(dimethyldiallylammonium chloride) solutions in DMF and water, respectively (Figure

3.8). Multilayer deposition was monitored using UV-visible spectroscopy by following the absorbance increase as a function of the deposition layer (Figure 3.9).

Scheme 3.4. Synthesis of anionic polymer **4f**.

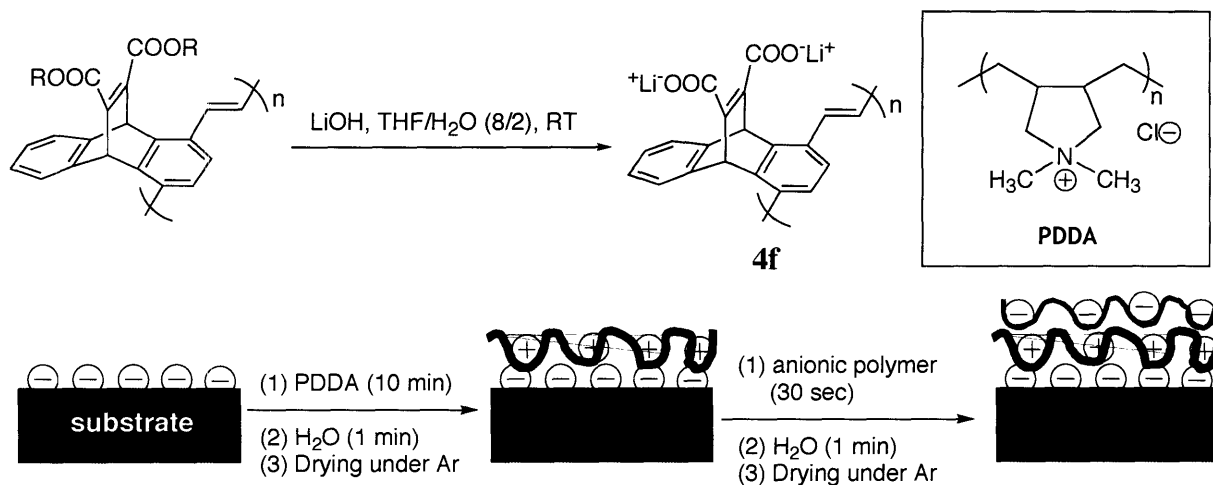


Figure 3.8. The Layer-by-Layer thin film prepared with anionic polymer **4f**.

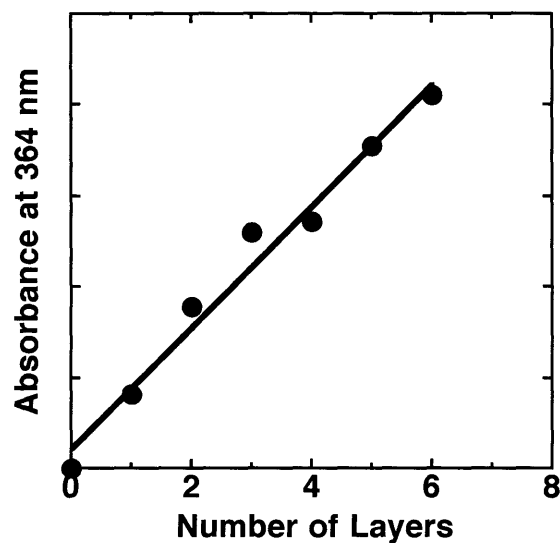


Figure 3.9. The growth of optical density of as a function of layer number deposited.

Conclusions

In summary, we have synthesized polymers bearing three-dimensional scaffolds that have novel structures and hyperconjugative/inductive electronic perturbations. The polymers show high solid-state fluorescence quantum yields and their modular design allow for the fine tuning of their electron affinity without affecting their band gap using hyperconjugative interactions. The hyperconjugative perturbations provide differential fluorescence sensory quenching responses to electron-rich and electron-deficient analytes in solution and thin films. The differences in the solution and thin film sensory responses of these polymers reveal the complexities associated with any direct comparison of quenching sensitivities. This latter point can be dramatically illustrated wherein comparisons of sensitivities of poly(phenylene ethynylene)s and polysiloles to TNT have been found to be the same order of magnitude in solution,¹¹ however thin films² of poly(phenylene ethynylene)s exhibit orders of magnitude more sensitive responses.¹²

Experimental Section

General Methods. NMR (¹H and ¹³C) spectra were recorded on Varian Mercury 300 MHz or Bruker Avance 400 MHz spectrometers. The chemical shift data for each signal are given in units of δ (ppm) relative to tetramethylsilane (TMS) where δ (TMS) = 0, and referenced to the residual solvent. High-resolution mass spectra were obtained with a Finnigan MAT 8200 system using sector double focus and an electron impact source with an ionizing voltage of 70 V. UV-vis spectra were obtained from a Cary 50 UV-Visible Spectrophotometer. Fluorescence spectra were measured with a SPEX Fluorolog- τ 3 fluorometer (model FL312,

450W xenon lamp) equipped with model 1935B polarization kit. The spectra in solution were obtained at room temperature using a quartz cuvette with a path length of 1 cm. Polymer thin film spectra were recorded by front-face (22.5°) detection. Fluorescence quantum yields of polymers in THF solution were determined relative equiabsorbing solutions of quinine sulfate ($\Phi_F = 0.53$ in 0.1 N sulfuric acid). The quantum yields for solid-state thin films were obtained relative to 0.01 mol% 9,10-diphenylanthracene in PMMA ($\Phi_F = 0.83$) as a reference. The time decay of fluorescence was determined by a phase-modulation method, using frequencies from 10 to 300 MHz. The molecular weights of polymers were determined by gel permeation chromatography PLgel column in series and a diode detector at 254 nm at a flow rate of 1.0 ml/min in THF. The molecular weights were reported relative to polystyrene standards purchased from Polysciences, Inc. Polymer thin films on a cover glass (18 x 18 mm) were spin cast on a EC101DT photoresist spinner (Headway Research, Inc.) using a spin rate of 3000 rpm from THF solution. Melting point (m.p.) determinations were performed using a Laboratory Devices MEL-TEMP instrument (open capillaries used) and were reported uncorrected.

Materials. All solvents were spectral grade unless otherwise noted. Anhydrous THF, xylene, isopropanol and carbon tetrachloride were purchased from Aldrich Chemical Co., Inc. All other compounds including analytes (Aldrich) were used as received. All air and water-sensitive synthetic manipulations were performed under an argon atmosphere using standard Schlenk techniques.

1,4-Dimethylantracene (1). To a solution of 1,4-dimethylantraquinone (1 g, 4.24 mmol) suspended in 40 mL of isopropanol was added sodium borohydride (1.6 g, 42.4 mmol) in portions over 1 h at room temperature with stirring. The reaction mixture was left to stir at

this temperature for an additional 30 min before heating to reflux overnight. The solution was then cooled to room temperature and quenched by pouring into 5% HCl solution. The mixture was left to stir for 1 hr and the solution was filtered to give a yellow solid. The solid was further recrystallized from ethanol to give **1** as a bright yellow solid (0.795 g, 92%): m.p. 70-72 °C (lit¹³. m.p. 74 °C); ¹H NMR (300 MHz, CDCl₃): 8.56 (2H, s), 8.06 (2H, dd, *J*=6.5 and 3.3 Hz), 7.50 (2H, dd, *J*=6.5 and 3.3 Hz), 7.22 (2H, s), 2.82 (6H, s); HR-MS (EI) calcd. for C₁₆H₁₄ (M⁺): 206.11, found: 206.11.

Compounds 2a and 2b. A general procedure is illustrated by the synthesis of **2a**.¹⁴

9,10-Dihydro-9,10-(1',2'-dicarbomethoxy)etheno-1,4-dimethyl anthracene (2a). To a solution of 1,4-dimethylantracene **1** (0.55 g, 2.67 mmol) in 10 mL xylene was added dimethylacetylenedicarboxylate (1.90 g, 13.34 mmol) at room temperature and stirred at 140 °C for 24 h. The mixture was allowed to cool to room temperature and the reaction solvent was removed under vacuum to give a solid. Further purification by recrystallization from a mixture of dichloromethane and methanol (1:3) gave the product **2a** as a white solid (0.84 g, 90%): m.p. 139-140 °C; ¹H NMR (300 MHz, CDCl₃): 7.38 (2H, dd, *J*=5.4 and 3.0 Hz), 7.03 (2H, dd, *J*=5.4 and 3.0 Hz), 6.75 (2H, s), 5.72 (2H, s), 3.81 (6H, s), 2.46 (6H, s); ¹³C NMR (75 MHz, CDCl₃): 166.2, 147.3, 144.0, 142.1, 130.1, 126.8, 125.6, 124.0, 52.8, 49.6, 18.7; HR-MS (EI) calcd. for C₂₂H₂₀O₄ (M⁺): 348.14, found: 348.13.

9,10-Dihydro-9,10-(1',2'-bis(trifluoromethyl))etheno-1,4-dimethyl anthracene (2b).

m.p. 155-156 °C; ¹H NMR (300 MHz, CDCl₃): 7.41 (2H, dd, *J*=5.4 and 3.0 Hz), 7.07 (2H, dd, *J*=5.4 and 3.0 Hz), 6.79 (2H, s), 5.67 (2H, s), 2.44 (6H, s); ¹³C NMR (75 MHz, CDCl₃): 167.3, 143.2, 141.3, 130.3, 127.2, 126.1, 124.1, 48.1, 18.3; HR-MS (EI) calcd. for C₂₀H₁₄F₆ (M⁺): 368.0994, found: 368.0995.

9,10-Dihydro-9,10-(1',2'-dicarbomethoxy)etheno-1,4-bis(bromomethyl) anthracene (3a).

A mixture of the methyl ester **2a** (200 mg, 0.575 mmol), N-bromosuccinimide (214 mg, 1.2 mmol) and 3 mg AIBN in 5 mL of carbon tetrachloride was stirred under reflux for 24 h. The mixture was cooled to room temperature and filtered to remove salts. The filtrate was washed with CCl₄ and the solution was evaporated to give a crude product. This was purified by column chromatography (5/1, hexane/ethyl acetate as eluant) to give **3a** as a white powder (174 mg, 60 %): m.p. 168-170 °C; ¹H NMR (300 MHz, CDCl₃): 7.53 (2H, dd, *J*=5.0 and 3.0 Hz), 7.09 (2H, dd, *J*=5.0 and 3.0 Hz), 6.98 (2H, s), 5.92 (2 H, s), 4.75 (2H, d, *J*=10.2 Hz), 4.55 (2H, d, *J*=10.2 Hz), 3.84 (6H, s); ¹³C NMR (75 MHz, CDCl₃): 166.0, 147.0, 145.0, 143.0, 133.1, 126.8, 126.3, 124.8, 53.0, 49.4, 30.4; HR-MS (EI) calcd. for C₂₂H₁₈O₄Br₂ (M⁺): 503.9566, found: 505.9524.

9,10-Dihydro-9,10-(1',2'-bis(trifluoromethyl))etheno-1,4-bis(bromomethyl)-anthracene (3b).

This compound was prepared in a similar procedure as **3a** except that benzene was used as a solvent and benzoyl peroxide as initiator. m.p. 168-170 °C; ¹H NMR (300 MHz, CDCl₃): 7.53 (2H, dd, *J*=5.1 and 3.0 Hz), 7.12 (2H, dd, *J*=5.1 and 3.0 Hz), 7.02 (2H, s), 5.87 (2H, s), 4.71 (2H, d, *J*=10.5 Hz), 4.53 (2H, d, *J*=10.5 Hz); ¹³C NMR (75 MHz, CDCl₃): 144.0, 142.2, 133.3, 127.3, 126.6, 124.9, 47.9, 29.6; HR-MS (EI) calcd. for C₂₀H₁₂F₆Br₂ (M⁺): 523.92, found: 523.92.

Polymer 4. A general procedure is illustrated by the synthesis of **4a**.

Polymer 4a. Compound **3a** (60 mg, 0.12 mmol) was placed in a 25 mL Schlenk flask with a stir bar. The flask was evacuated and back-filled with argon three times, followed by the addition of dry THF (3 mL). Under an atmosphere of argon, an excess of potassium *t*-butoxide (1 M solution in THF, 0.59 mmol) was added to the reaction solution and this was

left to stir for 2 hours at room temperature. The reaction mixture was then precipitated into a mixture of methanol and water (10:1). The polymer **4a** (30 mg, 73 %) was collected by filtration as a yellow-orange solid: $^1\text{H NMR}$ (300 MHz, CDCl_3): 8.0-7.8 (2H, br), 7.7-7.4 (4H, br), 7.2-6.9 (2H, br), 6.4-6.1 (2H, br), 1.6-1.4 (18H, br); $M_n = 123$ kDa, PDI = 2.5.

Polymer 4b. $^1\text{H NMR}$ (300 MHz, CDCl_3): 7.9-7.6 (6H, br), 7.4-7.3 (2H, br), 6.4-6.2 (2H, br); $M_n = 684$ kDa, PDI = 2.5.

Polymer 4d. $^1\text{H NMR}$ (300 MHz, CDCl_3): 7.8-6.5 (12H, br), 3.8 (4H, br), 1.5-0.86 (30H, br); $M_n = 890$ kDa, PDI = 1.7.

Acid-base response of Polymers 4a and 4b.

3 drops of trifluoroacetic acid (TFA) were added to 1 cm quartz cuvette containing polymer dissolved in CH_2Cl_2 at room temperature, and then its emission spectra were observed. In the case of polymer **4a**, the fluorescence spectra were recorded with the increase of concentration of pyridine added to the CH_2Cl_2 -TFA suspension of polymer **4a**.

Fluorescence quenching studies

Solution phase fluorescence quenching was investigated at different concentrations of *N,N*-dimethyl *p*-toluidine (DMT) and 2,4-dinitrotoluene (DNT) with constant concentrations of polymers (5.5×10^{-6} M) in THF. Additionally, the fluorescence lifetimes were determined as a function of concentration of analytes. The fluorescence quenching studies of polymer films were performed with excitation wavelengths of 400 nm with the vapors of DMT and DNT following the previous literature procedure.² The optical density of all polymer films was kept between 0.011 and 0.012. The fluorescence spectra were recorded immediately after exposing the polymer films to analytes for a specific time. The concentration used to make polymer films was 1mg per 1mL THF.

Rate constants for the quenching of fluorescence

Rate constants for the quenching of fluorescence were obtained by following a literature method.⁸ In the case of the mixture of static and dynamic quenching, the modified form of the Stern-Volmer equation, which is the second order in [Q], is applied (1). They accounts for the upward curvature observed in the Stern-Volmer plots of polymers.

$$F_0/F = (1 + K_S[Q])(1 + K_D[Q])\text{-----(1)}$$

The dynamic portion of the observed quenching was determined from the slope by lifetime measurements (2). The bimolecular quenching constant, k_q was calculated from the value of K_D (3).

$$\tau_0 / \tau = 1 + K_D[Q]\text{-----(2)}$$

$$K_D = k_q \tau_0\text{-----(3)}$$

Equation 1 can be rewritten by the multiplication of the terms in parentheses to give a plot of $(F_0/F - 1)$ versus [Q], which yields a straight line with an intercept of $K_S + K_D$ and a slope of $K_S K_D$ to give the Stern-Volmer quenching constants for static (K_S) and dynamic quenching (K_D) by 4. The average value of K_S obtained from both intercept and slope was taken for K_S .

$$(F_0/F - 1)/[Q] = (K_S + K_D) + K_S K_D [Q]\text{-----(4)}$$

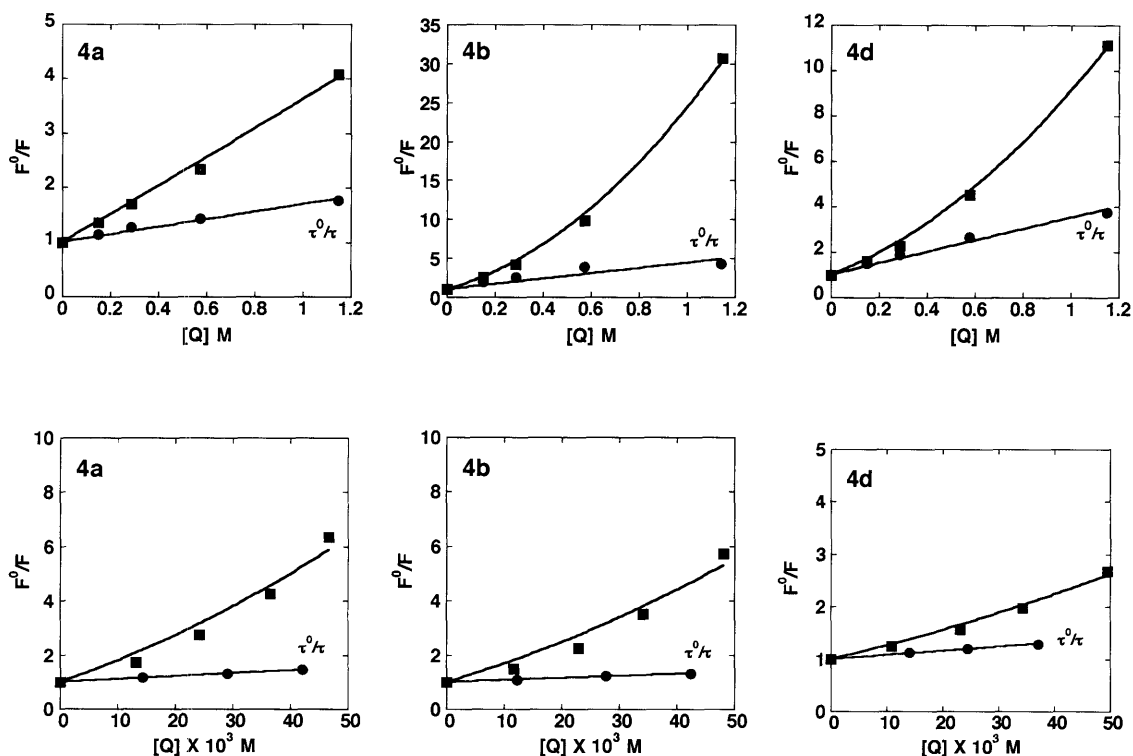


Figure 3.10. The Stern-Volmer plots of polymer **4a**, **4b** and **4d** with DMT (upper row) and DNT (lower row) in THF.

References

- (1) (a) Osaheni, J. A.; Jenekhe, S. A. *J. Am. Chem. Soc.* **1995**, *117*, 7389-7398. (b) Winnik, F. M. *Chem. Rev.* **1993**, *93*, 587-614. (c) An, B.-K.; Kwon, S.-K.; Jung, S.-D.; Park, S. Y. *J. Am. Chem. Soc.* **2002**, *124*, 14410-14415.
- (2) Yang, J.-S.; Swager, T. M. *J. Am. Chem. Soc.* **1998**, *120*, 11864-11873.
- (3) Kraft, A.; Grimsdale, A. C.; Holmes, A. B. *Angew. Chem. Int. Ed.* **1998**, *37*, 402-428.
- (4) (a) Chuah, B. S.; Cacialli, F.; dos Santos, D. A.; Feedar, N.; Davies, J. E.; Moratti, S. C.; Holmes, A. B.; Friend, R. H.; Brédas, J. L. *Synth. Met.* **1999**, *102*, 935-936 (b) Lux, A.;

Holmes, A. B.; Cervini, R.; Moratti, S. C.; Grüner, J.; Cacialli, F.; Friend, R. H. *Synth. Met.* **1997**, *84*, 293-294.

(5) We have previously found (Reference 2) that systems with lower energy traps lower the sensitivity of conjugated polymers to nitroaromatics.

(6) There are many examples of hyperconjugative interactions in [2.2.2] π -systems similar to those discussed herein: For hyperconjugative delocalized chromophores see: Yamamura, K.; Nakasuji, K.; Murata, I.; Inagaki, S. *J. Chem. Soc., Chem. Commun.* **1982**, *7*, 396-397. For hyperconjugative stereoelectronic effects see: Ohwada, T.; Okamoto, I.; Haga, N.; Shudo, K. *J. Org. Chem.* **1994**, *59*, 3975-3984.

(7) The quenching sensitivities to nitroaromatics of the polymers described herein are less than the pentyptycene-derived poly(*p*-phenylene ethynylene)s described in Reference 2.

(8) Lakowicz, J. R. *Principles of Fluorescence Spectroscopy*; Plenum Press: New York, **1986**.

(9) McQuade, D. T.; Pullen, A. E.; Swager, T. M. *Chem. Rev.* **2000**, *100*, 2537-2574.

(10) (a) Decher, G. *Science* **1997**, *277*, 1232-1237. (b) Ferreira, M.; Cheung, J. H.; Rubner, M. F. *Thin Solid Films* **1994**, *244*, 806-809.

(11) Sohn, H.; Sailor, M. J.; Magde, D. and Trogler, W. C. *J. Am. Chem. Soc.* **2003**, *125*, 3821-3830.

(12) Zahn, S.; Swager, T. M. *Angew. Chem. Int. Ed.* **2002**, *41*, 4225-4230.

(13) Traxler, J. T. *Synth. Commun.* **1977**, *7*, 161-166.

(14) Chan, T.-L.; Mak, T. C. W.; Poon, C.-D.; Wong, H. N. C.; Jia, J. H.; Wang, L. L. *Tetrahedron* **1986**, *42*, 655-661.

Chapter 4:

High Ionization Potential Conjugated Polymers

Adapted from:

Kim, Y.; Whitten, J. E.; Swager, T. M.
Submitted. 2005.

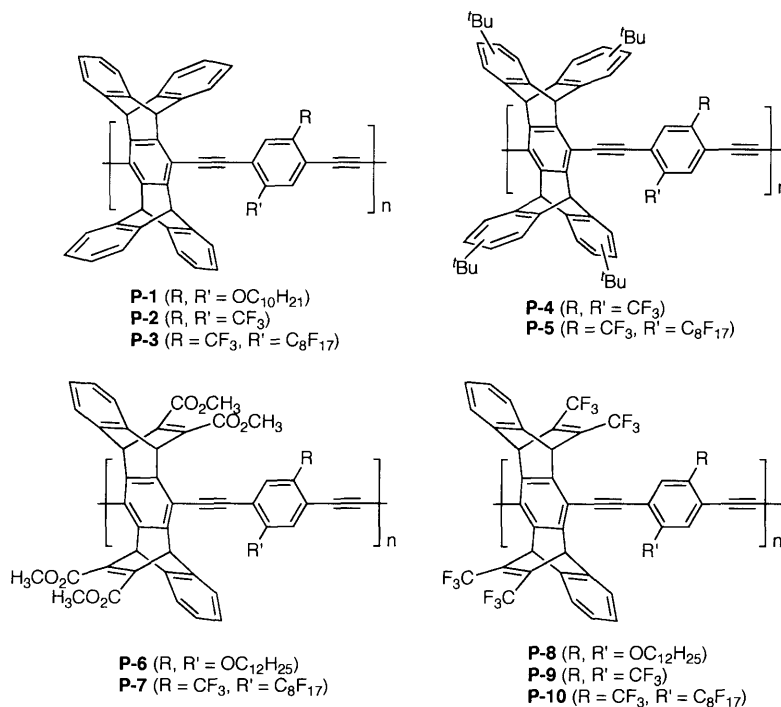
Introduction

Fluorescent conjugated polymers (CPs) have emerged as an important class of sensory materials for chemical and biochemical targets.¹ This interest has been driven by the ability of CPs to create large signal amplification relative to small molecule chemosensors due to the delocalization and rapid diffusion of excitons throughout the individual CP chains in solution² and in thin films.³ Building upon these principles, there is an ever-increasing demand for CPs with higher sensitivity and the ability to selectively target a wider scope of analytes. Receptor-coupled transduction schemes have been devised to impart selectivity to CP chemosensors,⁴ however much less work has been devoted to gaining selectivity by changing the electron-affinity of the polymers. The vast majority of luminescent CPs investigated so far has been of the low ionization potential variety (i.e., p-type materials), and the most efficient sensory transduction schemes involve electron transfer from the excited CP to an electron-acceptor.⁵ We have been engaged in developing high electron affinity CPs due to their potential to expand the range of chemosensory responses, an increasing interest in n-type materials for field effect transistors,⁶ their utility as the electron-transporting elements in polymer light emitting devices,⁷ and due to their potential to enhance photovoltaic devices.⁸

Previously, our group developed ultra-sensitive sensory materials based on pentiptycene-containing poly(*p*-phenylene ethynylene)s, which exploited fluorescence quenching upon response to vapors of electron-accepting analytes such as 2,4,6-trinitrotoluene (TNT) and 2,4-dinitrotoluene (DNT).³ The detection mechanism is fluorescence quenching through nonbonding electrostatic associations between the electron-rich polymer and the electron-poor nitroaromatic quenchers. Based upon this success, we have similarly been interested in whether a reciprocal process can be developed that is

sensitive to electron rich aromatics of biological importance such as indoles and phenols.⁹ We report in this chapter PPEs designed with [2.2.2] bicyclic ring systems incorporating electron-withdrawing perfluoroalkyl groups (Chart 1). Similar to our earlier designs,⁵ the non-compliant [2.2.2] bicyclic ring system is effective in preventing $\pi\pi$ stacking between the conjugated-polymer chains and introduces porosity of molecular dimensions that allows for rapid diffusion of analytes into and out of polymer thin films. The perfluoroalkyl groups are highly stable and powerful electron-withdrawing substituents,¹⁰ and we have produced new versatile electron-deficient CPs that are effective chemosensors for electron-rich aromatic compounds. The ionization potentials of the polymer films were determined using ultraviolet photoelectron spectroscopy (UPS), and these properties are related to their photooxidation behavior. The combined analysis provides an understanding for the design of highly emissive and high ionization potential materials for sensory functions.

Chart 1



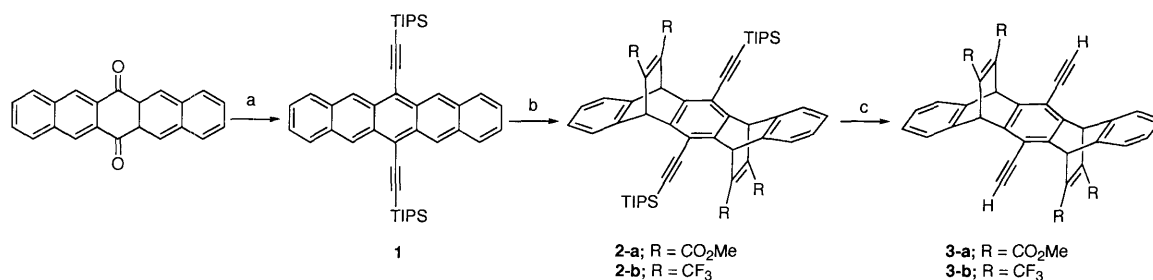
Results and Discussion

Synthesis

PPEs containing the [2.2.2] bicyclic ring systems were targeted to increase polymer solubility and solid-state quantum yields (Chart 1). Two types of structures were used: pentiptycenes based [2.2.2] bicyclic ring systems (**P-1** – **P-5**) and related [2.2.2] systems wherein one of the phenyl rings in the pentiptycene structures are replaced by an electron poor alkene (**P-6** – **P-10**). The latter groups serve to increase the polymer's electron affinity by a combination of hyperconjugative and inductive interactions.¹¹ The syntheses of pentiptycene monomers have been reported elsewhere.⁵ Scheme 4.1 summarizes an analogous synthesis leading to diacetylene monomers with electron-withdrawing [2.2.2] bicyclic ring systems, and Schemes 4.2 and 4.3 present our syntheses of the halide monomers. Monomer **3** is synthesized in Scheme 1 with an overall yield of 76%. This sequence involves a Diels-Alder reaction in xylene that assembles non-stereospecifically the [2.2.2.] bicyclic ring system, and deprotection with TBAF yields the key diethynyl monomer **3** for copolymerization with dihalide monomers by the Sonogashira-Hagihara reaction. The exact isomeric structures of monomers **3-a** and **3-b** were determined by single-crystal X-ray structures (Figure 4.1). Monomer **4** is synthesized in one step by iodination of commercially available 1,4-bis(trifluoromethyl)benzene. Monomer **6** is obtained in 79% overall yield by copper-promoted coupling reactions between perfluoroalkyl iodides and aromatic halides in DMSO followed by bromination (Scheme 4.3). The polymers shown in Chart 1 were synthesized by Pd(0)-catalyzed coupling reactions of diacetylene derivatives and diiodo or dibromo monomers having perfluoroalkyl or alkoxy substituents. Most of the polymers were completely soluble in common organic solvents such as THF, chloroform, dichloromethane

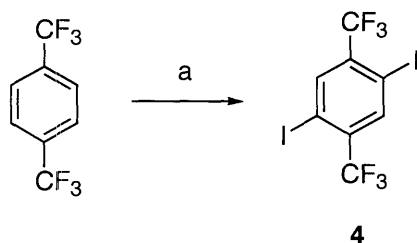
and chlorobenzene. However **P-2** and **P-9**, with (bis)trifluoromethyl groups on the phenyl ring, had limited solubility, which could be dramatically improved by the addition of bulky *t*-butyl groups on the pentiptycene moiety as **P-4**.¹² The photophysical properties and molecular weights of the resulting polymers are summarized in Table 4.1. The relative number average molecular weights (*M_n*) were estimated by gel permeation chromatography (GPC) relative to polystyrene standards (THF solvent) and ranged from 17,000 to 28,000 g/mol with polydispersity indices (*M_w/M_n*) from 1.2 to 2.9.

Scheme 4.1. Synthetic Route to Monomers **3-a** and **3-b**.^a



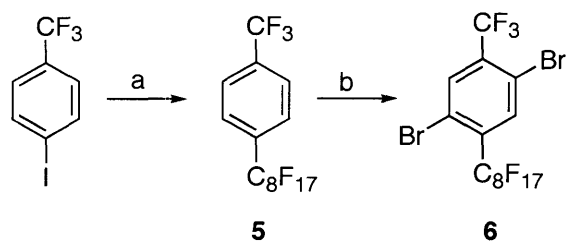
^a (a) (i) LiCCSi(isopropyl)₃, 0 °C to 25 °C (ii) SnCl₂·2H₂O, 50% acetic acid, acetone, 25 °C, 24 h, 92% (b) dimethylacetylenedicarboxylate or hexafluorobutyne, xylene, 140 °C, 48 h, 90%. (c) TBAF, THF, 25 °C, 0.5 h, 92%.

Scheme 4.2. Synthetic Route to Monomer **4**.^a



^a (a) Periodic acid, KI/H₂SO₄, 75 °C, 5 h, 65%.

Scheme 4.3. Synthetic Route to Monomer **6**.^a



^a(a) $\text{C}_8\text{F}_{17}\text{I}$, Cu, DMSO, 2,2'-bipyridine, 70 °C, 3 d, 90%. (b) $\text{H}_2\text{SO}_4/\text{TFA}$ (0.3 v/v), NBS, 60 °C, 2 d, 88%.

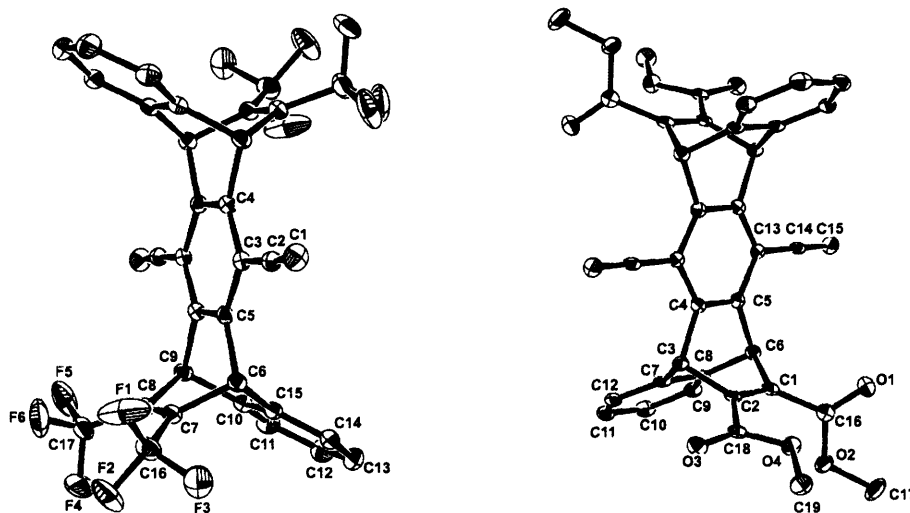


Figure 4.1. Single-crystal X-ray ORTEP structures of (left) **3-a** (50% probability) and (right) **3-b** (30% probability).

Photophysical studies.

The photophysical characteristics of the polymers were studied both in chloroform solution and in the solid state. The absorption maxima ($\lambda_{\text{max, abs}}$), the emission maxima ($\lambda_{\text{max, em}}$), the extinction coefficients at the maximum wavelengths (ϵ_{max}), fluorescence quantum yields (Φ_f in solution, and optical HOMO-LUMO energy gaps (E_g) are given in Table 4.1. The latter were measured as the threshold of the long wavelength side of the absorption peaks. The solution absorption spectra of all polymers lack fine structure, whereas the fluorescence spectra display clear vibronic peaks at room temperature. The emission maxima of the thin

films generally displayed a slight red-shift relative to those obtained in chloroform solution. However, the absorption spectra of polymers containing perfluoroalkyl groups (**P-3**, **P-4**, **P-5**, **P-8**, and **P-10**) display nearly identical maxima in solution and the solid state. The greater sensitivity of the emission maxima is likely the result of enhanced energy migration in thin films to minority polymer segments with lower band gaps and greater conjugation lengths.¹³ The π - π transitions of all of the materials are strongly allowed and give rise to large molar (per repeating unit) absorption coefficients (ϵ , Table 4.1). The extinction coefficients for the fluorinated polymers are lower than those of the non-fluorinated polymers, and this effect may be indicative of the role of oxygen in creating greater extension of the π -system and charge-transfer character.

Table 4.1. Photophysical Data of Polymers.

| Polymer | <i>M_n</i> (PDI) | <i>E_g</i> (eV) ^a | Solution | | Film | | $\epsilon_{\text{max}} / \text{M}^{-1}\text{cm}^{-1}$ (log ϵ) | Φ_{F} ^c |
|-------------|-------------------------------|--|------------------------------------|---------------------------------|------------------------------------|---------------------------------|--|--------------------------------|
| | | | $\lambda_{\text{max, abs}}$ /nm | Stokes shift/nm ^b | $\lambda_{\text{max, abs}}$ /nm | Stokes shift/nm ^b | | |
| P-1 | 64 kDa (2.54) | 2.65 ± 0.03 | 432 | 21 | 449 | 16 | 28,000 (4.45) | 0.67 |
| | | | 453, 482 | | 465, 489 | | | |
| P-3 | 18 kDa (1.71) | 2.77 ± 0.03 | 395 | 43 | 394 | 49 | 50,000 (4.70) | 0.65 |
| | | | 438, 466 | | 443, 472 | | | |
| P-4 | 22 kDa (2.91) | 2.76 ± 0.03 | 395 | 45 | 393 | 54 | 49,000 (4.69) | 0.55 |
| | | | 440, 467 | | 447, 473 | | | |
| P-5 | 18 kDa (2.15) | 2.77 ± 0.03 | 391 | 46 | 387 | 57 | 36,200 (4.56) | 0.56 |
| | | | 437, 465 | | 444, 470 | | | |
| P-6 | 21 kDa (1.82) | 2.65 ± 0.03 | 436 | 21 | 445 | 19 | 50,500 (4.70) | 0.59 |
| | | | 457, 486 | | 464, 496 | | | |
| P-7 | 17 kDa (1.96) | 2.78 ± 0.03 | 405 | 27 | 418 | 23 | 41,500 (4.62) | 0.87 |
| | | | 432, 459 | | 441, 496 | | | |
| P-8 | 28 kDa (2.00) | 2.66 ± 0.03 | 442 | 16 | 443 | 20 | 72,000 (4.86) | 0.57 |
| | | | 458, 488 | | 463, 492 | | | |
| P-10 | 18 kDa (1.24) | 2.80 ± 0.03 | 390 | 37 | 392 | 39 | 61,400 (4.79) | 0.84 |
| | | | 427, 459 | | 431, 459 | | | |

^a The optical band gap is based on the low energy onset in the UV-vis spectra.

^b The magnitude of the Stokes shift was calculated by $\Delta\lambda = \lambda_{\text{max, em}} - \lambda_{\text{max, abs}}$.

^c Fluorescence quantum yields were determined using quinine sulfate in 0.1 N sulfuric acid ($\Phi_{\text{F}} = 0.53$) as the fluorescence standard.

Figure 4.2 illustrates the absorption and emission spectra of **P-1** and **P-3** in chloroform solutions and as thin films. The spectra of **P-1** and **P-3** are respectively representative of the polymers containing alkoxy-substituted phenyl rings and the polymers containing perfluoroalkyl-substituted phenyl rings. **P-1** displays an absorption maxima at 432 nm and emission maxima at 453 nm with a low energy 0–1 peak at 482 nm, giving a vibrational splitting of $1,330\text{ cm}^{-1}$ consistent with C=C vibrations.¹⁴ The extinction coefficients (based upon the molar repeating units) are $38,000\text{ M}^{-1}\text{cm}^{-1}$ for **P-1**, $50,500\text{ M}^{-1}\text{cm}^{-1}$ for **P-6**, and $72,000\text{ M}^{-1}\text{cm}^{-1}$ for **P-8**. As revealed by the absorption and emission spectra, the replacement of alkoxy groups in **P-1** with perfluoroalkyl groups in **P-3**, leads to a 40 nm blue shift in $\lambda_{\text{max, abs}}$ to 395 nm ($\epsilon = 50,000\text{ M}^{-1}\text{cm}^{-1}$). The fluorescence spectrum of **P-3** in chloroform displays its maximum at 438 nm and a shoulder at 466 nm, indicative of vibronic fine structure (Figure 4.2). The emission of **P-3** thin film exhibits a Stokes shift of 49 nm, which is three times larger than that of **P-1**. Similarly large Stokes shifts, defined as the energy difference between the 0–0 transitions in the absorption and emission spectra, are also observed for the other fluorinated polymers relative to their alkoxy counterparts (i.e., **P-1** vs **P-3**, **P-4**, **P-5** and **P-6** vs **P-7** and **P-8** vs **P-10**). These results indicate that the perfluorinated alkyl groups, including simple trifluoromethyls, generally produce greater conformational relaxations in their excited state.

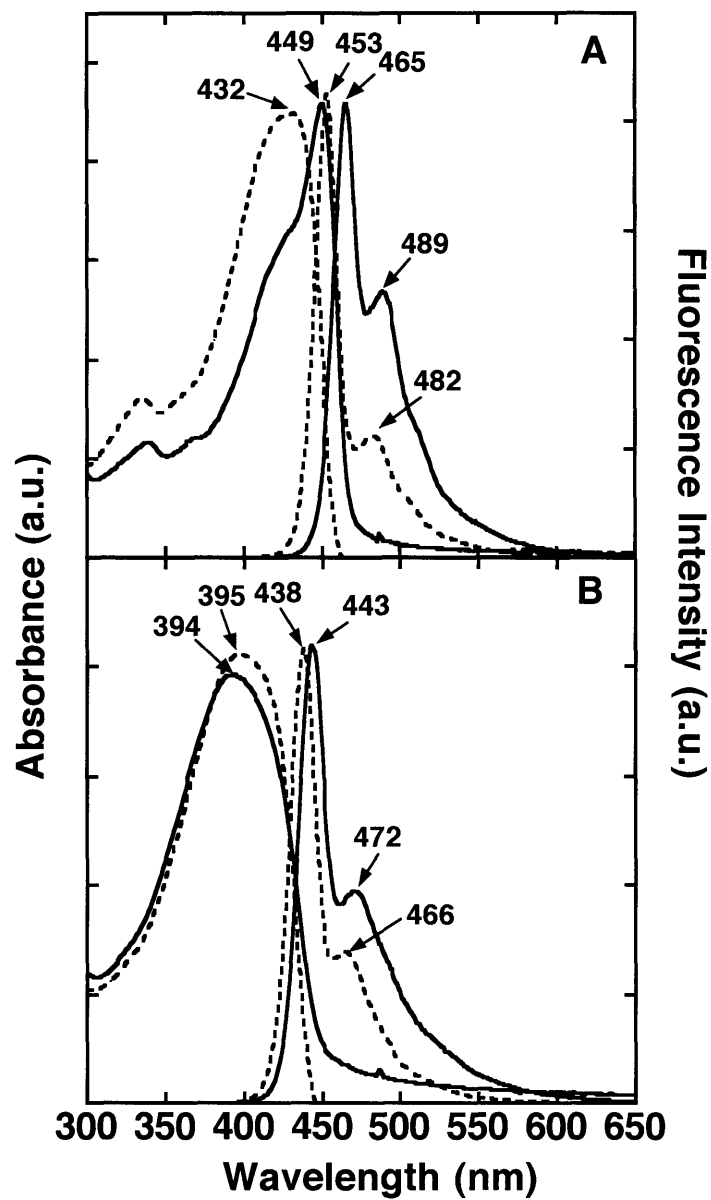


Figure 4.2. The absorption and emission spectra of (a) P-1 and (b) P-3 in chloroform (dotted line) and solid film (solid line).

The optical band gap (E_g) values were determined from the energy of the UV-vis absorption edge in solution. The band gaps of PPEs incorporating perfluoroalkyl groups were only slightly larger than for alkoxy substituted PPEs. This similarity does not parallel the larger energy increase in the absorption maximum and is a reflection of the conformational disorder of the perfluoroalkyl systems. Interestingly, the large steric bulk of *t*-butyl groups on pentiptycene moiety (**P-3** vs **P-4** and **P-5**) does not appear to cause an increase or decrease in the band gap. This result confirms that substitutions on the pendant phenyl rings do not disturb the conformation of the polymer chain. Notably, all polymers displayed high fluorescence quantum yields, and it appears that the conformational disorder and relaxations associated with the perfluoroalkyl groups do not promote non-radiative processes.

All of the polymers except **P-7** displayed similar shapes for emission curves in both solution and solid state, thereby indicating the absence of strong interchain electronic couplings. In the case of **P-7** we observed unusually strong red-shifted broad peak in emission spectra in thin films, although its emission in dilute solution was similar to the other polymers. The description of this behavior is beyond the scope of this present study, and an expanded investigation is underway on a series of related materials.¹⁵

Ionization potential determination

Ultraviolet photoelectron spectroscopy (UPS) using a He I ($h\nu = 21.22$ eV) excitation source and a concentric hemispherical electron energy analyzer was used to measure the ionization potentials of thin (ca. 100-300 Å) polymer films spin-coated on gold-covered silicon substrates. The ionization potential, or work function of the surface, was calculated by measuring the width of the UPS spectrum and subtracting it from the photon energy.¹⁶

Figure 4.3a shows UPS spectra for the **P-1**, **P-3**, and **P-10** films, which are typical of the spectra observed. Figure 4.3b shows an expansion of the low binding energy region. The secondary electron cutoffs and thresholds of the highest occupied molecular (HOMO) peaks were determined as described in literature.¹⁶ In the case of the HOMO, the threshold was taken as the intersection of lines drawn from the leading edge of the peak and the background. A summary of the results for all of the polymers is presented in Table 4.2. Because of uncertainties in determining the HOMO thresholds and sample-to-sample variations, we estimate the errors in the ionization energies to be ± 0.2 eV, as determined by multiple sample analyses. As expected, the **P-10** film has the highest ionization potential, with a value of 6.75 eV, which is 0.79 eV higher than that of **P-8** having alkoxy groups instead of perfluoroalkyl groups in the PPE backbone. The perfluoroalkyl substitution in the PPE system containing pentiptycene moiety allows for the tuning of ionization potential by as much as 0.50 eV (**P-1** vs **P-3**). The order is the following: **P-4** (5.79 eV), **P-1** (5.82 eV), **P-6** (5.94 eV), **P-8** (5.96 eV), **P-5** (5.98 eV), **P-3** (6.32 eV), **P-7** (6.40 eV), and **P-10** (6.75 eV). Based on simple electronegativity arguments, **P-1** would be expected to have the lowest ionization potential, and this is true within the error of the experiment.

Table 4.2. He I Ultraviolet Photoelectron Spectroscopy Results.

| Polymer | Cutoff (eV) ^a | HOMO Threshold (eV) ^a | Ionization Potential (eV) |
|-------------|--------------------------|----------------------------------|---------------------------|
| P-1 | 17.70 | 2.30 | 5.82 |
| P-3 | 17.08 | 2.18 | 6.32 |
| P-4 | 17.73 | 2.30 | 5.79 |
| P-5 | 17.62 | 2.38 | 5.98 |
| P-6 | 17.68 | 2.40 | 5.94 |
| P-7 | 17.39 | 2.57 | 6.40 |
| P-8 | 17.28 | 2.02 | 5.96 |
| P-10 | 16.63 | 2.16 | 6.75 |

^a The secondary electron cutoff and HOMO threshold energies are expressed relative to the spectroscopic Fermi level.

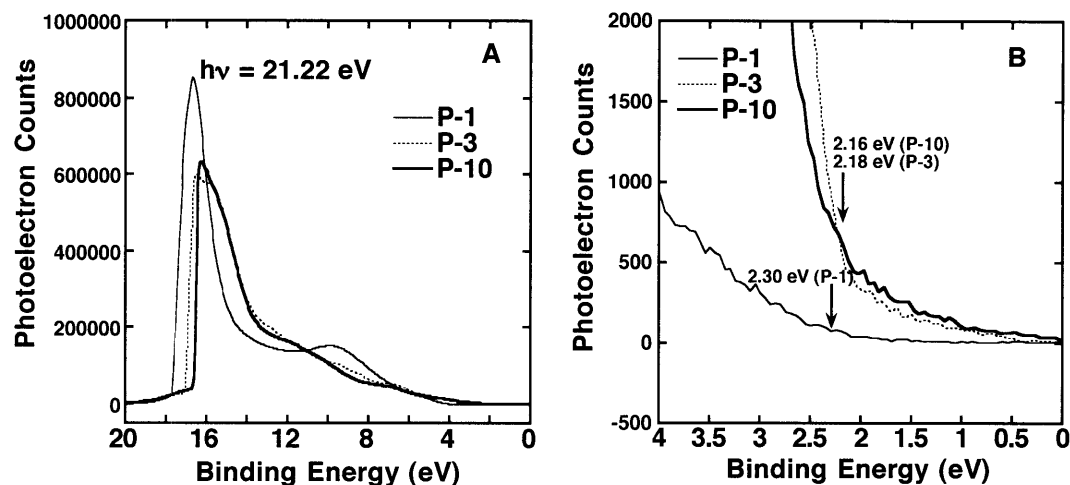


Figure 4.3. (a) He I ultraviolet photoelectron spectra of **P-1**, **P-3** and **P-10** polymer films spin-coated on gold substrates and (b) expanded graph of the HOMO threshold region. The arrows indicate the thresholds of the HOMOs. The binding energy scale is referenced to the spectroscopic Fermi level.

Photobleaching studies.

We recently reported that perfluoroalkyls could impart exceptional resistance to photobleaching upon irradiation of polymer thin films as compared to non-fluorinated polymers.¹⁷ The key feature of our system is the high ionization potential, and in accord, these materials are expected to have improved photostability. Figure 4.4 compares the photobleaching of polymer thin films with the same optical density, as monitored by fluorescence spectroscopy. The photooxidation studies were performed by continuous UV irradiation of polymer thin films using a 450 W Xe lamp as the irradiation source (slit width = 10 nm) under aerobic conditions. The percent of photobleaching was calculated from the loss in fluorescence intensity at the maximum emission wavelength. As shown in Figure 4.4, **P-1**, which displayed the lowest ionization potential, retains 50% of its fluorescence intensity after 30 min irradiation at an excitation wavelength of 380 nm, whereas 85% of the fluorescence intensity of **P-10**, the material with the highest ionization potential, remained under the same

irradiation conditions. This result demonstrates that the higher ionization potential significantly increases the materials resistance to photobleaching.

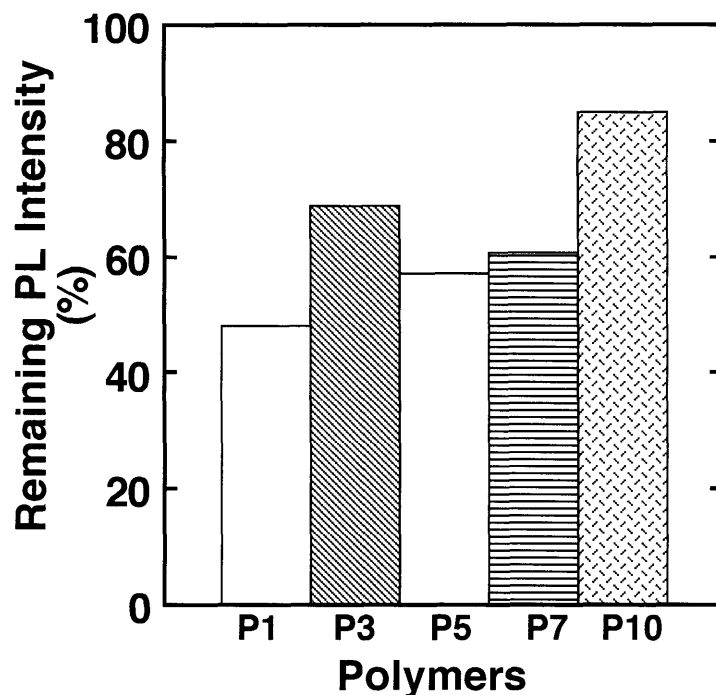


Figure 4.4. The fluorescence intensity of polymer thin films after UV irradiation for 30 min. The optical density of all of the polymer thin films was 0.1 ± 0.01 .

Steady-state and time-resolved fluorescence quenching studies in solution

The electron deficient nature of the polymers containing perfluoroalkyls directly attached to the polymer backbone phenyls and their large band gaps make them powerful excited state oxidants (electron acceptors). Hence their properties are the opposite of typical CP-based sensory materials that are excited state reductants (electron donors), and as a consequence we expect them to be insensitive to electron-accepting nitroaromatics, but highly sensitive to readily oxidized indoles and phenols. To explore their sensory potential, and also to determine to what degree their sensitivity is related to their ionization potential, we have

conducted quenching studies using steady-state and time-resolved fluorescence quenching techniques with several electron-donating molecules in solution and solid state.

We are interested in sensory responses to indole and phenols due to their biological significance as the aromatic portions of tryptophan and tyrosine, respectively.⁹ The change of fluorescence intensity of **P-10** upon titration with indole and a typical Stern-Volmer plot are shown in Figure 4.5. The quenching efficiencies of all of the polymers were determined by the Stern-Volmer quenching constants (K_{sv}) and the values ranged from 1 M⁻¹ to 26 M⁻¹ (Table 4.3). The K_{sv} value for **P-10** with indole, was 26 M⁻¹, a value 25 times larger than those of the lower ionization potential polymers **P-1** and **P-8** and twice that of **P-7**. Our fluorescence quenching studies all appear to be in accord with the polymers' ionization potentials. The greater quenching by **P-10** reflects the hyperconjugative and inductive influence of the electron-poor olefinic portion of the [2.2.2] bicyclic ring system. The quenching efficiency of **P-7** to indole was similar to that of **P-3**, and no new absorption or fluorescence peaks appeared upon addition of excess indole to chloroform solutions of the polymers. We investigated the response of **P-10**, which showed the highest sensitivity to indole, in more detail by conducting fluorescence lifetime measurements as a function of quencher concentration. Time-resolved fluorescence measurements indicated that the emission decay of **P-10** without quencher was a single-exponential with a lifetime of 0.40 ns. With increasing indole concentration, **P-10**'s lifetime was shorter, which indicates competitive dynamic quenching (Figure 4.5). The bimolecular quenching constant (k_q) calculated from the lifetime measurement was $1.4 \times 10^{10} \text{ M}^{-1}\text{s}^{-1}$, implying a highly diffusion-controlled quenching process.

Table 4.3. Stern-Volmer Quenching Constants of Polymers with Indole in THF.

| Polymers | K_{sv} (M^{-1}) |
|----------|--------------------------|
| P-1 | 0.9 |
| P-3 | 11.6 |
| P-7 | 11.8 |
| P-8 | 1.4 |
| P-10 | 25.6 |

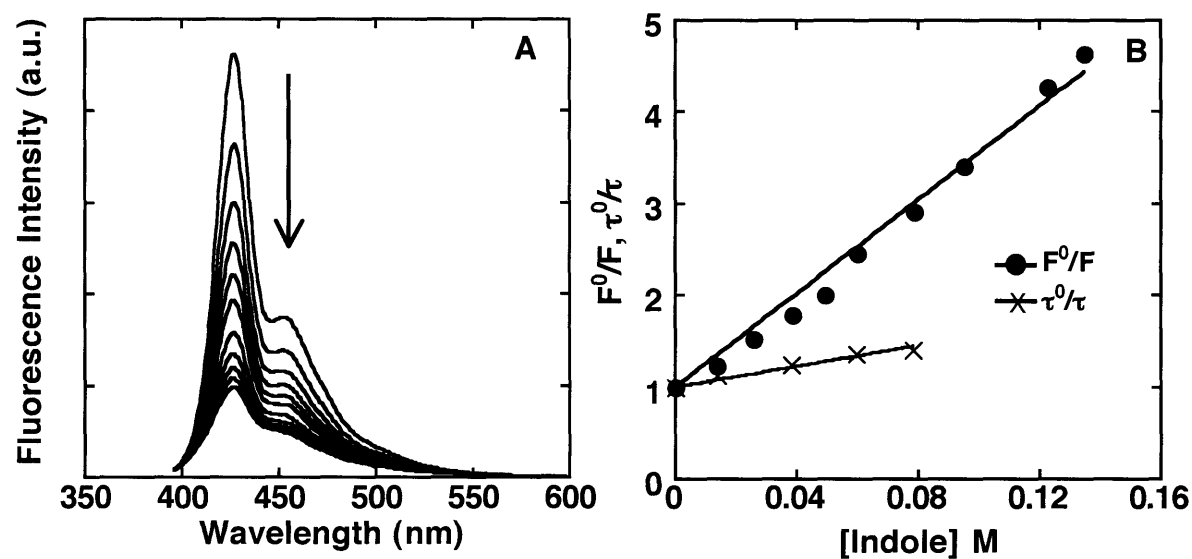


Figure 4.5. (a) The fluorescence spectra ($\lambda_{ex} = 380$ nm) of **P-10** as a function of added indole in THF: $[P-10] = 1.5 \times 10^{-6}$ M. $[Indole] = 0$ to 0.135 M (top to bottom) (b) The Stern-Volmer plot and lifetime measurements of **P-10** as a function of added indole in THF.

Fluorescence quenching study in polymer films

We have also determined the response and characteristics of the polymers in the solid state, for which they are most likely to be used in sensing applications. In these studies we found it useful to perform two types of determinations. To measure the spectroscopic properties and time dependant quenching profiles, we performed steady-state quenching experiments with polymer thin films prepared on glass substrates by spin-coating from chloroform solutions of the polymers. We measured the fluorescence intensity of polymer

thin films as a function of exposure time to indole vapor (an equilibrium vapor pressure of indole: 1.22×10^{-2} mmHg). In this scheme the indole reaches the polymer by slow diffusion, as there is no turbulence, and we can reproducibly obtain Stern-Volmer plots to determine the relative performance of our materials. We also performed measurements using a commercially available system developed for fluorescence vapor sensing.¹⁸ In these sensory systems, the polymers were coated on the inside of a glass capillary and analyte vapor was pulled through the capillary by flow of a carrier gas. The polymer was maintained at a precise temperature (40 °C) and was excited at 405 nm using a light-emitting diode. The luminescence intensity at 435 nm was monitored by a photodiode. Measurements from this sensor platform revealed the performance of the polymers under more realistic sensing conditions.

In order to investigate structural and steric effects on quenching response, the quenching efficiency of polymer thin films upon exposure to indole vapor was measured. Figure 4.6 shows Stern-Volmer plots of **P-1**, **P-3**, **P-5**, and **P-10** as a function of exposure time to indole vapor. **P-10**, with the highest ionization potential, showed the highest quenching efficiency, close to 90% fluorescence quenching after 5 min exposure, followed by **P-3** and then **P-5**. The stronger quenching of **P-3** also suggests that bulky *t*-butyl groups in **P-5** prevent efficient diffusion of indole through the cavity. Meanwhile relatively electron-rich (photo-reducing) **P-1**, which is known to display efficient sensory response for TNT,^{5(a)} exhibited a negligible response to indole vapor under the same conditions.

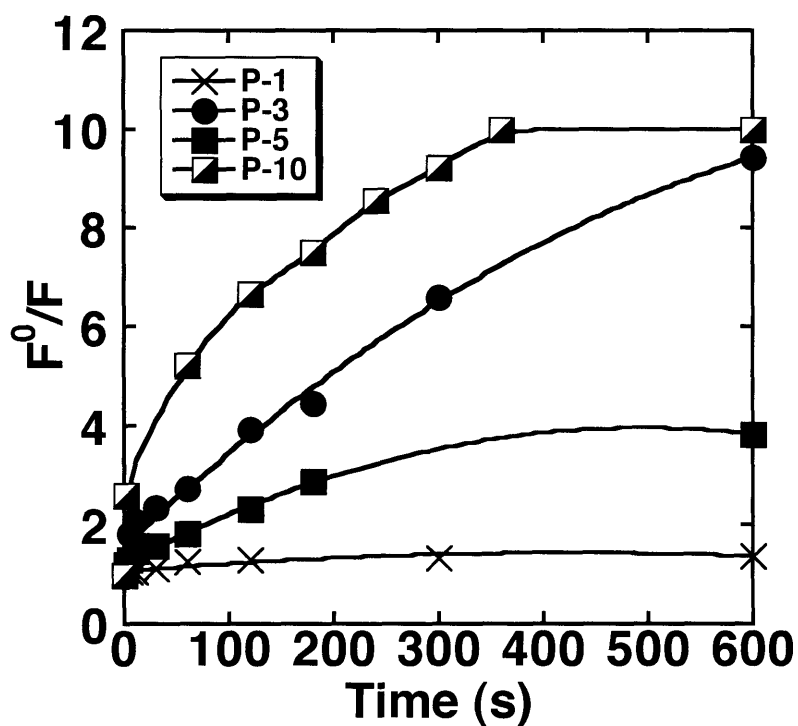


Figure 4.6. The Stern-Volmer plots of **P-1**, **P-3**, **P-5** and **P-10** in spin-cast films as function of exposure time to indole vapor.

Thin films of **P-10** displayed the most interesting responses to indole vapor and initially displayed rapid decreases in the 427 nm and 465 nm emission bands, with the appearance of an intense broad, featureless peak at 496 nm as shown in Figure 4.7 (a). The excitation or absorption spectra of **P-10** film did not show the appearance of the longer wavelength absorption band in presence or absence of analytes, which indicates that the new broad band centered at 496 nm does not originate from a ground-state charge transfer complex. We therefore attribute this long wavelength emission band to an exciplex (excited-state charge complex) between the excited state of **P-10** and indole. Interestingly, the exciplex peak is maximal upon initial exposure to indole, and continued exposure results in a reduction in the emission intensity. Hence, there is competition between energy transfer to

emissive exciplexes and electron transfer quenching. This unusual quenching behavior was further examined by exposing **P-10** film to other analyte vapors and by investigating absorption and emission spectra of **P-10** blend films with electron donating or accepting aromatic molecules.

The emission spectra of **P-10** films upon exposure to other electron-donating analytes such as dimethyl aniline (DMA), 1,4-dimethoxybenzene (DMB), and *N,N*-dimethyl *p*-toluidine (DMT) also displayed broad, red-shifted, and structureless peaks at longer wavelengths, depending on the oxidation potentials of the analytes (Figure 4.7 (b)). An exciplex peak was not observed with electron-accepting analytes such as 2,4-dinitrotoluene (DNT). **P-7**, having similar structure to that of **P-10**, also showed an exciplex peak on exposure to electron-donating analytes, but the peak is not clearly resolved in this case.¹⁵

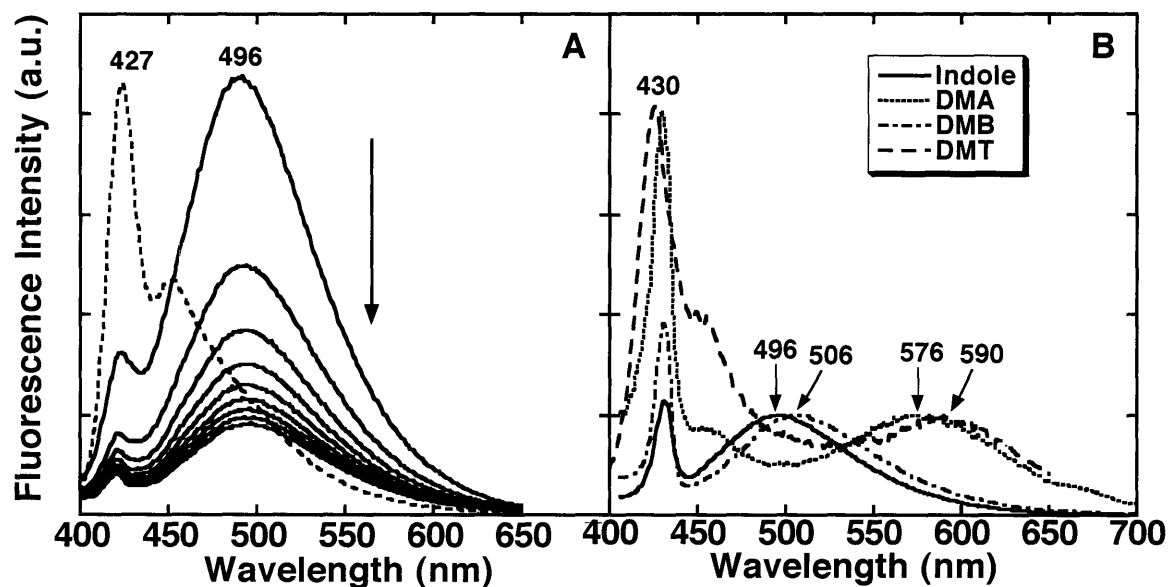


Figure 4.7. The time-dependent fluorescence spectra of (a) **P-10** film before (dotted line) and after exposure to indole vapor (solid line) at 1 s, 1, 2, 3, 4, 5, 6, 7, and 10 min (top to bottom). (b) The normalized fluorescence spectra of **P-10** films blended with indole, dimethyl aniline (DMA), 1,4-dimethoxybenzene (DMB), and *N,N*-dimethyl *p*-toluidine (DMT).

To best evaluate and contrast the relative responsiveness of **P-1** and **P-10** to indole (an electron-donating analyte) and 2,4-dinitrotoluene (DNT) (an electron-accepting analyte) we employed a commercially available system designed to detect chemical vapors.¹⁸ With this system we can readily sample vapor from the head-space of equilibrated containers to determine the relative responses of materials in a reproducible procedure. Simple inspection of the data shown in Figure 8 reveals the dramatically contrasting behaviors of **P-1** and **P-10**. Two-second exposure of indole vapor quenches (50%) the fluorescence from **P-10** (Figure 4.8b), and this material demonstrates excellent reversibility with an immediate recovery of the original fluorescence intensity upon removal of the vapor. In contrast two-second exposure of **P-10** to 2,4-DNT vapor gives no response other than that associated with thermal perturbations associated with the sampling. The usefulness of **P-10**'s sensory behavior is best demonstrated by comparison of the responses of **P-1** (Figure 4.8a), which displays ultra-sensitivity to TNT and 2,4-DNT. When subjected to two-second exposures to equilibrium vapors **P-1** exhibited 10% fluorescence quenching to vapor and 65% fluorescence quenching to 2,4-DNT. This reciprocal behavior confirms our assertions that the high ionization materials are key elements to augment the capabilities of fluorescent-based vapor sensors.

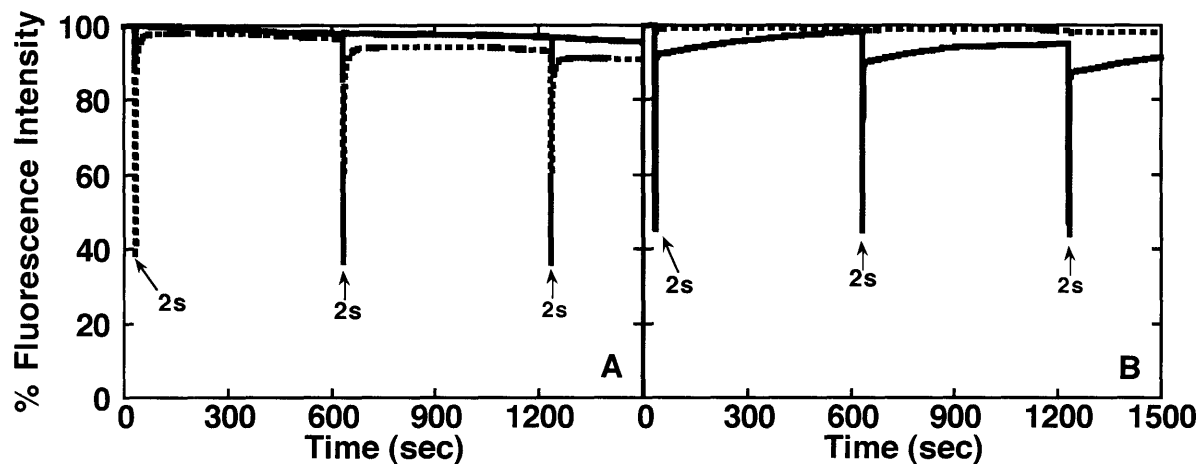


Figure 4.8. Plot of changes in fluorescence intensity of (a) **P-1** and (b) **P-10** film exposed to indole (blue solid) and 2,4-DNT (red dot) vapors for the indicated time.

Conclusion

We have synthesized new electron-deficient PPE derivatives containing perfluoroalkyl groups and determined that tuning of their ionization potentials (verified by UPS) can be used to impart dramatic selectivity changes in sensory responses. Sensing of electron-donating analytes by high ionization potential polymers was demonstrated by fluorescence quenching studies. Excited state charge-transfer complexes (exciplexes) observed for **P-7** and **P-10** films suggest prospects for new sensory schemes based upon the detection of exciplex emission.

Experimental Section

General Methods. NMR (^1H , ^{13}C , and ^{19}F) spectra were recorded on a Varian Mercury-300 MHz or Bruker Advance 400 MHz spectrometers. The ^1H and ^{13}C chemical shifts are given in units of δ (ppm) relative to tetramethylsilane (TMS) where $\delta(\text{TMS}) = 0$, and referenced to the residual solvent. ^{19}F -NMR chemical shifts are reported relative to trichlorofluoromethane as the reference. Melting point determinations were performed using a Laboratory Devices

MEL-TEMP instrument (open capillaries used) and were uncorrected. High-resolution mass spectra were obtained with a Finnigan MAT 8200 system using sector double focus and an electron impact source with an ionizing voltage of 70 V. The X-ray crystal structure was determined with a Siemens SMART/CCD diffractometer. The molecular weights of polymers were determined by using a PLgel 5 μm Mixed-C (300 x 7.5 mm) column and a diode detector at 254 nm at a flow rate of 1.0 mL/min in THF. The molecular weights are reported relative to polystyrene standards purchased from Polysciences, Inc. Polymer thin films deposited on a cover glass (18 mm x 18 mm) were prepared by spin casting using an EC101DT photo resist spinner (Headway Research, Inc.) from chloroform solutions of the polymers. The film thickness was determined for samples prepared on cover glasses using a profilometer (Veeco Dektak 6M). Samples for fluorescence quenching and photobleaching studies were prepared by spin-coating from chloroform solutions (1 mg/mL) at a rate of 3000 rpm. The same concentration was used to obtain polymer-coated glass capillaries for the Fido measurements. For these experiments, the capillary is attached to the spin-coater platform and a spin rate of 1000 rpm drives the polymer solution through the capillary. For UPS studies, solutions of 4 mg of polymer in 1 mL of chloroform were spin-coated to generate films (ca. 100-300 \AA) on gold surfaces at a spin rate of 3000 rpm.

Materials. All solvents were spectral grade unless otherwise noted. Anhydrous THF, xylene, DMSO, toluene and diisopropylamine were purchased from Aldrich Chemical Co., Inc. All other compounds were purchased from Aldrich and used as received. All air and moisture-sensitive synthetic manipulations were performed under an argon atmosphere using standard Schlenk techniques. Silica gel (40 μm) was obtained from J. T. Baker.

6,13-bis(triisopropylsilylethynyl)pentacene (1). This procedure is an adaptation of that reported by Anthony *et al.*¹⁹ Under an atmosphere of argon, 16.2 mL of *n*-butyllithium (40.5 mmol, 2.5 M solution in hexane) was added dropwise to 9.1 mL (40.5 mmol) of triisopropylsilyl acetylene in 50 mL of dry tetrahydrofuran at 0 °C. The mixture was kept at 0 °C for another 40 min before it was transferred to a solution of 6,13-pentacenequinone (5 g, 16.2 mmol) in 50 mL of dry tetrahydrofuran at 0 °C. The mixture was warmed to room temperature and stirred overnight. The reaction was quenched with 15 mL of 10% HCl and then subjected to a CHCl₃/H₂O workup. The solvent was removed and the resulting solid was collected by filtration. The crude solid was dissolved in 50 mL of acetone and then a solution of tin(II) chloride dihydrate (9.2 g, 40.5 mmol) in 50% of acetic acid (50 mL) was added dropwise. This mixture was stirred at room temperature for 24 h. The resulting blue solid product was filtered. The solid was then dissolved in hexane, washed with water and saturated sodium bicarbonate solution, and then dried over magnesium sulfate. The hexane solution is then poured onto a silica plug, which is flushed with hexane (200 mL), followed by 9:1 hexane/methylene chloride to elute a deep blue solid (9.5 g, 92%): m.p. 220-221 °C; ¹H NMR (300 MHz, CDCl₃): δ9.31 (s, 4H), 7.98 (dd, *J* = 6.6 and 3.0 Hz, 4H), 7.42 (dd, *J* = 6.6 and 3.0 Hz, 4H), 1.39 (s, 42H); HR-MS (EI) calcd. for C₄₄H₅₄Si₂ (M⁺): 638.38, found: 638.37. (lit.¹⁹ m.p. 210 °C).

6,13-bis(triisopropylsilylethynyl)-5,7,12,14-tetrahydro-5,7,12,14-(1',2'-tetra(carbomethoxy))ethenopentacene (2-a).

To a solution of **1** (1.00 g, 1.57 mmol) in 40 mL xylene in sealed vessel was added dimethylacetylenedicarboxylate (1.93 mL, 15.7 mmol) at room temperature and stirred at 140 °C for 48 h. The mixture was allowed to cool to room temperature and the reaction solvent

was removed under vacuum to give solid residues. The crude mixture was purified by silica column chromatography using 20% EtOAc in hexane as eluent to give pure mixture of two isomers (syn and anti) (1.3 g, 90%). The two isomers were separated by their solubility difference. Recrystallization using hexane gave the anti-isomer as a white solid (0.58 g, 40%). Further silica column chromatography (10% EtOAc in hexane) of the supernatant gave the syn-isomer as a white solid (0.55 g, 38%): **2-a-syn**; mp > 300 °C; ¹H NMR (300 MHz, CDCl₃): δ 7.27 (dd, *J* = 5.4 and 3.0 Hz, 4H), 6.97 (dd, *J* = 5.4 and 3.0 Hz, 4H), 5.90 (s, 4H), 3.79 (s, 12H), 1.29 (s, 42H); ¹³C NMR (75 MHz, CDCl₃): δ 165.6, 147.7, 143.6, 143.5, 125.8, 124.2, 115.5, 101.1, 99.7, 52.6, 51.2, 19.0, 11.6; HR-MS (EI) calcd. for C₅₆H₆₆O₈Si₂ (M⁺): 922.4291, found: 922.4263. **2-a-anti**; mp > 300 °C; ¹H NMR (300 MHz, CDCl₃): δ 7.33 (dd, *J* = 5.4 and 3.0 Hz, 4H), 7.04 (dd, *J* = 5.4 and 3.0 Hz, 4H), 5.89 (s, 4H), 3.73 (s, 12H), 1.29 (s, 42H); ¹³C NMR (75 MHz, CDCl₃): δ 165.5, 147.7, 143.6, 143.5, 125.9, 124.3, 115.5, 101.1, 99.7, 52.6, 51.1, 19.1, 11.6; HR-MS (EI) calcd. for C₅₆H₆₆O₈Si₂ (M⁺): 922.4291, found: 922.4263.

6,13-bis(triisopropylsilylethynyl)-5,7,12,14-tetrahydro-5,7,12,14-(1',2'-tetra(trifluoromethyl))ethenopentacene (2-b).

Hexafluoro-2-butyne (1.52 g, 9.39 mmol) was condensed in a 60 mL pressure tube by a dry ice/acetone cooling bath. A solution of **1** (2 g, 3.13 mmol) in xylene (10 mL) was slowly added through a septum. The pressure tube was then capped and heated in a 100 °C oil bath for 24 h. After being cooled to room temperature, the reaction mixture was concentrated in vacuo, and the residue was crystallized from hexane. The white crystalline material was collected by filtration and dried (1.7 g) to give **2-b-anti** as the major isomer. The mother liquor was concentrated and purified by silica column chromatography using 30% EtOAc in

hexane as eluent to give a second batch of **2-b-syn** (0.8 g). Total yield: 83%. **2-b-syn**; mp > 300 °C; ¹H NMR (300 MHz, CDCl₃): δ 7.31 (dd, *J* = 5.4 and 3.3 Hz, 4H), 7.04 (dd, *J* = 5.4 and 3.3 Hz, 4H), 5.92 (s, 4H), 1.28 (s, 42H); ¹⁹F NMR (282 MHz, CDCl₃): δ -61.7; HR-MS (EI) calcd. for C₅₂H₅₄F₁₂Si₂ (M⁺): 962.3571, found: 962.3421. **2-b-anti**; mp > 300 °C; ¹H NMR (300 MHz, CDCl₃): δ 7.41 (dd, *J* = 5.4 and 3.3 Hz, 4H), 7.14 (dd, *J* = 5.4 and 3.3 Hz, 4H), 5.92 (s, 4H), 1.28 (s, 42H); ¹⁹F NMR (282 MHz, CDCl₃): δ -61.8; HR-MS (EI) calcd. for C₅₂H₅₄F₁₂Si₂ (M⁺): 962.3571, found: 962.3421.

Compound 3-a. Tetrabutylammonium fluoride (1 M in THF; 0.015 mL, 0.146 mmol) was added to a stirred solution of **2-a-anti** (45 mg, 0.049 mmol) in THF (3 mL) at room temperature. The mixture was allowed to stir for 30 min at this temperature. The reaction mixture was concentrated in vacuo and the residue was passed through a short plug of silica. The crude product was crystallized from hexane and dichloromethane (10 : 1) to give **3-a-anti** as a white solid (27.5 mg, 92%): **3-a-anti**; mp > 300 °C; ¹H NMR (300 MHz, CDCl₃): δ 7.42 (dd, *J* = 5.4 and 3.3 Hz, 4H), 7.05 (dd, *J* = 5.4 and 3.3 Hz, 4H), 5.89 (s, 4H), 3.75 (s, 12H), 3.67 (s, 2H); ¹³C NMR (75 MHz, CDCl₃): δ 165.8, 147.2, 144.1, 143.4, 126.0, 124.4, 114.7, 85.7, 77.8, 52.7, 50.9; HR-MS (ESI) calcd. for C₃₈H₂₆O₈ ([M+Na]⁺): 633.1520, found: 633.1520.

3-a-syn was prepared by using **2-a-syn** in a similar procedure as **3-a-anti**. **3-a-syn**; mp > 300 °C; ¹H NMR (300 MHz, CDCl₃): δ 7.37 (dd, *J* = 5.4 and 3.0 Hz, 4H), 6.99 (dd, *J* = 5.4 and 3.0 Hz, 4H), 5.89 (s, 4H), 3.81 (s, 12H), 3.67 (s, 2H); ¹³C NMR (75 MHz, CDCl₃): δ 165.8, 147.2, 144.1, 143.4, 125.9, 124.4, 114.7, 85.7, 77.8, 52.8, 50.9; HR-MS (ESI) calcd. for C₃₈H₂₆O₈ ([M+Na]⁺): 633.1520, found: 633.1513.

Compound 3-b. Tetrabutylammonium fluoride (1 M in THF; 1.56 mL, 1.56 mmol) was added to a stirred mixture of both isomers of **2-b** (500 mg, 0.52 mmol) in THF (20 mL) at room temperature. The mixture was allowed to stir for 30 min at this temperature. The reaction mixture was concentrated in vacuo and the residue was passed through a short plug of silica. The crude product was concentrated and purified by silica column chromatography (10% EtOAc in hexane) to give **3-b** as a white solid mixture of two isomers (283 mg, 84%): **3-b-anti**; mp > 300 °C; ¹H NMR (300 MHz, CDCl₃): δ 7.50 (dd, *J* = 5.4 and 3.3 Hz, 4H), 7.15 (dd, *J* = 5.4 and 3.3 Hz, 4H), 5.89 (s, 4H), 3.76 (s, 2H); ¹⁹F NMR (282 MHz, CDCl₃): δ -61.9; HR-MS (EI) calcd. for C₃₄H₁₄F₁₂ (M⁺): 650.09, found: 650.09. **3-b-syn**; mp > 300 °C; ¹H NMR (300 MHz, CDCl₃): δ 7.41 (dd, *J* = 5.4 and 3.3 Hz, 4H), 7.06 (dd, *J* = 5.4 and 3.3 Hz, 4H), 5.89 (s, 4H), 3.76 (s, 2H); ¹⁹F NMR (282 MHz, CDCl₃): δ -61.7; HR-MS (MALDI) calcd. for C₃₄H₁₄F₁₂ ([M+H]⁺): 651.0977, found: 651.1009.

2,5-diiodo-1,4-bis(trifluoromethyl)benzene (4). To a solution of 30 mL H₂SO₄ was added periodic acid (3.18 g, 14 mmol) and potassium iodide (6.90 g, 42 mmol) at 0 °C and then 1,4-bis(trifluoromethyl)benzene (2.17 mL, 14 mmol) was added. The reaction mixture was then stirred at 75 °C for 5 h. After cooling to room temperature, the resulting solution was poured into ice-water and then extracted with diethyl ether (100 mL) and 10% sodium thiosulfate (50 mL). The organic layer was washed with 10% sodium thiosulfate (3 x 50 mL), dried over MgSO₄, filtered, and concentrated. The residue was recrystallized from hexane to give **4** as a white solid (4.24 g, 65%): m.p. 118-119 °C; ¹H NMR (300 MHz, CDCl₃): δ 8.20 (s, 2H); ¹⁹F NMR (282 MHz, CDCl₃): δ -64.2; HR-MS (EI) calcd. for C₈H₂F₆I₂ (M⁺): 465.8145, found: 465.8159.

4-(perfluorooctyl)- α,α,α -trifluorotoluene (5). A $C_8F_{17}I$ (12 g, 22 mmol) was added dropwise over 10 min to a stirred mixture of 4-iodobenzotrifluoride (3 g, 11 mmol), copper powder (5.6 g, 88 mmol), 2,2'-bipyridine (120 mg, 0.8 mmol), DMSO (30 mL) at 70 °C. The reaction mixture was subsequently stirred for a further 72 h at this temperature. After cooling to room temperature, the mixture was poured into a beaker containing ether (100 mL) and water (100 mL). After filtering, the organic layer was separated, washed with water (3 x 50 mL) and dried over $MgSO_4$. Sublimation under vacuum gave the product **5** as a white solid (5.6 g, 90%): m.p. 48-50 °C; 1H NMR (300 MHz, $CDCl_3$): δ 7.77 (dd, $J=8.1$ and 8.4 Hz, 4H); ^{19}F NMR (282 MHz, $CDCl_3$): δ -64.0, -81.4, -111.6, -121.4, -122.0, -122.1, -122, 9, -126, 3; HR-MS (EI) calcd. for $C_{15}H_4F_{20}$ (M^+): 563.9988, found (M^+): 563.9996.

1-perfluorooctyl-4-trifluoromethyl-2,5-dibromobenzene (6). Into a 500 mL round-bottom flask were placed 120 mL trifluoroacetic acid, compound **5** (12 g, 21.3 mmol), and 36 mL sulfuric acid (98%). The mixture was stirred vigorously and NBS (11.4 g, 63.8 mmol) was added in portions at 60 °C over 5-hour period. After stirring at 60 °C for 2 d, the mixture was poured into 200 mL of ice-water. The precipitates were filtered and sublimed to give a white solid **6** (13.5 g, 88%): m.p. 53-54 °C; 1H NMR (300 MHz, $CDCl_3$): δ 8.04 (s, 1H), 7.92 (s, 1H); ^{19}F NMR (282 MHz, $CDCl_3$): δ -64.2, -81.3, -108.0, -119.8, -121.9, -122.3, -123.2, -126.6; HR-MS (EI) calcd. for $C_{15}H_2F_{20}Br_2$ (M^+): 719.8198, found (M^+): 719.8221.

Polymers 1-10. A general procedure is illustrated by the synthesis of polymer **10**. Compound **3-b** (27.8 mg, 0.043 mmol), compound **6** (30 mg, 0.042 mmol), CuI (0.47 mg, 0.003 mmol), and $Pd(PPh_3)_4$ (4.8 mg, 0.0042 mmol) were placed in a 25 ml Schlenk tube with a stir bar. The flask was evacuated and back-filled with argon three times, followed by the addition of degassed diisopropylamine/toluene (1:2, 4.5 mL) under an atmosphere of argon.

This mixture was heated at 70 °C for 3 days and then subjected to a CHCl₃/H₂O workup. The combined organic phase was washed with 10% NH₄Cl and then dried (MgSO₄). The solvent was removed in vacuo, and the residue dissolved in chloroform was reprecipitated in methanol. The resulting precipitate was filtered and washed with MeOH and acetone to give a yellow solid (35 mg, 69%). Removal of oligomer and impurities was achieved by subjecting the solid to sequential extractions in Soxhlet apparatus with MeOH, acetone, followed with chloroform. The chloroform fraction was characterized. **P-3** (69%): ¹H NMR (400 MHz, CDCl₃): 8.6-8.5 (br, 1H), 8.4-8.3 (br, 1H), 7.6-7.4 (br, 8H), 7.2-7.0 (br, 8H), 6.1-6.0 (br, 2H), 5.9-5.8 (br, 2H). **P-4** (82%): ¹H NMR (300 MHz, CDCl₃): δ 8.5-8.4 (br, 2H), 7.6-7.4 (br, 8H), 7.2-7.0 (br, 4H), 6.1-5.9 (br, 4H), 1.4-1.2 (br, 36H). **P-5** (%): ¹H NMR (400 MHz, CDCl₃): δ 8.5-8.3 (br, 2H), 7.6-7.3 (br, 8H), 7.2-7.0 (br, 4H), 6.1-5.7 (br, 4H), 1.4-1.2 (br, 36H). **P-6** (71%): ¹H NMR (300 MHz, CDCl₃): δ 7.6-7.5 (br, 4H), 7.4-7.3 (br, 2H), 7.2-7.0 (br, 4H), 6.2-6.1 (br, 4H), 4.4-4.3 (br, 4H), 3.8-3.7 (br, 12H), 2.2-2.0 (br, 4H), 1.7-1.5 (br, 8H), 1.4-1.2 (br, 28H), 0.9-0.8 (br, 6H). **P-7** (65%): ¹H NMR (300 MHz, CDCl₃): δ 8.5-8.4 (br, 1H), 8.3-8.2 (br, 1H), 7.6-7.4 (br, 4H), 7.2-7.0 (br, 4H), 6.2-5.9 (br, 4H), 3.9-3.6 (br, 12H). **P-8** (74%): ¹H NMR (300 MHz, CDCl₃): δ 7.7-7.6 (br, 4H), 7.6-7.4 (br, 2H), 7.2-7.0 (br, 4H), 6.2-6.0 (br, 4H), 4.4-4.2 (br, 4H), 2.2-2.0 (br, 4H), 1.7-1.5 (br, 4H), 1.5-1.4 (br, 4H), 1.4-1.2 (br, 28H), 0.9-0.8 (br, 6H). **P-10** (69%): ¹H NMR (300 MHz, THF-*d*₈): δ 8.6-8.5 (br, 1H), 8.5-8.4 (br, 1H), 7.7-7.5 (br, 4H), 7.3-7.0 (br, 4H), 6.2-6.0 (br, 4H).

Photophysical methods. UV-vis spectra were obtained from Hewlett-Packard 8452A diode array or Cary 50 UV-Visible spectrophotometers. Fluorescence studies were conducted with a SPEX Fluorolog-τ2 fluorometer (model FL112, 450 W xenon lamp) equipped with a model 1935B polarization kit. The spectra in solution were obtained at 25 °C using a quartz cuvette

with a path length of 1 cm. Polymer thin film spectra were recorded by front-face (22.5°) detection. Fluorescence quantum yields of polymers in CHCl_3 solution were determined relative to equiabsorbing solutions of quinine sulfate ($\Phi_F = 0.53$ in 0.1 N sulfuric acid). The solid state quantum yields were obtained relative to 10^{-3} M 9,10-diphenylanthracene in poly(methyl methacrylate) (PMMA) ($\Phi_F = 0.83$) as a reference. The time decay of fluorescence was determined by a phase-modulation method, using frequencies from 10 to 300 MHz.

Fluorescence Quenching Studies. Fluorescence quenching and absorption experiments in solution were carried out by micro-titration in a fluorescence cuvette. In a typical titration quenching experiment, 2.5 mL of polymer solution was placed in a 1 cm quartz fluorescence cell. The UV-visible absorption and fluorescence spectra were recorded at room temperature. Then absorption and fluorescence spectra were repeatedly acquired after the addition of microliter aliquots of a polymer solution that contained the quencher. The fluorescence quenching studies of polymer films were performed following the literature procedure.¹¹ The fluorescence spectra were recorded immediately after exposing the polymer films to the vapor of analyte for a specific period of time at excitation wavelength of 380 nm. The equilibrium vapor pressures of the analyte are assumed to be similar to the documented values.²⁰

Photoelectron Spectroscopy. The samples for ultraviolet photoelectron spectroscopy (UPS) measurements were prepared by spin-coating polymer solutions in chloroform (4 mg/1mL) onto gold substrates at a rate of 3000 rpm for 60 s. The gold substrates were prepared by thermally depositing approximately 2000 Å of gold on ca. 1 cm² x 1 cm² pieces of Si(111) wafers. The polymer-coated gold substrates were attached to metal sample stubs using vacuum-compatible silver paint, and this was also used to electrically connect the edges of the

samples to the sample stubs. The UPS experiments were performed in a VG ESCALAB MKII photoelectron spectrometer having a base pressure of 1×10^{-9} mbar. A differentially pumped He I lamp emitting 21.22 eV radiation was used as the excitation source, and photoelectrons were detected normal to the sample plane by a concentric hemispherical analyzer operating with a pass energy of 2 eV. During UPS measurements, the sample stub (and sample) was biased -6.32 V relative to ground, enabling the low kinetic energy portion of the spectrum to be measured. The work function of the sample was calculated as the difference between the photon energy (21.22 eV) and the spectrum width, with the latter determined by measuring the secondary electron cutoff on the low kinetic energy side of the spectrum and the edge of the highest occupied molecular orbital (HOMO) on the high kinetic energy side.

X-ray crystal structure determination. Crystals suitable for X-ray analysis were grown by slow evaporation of CH₂Cl₂-Hexane solutions of one isomer of **3-a** and **3-b**, respectively. Crystal structure determination was performed by Dr. William Davis and Peter Müller (MIT X-ray Crystallography Facility) using a Bruker Smart diffractometer equipped with a Kappa CCD area detector using radiation from a Mo-K_α source monochromated through graphite ($\lambda = 0.71073$ Å). Structures were solved and refined using the Bruker SHELXTL package. Crystal structure data are reproduced below (Table 4.4 – 4.12).

Table 4.4. Crystal data and structure refinement for Compound **3-a** and **3-b**.

| | 3-a | 3-b |
|-----------------------------------|---|---|
| Empirical formula | C ₃₉ H ₂₈ Cl ₂ O ₈ | C _{34.20} H _{14.40} Cl _{0.40} F ₁₂ |
| Formula weight | 695.51 | 667.44 |
| Temperature | 100(2) K | 193(2) K |
| Wavelength | 0.71073 Å | 0.71073 Å |
| Crystal system | Monoclinic | Monoclinic |
| Space group | C2/c | P2(1)/n |
| Unit cell dimensions | a = 23.75(2) Å $\alpha = 90^\circ$. b = 8.456(9) Å $\beta = 118.39^\circ$. c = 18.780(20) Å $\gamma = 90^\circ$. | a = 8.4828(8) Å $\alpha = 90^\circ$ b = 13.0644(13) Å $\beta = 101.579^\circ$ c = 13.703(2) Å $\gamma = 90^\circ$ |
| Volume | 3318(6) Å ³ | 1487.7(3) Å ³ |
| Z | 4 | 2 |
| Density (calculated) | 1.392 Mg/m ³ | 1.490 Mg/m ³ |
| Absorption coefficient | 0.251 mm ⁻¹ | 0.174 mm ⁻¹ |
| F(000) | 1440 | 669 |
| Crystal size | 0.20 x 0.15 x 0.10 mm ³ | 0.22 x 0.21 x 0.16 mm ³ |
| Theta range for data collection | 1.95 to 24.99°. | 2.18 to 28.28°. |
| Index ranges | -28 ≤ h ≤ 24, 0 ≤ k ≤ 10, 0 ≤ l ≤ 22 | -11 ≤ h ≤ 11, -15 ≤ k ≤ 17, -17 ≤ l ≤ 8 |
| Reflections collected | 2907 | 7783 |
| Independent reflections | 2907 [R(int) = 0.0509] | 3466 [R(int) = 0.0170] |
| Completeness to theta = 24.99° | 99.9 % | 93.8 % |
| Absorption correction | Semi-empirical from equivalents | None |
| Max. and min. transmission | 0.9753 and 0.9515 | |
| Refinement method | Full-matrix least-squares on F ² | Full-matrix least-squares on F ² |
| Data / restraints / parameters | 2907 / 0 / 224 | 3466 / 0 / 281 |
| Goodness-of-fit on F ² | 1.211 | 1.174 |
| Final R indices [I > 2σ(I)] | R1 = 0.0544, wR2 = 0.1243 | R1 = 0.0539, wR2 = 0.1445 |
| R indices (all data) | R1 = 0.0566, wR2 = 0.1258 | R1 = 0.0612, wR2 = 0.1491 |
| Largest diff. peak and hole | 0.415 and -0.263 e.Å ⁻³ | 0.510 and -0.324 e.Å ⁻³ |

Table 4.5. Selected bond lengths [Å] and angles [°] for compound **3-a**.

| Selected bond lengths [Å] | | Selected bond angles [°] | |
|---------------------------|----------|--------------------------|------------|
| O(1)-C(16) | 1.207(3) | C(16)-O(2)-C(17) | 115.9(2) |
| O(2)-C(16) | 1.331(3) | C(18)-O(4)-C(19) | 115.5(2) |
| O(2)-C(17) | 1.442(3) | C(2)-C(1)-C(16) | 126.4(2) |
| O(3)-C(18) | 1.197(3) | C(2)-C(1)-C(6) | 113.9(2) |
| O(4)-C(18) | 1.328(3) | C(16)-C(1)-C(6) | 119.6(2) |
| O(4)-C(19) | 1.446(3) | C(1)-C(2)-C(18) | 128.3(2) |
| C(1)-C(2) | 1.332(4) | C(1)-C(2)-C(3) | 113.8(2) |
| C(1)-C(16) | 1.474(3) | C(18)-C(2)-C(3) | 117.9(2) |
| C(1)-C(6) | 1.527(3) | C(4)-C(3)-C(7) | 105.82(19) |
| C(2)-C(18) | 1.488(4) | C(4)-C(3)-C(2) | 105.16(19) |
| C(2)-C(3) | 1.527(3) | C(7)-C(3)-C(2) | 105.62(19) |
| C(3)-C(4) | 1.521(3) | C(5)-C(4)-C(13)#1 | 121.3(2) |
| C(3)-C(7) | 1.526(4) | C(5)-C(4)-C(3) | 113.0(2) |
| C(4)-C(5) | 1.386(3) | C(13)#1-C(4)-C(3) | 125.6(2) |
| C(4)-C(13)#1 | 1.392(3) | C(4)-C(5)-C(13) | 121.4(2) |
| C(5)-C(13) | 1.399(3) | C(4)-C(5)-C(6) | 112.7(2) |
| C(5)-C(6) | 1.520(3) | C(13)-C(5)-C(6) | 125.9(2) |
| C(6)-C(8) | 1.526(3) | C(5)-C(6)-C(8) | 105.11(19) |
| C(7)-C(12) | 1.384(4) | C(5)-C(6)-C(1) | 105.55(19) |
| C(7)-C(8) | 1.391(4) | C(8)-C(6)-C(1) | 106.0(2) |
| C(8)-C(9) | 1.380(4) | C(12)-C(7)-C(8) | 121.0(2) |
| C(9)-C(10) | 1.387(4) | C(12)-C(7)-C(3) | 126.4(2) |
| C(10)-C(11) | 1.385(4) | C(8)-C(7)-C(3) | 112.6(2) |
| C(11)-C(12) | 1.392(4) | C(9)-C(8)-C(7) | 120.2(2) |
| C(13)-C(4)#1 | 1.392(3) | C(9)-C(8)-C(6) | 127.0(2) |
| C(13)-C(14) | 1.439(4) | C(7)-C(8)-C(6) | 112.8(2) |
| C(14)-C(15) | 1.180(4) | C(8)-C(9)-C(10) | 119.4(2) |
| | | C(11)-C(10)-C(9) | 120.2(2) |
| | | C(10)-C(11)-C(12) | 120.9(2) |
| | | C(7)-C(12)-C(11) | 118.4(2) |
| | | C(4)#1-C(13)-C(5) | 117.3(2) |
| | | C(4)#1-C(13)-C(14) | 121.2(2) |

| | |
|-------------------|----------|
| C(5)-C(13)-C(14) | 121.5(2) |
| C(15)-C(14)-C(13) | 177.9(3) |
| O(1)-C(16)-O(2) | 124.4(2) |
| O(1)-C(16)-C(1) | 123.4(2) |
| O(2)-C(16)-C(1) | 112.2(2) |
| O(3)-C(18)-O(4) | 124.9(2) |
| O(3)-C(18)-C(2) | 123.7(2) |
| O(4)-C(18)-C(2) | 111.3(2) |

Symmetry transformations used to generate equivalent atoms:

#1 $-x-1/2, -y+1/2, -z$

Table 4.6. Selected bond lengths [Å] and angles [°] for compound **3-b**.

| Selected bond lengths [Å] | | Selected bond angles [°] | |
|---------------------------|-----------|--------------------------|------------|
| C(1)-C(2) | 1.186(2) | C(1)-C(2)-C(3) | 175.93(17) |
| C(2)-C(3) | 1.438(2) | C(4)-C(3)-C(5) | 116.86(13) |
| C(3)-C(4) | 1.402(2) | C(4)-C(3)-C(2) | 120.29(13) |
| C(3)-C(5) | 1.406(2) | C(5)-C(3)-C(2) | 122.81(13) |
| C(4)-C(5)#1 | 1.391(2) | C(5)#1-C(4)-C(3) | 122.03(13) |
| C(4)-C(9)#1 | 1.527(2) | C(5)#1-C(4)-C(9)#1 | 112.76(13) |
| C(5)-C(4)#1 | 1.392(2) | C(3)-C(4)-C(9)#1 | 125.21(13) |
| C(5)-C(6) | 1.529(2) | C(4)#1-C(5)-C(3) | 121.10(13) |
| C(6)-C(15) | 1.527(2) | C(4)#1-C(5)-C(6) | 112.66(13) |
| C(6)-C(7) | 1.537(2) | C(3)-C(5)-C(6) | 126.23(13) |
| C(7)-C(8) | 1.330(2) | C(15)-C(6)-C(5) | 106.22(12) |
| C(7)-C(16) | 1.501(2) | C(15)-C(6)-C(7) | 105.46(12) |
| C(8)-C(17) | 1.503(2) | C(5)-C(6)-C(7) | 105.24(12) |
| C(8)-C(9) | 1.533(2) | C(8)-C(7)-C(16) | 129.04(16) |
| C(9)-C(10) | 1.526(2) | C(8)-C(7)-C(6) | 113.82(14) |
| C(9)-C(4)#1 | 1.527(2) | C(16)-C(7)-C(6) | 117.13(14) |
| C(10)-C(11) | 1.381(2) | C(7)-C(8)-C(17) | 127.32(17) |
| C(10)-C(15) | 1.396(2) | C(7)-C(8)-C(9) | 113.84(14) |
| C(11)-C(12) | 1.396(3) | C(17)-C(8)-C(9) | 118.82(16) |
| C(12)-C(13) | 1.381(3) | C(10)-C(9)-C(4)#1 | 105.55(12) |
| C(13)-C(14) | 1.394(3) | C(10)-C(9)-C(8) | 106.34(12) |
| C(14)-C(15) | 1.385(2) | C(4)#1-C(9)-C(8) | 105.07(12) |
| C(16)-F(1') | 1.154(7) | C(11)-C(10)-C(15) | 120.82(15) |
| C(16)-F(3') | 1.258(9) | C(11)-C(10)-C(9) | 126.39(15) |
| C(16)-F(1) | 1.286(3) | C(15)-C(10)-C(9) | 112.78(13) |
| C(16)-F(2) | 1.317(3) | C(10)-C(11)-C(12) | 118.86(17) |
| C(16)-F(3) | 1.357(3) | C(13)-C(12)-C(11) | 120.33(17) |
| C(16)-F(2') | 1.454(9) | C(12)-C(13)-C(14) | 120.95(17) |
| C(17)-F(6') | 1.149(12) | C(15)-C(14)-C(13) | 118.73(17) |
| C(17)-F(5') | 1.156(12) | C(14)-C(15)-C(10) | 120.29(15) |
| C(17)-F(4) | 1.295(4) | C(14)-C(15)-C(6) | 127.19(15) |
| C(17)-F(5) | 1.300(3) | C(10)-C(15)-C(6) | 112.52(13) |
| C(17)-F(6) | 1.372(3) | F(1')-C(16)-F(3') | 117.3(10) |
| C(17)-F(4') | 1.511(9) | F(1')-C(16)-F(1) | 125.7(4) |
| F(1)-F(3') | 0.809(12) | F(3')-C(16)-F(1) | 37.1(6) |
| F(1)-F(2') | 1.428(9) | F(1')-C(16)-F(2) | 44.8(10) |
| F(2)-F(1') | 0.953(19) | F(3')-C(16)-F(2) | 134.0(4) |
| F(2)-F(2') | 1.344(12) | F(1)-C(16)-F(2) | 110.4(3) |
| F(3)-F(1') | 1.214(19) | F(1')-C(16)-F(3) | 57.1(10) |
| F(3)-F(3') | 1.561(15) | F(3')-C(16)-F(3) | 73.2(7) |
| F(4)-F(6') | 0.57(3) | F(1)-C(16)-F(3) | 106.0(3) |
| F(4)-F(4') | 1.508(11) | F(2)-C(16)-F(3) | 101.4(2) |

| | | | |
|-------------|-----------|-------------------|------------|
| F(5)-F(5') | 0.93(3) | F(1')-C(16)-F(2') | 99.4(9) |
| F(5)-F(4') | 1.397(13) | F(3')-C(16)-F(2') | 99.1(7) |
| F(6)-F(5') | 1.31(3) | F(1)-C(16)-F(2') | 62.5(4) |
| F(6)-F(6') | 1.56(3) | F(2)-C(16)-F(2') | 57.7(5) |
| C(18S)-Cl | 1.68(2) | F(3)-C(16)-F(2') | 143.2(4) |
| C(18S)-Cl#2 | 1.716(19) | F(1')-C(16)-C(7) | 120.6(4) |
| Cl-C(18S)#2 | 1.716(19) | F(3')-C(16)-C(7) | 110.1(5) |
| | | F(1)-C(16)-C(7) | 113.73(19) |
| | | F(2)-C(16)-C(7) | 114.4(2) |
| | | F(3)-C(16)-C(7) | 109.91(16) |
| | | F(2')-C(16)-C(7) | 106.5(4) |
| | | F(6')-C(17)-F(5') | 117.4(14) |
| | | F(6')-C(17)-F(4) | 26.0(14) |
| | | F(5')-C(17)-F(4) | 129.6(8) |
| | | F(6')-C(17)-F(5) | 122.2(9) |
| | | F(5')-C(17)-F(5) | 43.8(16) |
| | | F(4)-C(17)-F(5) | 112.3(3) |
| | | F(6')-C(17)-F(6) | 76.1(14) |
| | | F(5')-C(17)-F(6) | 61.9(17) |
| | | F(4)-C(17)-F(6) | 101.9(3) |
| | | F(5)-C(17)-F(6) | 104.2(3) |
| | | F(6')-C(17)-C(8) | 121.1(9) |
| | | F(5')-C(17)-C(8) | 116.3(8) |
| | | F(4)-C(17)-C(8) | 114.0(2) |
| | | F(5)-C(17)-C(8) | 112.6(2) |
| | | F(6)-C(17)-C(8) | 110.9(2) |
| | | F(6')-C(17)-F(4') | 88.2(12) |
| | | F(5')-C(17)-F(4') | 101.2(14) |
| | | F(4)-C(17)-F(4') | 64.5(5) |
| | | F(5)-C(17)-F(4') | 59.0(6) |
| | | F(6)-C(17)-F(4') | 145.8(4) |
| | | C(8)-C(17)-F(4') | 103.3(3) |
| | | F(3')-F(1)-C(16) | 69.6(7) |
| | | F(3')-F(1)-F(2') | 133.3(10) |
| | | C(16)-F(1)-F(2') | 64.6(4) |
| | | F(1')-F(2)-C(16) | 58.5(5) |
| | | F(1')-F(2)-F(2') | 120.1(7) |
| | | C(16)-F(2)-F(2') | 66.3(4) |
| | | F(1')-F(3)-C(16) | 53.0(5) |
| | | F(1')-F(3)-F(3') | 95.1(6) |
| | | C(16)-F(3)-F(3') | 50.5(4) |
| | | F(6')-F(4)-C(17) | 62.4(13) |
| | | F(6')-F(4)-F(4') | 121.5(16) |
| | | C(17)-F(4)-F(4') | 64.7(4) |
| | | F(5')-F(5)-C(17) | 59.8(7) |
| | | F(5')-F(5)-F(4') | 125.2(10) |

| | |
|--------------------|-----------|
| C(17)-F(5)-F(4') | 68.0(5) |
| F(5')-F(6)-C(17) | 51.0(9) |
| F(5')-F(6)-F(6') | 86.0(9) |
| C(17)-F(6)-F(6') | 45.5(4) |
| F(2)-F(1')-C(16) | 76.7(9) |
| F(2)-F(1')-F(3) | 145.2(8) |
| C(16)-F(1')-F(3) | 69.9(7) |
| F(2)-F(2')-F(1) | 100.9(7) |
| F(2)-F(2')-C(16) | 56.0(4) |
| F(1)-F(2')-C(16) | 53.0(3) |
| F(1)-F(3')-C(16) | 73.3(7) |
| F(1)-F(3')-F(3) | 122.7(10) |
| C(16)-F(3')-F(3) | 56.3(5) |
| F(5)-F(4')-F(4) | 95.7(6) |
| F(5)-F(4')-C(17) | 52.9(4) |
| F(4)-F(4')-C(17) | 50.8(3) |
| F(5)-F(5')-C(17) | 76.4(16) |
| F(5)-F(5')-F(6) | 140.0(14) |
| C(17)-F(5')-F(6) | 67.1(10) |
| F(4)-F(6')-C(17) | 91.5(14) |
| F(4)-F(6')-F(6) | 149.2(15) |
| C(17)-F(6')-F(6) | 58.4(11) |
| Cl-C(18S)-Cl#2 | 121.6(10) |
| C(18S)-Cl-C(18S)#2 | 58.4(10) |

Symmetry transformations used to generate equivalent atoms:

#1 -x+1,-y,-z+1 #2 -x+2,-y+1,-z+1

Table 4.7. Atomic coordinates ($\times 10^4$) and equivalent isotropic displacement parameters ($\text{\AA}^2 \times 10^3$) for compound **3-a**. $U(\text{eq})$ is defined as one third of the trace of the orthogonalized U_{ij} tensor.

| | x | y | z | U(eq) |
|--------|----------|----------|----------|-------|
| O(1) | -9(1) | 1262(2) | 1152(1) | 20(1) |
| O(2) | -178(1) | 2820(2) | 101(1) | 20(1) |
| O(3) | -1452(1) | 3680(2) | -1647(1) | 26(1) |
| O(4) | -894(1) | 1480(2) | -1546(1) | 25(1) |
| C(1) | -1041(1) | 1374(3) | 19(1) | 14(1) |
| C(2) | -1417(1) | 1621(3) | -769(1) | 15(1) |
| C(3) | -2102(1) | 1031(3) | -1081(1) | 14(1) |
| C(4) | -2343(1) | 1854(3) | -557(1) | 14(1) |
| C(5) | -1953(1) | 1602(3) | 264(1) | 13(1) |
| C(6) | -1378(1) | 567(3) | 440(1) | 14(1) |
| C(7) | -2042(1) | -715(3) | -851(1) | 15(1) |
| C(8) | -1659(1) | -962(3) | -25(2) | 15(1) |
| C(9) | -1574(1) | -2470(3) | 291(2) | 17(1) |
| C(10) | -1859(1) | -3738(3) | -225(2) | 21(1) |
| C(11) | -2226(1) | -3490(3) | -1050(2) | 22(1) |
| C(12) | -2325(1) | -1972(3) | -1373(2) | 18(1) |
| C(13) | -2104(1) | 2237(3) | 840(1) | 13(1) |
| C(14) | -1712(1) | 1932(3) | 1691(2) | 15(1) |
| C(15) | -1401(1) | 1641(3) | 2386(2) | 19(1) |
| C(16) | -358(1) | 1792(3) | 489(1) | 15(1) |
| C(17) | 489(1) | 3261(3) | 508(2) | 27(1) |
| C(18) | -1254(1) | 2407(3) | -1357(1) | 16(1) |
| C(19) | -717(2) | 2129(4) | -2123(2) | 36(1) |
| C(1S) | 0 | 3458(4) | 2500 | 26(1) |
| Cl(1S) | 514(1) | 4623(1) | 3341(1) | 27(1) |

Table 4.8. Anisotropic displacement parameters ($\text{\AA}^2 \times 10^3$) for compound **3-a**. The anisotropic displacement factor exponent takes the form: $-2\pi^2 [h^2 a^{*2} U^{11} + \dots + 2 h k a^* b^* U^{12}]$.

| | U ¹¹ | U ²² | U ³³ | U ²³ | U ¹³ | U ¹² |
|--------|-----------------|-----------------|-----------------|-----------------|-----------------|-----------------|
| O(1) | 13(1) | 23(1) | 21(1) | 0(1) | 4(1) | 0(1) |
| O(2) | 11(1) | 23(1) | 25(1) | 2(1) | 7(1) | -5(1) |
| O(3) | 27(1) | 22(1) | 30(1) | 8(1) | 14(1) | 5(1) |
| O(4) | 32(1) | 21(1) | 33(1) | 0(1) | 25(1) | 0(1) |
| C(1) | 12(1) | 11(1) | 22(1) | -1(1) | 9(1) | 3(1) |
| C(2) | 13(1) | 12(1) | 20(1) | -3(1) | 8(1) | 1(1) |
| C(3) | 11(1) | 16(1) | 15(1) | 0(1) | 5(1) | 0(1) |
| C(4) | 13(1) | 10(1) | 19(1) | -2(1) | 8(1) | -4(1) |
| C(5) | 9(1) | 11(1) | 18(1) | 0(1) | 5(1) | -2(1) |
| C(6) | 11(1) | 16(1) | 16(1) | 0(1) | 6(1) | 0(1) |
| C(7) | 9(1) | 16(1) | 21(1) | -1(1) | 9(1) | 1(1) |
| C(8) | 8(1) | 17(1) | 22(1) | -2(1) | 9(1) | 1(1) |
| C(9) | 13(1) | 19(1) | 23(1) | 2(1) | 10(1) | 3(1) |
| C(10) | 17(1) | 15(1) | 35(2) | 3(1) | 16(1) | 1(1) |
| C(11) | 20(1) | 17(1) | 33(2) | -8(1) | 15(1) | -5(1) |
| C(12) | 13(1) | 21(1) | 21(1) | -2(1) | 8(1) | -1(1) |
| C(13) | 10(1) | 12(1) | 16(1) | 0(1) | 5(1) | -3(1) |
| C(14) | 10(1) | 12(1) | 24(1) | -2(1) | 10(1) | -1(1) |
| C(15) | 17(1) | 22(1) | 17(1) | 0(1) | 6(1) | -1(1) |
| C(16) | 13(1) | 12(1) | 19(1) | -4(1) | 8(1) | 2(1) |
| C(17) | 15(1) | 28(1) | 37(2) | 3(1) | 12(1) | -5(1) |
| C(18) | 11(1) | 18(1) | 14(1) | -4(1) | 2(1) | -4(1) |
| C(19) | 48(2) | 39(2) | 42(2) | 2(1) | 38(2) | -2(1) |
| C(1S) | 26(2) | 19(2) | 24(2) | 0 | 3(2) | 0 |
| Cl(1S) | 26(1) | 24(1) | 26(1) | -4(1) | 7(1) | -6(1) |

Table 4.9. Hydrogen coordinates ($\times 10^4$) and isotropic displacement parameters ($\text{\AA}^2 \times 10^3$) for compound **3-a**.

| | x | y | z | U(eq) |
|--------|-------|-------|-------|-------|
| H(3) | -2380 | 1220 | -1673 | 17 |
| H(6) | -1091 | 394 | 1031 | 17 |
| H(9) | -1323 | -2637 | 857 | 21 |
| H(10) | -1801 | -4780 | -12 | 25 |
| H(11) | -2413 | -4368 | -1399 | 27 |
| H(12) | -2581 | -1802 | -1938 | 22 |
| H(15) | -1151 | 1406 | 2945 | 23 |
| H(17A) | 592 | 3769 | 1025 | 40 |
| H(17B) | 574 | 4000 | 168 | 40 |
| H(17C) | 754 | 2314 | 608 | 40 |
| H(19A) | -1104 | 2406 | -2623 | 55 |
| H(19B) | -470 | 1343 | -2243 | 55 |
| H(19C) | -455 | 3079 | -1896 | 55 |
| H(1S1) | -261 | 2769 | 2655 | 32 |
| H(1S2) | 261 | 2769 | 2345 | 32 |

Table 4.10. Atomic coordinates ($\times 10^4$) and equivalent isotropic displacement parameters ($\text{\AA}^2 \times 10^3$) for compound **3-b**. $U(\text{eq})$ is defined as one third of the trace of the orthogonalized U_{ij} tensor.

| | x | y | z | $U(\text{eq})$ |
|--------|-----------|----------|----------|----------------|
| C(1) | 4850(2) | -1446(2) | 7595(1) | 43(1) |
| C(2) | 4979(2) | -1006(1) | 6858(1) | 30(1) |
| C(3) | 5028(2) | -503(1) | 5931(1) | 26(1) |
| C(4) | 4127(2) | -886(1) | 5034(1) | 26(1) |
| C(5) | 5912(2) | 397(1) | 5873(1) | 25(1) |
| C(6) | 6999(2) | 942(1) | 6743(1) | 27(1) |
| C(7) | 6365(2) | 2045(1) | 6713(1) | 32(1) |
| C(8) | 6295(2) | 2510(1) | 5842(1) | 34(1) |
| C(9) | 6906(2) | 1852(1) | 5069(1) | 30(1) |
| C(10) | 8599(2) | 1506(1) | 5557(1) | 29(1) |
| C(11) | 9976(2) | 1626(1) | 5176(1) | 40(1) |
| C(12) | 11432(2) | 1255(2) | 5721(2) | 48(1) |
| C(13) | 11489(2) | 783(2) | 6629(2) | 45(1) |
| C(14) | 10102(2) | 662(1) | 7017(1) | 35(1) |
| C(15) | 8653(2) | 1018(1) | 6470(1) | 28(1) |
| C(16) | 5910(2) | 2450(2) | 7644(2) | 45(1) |
| C(17) | 5657(3) | 3563(2) | 5548(2) | 55(1) |
| F(1) | 4527(4) | 2140(3) | 7772(3) | 113(2) |
| F(2) | 6025(4) | 3451(2) | 7746(2) | 78(1) |
| F(3) | 6990(3) | 2128(2) | 8455(1) | 69(1) |
| F(4) | 6577(5) | 4296(3) | 5968(4) | 107(2) |
| F(5) | 5246(5) | 3677(2) | 4588(2) | 86(1) |
| F(6) | 4264(4) | 3744(2) | 5884(3) | 90(1) |
| F(1') | 6754(14) | 3002(13) | 8162(9) | 99(5) |
| F(2') | 4541(14) | 3126(7) | 7325(8) | 86(3) |
| F(3') | 5229(17) | 1760(7) | 8051(9) | 90(5) |
| F(4') | 6836(16) | 3977(6) | 4954(10) | 92(3) |
| F(5') | 4460(30) | 3603(11) | 4967(18) | 164(11) |
| F(6') | 5970(30) | 4246(11) | 6079(10) | 147(12) |
| C(18S) | 10670(20) | 4605(14) | 4839(17) | 48(5) |
| Cl | 8716(4) | 4431(2) | 4320(3) | 68(1) |

Table 4.11. Anisotropic displacement parameters ($\text{\AA}^2 \times 10^3$) for compound **3-b**. The anisotropic displacement factor exponent takes the form: $-2\pi^2 [h^2 a^*2U^{11} + \dots + 2 h k a^* b^* U^{12}]$.

| | U ¹¹ | U ²² | U ³³ | U ²³ | U ¹³ | U ¹² |
|--------|-----------------|-----------------|-----------------|-----------------|-----------------|-----------------|
| C(1) | 50(1) | 46(1) | 34(1) | 12(1) | 8(1) | 1(1) |
| C(2) | 31(1) | 29(1) | 29(1) | 1(1) | 4(1) | 0(1) |
| C(3) | 27(1) | 25(1) | 26(1) | 2(1) | 7(1) | 2(1) |
| C(4) | 29(1) | 22(1) | 28(1) | 0(1) | 7(1) | 1(1) |
| C(5) | 26(1) | 25(1) | 25(1) | -1(1) | 6(1) | 2(1) |
| C(6) | 31(1) | 26(1) | 24(1) | -1(1) | 6(1) | 0(1) |
| C(7) | 32(1) | 28(1) | 35(1) | -7(1) | 7(1) | 0(1) |
| C(8) | 36(1) | 25(1) | 37(1) | -4(1) | 2(1) | 2(1) |
| C(9) | 36(1) | 24(1) | 28(1) | 2(1) | 5(1) | -3(1) |
| C(10) | 33(1) | 25(1) | 30(1) | -3(1) | 7(1) | -3(1) |
| C(11) | 42(1) | 41(1) | 38(1) | -1(1) | 13(1) | -8(1) |
| C(12) | 35(1) | 53(1) | 59(1) | -3(1) | 19(1) | -4(1) |
| C(13) | 31(1) | 43(1) | 58(1) | -1(1) | 5(1) | 3(1) |
| C(14) | 36(1) | 29(1) | 39(1) | 1(1) | 2(1) | 0(1) |
| C(15) | 32(1) | 23(1) | 30(1) | -2(1) | 6(1) | -2(1) |
| C(16) | 50(1) | 43(1) | 48(1) | -15(1) | 18(1) | -1(1) |
| C(17) | 71(1) | 31(1) | 56(1) | -3(1) | -9(1) | 11(1) |
| F(1) | 67(2) | 187(4) | 102(2) | -94(3) | 55(2) | -62(2) |
| F(2) | 131(3) | 43(1) | 65(1) | -18(1) | 29(1) | 16(1) |
| F(3) | 92(2) | 80(1) | 33(1) | -13(1) | 7(1) | 26(1) |
| F(4) | 117(2) | 26(1) | 146(4) | 2(2) | -49(2) | -8(1) |
| F(5) | 153(4) | 49(1) | 49(1) | 12(1) | 1(2) | 41(2) |
| F(6) | 87(2) | 73(2) | 109(2) | 5(1) | 15(2) | 51(1) |
| F(1') | 73(6) | 147(11) | 93(8) | -92(8) | 54(6) | -75(7) |
| F(2') | 102(7) | 66(5) | 113(7) | 10(5) | 78(6) | 40(5) |
| F(3') | 160(13) | 46(4) | 102(8) | 3(4) | 119(10) | -1(6) |
| F(4') | 133(9) | 32(4) | 128(8) | 33(4) | 67(7) | 9(4) |
| F(5') | 165(16) | 76(8) | 179(19) | 42(12) | -138(15) | -14(10) |
| F(6') | 340(30) | 47(8) | 45(5) | -27(5) | 24(11) | 80(13) |
| C(18S) | 46(10) | 33(9) | 73(13) | -20(9) | 35(10) | -6(8) |
| Cl | 74(2) | 60(2) | 70(2) | -7(1) | 14(2) | -8(1) |

Table 4.12. Hydrogen coordinates ($\times 10^4$) and isotropic displacement parameters ($\text{\AA}^2 \times 10^3$) for compound **3-b**.

| | x | y | z | U(eq) |
|--------|-------|-------|------|-------|
| H(1) | 4746 | -1799 | 8185 | 52 |
| H(6) | 7028 | 597 | 7398 | 33 |
| H(9) | 6864 | 2213 | 4421 | 35 |
| H(11) | 9933 | 1955 | 4553 | 47 |
| H(12) | 12388 | 1328 | 5467 | 57 |
| H(13) | 12489 | 537 | 6995 | 54 |
| H(14) | 10149 | 341 | 7644 | 42 |
| H(18A) | 11248 | 4701 | 4286 | 57 |
| H(18B) | 11062 | 3955 | 5171 | 57 |

References

- (1) (a) McQuade, D. T.; Pullen, A. E.; Swager, T. M. *Chem. Rev.* **2000**, *100*, 2537–2574. (b) Huang, H.; Wang, K.; Tan, W.; An, D.; Yang, X.; Huang, S.; Zhai, Q.; Zhou, L.; Jin, Y. *Angew. Chem. Int. Ed.* **2004**, *43*, 5635–5638.
- (2) Zhou, Q.; Swager, T. M. *J. Am. Chem. Soc.* **1995**, *117*, 7017–7018.
- (3) Yang, J.-S.; Swager, T. M. *J. Am. Chem. Soc.* **1998**, *120*, 5321–5322.
- (4) For recent examples not covered in earlier reviews see: (a) Kim, J.; McQuade, D. T.; McHugh, S.; Swager, T. M. *Angew. Chem. Int. Ed.* **2000**, *39*, 3868–3872. (b) Vigalok, A.; Zhu, Z.; Swager, T. M. *J. Am. Chem. Soc.* **2001**, *123*, 7917–7918. (c) Takeuchi, M.; Shioya, T.; Swager, T. M. *Angew. Chem. Int. Ed.* **2001**, *40*, 3372–3376. (d) Vigalok, A.; Swager, T. M. *Adv. Mater.* **2002**, *14*, 368–371. (e) Yu, H.-H.; Pullen, A. E.; Büschel, M. G.; Swager, T. M. *Angew. Chem. Int. Ed.* **2004**, *43*, 3700–3703.
- (5) (a) Yang, J.-S.; Swager, T. M. *J. Am. Chem. Soc.* **1998**, *120*, 11864–11873. (b) Chen, L.; McBranch, D. W.; Wang, H.-L.; Helgeson, R.; Wudl, F.; Whitten, D. G. D. *Proc. Natl. Acad. Sci. USA.* **1999**, *96*, 12287–12292.

- (6) Facchetti, A.; Yoon, M.-H.; Stern, C. L.; Hutchison, G. R.; Ratner, M. A.; Marks, T. J. *J. Am. Chem. Soc.* **2004**, *126*, 13480–13501.
- (7) (a) Yu, L.-S.; Chen, S.-A. *Adv. Mater.* **2004**, *16*, 744–748. (b) Hughes, G.; Bryce, M. R. *J. Mater. Chem.* **2005**, *15*, 94–107.
- (8) (a) Alam, M. M.; Jenekhe, S. A. *Chem. Mater.* **2004**, *16*, 4647–4656. (b) Neuteboom, E. E.; Meskers, S. C. J.; van Hal, P. A.; van Duren, J. K. J.; Meijer, E. W.; Janssen, R. A. J.; Dupin, H.; Pourtois, G.; Cornil, J.; Lazzaroni, R.; Brédas, J.-L.; Beljonne, D. *J. Am. Chem. Soc.* **2003**, *125*, 8625–8638.
- (9) (a) Bernardo, A. R.; Stoddart, J. F.; Kaifer, A. E. *J. Am. Chem. Soc.* **1992**, *114*, 10624–10631. (b) Deranleau, D. A.; Schwyzer, R. *Biochemistry* **1970**, *9*, 126–134.
- (10) Krebs, F. C.; Spanggaard, H. *J. Org. Chem.* **2002**, *67*, 7185–7192.
- (11) Kim, Y.; Zhu, Z.; Swager, T. M. *J. Am. Chem. Soc.* **2004**, *126*, 452–453.
- (12) Long, T. M.; Swager, T. M. *J. Am. Chem. Soc.* **2003**, *125*, 14113–14119.
- (13) (a) Qui, S.; Lu, P.; Liu, X.; Shen, F.; Liu, L.; Ma, Y.; Shen, J. *Macromolecules* **2003**, *36*, 9823–9829. (b) Blatchford, J. W.; Jessen, S. W.; Lin, L.-B.; Gustafson, T. L.; Fu, D.-K.; Wang, H.-L.; Swager, T. M.; MacDiarmid, A. G.; Epstein, A. J. *Phys. Rev. B* **1996**, *54*, 9180–9189.
- (14) Bush, T. E.; Scott, G. W. *J. Phys. Chem.* **1981**, *85*, 144–146.
- (15) Kim, Y.; Bouffard, J.; Kooi, S.; Swager, T. M. to be published.
- (16) (a) *Conjugated Polymer Surfaces and Interfaces*; Salaneck, W. R.; Stafström, S.; Brédas, J.-L., Cambridge University Press: Cambridge, **1996**. (b) Salaneck, W. R.; Lögdlund, M.; Fahlman, M.; Greczynski, G.; Kugler, Th. *Mater. Sci. Eng.* **2001**, 121–146. (c) Liao, L.-S.; Lee, C. S.; Lee, S. T.; Inbasekaran, M.; Wu, W. W. in *Conjugated Polymer and Molecular*

Interfaces; Salaneck, W. R.; Seki, K.; Kahn, A.; Pireaux, J.-J., Eds; Marcel Dekker: New York, **2002**, pp. 401–441.

(17) Kim, Y.; Swager, T. M. *Chem. Commun.* **2005**, 372–374.

(18) These systems are known as Fido sensors and are available from Nomadics Inc in Stillwater, OK.

(19) Anthony, J. E.; Brooks, J. S.; Eaton, D. L.; Parkin, S. R. *J. Am. Chem. Soc.* **2001**, *123*, 9482–9483.

(20) *Handbook of physical properties of organic chemicals*; Howard, P.H.; Meylan, W. M., Eds; CRC Press: Boca Raton, **1997**.

Chapter 5:
Highly Emissive Conjugated Polymer Excimers

Adapted from:

Kim, Y.; Bouffard, J.; Kooi, S. E.; Swager, T. M.
To be submitted.

Introduction

Interchain interactions often play a dominant role in determining the photophysical properties of conjugated polymers (CPs). Most often strong electronic couplings between the delocalized portion of the polymer's backbone give rise to low fluorescence quantum yields and researchers have focused on strategies for solid state organizations that discourage these interactions. Strong interchain interactions are most prevalent in CPs having large band gaps and presumably more localized wavefunctions (less diffuse orbitals which overlap more strongly). Poly(phenylene ethynylene)s (PPEs) are a class of polymers with a particularly high tendency to produce interchain interactions. The strong interchain interactions in PPEs produce a red shift in the CP's absorbance spectrum that is due to both planarization as well as cofacial π -electron delocalization. These effects have been studied in precisely organized PPE monolayers at an air-water interface.¹ The red shifted emission spectra from CP aggregates are often referred to as having excimer-like character due to their broad featureless spectral character, reduced quantum yields, and longer excited state lifetimes.² The interchain spacing of PPE aggregates has been studied in organized Langmuir monolayers and it was found that excimer-like features dominate when the interchain spacing is less than 4.3 Å.³ It is also found that the absorption spectrum is red-shifted by these close interactions. With few exceptions⁴ strong interactions between the delocalized states of CPs produce greatly diminished quantum yields.

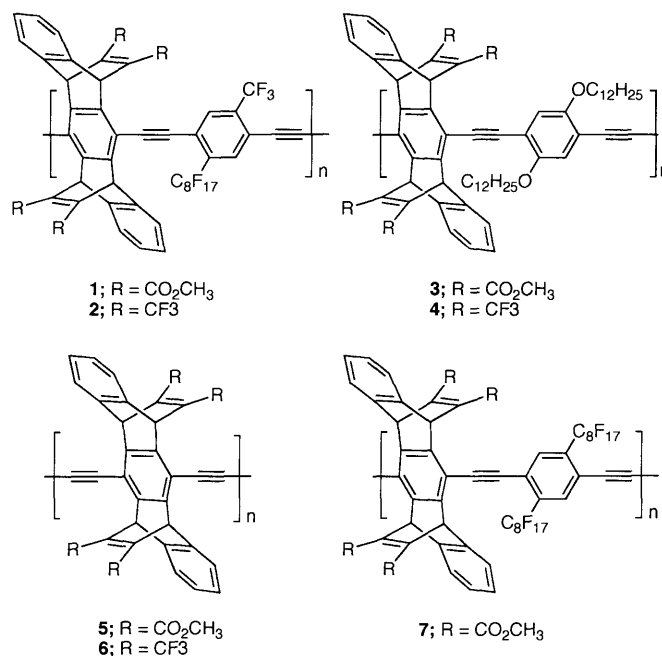
In small molecule photophysics the term excimer is reserved for excited state dimeric complexes that display a repulsive intermolecular interaction in their ground state. As mentioned, typical CP aggregates have strong ground state interactions with

significant interchain mixing of the wave functions. Classical excimers wherein the CP's ground states and their associated absorption spectra are unaffected by the neighboring polymer chains are less common. We had previously discovered a singular example of excimer behavior in systems with elaborated pentiptycene frameworks appended to the polymer.⁵ In this case we found that rigid bicyclic [2.2.2] scaffolds with naphthalenes constituting one of the bridging groups displayed excimer behavior. We suggested that this rigid scaffold, which was designed to prevent strong interactions between the polymer backbones, might itself associate via the naphthalene with a neighboring polymer's backbone to produce an excited state complex.

This chapter details new polymer structures also having [2.2.2] ring systems that faithfully prevent strong ground state interactions. We detail how a series of PPEs (**1**, **3**, and **7**, Chart 1) and a related poly(phenylene diethynylene) (**5**, Chart 1) all containing a [2.2.2] ring system having an bridge disubstituted with esters display bright excimer emissions. These systems were initially of interest to us as systems wherein we could use hyperconjugative and inductive interactions of the electron-poor alkene in the [2.2.2] system to tune the electronics of the polymers and employ the ester groups in biological conjugation chemistries.⁶ However, as reported in this chapter we have come to recognize this [2.2.2] ring system common to **1**, **3**, **5**, and **7** to be an important structure for producing strong excimer emissions in a variety of phenylene ethynylene containing polymers. The special nature of this structure is revealed in that homologues also having electron-withdrawing trifluoromethyl substituted bridging olefins (**2**, **4**, and **6**, Chart 1) exhibited indistinguishable absorption spectra, but gave no evidence of excimer formation. Elucidation of the factors that can produce excimers in these systems is of

interest for extending the utility and basic photophysics of CPs in optoelectronic devices and sensors.

Chart 1



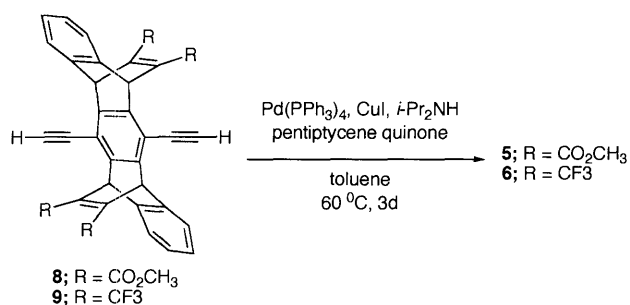
Results and Discussion

Synthesis

The preparation of polymers **1-4** was described in chapter 4⁷ and their respective number average molecular weights are 17000 (PDI = 2.0, DP = 15), 18000 (PDI = 1.2, DP = 15), 21000 (PDI = 1.8, DP = 20), and 28000 (PDI = 2.0, DP = 26). Poly(phenylene diethynylene)s **5** and **6** were synthesized from homopolymerization⁸ (Scheme 5.1) of diacetylene monomers **8** and **9** which were also used in the preparation of polymers **1-4**. Neither polymer **5** nor **6** is adorned, as is typical for soluble CPs, with long flexible sidechains, yet they are completely soluble in common organic solvents such as chloroform, THF and dichloromethane. High solubility in polymers having [2.2.2] ring

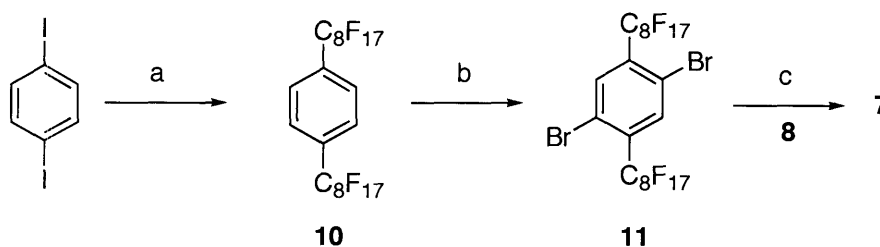
systems has been attributed to the fact that strong intermolecular interactions are blocked by the rigid scaffolds.⁹ The molecular weights (M_n) were 15000 (PDI = 1.3, DP = 24) and 12000 (PDI = 1.4, DP = 19) for polymer **5** and **6**, respectively.

Scheme 5.1. Synthesis of polymers **5** and **6**.



In an effort to add bulk to the polymer backbone that will be unfavourable to interchain contacts, we prepared polymer **7** having bis-perfluorooctyl groups as shown in Scheme 5.2. Monomer **11** is obtained in 11% overall yield by a copper-promoted coupling reaction between perfluorooctyl iodide and 1,4-diiodobenzene in DMSO followed by bromination. The low synthetic yield of monomer **11** is attributed to its low solubility and that of its intermediate. Polymer **7** prepared by Sonogashira-Hagihara cross-coupling reaction exhibits good solubility in common organic solvents (M_n = 14000, PDI = 1.5, DP = 9).

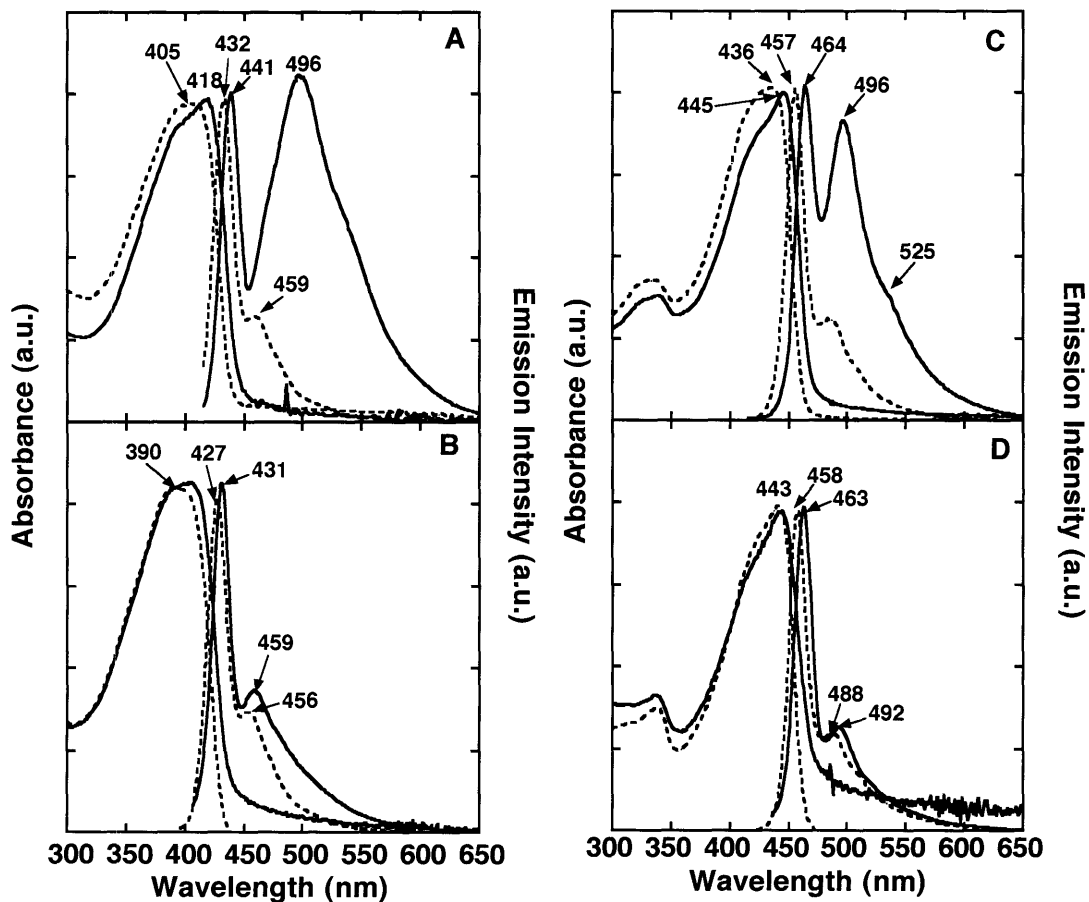
Scheme 5.2. Synthesis of polymer **7**.^a



^a(a) $\text{C}_8\text{F}_{17}\text{I}$, Cu, DMSO, 140 °C, 3 d, 35%. (b) $\text{H}_2\text{SO}_4/\text{TFA}$ (0.3 v/v), NBS, 70 °C, 2 d, 30%. (c) CuI, $\text{Pd(PPh}_3)_4$, $(i\text{-Pr})_2\text{NH/Toluene}$ (1:2), 70 °C, 3 d, 61%.

Photophysical studies.

The absorption and emission spectra of these polymers were investigated in solution and solid state (Figure 5.1). The most striking result is that all of the polymers containing ester groups appended to the double bond as one bridge in the [2.2.2] bicyclic rings (polymer **1**, **3**, **5**, and **7**) display new intense solid state emission peaks that are red shifted from their solution spectra. In contrast, the polymers containing trifluoromethyl substituted olefins (**2**, **4**, and **6**) display solid-state spectra that are very similar to those obtained in solution.



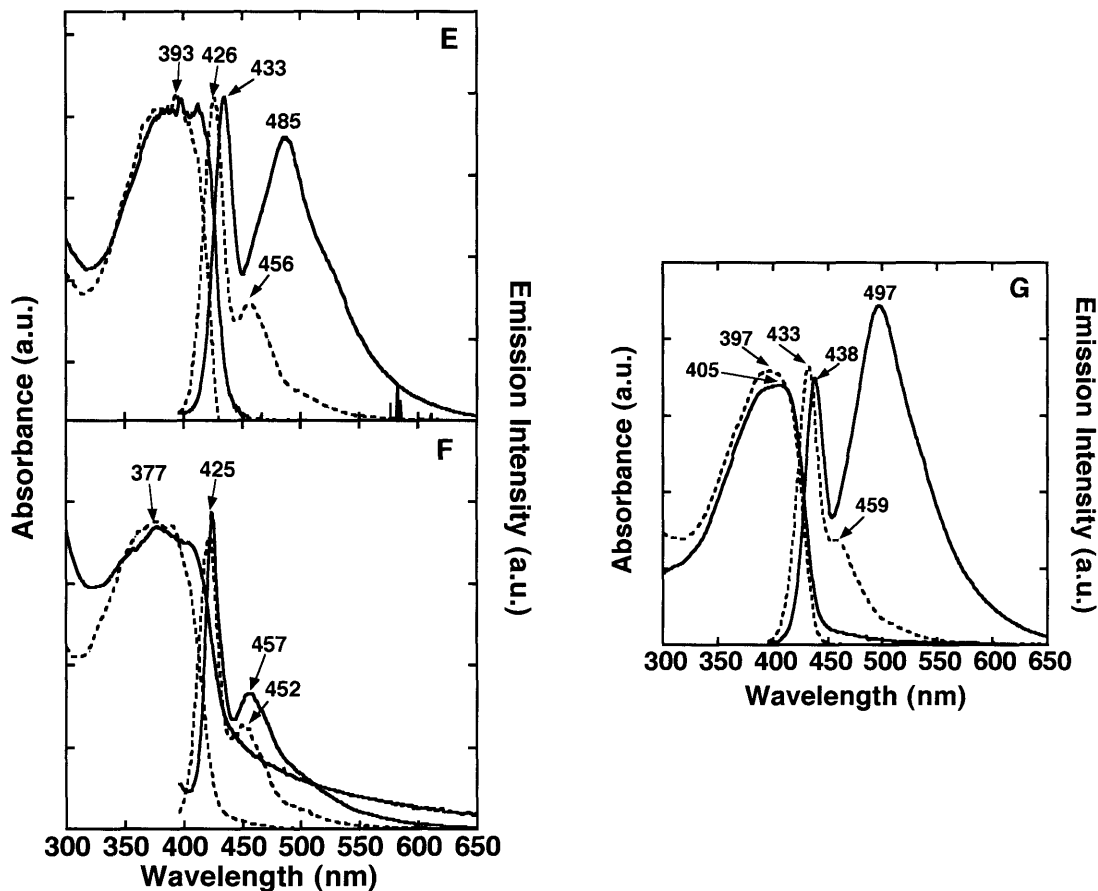


Figure 5.1. Normalized absorption and emission spectra of polymers (A) 1, (B) 2, (C) 3, (D) 4, (E) 5, (F) 6, and (G) 7 in chloroform (dotted line) and solid films (solid line). Polymers 1, 2, 5, 6 and 7 were excited at 380 nm and polymers 3 and 4 were excited at 420 nm.

To probe the origin of the red-shifted emissive peak, we investigated the effect of the film thickness on the emission spectra. As the thickness of polymer 1 film increases (Figure 5.2 (a)), so does the intensity of the long wavelength emission relative to that of shorter wavelength (I_{496}/I_{438}). Two factors may contribute to the enhanced long wavelength emission in thicker films. In thin films interfaces can dictate polymer organization and create conformations unfavourable to the long wavelength emission. Hence, with thicker films the amount of polymer away from the interfaces increases and

if this material is organized in a way that gives the new emission we expect an enhancement. Alternatively, in addition to this organizational explanation, energy migration may be enhanced in thicker films.¹⁰ In this case we must infer that the energy of the polymer segments responsible for the low energy emission is favourable (i.e. lower energy than its surroundings) for energy transfer to occur. We additionally studied spin-cast films wherein polymer **1** is interned within a poly(methyl methacrylate) (PMMA) matrix with different weight ratios (polymer **1**/PMMA). As shown in Figure 5.2 (b), mixed films wherein the polymer **1**/PMMA ratio is less than 0.03 behave like a solution, demonstrating that long wavelength emission may be avoided by reducing interchain interactions. Therefore, PMMA films containing small amounts of polymer **1** exhibit a strong blue fluorescence, whereas films of pure polymer **1** exhibit a strong green fluorescence due to the new emission.

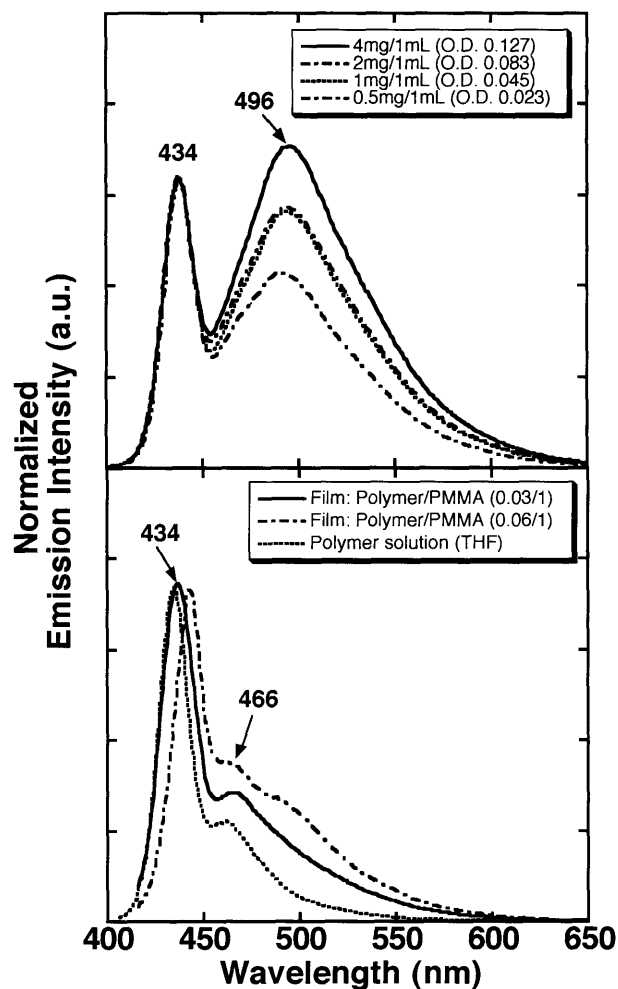


Figure 5.2. The emission spectra of polymer **1** films as a function of film thickness (top) and normalized emission spectra of polymer **1** in THF and as spin-cast films in PMMA (O.D: 0.05 for 0.03/1 and 0.3 for 0.06/1) (bottom). Films and solution were excited at 400 nm and 390 nm, respectively.

The concentration dependence of the emission characteristics of polymer **1** in solution shows a behavior similar to that of small molecule excimers. In dilute THF solutions (5×10^{-6} - 5×10^{-5} M), polymer **1**'s spectroscopic characteristics were constant and the emission spectra displayed emission maximum at 432 with a vibrational band at 459 nm ($\Delta E^{01} = 1,362 \text{ cm}^{-1}$) and the emission intensity scales linearly with concentration, indicating that the emission is emanating from an isolated chain singlet excited state, A^* .

However, at high concentrations of **1** (0.1 w% in THF) was observed a new red-shifted emission peak which is consistent with emission from a singlet excimer excited state, AA*. Unlike most CP aggregates, which are red-shifted in both emission and absorption, a new red-shifted peak of polymer **1** film was not observed in its absorption spectra at any concentration or in thin films. Moreover the absorption and excitation spectra of polymer **1** film are identical. Hence these solution studies and the thin film investigations clearly point toward the new long wavelength emission being characterized as an excimer.

The photophysical studies of other polymers were similarly carried out in solution and solid state. The same trends displayed by polymer **1** were observed for the polymers having alkenes bearing esters as one of the bridges in the [2.2.2] bicyclic ring system (**3**, **5**, **7**). Similar film thickness behaviors are consistently observed for these polymers as shown in Figure 5.3. We emphasize that none of these behaviors was observed for polymers **2**, **4** and **6** films at any thicknesses prepared ($> O.D\ 0.15$).

In considering the structure of polymer **1** it is tempting to suggest that the new excimer emission is due to an association involving the more sterically accessible phenylene which lacks the [2.2.2] ring system. However, polymer **5** that has only [2.2.2] substituted phenylenes in the polymer backbone still displays excimer behavior in thin films, though with weaker intensity (I_{AA^*}/I_{A^*}) than those observed for films of polymer **1** with similar optical density. Moreover, polymer **7** bearing two bulky perfluorooctyl groups, which was originally prepared to reduce interchain contacts, exhibits a stronger tendency for excimer formation (larger I_{AA^*}/I_{A^*}) than polymer **1** (Figure 5.3). The stabilization energy of the excimers, which is the energy difference between the single

chain A* and excimer AA* emission maxima, is almost the same for films of polymers **1** (0.33 eV), **5** (0.31 eV), and **7** (0.33 eV). These values are also consistent with the stabilization energies for excimers of conjugated polymers reported in the literature.^{4,11}

Polymer **3** differs significantly from polymers **1** and **7** in that it has electron-donating alkoxy substituents instead of perfluoroalkyl groups attached to alternating phenylenes. The oxygen groups tend to raise HOMO levels and hence **3** has a lower band-gap than the other polymers and further displays an excimer emission, which in concert with **1**, **5**, and **7**, increases in intensity with film thickness (Figure 5.4), but is generally less intense and has a smaller stabilization energy (0.25 eV) than the other excimer forming polymers. However, due to the smaller excimer stabilization energy associated with polymer **3**, the exciplex emission may overlap with higher-order vibronic transitions associated with a single-chain emission and that as a consequence the relative contributions of each of these species to the red-shifted emission remains undetermined.

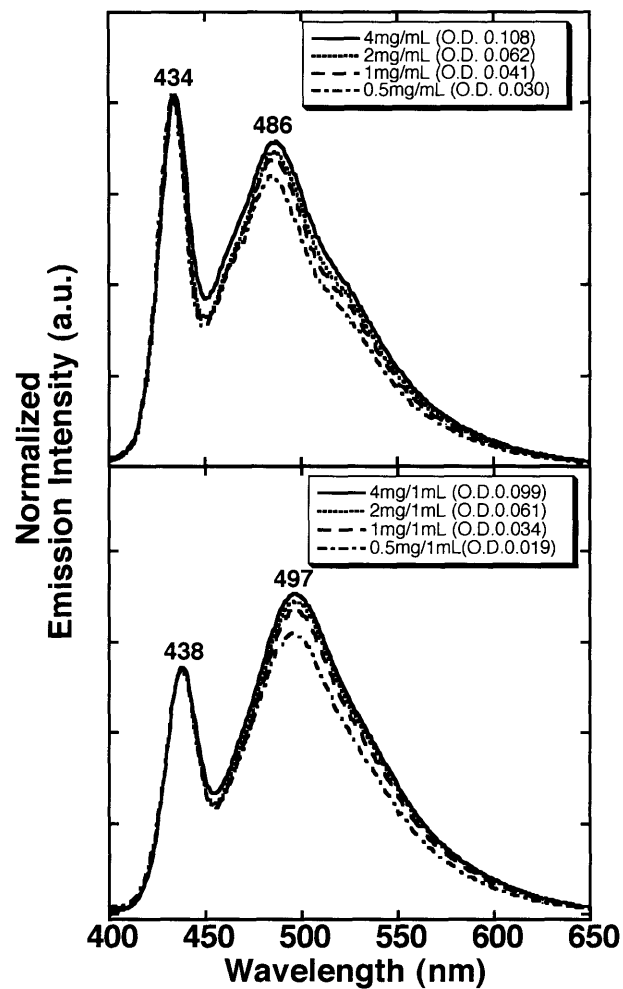


Figure 5.3. The emission spectra of polymer 5 (top) and polymer 7 (bottom) films as a function of film thickness.

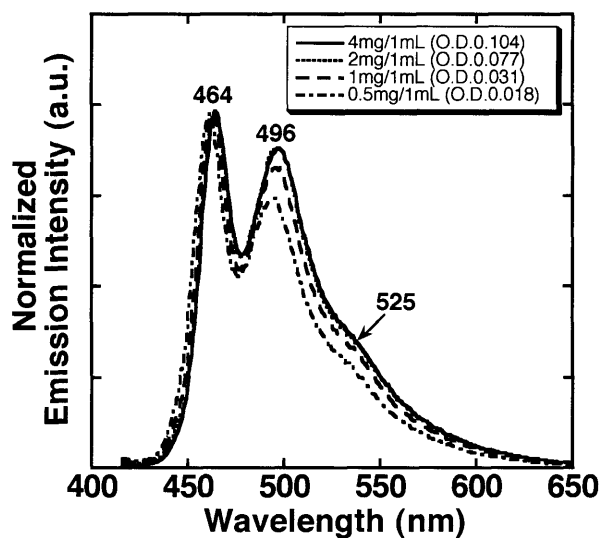


Figure 5.4. The emission spectra of polymer **3** films as a function of film thickness.

Time-resolved photoluminescence decay dynamics

To rule out the possibility that our excimer emission is not merely a vibrational band enhanced by certain nuclear coordinates of the polymers in thin films and concentrated solutions, we measured time-resolved photoluminescence decay dynamics of polymer **1** and **2** in solution and thin films using a streak camera technique (Figure 5.5).¹² In particular the observation of different lifetimes for the two emission peaks observed will confirm that they are not from the same emissive state. Polymer **2** does not display the excimer behavior in thin films and hence it serves as a reference. In dilute solution (ca. 10^{-6} M, THF) wherein we observe emission strictly from isolated chains, A^* , both polymers **1** and **2** exhibited a single exponential decay with lifetimes of 0.46 ns and 0.36 ns respectively. The excited state decay dynamics of thin films of CPs are typically shorter and multi-exponential in character, which is an indication of different organizations and energy transfer processes. Thin film of polymer **2** ($OD = 0.10 \pm 0.02$)

were found to have a single exponential lifetime of 0.14 ns at 434 nm and it has bi-exponential lifetimes of 0.13 ns (94.1%) with a small portion (5.9%) of a longer lived excited state (0.99 ns) at 461 nm. The PL decay dynamics of polymer **1** are more interesting and thin films (OD = 0.10 ± 0.02) were best described by bi-exponential lifetimes of 0.09ns and 0.34 ns at 443 nm and 0.10 ns and 0.99 ns at 494 nm, respectively. In this case the contribution of the longer lived excited state at 496 nm is increased (26.2%). The faster decays at shorter wavelength for both polymer **1** and **2** films are suggestive of fast exciton diffusion to low energy sites. The longer-lived emitting species at 494 nm for polymer **1** film is consistent with the expected longer radiative lifetimes typical of excimers and its large difference from the 443 nm emission clearly confirm that it is a different emissive state.

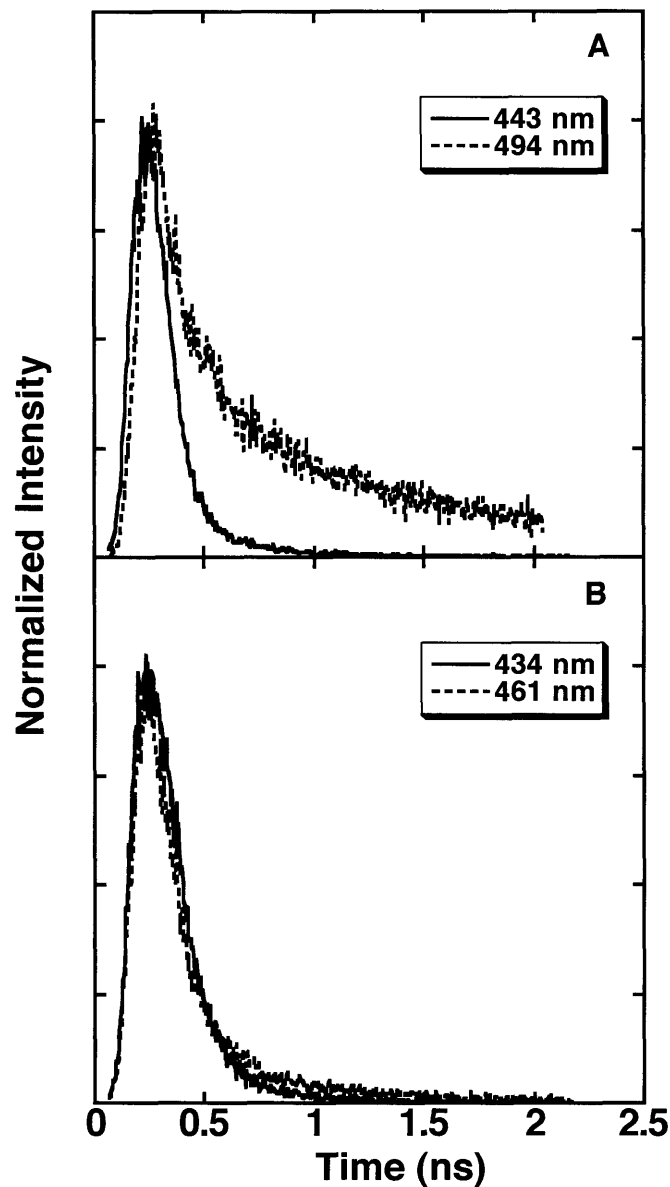


Figure 5.5. Time-resolved emission decays of polymer films (a) 1 and (b) 2. Polymer 1 bi-exponential decays gave lifetimes of 0.09ns (96.3%) and 0.34 ns (3.7%) for 443 nm and 0.10 ns (73.8%) and 0.99 ns (26.2%) for 494 nm. Polymer 2 a single exponential decay that was fit a lifetime of 0.14 ns for 434 nm and bi-exponential decay yielded lifetimes of 0.13ns (94.1%) and 0.99 ns (5.9%) for 461 nm.

One of the most striking features of the excimers reported in this chapter is their relatively high quantum yields that are apparent from casual inspection. The quantum

yields for polymers **1** and **2** are similar in solution (0.87 and 0.84, respectively) and the solid state (0.21 and 0.22 respectively). This result indicates excimer emission from polymer **1** thin film does not affect its quantum yield more than would be expected from a solid-state structure devoid of excimers. We also determined the quantum yield of polymer **1**:PMMA films at concentrations below those producing excimers (2 wt% polymer **1** /PMMA) and determined a value of 0.81, which compares favourably with the solution values. Of the excimer forming materials, polymer **3** stands out as having lower quantum yields both in solution (0.59) as well as in solid state (0.05). It is possible that the donation properties of the alkoxy groups give rise to non-radiative transitions having charge transfer characteristics.

X-ray diffraction studies

Central to understanding interchain interactions in CPs is the determination of the structure of aggregates. Given the pivotal nature of [2.2.2] ring system in excimer formation we sought to investigate if any unusual interactions could be identified in crystals of the monomers **8** and **9**. Although both the syn- and anti-isomers are produced in approximately 1:1 ratio in the synthesis we found that the anti-isomers gave crystals suitable for X-ray diffraction studies. As shown in Figure 5.6, the perpendicular distances (*a*) for **8** and **9** between two central aromatic rings in neighbouring molecules are similar, with values of 8.456 Å and 8.483 Å, respectively. The most interesting aspect of the structures is the parallel alignment and close spacing (*b*) of 4.029 Å for **8** and 4.228 Å for **9** between phenylenes constituting one of the bridges of the [2.2.2] bicyclic system. The closer spacing of 4.029 Å in **8** is sufficient to cause intermolecular

electronic coupling^{1,3} and we note that this monomer is responsible for producing excimer properties. This feature suggests that electronic interactions with the pendant groups of the [2.2.2] ring system are responsible for the excimers observed for polymer **1**, **3**, **5**, and **7**. The greater steric demands of the trifluoromethyl groups in monomer **9** may prevent interactions and we see no evidence of strong interpolymer electronic interactions for polymers **2**, **4**, and **6**.

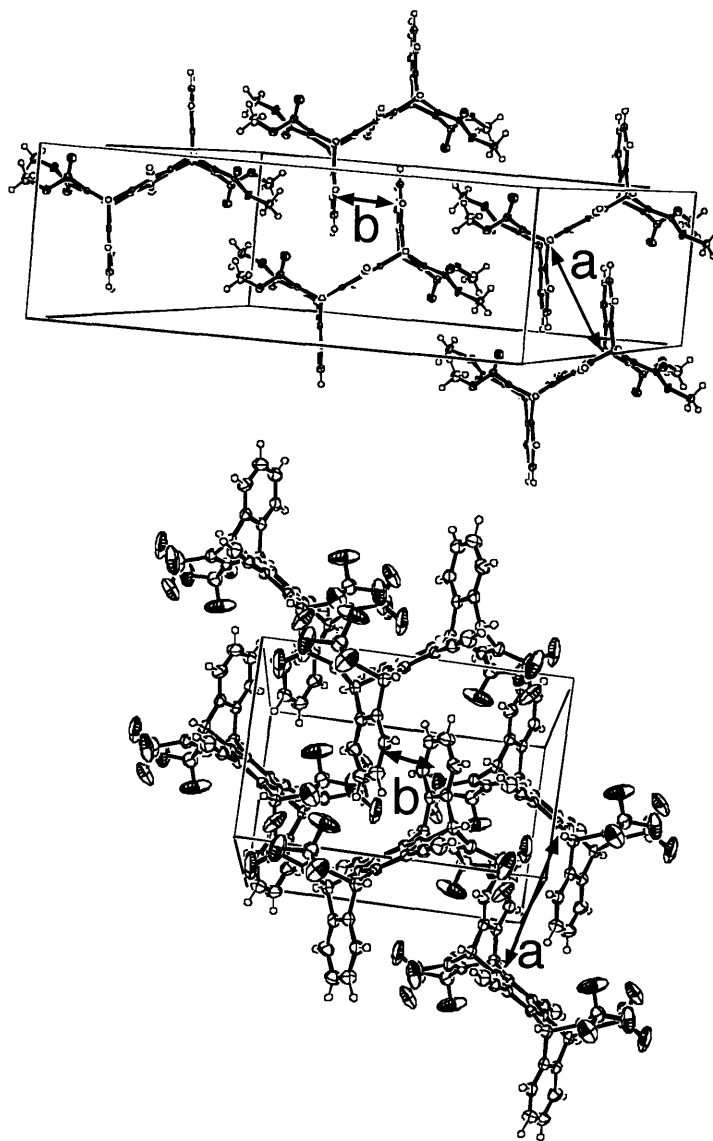


Figure 5.6. A perspective view of crystal packing of monomers **8** (top) and **9** (bottom).

Computer modeling of model compounds

To further investigate interchain interactions which can result in the different photophysical behaviors of polymer films (**1** vs **3**), we performed computer modeling of model compounds **12** and **13** with energy minimization using Gaussian (semi-empirical PM3 calculation). Both perfluoroalkyl side chains in compound **12** and alkyloxy side chains in compound **13** adopt a regular all trans conformation. As shown in Figure 5.7, the compound **12** has a little twisted geometry where a torsion angle of 22° is observed between the [2.2.2] bicyclic ring-based phenyl ring and the perfluoroalkylphenyl ring, whereas the phenyl ring having the alkoxy side chains ($\text{OC}_{11}\text{H}_{23}$) and conjugated backbones in compound **13** lie on the same plane.

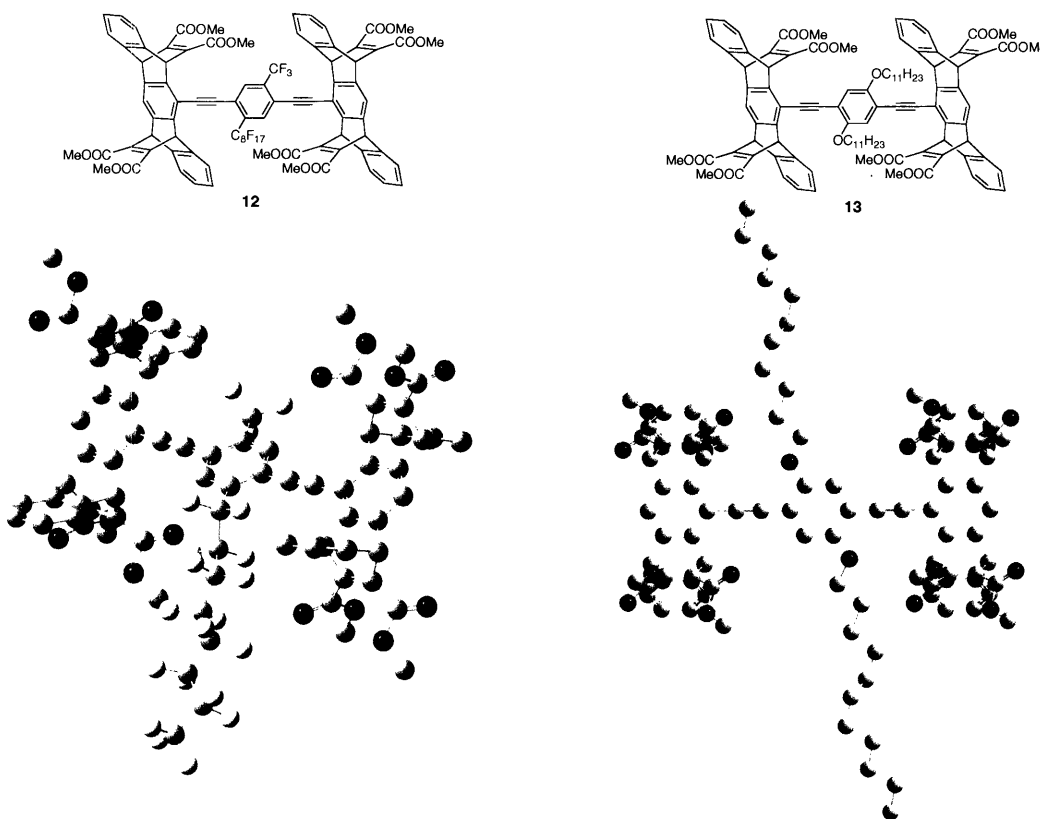


Figure 5.7. Semi-empirical simulations (PM3) of model compounds with energy minimization. The structure is shown in inset. (Hydrogens are omitted in images for clarity.)

Study of interchain interaction on Langmuir-Blodgett monolayer

Structural correlations in polymer aggregates are complicated by the disorder that is inherent to polymers assembling from solution random coil conformations. However, the conformational disorder in PPEs can be greatly restricted by confining them to a monolayer at the air-water interface. When densely assembled in this two-dimensional state the polymer chains exhibit high persistence length¹³ and the adjacent polymer chains are organized in a parallel fashion. As a result, Langmuir-Blodgett techniques have proven their utility in the study of conjugated polymers and in controlling the structure of their self-assembled films,¹⁴ and we have shown that *in situ* spectroscopic measurements can be used to better understand inter- and intra-chain effects.¹ To utilize these methods to elucidate the interactions generating excimers, we have studied polymer 7, which form highly stable and luminescent Langmuir monolayers with an extrapolated area of 170 Å² per repeating unit (Figure 5.8). Perfluoroalkyl side chains such as those present in polymer 7 are best known for their hydrophobicity,¹⁵ and hence they are predicted to remain outside the water subphase. Given their *para*-substitution we would expect the phenylene to organize with a *face-on* orientation of the arene ring coplanar to the air-water interface. The preferred orientation of the arene ring bearing the more hydrophilic ester substituted bicyclic framework is not as easily predicted. However, the characteristic bathochromic shifts observed in the fluorescence excitation (24 nm) and emission (7 nm) maxima of polymer 7 in Langmuir films (Figure 5.8) with respect to their solution values are consistent with an extended effective conjugation length associated with an entirely *face-on* organization of the polymer main chain at the air-water interface. As the monolayer is compressed, the surface pressure

increases until the monolayer folds into multilayers at 33 mNm^{-1} . As indicated by the P-A isotherm for polymer **7** (Figure 5.8, inset), the folding into multilayers is largely irreversible, possibly due to the formation of aggregates promoted by the association of perfluoroalkyl side-chains that are more conformationally rigid than simple alkanes. The fluorescence excitation and emission spectra of Langmuir monolayers of polymer **7** show minimal variations as the surface pressure is increased, and do not present an excimer emission band at 497 nm. However, as the monolayer is folded into multilayers, a strong excimer emission appears. We interpret these observations to be consistent with the requirement for coincident orientation of the polymers and subtle organizations between adjacent polymer chains to give rise to the excimer emission. We further find this observation to be consistent with our earlier suggestion based on **8**'s crystal structure that the fused pendant arene groups defining the [2.2.2] ring systems are responsible for the excimer emission. Below the pressure at which the monolayer collapses into multilayers, the arene rings of the polymer main chain are constrained to the plane of the air-water interface due to its *face-on* structure. As the monolayer collapses into multilayers, this conformational restriction is released and face-to-face interaction between pendant arene units on adjacent polymer chains becomes possible.

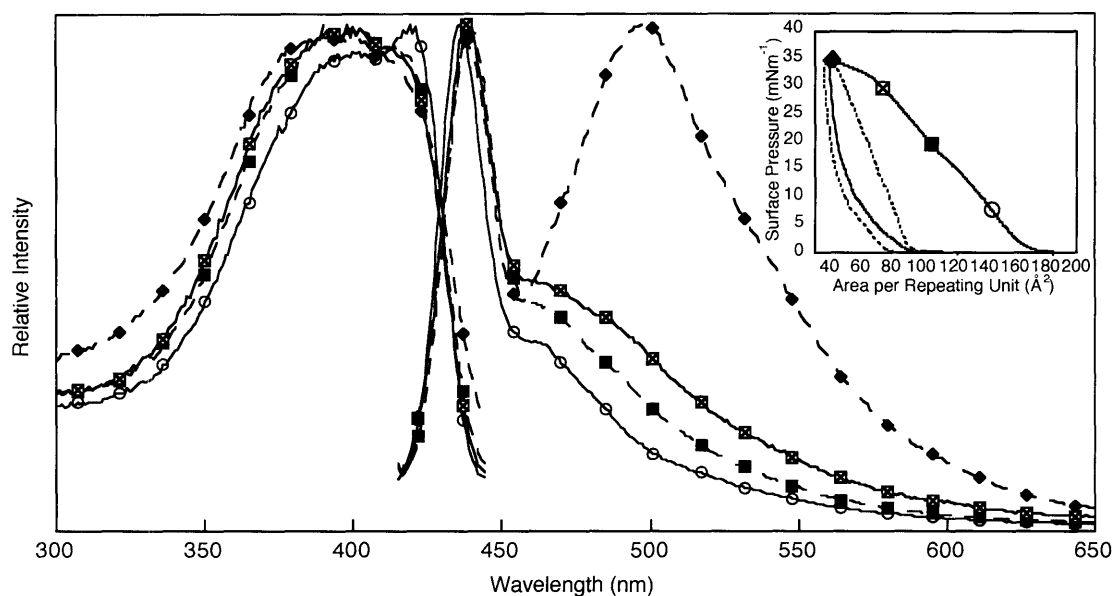


Figure 5.8. Normalized fluorescence excitation and emission spectra of Langmuir monolayers of polymer 7 of during cycles of compressions and expansions. Inset: Pressure-area (P-A) isotherms of polymer 7, first (solid line) and second (dashed line) compression cycles.

Conclusion

In summary, spectroscopic results showed the existence of highly emissive excimers in polymer 1, 3, 5 and 7 films with ester groups appended on [2.2.2] bicyclic ring systems. The photophysical behaviors from these systems are consistent with classical exciplexes known for low molecular weight systems. The present evidence suggests that the pendant arene groups of the [2.2.2] bicyclic ring system are responsible for generating the intermolecular interactions the produce a bright excimer emission. The ability to design excimers on demand has important ramifications for the development of sensors as well as light emissive devices. The [2.2.2] bicyclic ring system reported in this chapter represents a significant advance to that goal by faithfully generating excimer emission in four different polymers. Our ongoing investigations are directed at

discovering other excimer promoting structures and exploiting this behavior in sensory schemes.

Experimental Section

General Methods. NMR (^1H and ^{19}F) spectra were recorded on a Varian Mercury-300 MHz. The ^1H chemical shifts are given in units of δ (ppm) relative to tetramethylsilane (TMS) where δ (TMS) = 0, and referenced to the residual solvent. ^{19}F -NMR chemical shifts are reported in units of δ (ppm) or Hz relative to trichlorofluoromethane as the reference. Melting point determinations were performed using a Laboratory Devices MEL-TEMP instrument (open capillaries used) and are reported uncorrected. High-resolution mass spectra were obtained with a Finnigan MAT 8200 system using sector double focus and an electron impact source with an ionizing voltage of 70 V. The molecular weights of polymers were determined by using three PLgel 5 μm (300 x 7.5 mm) columns in series and a diode detector at 254 nm at a flow rate of 1.0 ml/min in THF. The molecular weights are reported relative to polystyrene standards purchased from Polysciences, Inc. Polymer thin films were prepared by spin casting from 0.05 - 0.4 wt% solutions in CHCl_3 on glass substrates (18 mm x 18 mm) using an EC101DT photo resist spinner (Headway Research, Inc.). Thin films of solid solutions of a conjugated polymer in PMMA were similarly prepared from CHCl_3 solutions. UV-vis spectra were obtained from Hewlett-Packard 8452A diode array or Cary 50 UV-Visible Spectrophotometers. Fluorescence studies were conducted with a SPEX Fluorolog- τ 2 fluorometer (model FL112, 450 W xenon lamp) equipped with a model 1935B polarization kit. The spectra in solution were obtained at 25 $^\circ\text{C}$ using a quartz cuvette

with a path length of 1 cm. Polymer thin film spectra were recorded by front-face (22.5°) detection. Fluorescence quantum yields of polymers in CHCl₃ solution were determined relative to equiabsorbing solutions of quinine sulfate ($\Phi_F = 0.53$ in 0.1 N sulfuric acid). The solid state quantum yields were obtained relative to 9,10-diphenylanthracene in poly(methyl methacrylate) (PMMA) ($\Phi_F = 0.83$, 10⁻³ M) as a reference. Time resolved fluorescence measurements were performed by exciting the samples with 170 femtosecond pulses at 390 nm from a Coherent RegA Ti:Sapphire amplifier. The resulting fluorescence was spectrally and temporally resolved with a Hamamatsu C4770 Streak Camera system.

Materials. All solvents were spectrophotometric grade unless otherwise noted. Anhydrous THF, DMSO, toluene and diisopropylamine were purchased from Aldrich Chemical Co., Inc. All other compounds were purchased from Aldrich and used as received. All air and moisture-sensitive synthetic manipulations were performed under an argon atmosphere using standard Schlenk techniques. Silica gel (40 μm) was obtained from J. T. Baker.

1,4-bis(perfluorooctyl)benzene (10). Perfluorooctyl iodide (18.2 g, 33 mmol) was added dropwise over 10 min to a stirred mixture of copper powder (4.3 g, 67.5 mmol) in dry DMSO (30 mL) at 140 °C. After 45 min, 1,4-diiodobenzene (5.0 g, 15 mmol) was added and the mixture was stirred for 3 days at this temperature. After cooling to room temperature, aqueous ammonia (50 mL) was added and the supernatant was decanted. The solid was washed with several portions of aqueous ammonia. The solid was then partially dissolved in boiling toluene (500 mL) and filtered, giving a light yellow filtrate with a white precipitate. The filtrate was cooled to room temperature, and the resulting

second crop, which precipitated upon cooling, was filtered. The combined white precipitates were washed with toluene (2 x 100 mL) and methylene chloride (2 x 100 mL) and dried to give the product **10** as a white solid (4.7 g, 35%): m.p. 98-100 °C; ¹H NMR (300 MHz, CDCl₃): δ 7.77 (s, 4H); ¹⁹F NMR (282 MHz, CDCl₃): δ -81.5, -111.8, -121.7, -122.2, -122.4, -123.1, -126.5; HR-MS (EI) calcd. for C₂₂H₄F₃₄ ([M]⁺): 913.9765, found ([M]⁺): 913.9738.

2,5-dibromo-1,4-bis(perfluorooctyl)benzene (11). Into a 100 mL round-bottomed flask were placed 20 mL trifluoroacetic acid, compound **10** (300 mg, 0.328 mmol), and 6 mL H₂SO₄ (98%). The mixture was stirred vigorously and N-bromosuccinimide (175 mg, 0.984 mmol) was added in portions at 70 °C over a 5-hour period. After stirring at 70 °C for 2 d, the mixture was poured into 50 mL of ice-water. The precipitates were filtered and recrystallized from toluene to give a white solid **11** (105 mg, 30%): m.p. 129-130 °C; ¹H NMR (300 MHz, CDCl₃): δ 7.95 (s, 2H); ¹⁹F NMR (282 MHz, CDCl₃): δ -81.1, -108.1, -119.7, -121.6, -122.3, -123.1, -126.5; HR-MS (EI) calcd. for C₂₂H₂F₃₄Br₂ ([M]⁺): 1069.7975, found ([M]⁺): 1069.7939.

Polymers 1-7. The synthesis and characterization of the conjugated polymers **1-4** have been reported. A general procedure for polymer **5** and **6** is illustrated by the synthesis of polymer **5**.⁸

Polymers 5. Diacetylene monomer **8** (25 mg, 0.041 mmol), pentyptycene quinone (24.5 mg, 0.053 mmol), CuI (2.4 mg, 0.012 mmol), and Pd(PPh₃)₄ (1.2 mg, 0.001 mmol) were combined under Ar in a 25-mL Schlenk tube. To this were added 3 mL of toluene and 0.5 mL of diisopropylamine. The solution was stirred at 60 °C under Argon for 72 h. The reaction mixture was then cooled, taken up in 50 mL of chloroform, and extracted

with 10% NH₄Cl (3 x 40 mL). The organic phase was then dried (MgSO₄), and the solvent was removed under reduced pressure. This solid was redissolved in a minimum hot solvent and reprecipitated from methanol to give a green solid (16 mg, 64%). The solid was collected by filtration and washed repeatedly with hot methanol. Removal of oligomers and impurities was achieved by subjecting the solid to sequential extractions in a Soxhlet apparatus with MeOH, acetone, followed with chloroform. The chloroform fraction was characterized. ¹H NMR (300 MHz, THF-*d*₈): δ7.70 (br, 4H), 7.13 (br, 4H), 6.19 (br, 2H), 6.16 (br, 2H), 3.79 (br, 12H). **Polymer 6** (55%). ¹H NMR (300 MHz, THF-*d*₈): . 7.7-7.4 (br, 4H), 7.2-7.0 (br, 4H), 6.2-6.1 (br, 4H).

Polymer 7. Compound **8** (18 mg, 0.029 mmol), compound **11** (30 mg, 0.028 mmol), CuI (0.30 mg, 0.006 mmol), and Pd(Ph₃)₄ (3.2 mg, 0.003 mmol) were placed in a 25 ml Schlenk tube with a stir bar. The flask was evacuated and back-filled with argon three times, followed by the addition of diisopropylamine/toluene (1:2, 3 mL) under an atmosphere of argon. This mixture was heated at 70 °C for 3 days and then subjected to a CHCl₃/H₂O workup. The combined organic phase was washed with 10% NH₄Cl, and then dried (MgSO₄). The solvent was removed in vacuo, and the residue dissolved in chloroform was reprecipitated in methanol. The resulting precipitate was filtered and washed with MeOH to give a yellow solid (28 mg, 67%). Removal of oligomer and impurities was achieved by subjecting the solid to sequential extractions in Soxhlet extractor with MeOH, acetone, followed with chloroform. The chloroform fraction was characterized. ¹H NMR (300 MHz, THF-*d*₈): δ7.8-7.6 (br, 2H), 7.5-7.3 (br, 4H), 7.2-7.0 (br, 4H), 6.2-6.0 (br, 4H), 3.8-3.6 (br, 12H).

References

- (1) (a) Kim, J.; Swager, T. M. *Nature* **2001**, *411*, 1030–1034. (b) Kim, J.; Levitsky, I. A.; McQuade, D. T.; Swager, T. M. *J. Am. Chem. Soc.* **2002**, *124*, 7710–7718.
- (2) (a) Cornil, J.; dos Santos, D. A.; Crispin, X.; Silbey, R.; Brédas, J.-L. *J. Am. Chem. Soc.* **1998**, *120*, 1289–1299. (b) Blatchford, J. W.; Jessen, S. W.; Lin, L.-B.; Gustafson, T. L.; Fu, D.-K.; Wang, H.-L.; Swager, T. M.; MacDiarmid, A. G.; Epstein, A. J. *Phys. Rev B* **1996**, *54*, 9180–9189.
- (3) McQuade, D. T.; Kim, J.; Swager, T. M. *J. Am. Chem. Soc.* **2000**, *122*, 5885–5886.
- (4) We have found that systems having an apparent oblique orientation between polymer chains can display strong red shifts in their absorption and emission and also maintain high quantum yields. (a) Deans, R.; Kim, J.; Machacek, M.; Swager, T. M. *J. Am. Chem. Soc.* **2000**, *122*, 8565–8566. (b) Zahn, S.; Swager, T. M. *Angew. Chem. Int. Ed.* **2002**, *41*, 4225–4230.
- (5) Yang, Y.-S.; Swager, T. M. *J. Am. Chem. Soc.* **1998**, *120*, 11864–11873.
- (6) Kim, Y.; Zhu, Z.; Swager, T. M. *J. Am. Chem. Soc.* **2004**, *126*, 452–453.
- (7) Kim, Y.; Whitten, J.; Swager, T. M. submitted for publication.
- (8) Williams, V. E.; Swager, T. M. *J. Polym. Sci. A* **2000**, *38*, 4669–4676.
- (9) Williams, V. E.; Swager, T. M. *Macromolecules* **2000**, *33*, 4069–4073.
- (10) Levitsky, I. A.; Kim, J.; Swager, T. M. *J. Am. Chem. Soc.* **1999**, *121*, 1466–1472.
- (11) Li, H.; Powell, D. R.; Hayashi, R. K.; West, R. *Macromolecules* **1998**, *31*, 52–58.
- (12) Osaheni, J. A.; Jenekhe, S. A. *Macromolecules* **1994**, *27*, 739–742. The samples were excited at 391 nm with the doubled light. The laser repetition rate was 250 kHz, the pulsewidth was about 150 fs, and the average power was 15.4 W.

(13) PPEs have a relatively high persistence length of 15 nm in solution: Cotts, P. M.; Swager, T. M.; Zhou, Q. *Macromolecules* **1996**, *29*, 7323–7328.

(14) (a) Wegner, G. *Thin Solid Films* **1992**, *216*, 105–116. (b) Robitaille, L.; Leclerc, M. *Macromolecules*, **1994**, *27*, 1847–1851. (c) Kim, J.; McHugh, S.; Swager, T. M. *Macromolecules* **1999**, *32*, 1500–1507. (d) Rietzel, N.; Greve, D. R.; Kjaer, K.; Howes, P. B.; Jayaraman, M.; Savoy, S.; McCullough, R. D.; McDevitt, J. T.; Bjornholm, T. *J. Am. Chem. Soc.* **2000**, *122*, 5788–5800.

(15) Hong, X. M.; Tyson, J. C.; Collard, D. M. *Macromolecules* **2000**, *33*, 3502–3504.

Chapter 6:
Electron-Deficient Polyelectrolytes
For Biosensory Applications

Introduction

Fluorescent conjugated polymers (FCPs) are an emerging class of optical sensory materials due to their high sensitivity.¹ Recently, water-soluble ionic FCPs have been exploited with great interest for the detection of biological species, including sugars,² bacteria,³ proteins,⁴ and DNA.⁵ In general, the signal transduction mechanisms are based on analyte-modulated emission wavelength changes from facile energy transfer from polymer to dye acceptors or oxidative photoinduced electron transfer (PET) which results in a change of polymer's fluorescence intensity.⁶ In contrast to energy transfer-based systems where long-range dipole-dipole interactions dictate the response, PET-based sensors function by short-range electron transfer fluorescence quenching mechanisms. An efficient fluorescence quenching by PET process requires a strong electronic interaction between the donor and acceptor. In addition, the excited-state redox potentials for the electron transfer process must be energetically favorable.

In Chapter 4, we described a series of electron-deficient poly(*p*-phenylene ethynylene) (PPE) derivatives and demonstrated that they were able to selectively detect electron-donating aromatic compounds as a result of a combination of both dynamic and static quenching processes.⁷ In those systems the conjugated polymer backbones behave as excited-state oxidants of electron-donating analytes. The initial promising sensory results for the detection of indole in organic solvents or vapor phase, suggested to us that these materials should be useful in biosensing applications. In addition to high electron affinity of this material, which endows it with high photostability, it incorporates a three-dimensional [2.2.2] bicyclic ring system that increases the fluorescence quantum yield of polymer in aqueous solution where

most water-soluble FCPs suffer from low aggregation induced quantum yields.⁸ High quantum yields are required for the optimal sensory sensitivities of FCPs.

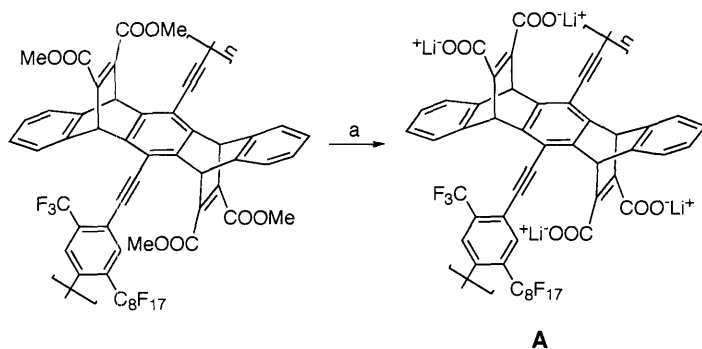
We report in this chapter synthesis and photophysical behavior of a water-soluble photo-oxidizing FCP, which is substituted with electron-withdrawing perfluoroalkyl and carboxylate groups. The fluorescence-based sensing responses of this polymer were examined to evaluate its potential application as PET-based sensors for the detection in aqueous buffer system of several amino acids, neurotransmitters, and proteins possessing electron-donating aromatic moieties.

Results and Discussion

Synthesis

We synthesized a water-soluble photo-oxidizing FCP, polymer **A**, through a postpolymerization alkaline hydrolysis (aqueous LiOH in THF-H₂O) of its ester precursor polymer (*M_n* 17 kDa, PDI=1.96), obtained by a Pd(0)/Cu(I)-catalyzed coupling of the corresponding monomers (Scheme 6.1). After hydrolysis, the reaction mixture was subjected to dialysis against distilled water to remove oligomers and low molecular weight polymer (MW cutoff: 10,000). The neutral precursor polymer is readily soluble in common organic solvents such as THF, chloroform, toluene, and xylenes but insoluble in water. However, the anionic polymer **A** was insoluble in organic solvents but completely soluble in water and DMF.

Scheme 6.1. Synthesis of polymer **A**.^a



^a(a) (i) LiOH, THF-H₂O (4:1), 50 °C, 2 d. (ii) dialysis, 3 d.

Photophysical properties

The photophysical properties of polymer **A** were investigated in aqueous solution. Absorption and fluorescence spectra of polymer **A** were obtained in water at different pH (pH 1 to 10) and phosphate buffer solutions (100 mM, pH 7.4) (Figure 6.1). The polymer features a strong absorption band which arises from a π - π^* transition with strong blue (or green) fluorescence. The emission spectra are strongly pH-dependent whereas the concomitant changes in the absorption spectra of polymers are minor. At neutral and basic media, the absorption and emission spectra of polymer **A** closely resemble the spectra of neutral precursor polymer in organic solvents ($\lambda_{\max(\text{abs})}$: 405 nm, $\lambda_{\max(\text{emi})}$: 432, 459 nm).⁹ The fluorescence of polymer **A** at high pH (pH ~ 10) appears as a relatively narrow and structured band, which is Stokes shifted by 39 nm from the absorption band. In contrast, under acidic conditions the fluorescence of polymer **A** broadens to give a less intense new band that is red-shifted from fluorescence maxima at high pH. This broad, red-shifted emission band is similar to that observed in the emission spectra of neutral polymer at high concentrated solutions and in the solid state. This suggests that the polymer **A** exists as isolated completely

soluble polymer chains at high pH and as aggregated chains at low pH due to hydrophobic and π - π interactions between polymers.¹⁰ These aggregates may also be stabilized by hydrogen bonding between COOH residues on adjacent chains.¹¹ The fluorescence quantum yield of anionic polymer A in water (pH 6~7) measured relative to quinine sulfate ($\Phi_F = 0.53$ in 0.1 N H₂SO₄) was 0.20, which is relatively high compared with known ionic PPE derivatives in aqueous solutions ($\Phi_F = 0.03$ –0.10).⁸

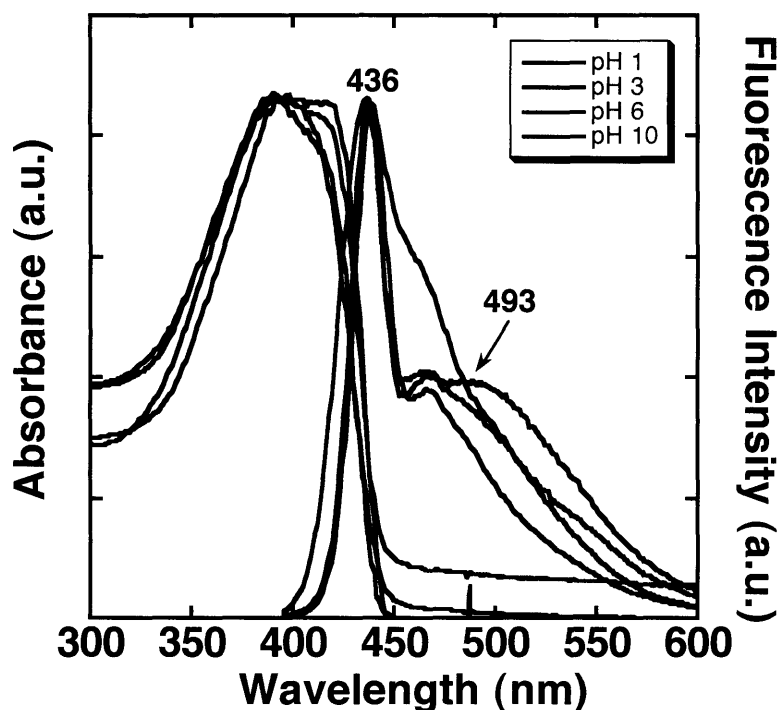


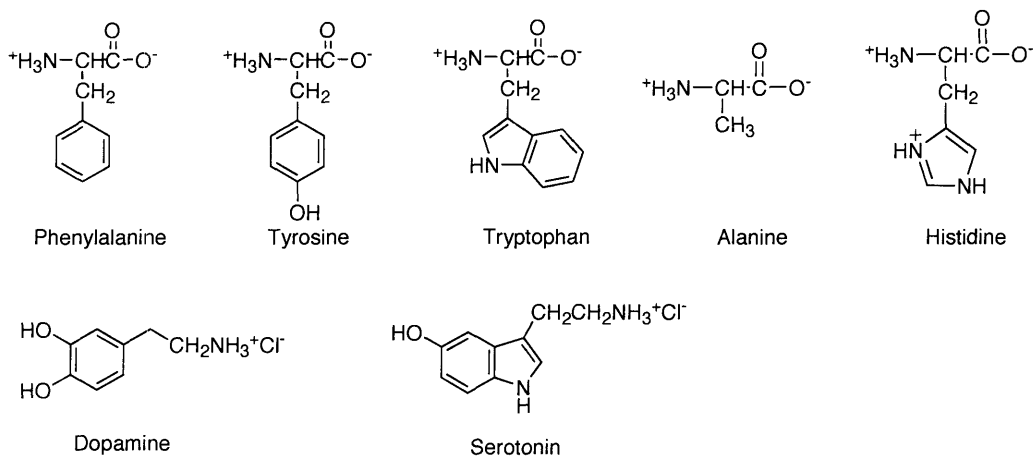
Figure 6.1. Normalized absorption and emission spectra of polymer A as a function of the solution pH. The optical density of polymer is 0.12 to 0.15 and the pH was adjusted with 0.1 N HCl or 0.1 N NaOH. ($\Phi_F = 0.03$ (pH 1), 0.05 (pH 3), 0.22 (pH 10))

Fluorescence quenching in solution

As detailed in Chapter 4, due to its high ionization potential the neutral precursor polymer showed a sensitivity opposite that of typical conjugated polymers in organic solvents. Namely it is sensitive to molecules that are easily oxidized such as indole.⁷ On the basis of these results, we anticipated that for polymer **A**, the effects of the electron-deficient polymer backbone as well as negatively charged carboxylated groups would contribute to give a high quenching efficiency with cation bearing analytes having electron-donating aromatic moieties in aqueous media.

Polymer **A**'s response to biologically important amino acids, neurotransmitters, and protein (Chart 1) was investigated. A feature common to all of the analytes selected (except alanine) is the presence of an aromatic system.

Chart 1



The relative fluorescence quenching efficiency of polymer **A** with given analytes was quantified in solution by determining the Stern-Volmer quenching constant (K_{SV}) using Stern-Volmer equation; $F^\circ/F = 1 + K_{\text{SV}}[\text{quencher}]$ (Table 6.1).

Table 6.1. Stern-Volmer quenching constants (M^{-1}) of polymer **A** with given analytes in aqueous media at 25 °C.

| Analytes ^a | PBS ^b | Water (pH 6) |
|-----------------------|-----------------------------|-----------------------------|
| Tryptophan | 1,400 ± 50 | 1,100 ± 30 |
| Tyrosine | NA ^c | NA ^c |
| Phenylalanine | ND ^d | ND ^d |
| Histidine | ND ^d | ND ^d |
| Alanine | ND ^d | ND ^d |
| Serotonin | 1.1 ± 0.2 × 10 ⁵ | 4.4 ± 0.3 × 10 ⁵ |
| Dopamine | 1.1 ± 0.1 × 10 ⁴ | 3.0 ± 0.2 × 10 ⁴ |
| Lysozyme | 6.1 ± 0.3 × 10 ⁶ | |

^aResults by L-amino acids were shown, but no difference was observed for D versus L.

^bPhosphate buffer solution (100 mM, pH 7.4). ^cNot available due to low solubility of tyrosine in neutral condition. ^dNo fluorescence intensity change was detected.

Figure 6.2 shows the changes of emission intensity of anionic polymer **A** upon titration with tryptophan in phosphate buffer solution (100 mM, pH 7.4). The addition of tryptophan to solution of polymer **A** results in a large decrease in the fluorescence intensity, which is not accompanied by new red-shifted emission peak. This result suggests that the fluorescence reduction is the result of analyte induced conformational changes but by an electronic interaction that produces facile quenching.

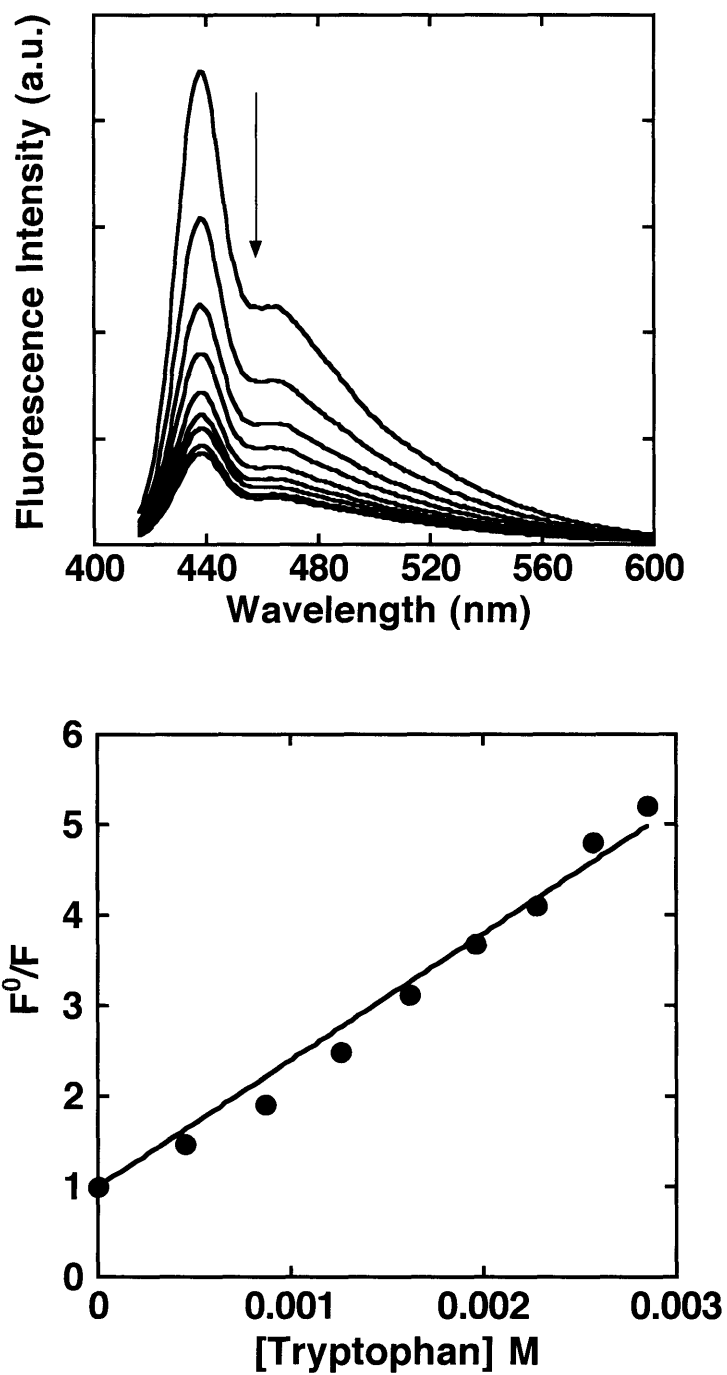


Figure 6.2. The changes in emission spectra (top) and S-V plot (bottom) of polymer A upon addition of tryptophan in phosphate buffer (pH 7.4). [Trp] = 0 to 3×10^{-3} M (top to bottom).

Since the predominant ionic form of amino acids is dependent on pH of solution, it will control the type of the interaction between the amino acids and anionic polymer. We would expect that on average, tryptophan (pI 5.89) would be negatively charged in the buffer solution (pH 7.4), suggesting that electrostatic repulsion may be predominate, making it less reactive with the anionic polymer **A**. Nevertheless, anionic polymer **A** exhibited K_{SV} of 1,400 M^{-1} with tryptophan, which is a 100-fold larger quenching efficiency relative to that observed for the neutral precursor polymer with indole in THF ($K_{SV} \sim 12 M^{-1}$). K_{SV} for tyrosine could not be obtained due to solubility problem in neutral conditions. Thus, to directly compare their fluorescence quenching responses, the K_{SV} was obtained in basic media (pH 10). The K_{SV} for tryptophan-polymer **A** ($80 M^{-1}$) was larger than that for tyrosine-polymer **A** ($16 M^{-1}$) at high pH. This effect is probably due to the greater electronic donor ability and hydrophobic character of the aromatic subunit of former compound.⁸ The presence of a hydrophobic interaction is supported by examining the effect of surfactant on the fluorescence quantum yield and quenching efficiency of this polymer. As generally observed in ionic FCPs, the fluorescence quantum yield of anionic polymer **A** at pH = 6~7 increased four-fold in the presence of surfactant (neutral, 0.8% Triton, X-100), suggesting that there is a hydrophobic interaction between the polymer chains in aqueous media.¹⁰ The addition of surfactant to a polymer **A** solution with tryptophan in water decreased the quenching efficiency by 35-fold, which is attributed to the a decreased interaction between conjugated polymer and quencher which lowers the efficiency of electron transfer processes.

Aromatic amino acids lacking an easily oxidizable aromatic ring (phenylalanine or alanine) did not produce fluorescence quenching responses with polymer **A** at high concentrations of quencher (up to 0.03 M) and at any pH. In addition, histidine, which has

isoelectric point higher than the pH of the buffer (pI 7.59), was expected to have ionic interactions as well as π - π interaction. However histidine did not produce any fluorescence quenching of polymer **A** even at high concentrations (up to 0.04 M) at any pH. These results suggest that efficient PET is the dominant factor in fluorescence quenching mechanism of a photo-oxidizing polymer **A** with amino acids with electron-donating aromatic units.

Fluorescence quenching responses of the electron-deficient anionic polymer **A** were further investigated with structurally related compounds such as an indole-based neurotransmitter, serotonin, and a catechol-based neurotransmitter, dopamine, in phosphate buffer solution (100 mM, pH 7.4). Specific detection of these analytes is important as a result of their significance to a number of biological processes.¹² Serotonin showed a larger fluorescence quenching response to polymer **A** than dopamine, as expected from its superior electron-donating abilities (Figure 6.3). In addition, the K_{SV} constants of the anionic polymer **A** with neurotransmitters, dopamine and serotonin, are higher than those for tyrosine or tryptophan. This larger fluorescence quenching originates from the formation of association complexes produced by electrostatic interactions between the positive charge on the neurotransmitter side chains and the anionic polymer. These data imply that while the intrinsic ET property conferred by the indole side chain of tryptophan quenches the fluorescence, the efficiency can be tuned over more than 2 orders of magnitude by controlling the analyte's charge.

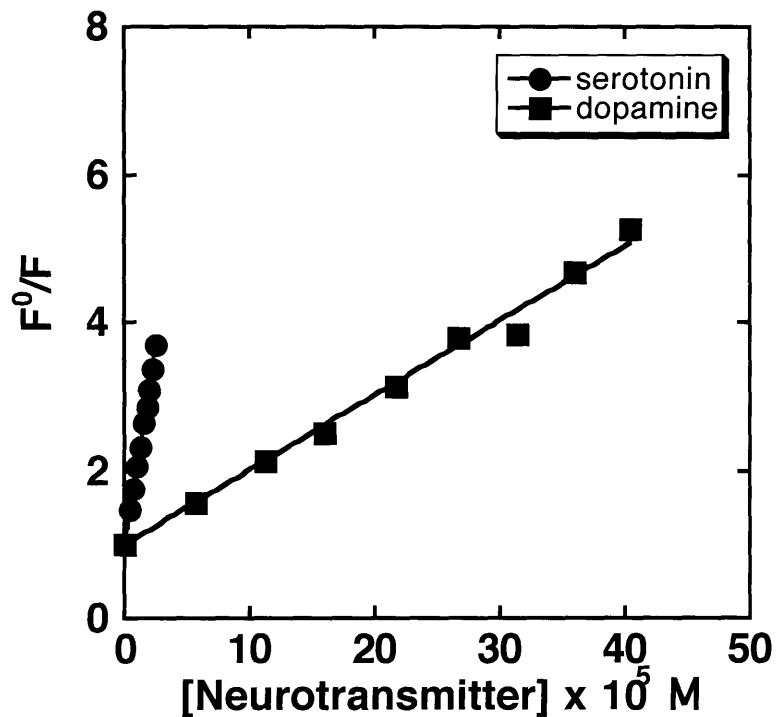


Figure 6.3. The S-V plots of anionic polymer A upon titration with neurotransmitters in phosphate buffer solution (pH 7.4).

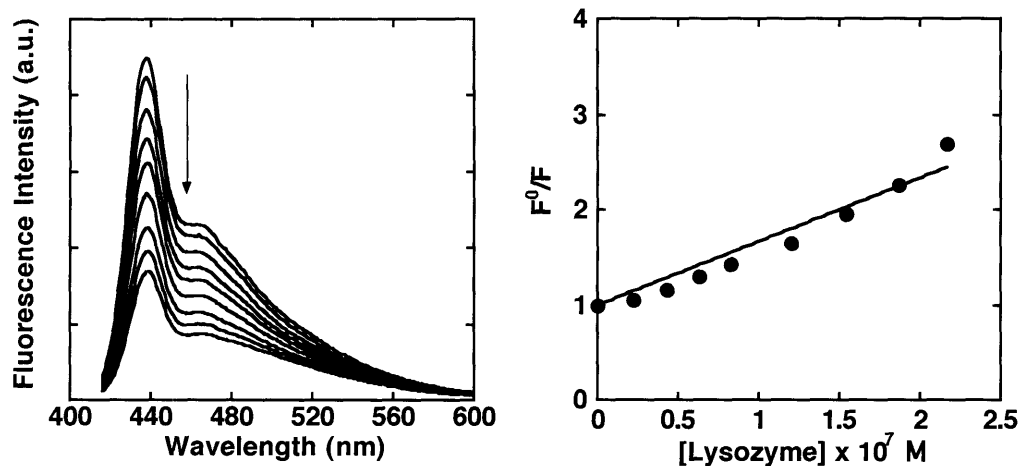


Figure 6.4. The changes in emission spectra (left) and S-V plot (right) of anionic polymer A upon addition of lysozyme in phosphate buffer (pH 7.4). [Lysozyme] = 0 to 2.5×10^{-7} M (top to bottom).

As shown in Figure 6.4, anionic polymer **A** was also investigated as a molecular probe to detect water-exposed tryptophan and tyrosine residues in a protein. As one example, lysozyme (chicken egg white, MW 14,307), which contains 6 tryptophans, showed a high fluorescence quenching response with polymer **A** ($K_{SV} \sim 6 \times 10^6 \text{ M}^{-1}$) in phosphate buffer solution (pH 7.4). Upon continued addition of lysozyme,¹³ the emission spectra of anionic polymer **A** did not show any saturation of quenching response or the presence of new peak, indicating the complete quenching responses of anionic polymer **A**. These results suggest that the mode of fluorescence quenching for polymer **A** with lysozyme is also an electron transfer process rather than the formation of weakly emissive aggregates, which was previously observed for a simple non-oxidizing polyanionic polymer.^{4b} We propose that complexation of anionic polymer **A** with the positively charged polyelectrolyte, lysozyme, would lead to the contraction of distance between polymer and analyte. The short distance will enhance the efficiency of electron transfer by increasing the local concentration of the quencher.

Conclusion

A new water-soluble photo-oxidizing FCP has been synthesized and characterized. In solution the fluorescence spectra of the polymer vary strongly with pH of solution due to aggregation of the anionic polymer at low pH. This work has shown that a water-soluble photo-oxidizing FCP could serve as a PET-based sensor for amino acids, neurotransmitters and proteins with electron-donating aromatic compounds in aqueous media. The results show that the quenching efficiency is strongly dependent on electrostatic interaction of the anionic

polymer and quencher as well as hydrophobic and electron transfer interactions between the polymer chains and quencher.

Experimental Section

Materials and Methods. Amino acids and serotonin and dopamine hydrochlorides were purchased from Aldrich. Chicken egg white lysozyme (14,307) was purchased from Sigma. All other chemicals were of analytical grade. Aqueous solutions were always freshly prepared with distilled water. Neurotransmitter solutions were used immediately after preparation. UV-vis spectra were obtained from Hewlett-Packard 8452A diode array or Cary 50 uv-visible spectrophotometer. Fluorescence spectra were measured with a SPEX Fluorolog- τ 2 fluorometer (model FL112, 450W xenon lamp) equipped with model 1935B polarization kit. The spectra in solution were obtained at 25 °C using a quartz cell with a path length of 1 cm.

Synthesis of anionic polymer A. A 50 mL round-bottom flask with a magnetic spin bar was charged with 20 mg of neutral polymer (0.017 mmol based on repeat unit). The polymer was dissolved in 8 mL of THF. To this was added aqueous LiOH (20 mg, 2 mL) and the mixture was stirred at 50 °C for 2 days. After removal of volatile fractions, the reaction mixture was subjected to dialysis against pure water (Pierce, Snakeskin, MWCO10000) for 3 days to give the anionic polymer A (12 mg). The NMR characterization of anionic polymer A was carried out in acid form obtained by treatment of HCl: ^1H NMR (300 MHz, $\text{THF-}d_3$): δ 8.9-8.8 (br, 1H), 8.7-8.6 (br, 1H), 7.5-7.4 (br, 4H), 7.1-7.0 (br, 4H), 6.5-6.4 (br, 4H), 5.9-4.0 (br, 4H).

Determination of Stern-Volmer Quenching Constants. The fluorescence quenching of was monitored by measuring the fluorescence intensity of the polymer upon addition of the

quencher. In order to determine S-V constants, a solution of polymer in phosphate buffer (100 mM, pH 7.4) was titrated with aliquots from a stock solution of the quencher containing polymer in order to keep the concentration of polymer constant during the titration. The Stern-Volmer quenching constants were determined by the fluorescence intensity at maximum emission wavelength using the following equation: $F^0/F = 1 + K_{SV}[Q]$.

References

- (1) (a) McQuade, D. T.; Pullen, A. E.; Swager, T. M. *Chem. Rev.* **2000**, *100*, 2537–2574. (b) Chen, L.; McBranch, D. W.; Wang, H.-L.; Helgeson, R.; Wudl, F.; Whitten, D. G. *Proc. Natl. Acad. Sci. U.S.A.* **1999**, *96*, 12287–12292. (c) Faïd, K.; Leclerc, M. *Chem. Commun.* **1996**, *24*, 2761–2762.
- (2) DiCesare, N.; Pinto, M.; Schanze, K. S.; Lakowicz, J. R. *Langmuir* **2002**, *18*, 7785–7787.
- (3) Disney, M. D.; Zheng, J.; Swager, T. M.; Seeberger, P. H. *J. Am. Chem. Soc.* **2004**, *126*, 13343–13346.
- (4) (a) Dwight, S. J.; Gaylord, B. S.; Hong, J. W.; Bazan, G. C. *J. Am. Chem. Soc.* **2004**, *126*, 16850–16859. (b) Fan, C.; Plaxco, K. W.; Heeger, A. J. *J. Am. Chem. Soc.* **2002**, *124*, 5642–5643.
- (5) (a) Ho, H. A.; Boissinot, M.; Bergeron, M. G.; Corbeil, G.; Dore, K.; Boudreau, D.; Leclerc, M. *Angew. Chem. Int. Ed. Engl.* **2002**, *41*, 1548–1551. (b) Nilsson, K. P. R.; Inganäs, O. *Nat. Mater.* **2003**, *2*, 419–410. (c) Liu, B.; Bazan, G. C. *J. Am. Chem. Soc.* **2004**, *126*, 1942–1943.
- (6) (a) McQuade, D. T.; Hegedus, A. H.; Swager, T. M. *J. Am. Chem. Soc.* **2000**, *122*, 12389–12390. (b) Murphy, C. B.; Zhang, Y.; Troxler, T.; Ferry, V.; Martin, J. J.; Jones, W. E., Jr. *J.*

- Phys. Chem. B* **2004**, *108*, 1537–1543. (b) Fan, L.-J.; Zhang, Y.; Jones, W. E., Jr. *Macromolecules* **2005**, *38*, 2844–2849.
- (7) Kim, Y.; Whitten, J.; Swager, T. M. to be published.
- (8) (a) Tan, C.; Pinto, M.; Schanze, K. S. *Chem. Commun.* **2002**, *5*, 446–447. (b) Kuroda, K.; Swager, T. M. *Chem. Commun.* **2003**, 26–27. (c) Pinto, M.; Schanze, K. S. *Synthesis* **2002**, *9*, 1293–1309.
- (9) Kim, Y.; Bouffard, J.; Swager, T. M. to be published.
- (10) Wosnick, J. H.; Mello, C. M.; Swager, T. M. *J. Am. Chem. Soc.* **2005**, *127*, 3400–3405.
- (11) Kim, B. S.; Chen, L.; Gong, J. P.; Osada, Y. *Macromolecules* **1999**, *32*, 3964–3969.
- (12) (a) Goodnow, T. M.; Reddington, M. V.; Stoddart, J. F.; Kaifer, A. E. *J. Am. Chem. Soc.* **1991**, *113*, 4335–4337. (b) Secor, K. E.; Glass, T. E. *Org. Lett.* **2004**, *6*, 3727–3730.
- (13) Chicken egg white lysozyme (MW = 14,307) was used.

Curriculum Vitae

Youngmi Kim

EDUCATION

- 9/2000 – present **Massachusetts Institute of Technology**, Cambridge, MA
Ph.D. in Chemistry
Research Advisor: Professor Timothy M. Swager
- 3/1992 – 2/1994 **Pohang University of Science and Technology**, Pohang, Korea
M.S. in Organic Chemistry
Research Advisor: Professor Dong-Han Kim
- 3/1988 – 2/1992 **Kyungpook National University**, Daegu, Korea
B.S. in Chemical Education

EXPERIENCE

- 1/2001 – present **Massachusetts Institute of Technology**, Cambridge, MA
Research Assistant, Laboratory of Professor Timothy M. Swager
- Synthesis and characterization of various poly(*p*-phenylenevinylene)s (PPVs) and poly(*p*-phenyleneethynylene)s (PPEs) containing perfluoroalkyl groups.
 - Study of their chemical and photophysical properties.
 - Investigation of potential applications as (bio)sensory and molecular optoelectronic device materials.
- 9/2000 – 12/2001 *Teaching Assistant*
Laboratory instructor in general chemistry lab
- 1/1999 – 6/2000 **Korea Atomic Energy Research Institute**, Daejeon, Korea
Senior Researcher at Radioisotope and Radiation Application Team
- Development of imaging agents for Tc-99m-based central neural system (CNS) receptors
- 3/1994 – 12/1998 *Researcher at Radioisotope and Radiation Application Team*
- Synthesis and characterization of Tc-99m and Re-188 complexes with Schiff base and phosphine ligands for myocardial perfusion imaging agents.
 - Synthesis of biodegradable and biocompatible ¹⁶⁶Ho-Chitosan complex and its aggregates.
 - Synthesis of Tc-99m carbonyl complex and their complexes with amino acids and investigation for renal and brain imaging agents.
 - Development of radiopharmaceuticals of Ca-45, P-32, I-131/125 for therapy and diagnosis.
- 3/1992 – 2/1994 **Pohang University of Science and Technology**, Pohang, Korea
Research Assistant, Laboratory of Professor Dong-Han Kim
- Synthesis of four stereoisomers of 2-benzyl-3,4-epoxybutanoic acid and investigation of their activities against carboxypeptidase A.
- 3/1992 – 12/1992 *Teaching Assistant*
Laboratory instructor in general chemistry lab and recitation instructor in general Chemistry

TRAINING EDUCATIONS and CERTIFICATIONS

- 10/1999 Certificate, IAEA Regional Training Workshop, Daejon, Korea
- 1/1998 – 5/1998 IAEA Fellowship Program,
Department of Chemistry, University of Missouri-Columbia, USA
(Professor Dr. Silvia Jurisson)
- 5/1996 – 7/1996 Certificate, Training Course for Radioisotope Application, Daejon, Korea
- 6/1995 Certificate, Regional Training Course by IAEA, Bangkok, Thailand

HONORS and AWARDS

- 1/1998 Fellowship (Awarded by IAEA)
Department of Chemistry, University of Missouri-Columbia, USA
- 10/1996 Award for Superior paper (Awarded by the Society of Korea Nuclear Medicine)
Title: Study on the preparation of new ¹⁶⁶Ho-Chitosan complex
and its macroaggregates for a potential use of internal
radiotherapy. *Kor. J. Nucl. Med.*, **1996**, 30, 351.
- 5/1996 Award for Superior Project (Awarded by Korea Atomic Energy Research Institute)
- 3/1988 Honor of 1st class, Full scholarship (Awarded by Kyungpook National University)

PUBLICATIONS

1. **Kim Y.**; Swager T. M. Ultra-stable n-type PPVs. *Chem. Comm.* **2005**, 5, 372.
2. **Kim, Y.**; Zhu, Z.; Swager. T. M. Hyperconjugative and Inductive Perturbations in Poly(*p*-phenylene vinylenes). *J. Am. Chem. Soc.* **2004**, 126, 452.
3. Jang, B.-S.; **Kim, Y.**; Choi, S.-M.; Shin, B.-C.; Choi, S.-J.; Hong, Y.-D.; Gwon, H.-J.; Park, K.-B.; Yun, H.-I. Synthesis of ^{99m}Tc-tricarbonyl precursors for labeling of bioactive molecules. *J. Kor. Nuc. Soci.* **2002**, 34, 146.
4. Hong, Y.-D.; Park, K.-B.; Jang, B.-S.; Choi, S.-J.; Choi, S.-M; **Kim, Y.** Holmium-166-DTPA as a liquid source for endovascular brachytherapy. *Nucl. Med. Biol.* **2002**, 29, 833.
5. Joh, C. W.; Park, C. H.; Kang, H. J.; Oh, Y. T.; Chun, M. S.; Kim, H. S.; Choi, B. I. W.; Park, K. B.; **Kim, Y.**; Kim, K. H.; Vahc, Y. W.; Jang, J. S.; Lee, B. K. Measurement of radiation absorbed dose in endovascular Ho-166 brachytherapy using a balloon angio-catheter. *Nucl. Med. Comm.* **2000**, 21, 959.
6. Oh Y T; Kim H S; Chun M; Kang H; Yoon M H; Kim J S; Kang S H; Joh C W; **Kim Y.**; Choi B I; Park K B; Park C. H. The effect of external electron beam on neointima in rat carotid artery injury model. *International journal of radiation oncology, biology, physics.* **1999**, 44, 643.
7. Kim, K. W.; **Kim Y.**; Park, K.-B. A study on the dose distribution produced by ³²P source form in the treatment for inhibiting restenosis of coronary artery. *Kor. J. Med. Phys.* **1999**, 10, 1.
8. Suzuki, Y. S.; Momose, Y.; Higashi, N.; Shigematsu, A.; Park, K.-B.; **Kim, Y.**; Kim, J.-R.; Ryu, J.-M. Biodistribution and kinetics of holmium-166-chitosan complex (DW-166HC) in rats and mice. *J. Nucl. Med.* **1998**, 39, 2161.
9. Lee, J. D.; **Kim Y.**; Park, K.-B. Radionuclide Therapy of skin cancers and Bowen's disease using a specially designed skin patch. *J. Nucl. Med.* **1997**, 38, 697.
10. Park, K.-B.; **Kim Y.**; Shin, B.-C.; Kim, J.-R. Study on the preparation of new ¹⁶⁶Ho-Chitosan complex and its macroaggregates for a potential use of internal radiotherapy. *Kor. J. Nucl. Med.* **1996**, 30, 351.
11. Kim, D. H.; **Kim Y.**; Li Z.-H.; Kim K.-B; Choi, S. Y.; Yun, M.; Kim S. A new type of carboxypeptidase A inhibitor: Design, Synthesis, and Mechanistic Implication, *Pure & Appl. Chem.* **1994**, 66, 721.

12. Kim, D. H.; **Kim Y.** Convenient preparation of all four possible stereoisomers of 2-benzyl-3,4-epoxybutanoic acid, Pseudomechanism-based inactivator for carboxypeptidase A via α -chymotrypsin-catalyzed hydrolysis. *J. Kor. Chem. Soci.* **1993**, *17*, 967.

PATENTS

1. Swager T. M.; **Kim Y.** Ultrastable, fluorescent, soluble, semiconductive organic polymers. US Provisional Patent Application Serial No.: 60/526,886.
2. Park, K.-B.; **Kim Y.**; Kim, J.-R. Radioactive chitosan complex for radiation therapy. Korean Patent Number.190975 (1998), US 5,762,903 (1998), EU 5,762,903 (1998).

PRESENTATIONS

1. "Synthesis and properties of electron deficient conjugated polymers" **Kim, Y.**; Zhu, Z.; Swager. T. M. 223rd National ACS Meeting, Orlando, FL, April 7 -11, **2002**.
2. "Electron deficient conjugated polymers: Highly stable molecular electronic materials" **Kim, Y.**; Zhu, Z.; Swager. T. M. Materials Research Society, Boston, MA, November 29 - December 02, **2003**.
3. "Hyperconjugative and Inductive Perturbations in Poly(phenylenevinylenes)" **Kim, Y.**; Swager. T. M. 6th International Symposium on Functional pi-electron (fpi) Systems, Ithaca, NY, June 14 -18, **2004**.

ACKNOWLEDGMENTS

I well remember the Commencement Day of 2001. I was watching a stream of graduates, and feeling a strong emotion. Those memories are still vivid in my mind: wondering whether studying away from home was really the right decision for our family, and whether I could finish all these things that seemed endless to me. Now I sit down to look back over the last five years filled with a lot of ups and downs. As I think about my years at MIT, I am overwhelmed at the number of people who have offered inspiration, support and encouragement to make this thesis possible. I will never be able to appropriately express my gratitude in a few words here, but there are many people who deserve special thanks.

I would first like to thank my thesis advisor, Tim Swager, for taking a shy and unconfident Korean student who could barely express herself into his group in the fall of 2000 and for guiding and supporting me throughout the past five years. It has been a great pleasure working with him during my PhD degree study. I have been a big fan of Tim, although my husband is very jealous about that. When I had little confidence in myself and my results, his unparalleled enthusiasm, variety of ideas, and confidence in me have always inspired me to push a little harder and to dig a little deeper. I am also grateful for the experience he provides to his students. Without his unlimited support and understanding, I would not have obtained significant results. He is now my standard as a boss for whatever I do in the future! One of the best things about working in Tim's group is the wonderful colleagues I have had. I would like to thank the former and current members for useful discussions, friendship, and technical assistance.

I knew nothing about conjugated polymers when I first joined the group. I was very fortunate to have Drs. Mark MacLachlan and Dave Simone as benchmates. They taught me a lot of synthetic skills and generously devoted a lot of their time to helping me out. They patiently answered all of my stupid questions and made my life at the lab quite enjoyable.

Among the many post-docs that came through the group, I wish especially to thank two Korean post-docs, Drs. Dongwhan Lee and Tae-hyun Kim, who contributed much to my first two years at MIT. I feel a tremendous amount of gratitude for their approach to science, for their help as I prepared my first-year oral exam, for proofreading my terrible drafts, and so much more. They have meant a lot to me. I will never forget the laughs and concerns we shared at lunchtime. I feel sorry for not giving enough attention to Hyuna Kang, Inja Song, and Changsik Song as much as I got the benefits from Dongwhan and Taehyun. I wish good luck to them for great results as Dr. Jinsang Kim made Tim happy.

I was also lucky to be surrounded by great colleagues in the office. Sam Thomas was always willing to answer my questions, including those on photophysics. I wish good luck to him, and I am waiting to see his own group website. John Amara was also willing to help me with anything I asked. I thank Dr. Koushik Venkatesan for his valuable time to help me and let me use his computer, as well as for his smiles and kindness. Dr. Guy Joly is a serious chemist and a serious joker; I wish I could have more time to work with them both.

Jessica Liao, Gigi Bailey, Juan Zheng, Drs. Anne McNeil and Dahui Zhao were all really valuable to me. Whenever and whatever we talked, I always felt their

friendship. They never hesitated to help me and listen to me. I owe them more than I can say. I hope that Jessica get fantastic results with my anionic polymer. I also wish good luck to Anne McNeil and Andrew Satrijo, who took over some parts of my project.

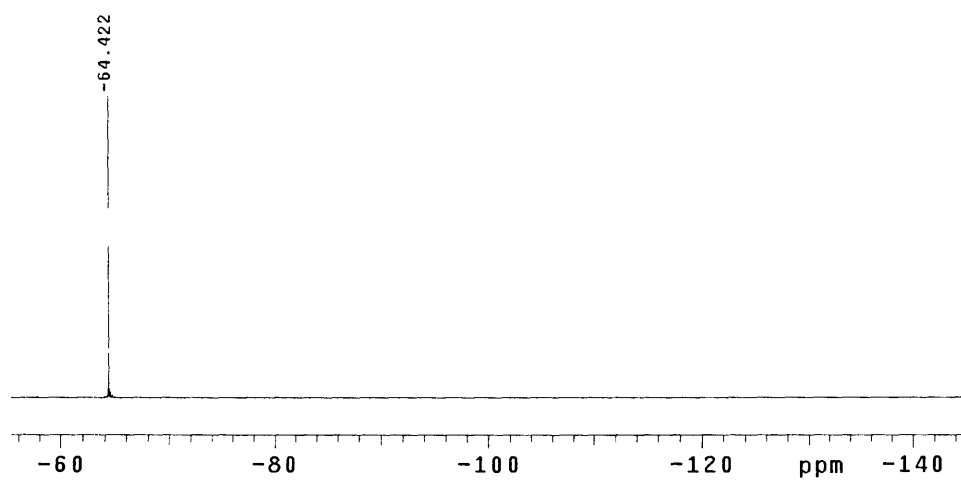
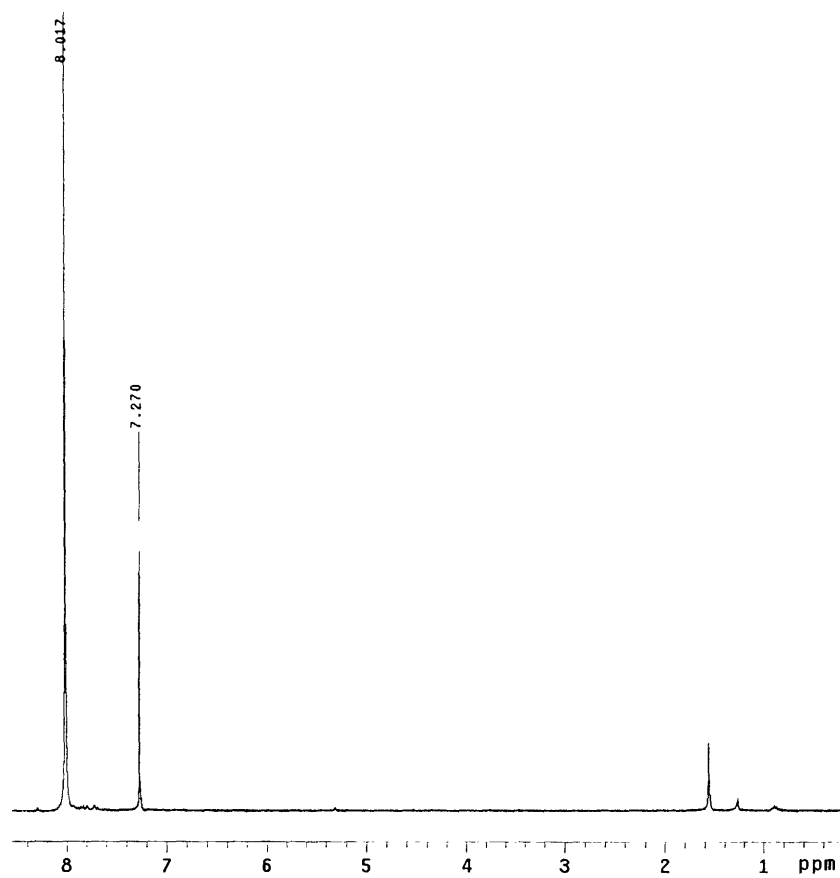
There are no words to adequately express my thanks to Jean Bouffard, my amazing benchmate. I was extremely lucky to have this very devoted chemist working next to me as a good consultant to talk about chemistry as well as so many other things. He gave me a lot of encouragement and laughter whenever I was depressed or exhausted. I can't be happy with any future benchmate since he completely spoiled me! I'll be forever grateful for his friendship that made a huge difference in my last couple of years at MIT.

Everybody has been always willing to baby-sit Hyunmo. I must say that I am so sorry for bothering them, and I am also so grateful for their valuable time. Many thanks go to Professor James Whitten and Dr. Steve Kooi for great contributions to my paper as collaborators. I would like to thank Rebekah Bjork and Simone Nakhoul for helping me considerably. I am indebt to Dr. Zhengguo Zhu for his compounds. Whenever I needed some compounds, I used to run and check his leftover compounds. I must thank Dr. Mark Wall of the MIT DCIF for his help with experimental aspects of NMR spectrometry, and Drs. Bill Davis and Peter Müller of the MIT x-ray crystallography lab for solving the crystal structures presented in Chapter 4 of my thesis. I appreciate the funding from ISN. I would like to thank Jean and Anne for taking their precious time to proofread my thesis and for giving their helpful comments and suggestions. Outside of my lab, Laura Moses from the Office of the Arts was my best friend and counselor. I miss the tea time we had, and I wish her a great life in South Carolina.

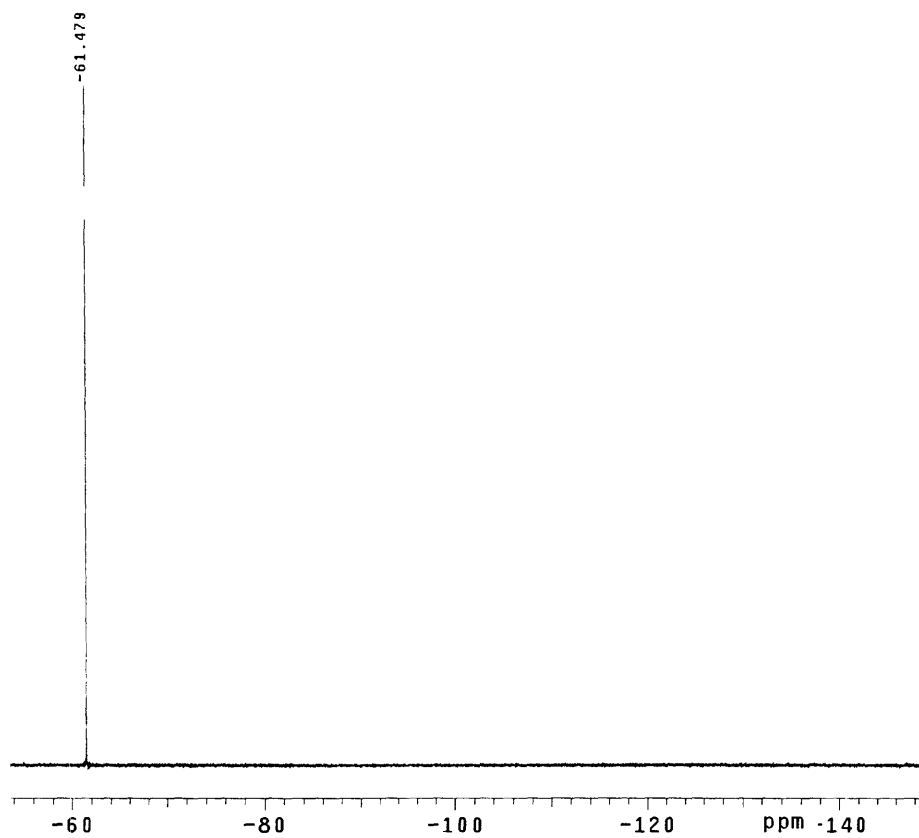
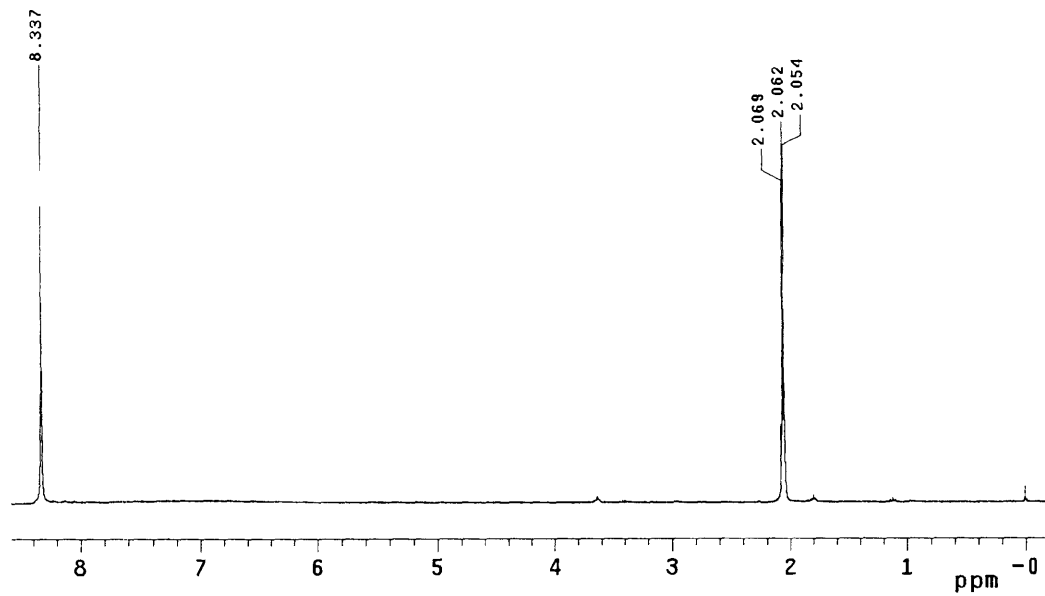
Last, but not least, I owe an enormous debt of gratitude to my family. My mother always does everything for me without expecting anything from me. She has always been concerned about me and my family here. (But she should know that my life here is not terrible at all. Moreover, the last five years have been the most valuable period of my life, which cannot be replaced by any materialistic thing.) Most of all, I have to thank my husband Bon-Cheol. I was never that brave woman who quitted a stable job to come here to study, the mother who left a three-year-old boy in Korea. Without his encouragement, support, and confidence in me, I would not have been able even to consider a PhD. Now, I am proud of myself. This is not because I have an MIT PhD, but because I came to this point without giving up. However, I know that the energy for me comes from my son Hyunmo. After he joined us at the beginning of my second year, all the advantages we had as a student couple for the first year were gone, and our daily life became very difficult. I felt as if I took all my exams twice, since my husband also had similar exams at his school. But Hyunmo was willing to lend all his fun, and was patient enough with my late return, or with staying with only one parent due to our schedules. He was an unbelievably good boy to us! Without the benefit of the love and sacrifice from Bon-Cheol and Hyunmo, I might not have completed my degree. I dedicate this to my son and my husband; I'm glad that our family can now have dinner together and spend more time together.

Appendix A:
NMR Spectra of Chapter 2

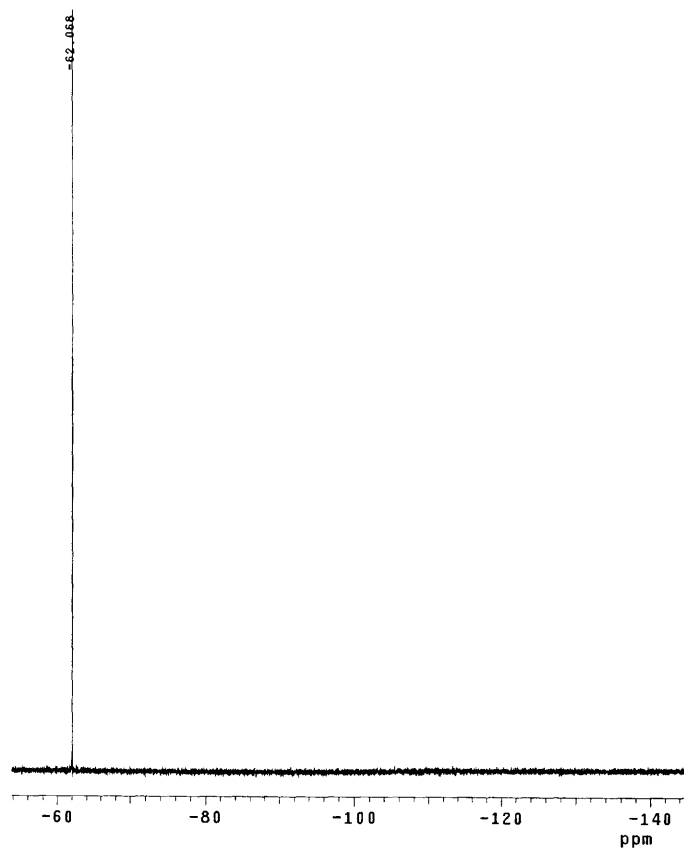
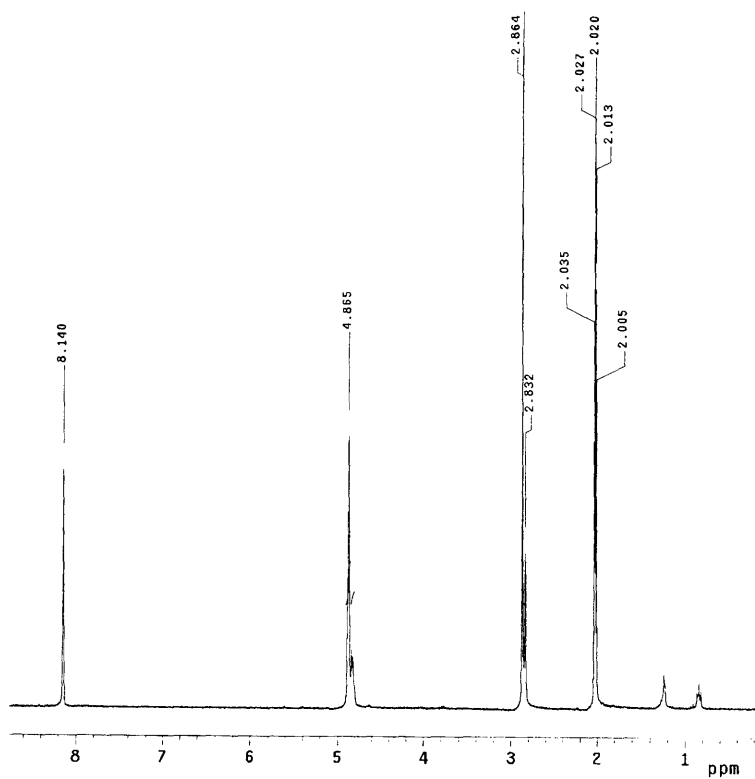
^1H NMR and ^{19}F NMR of **2** (CDCl_3)



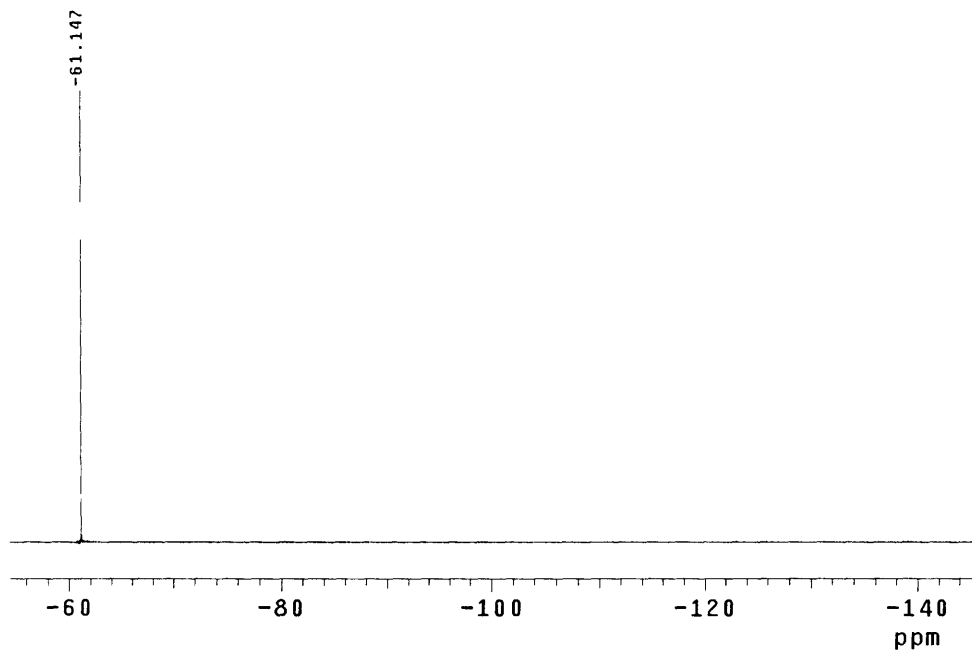
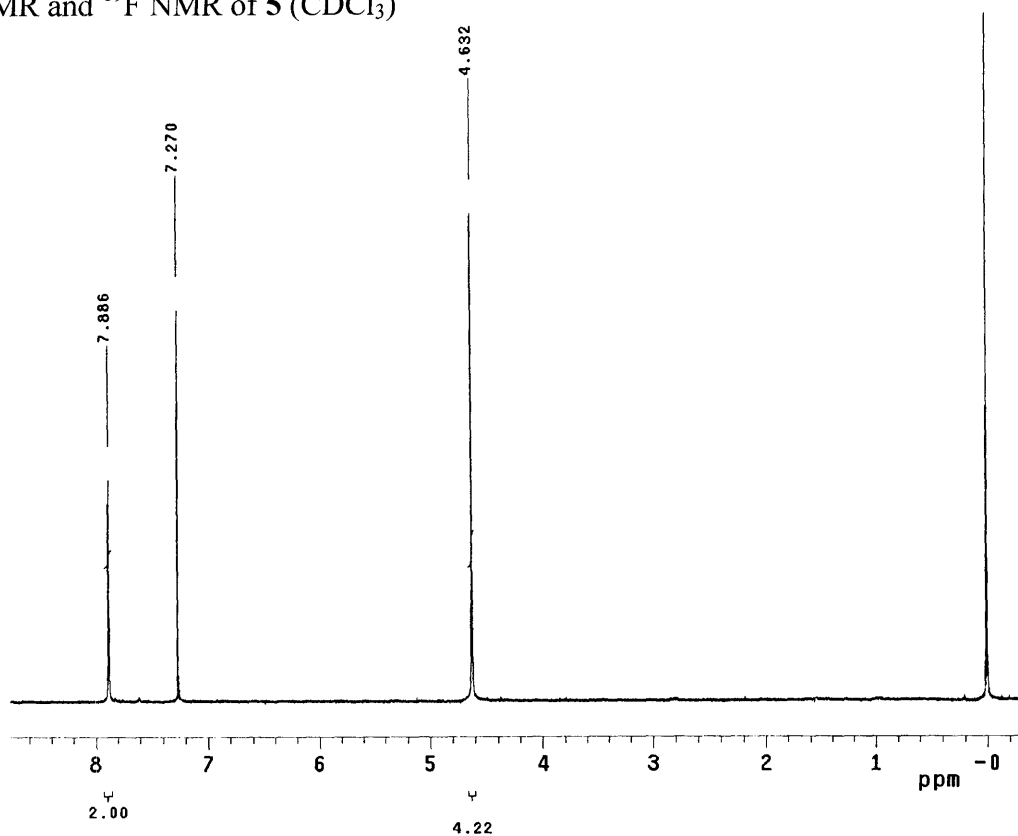
^1H NMR and ^{19}F NMR of **3** (Acetone- d_6)



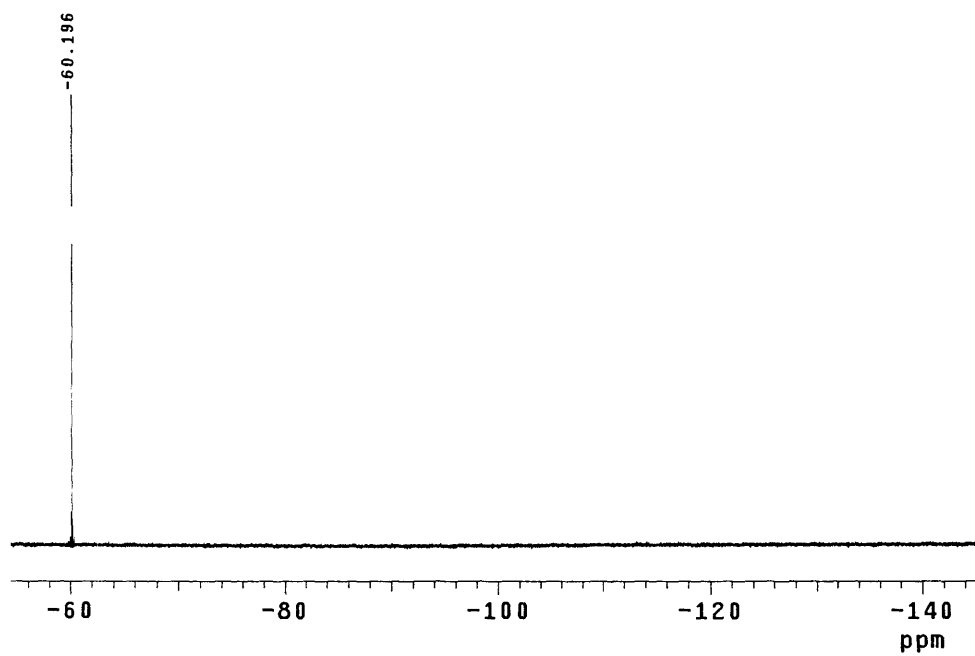
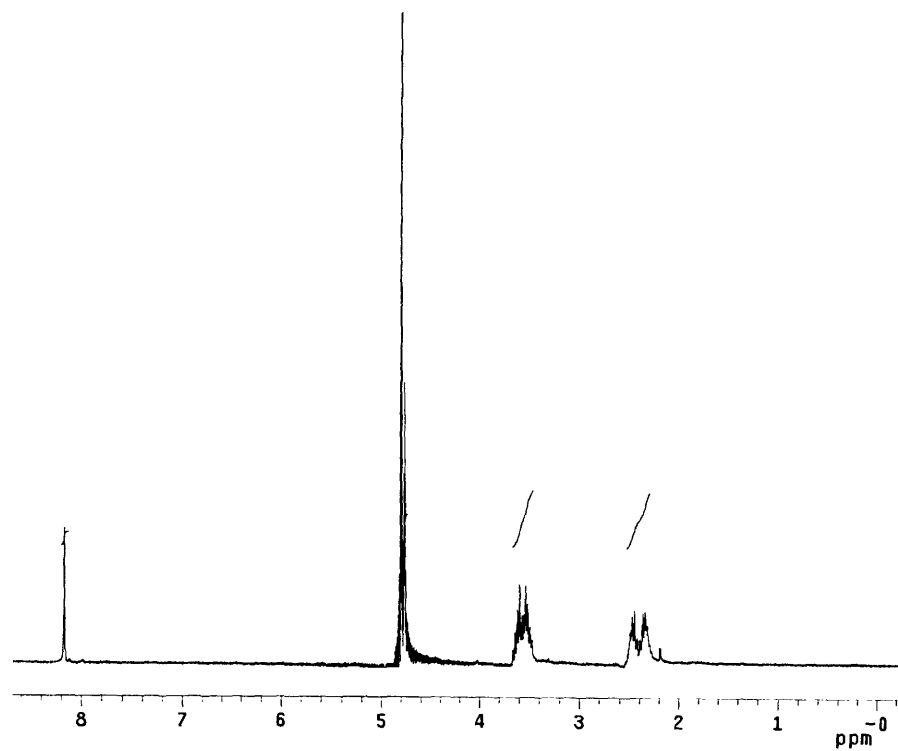
^1H NMR and ^{19}F NMR of **4** (Acetone- d_6)



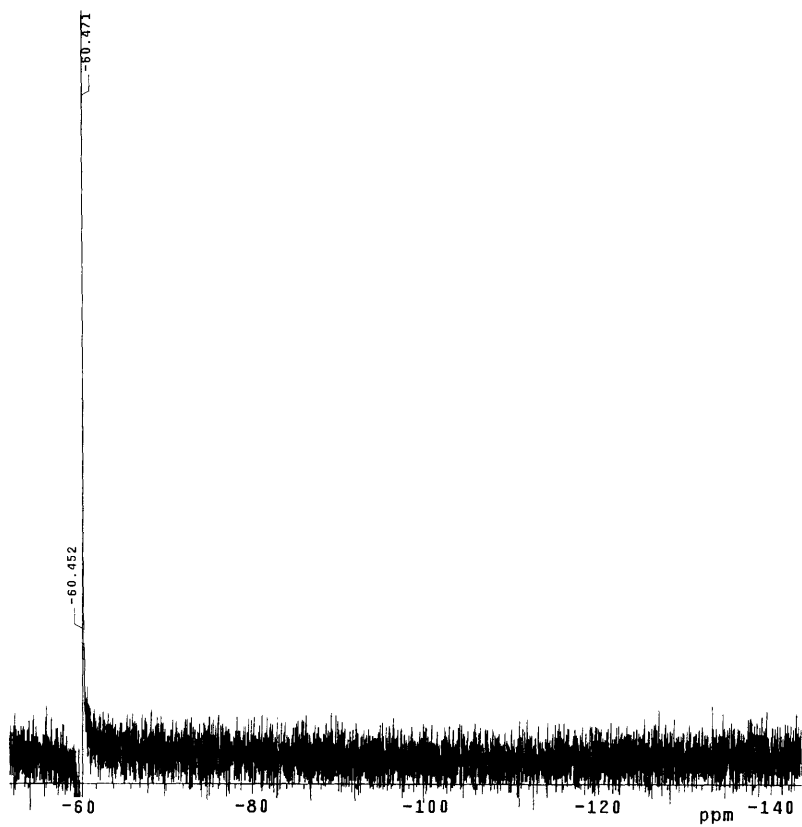
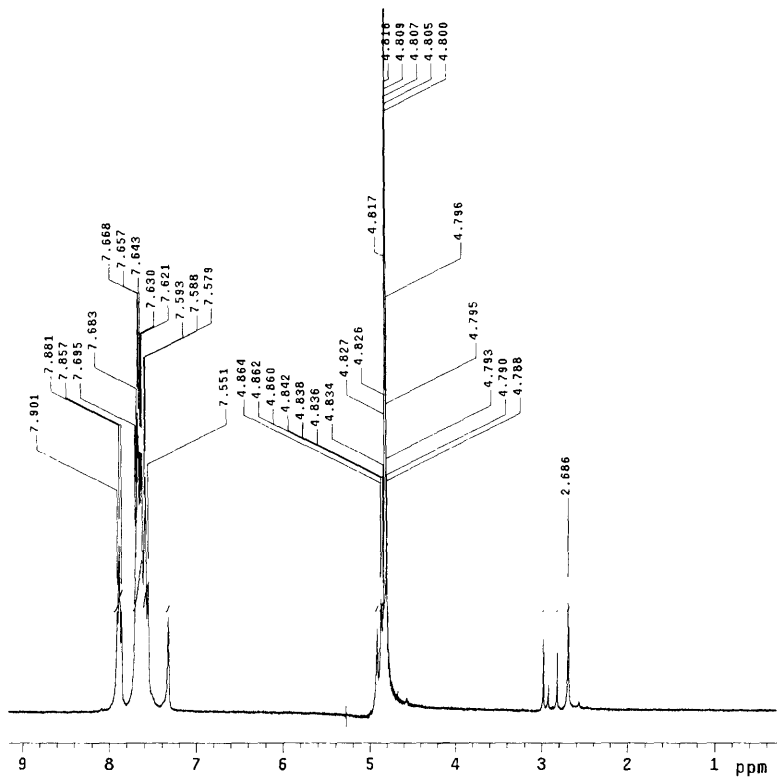
^1H NMR and ^{19}F NMR of **5** (CDCl_3)



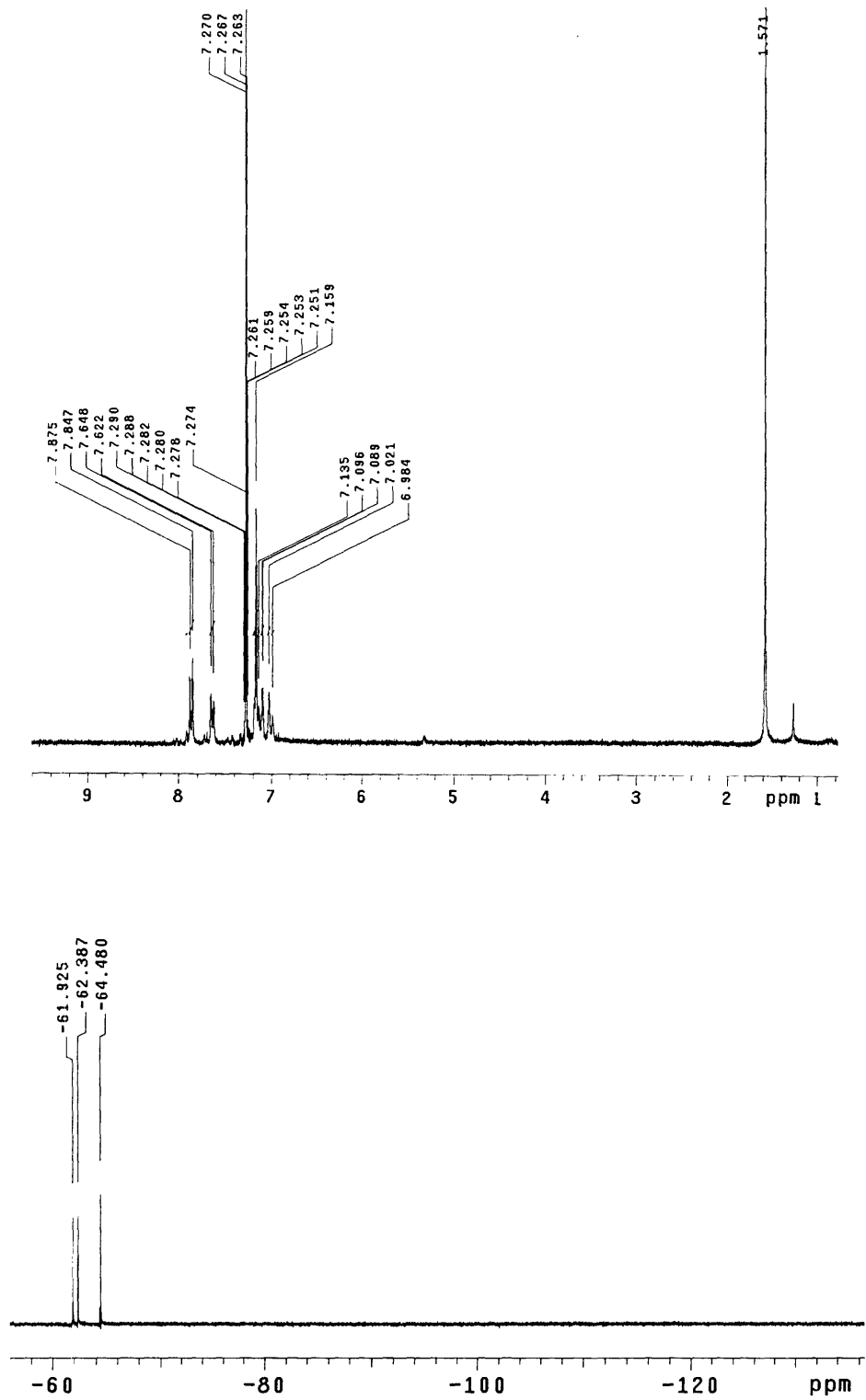
^1H NMR and ^{19}F NMR of **6** (D_2O)



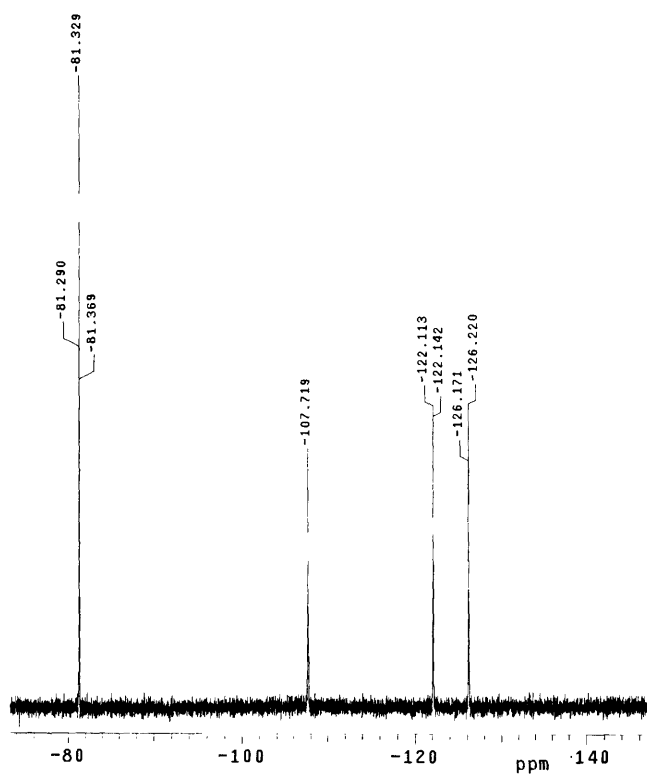
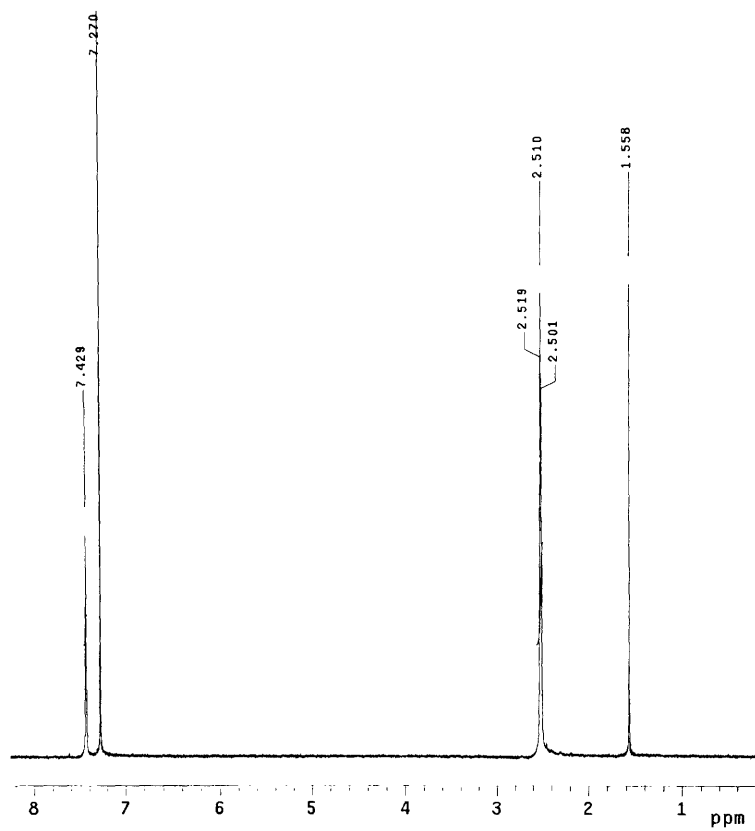
^1H NMR and ^{19}F NMR of **9** (CDCl_3)



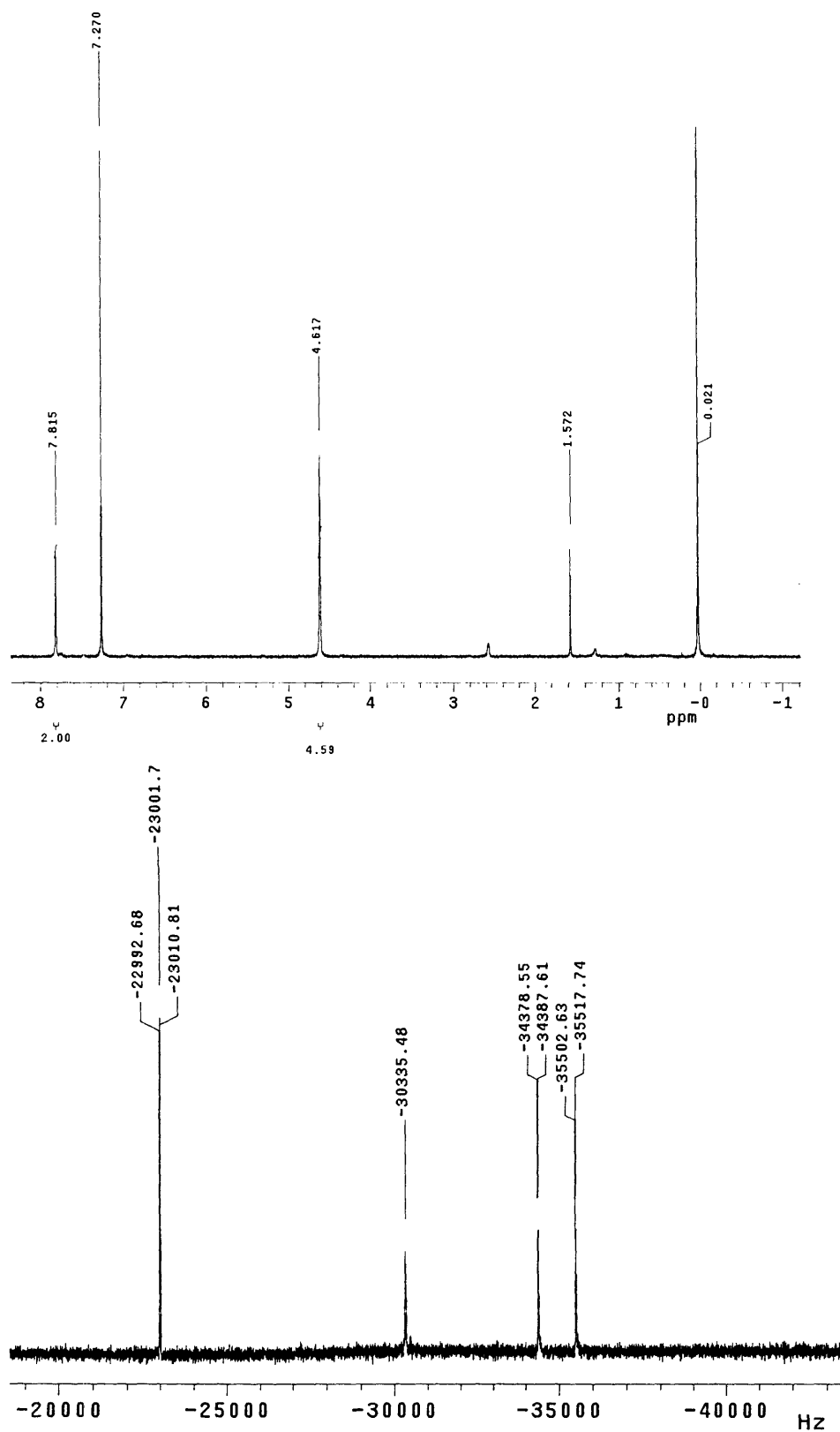
^1H NMR and ^{19}F NMR of **10** (CDCl_3)



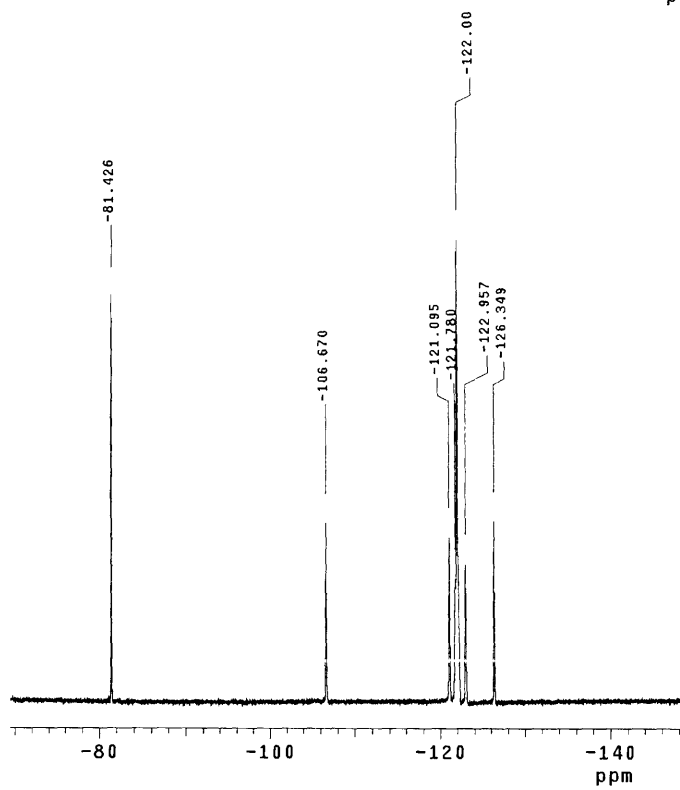
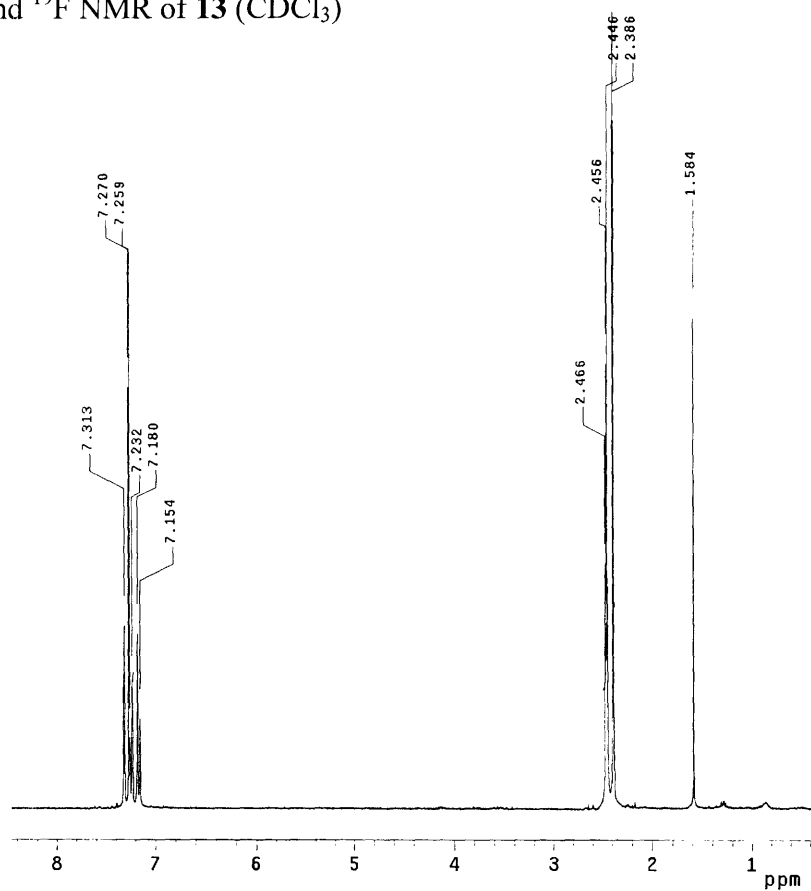
^1H NMR and ^{19}F NMR of **11** (CDCl_3)



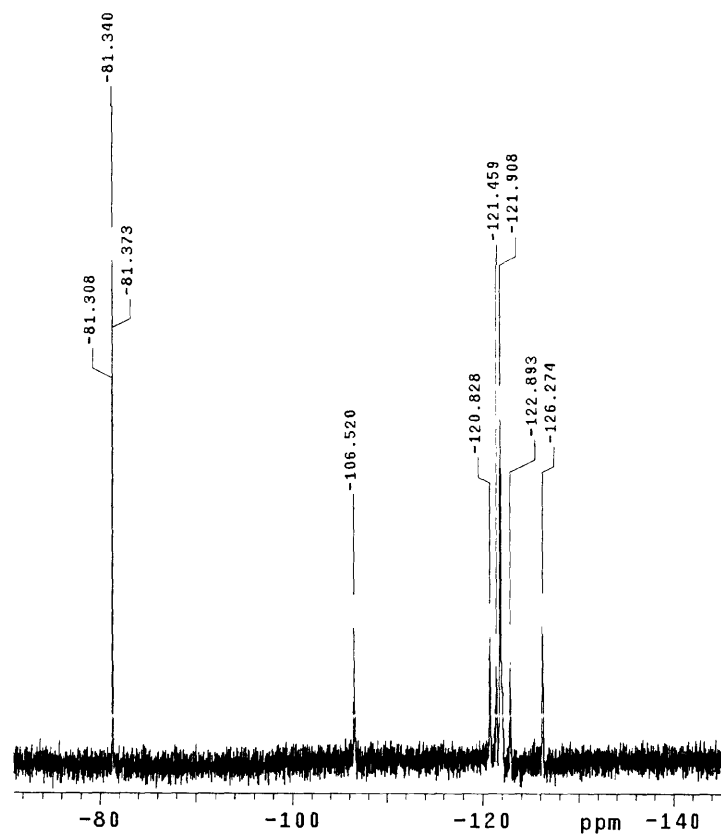
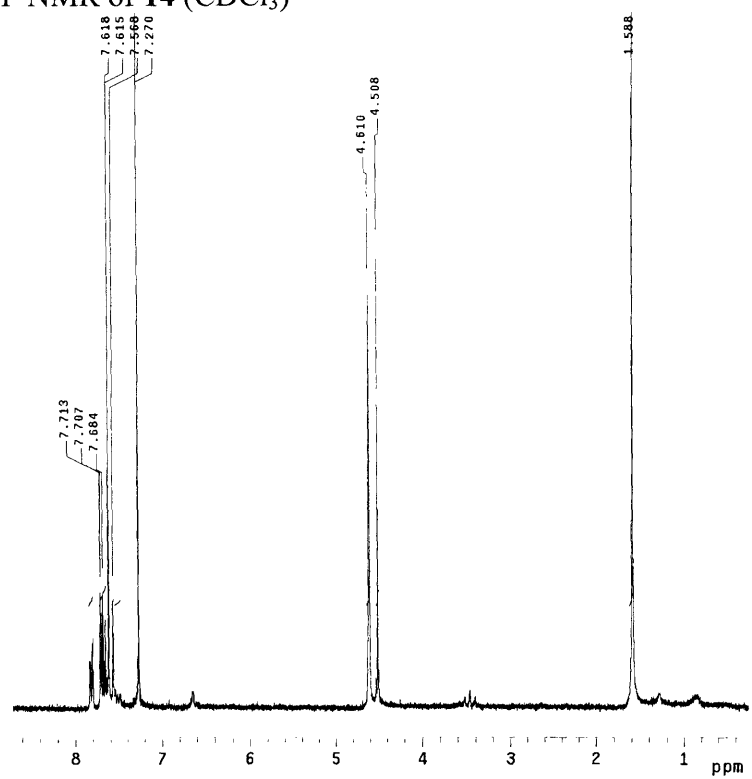
^1H NMR and ^{19}F NMR of 12 (CDCl_3)



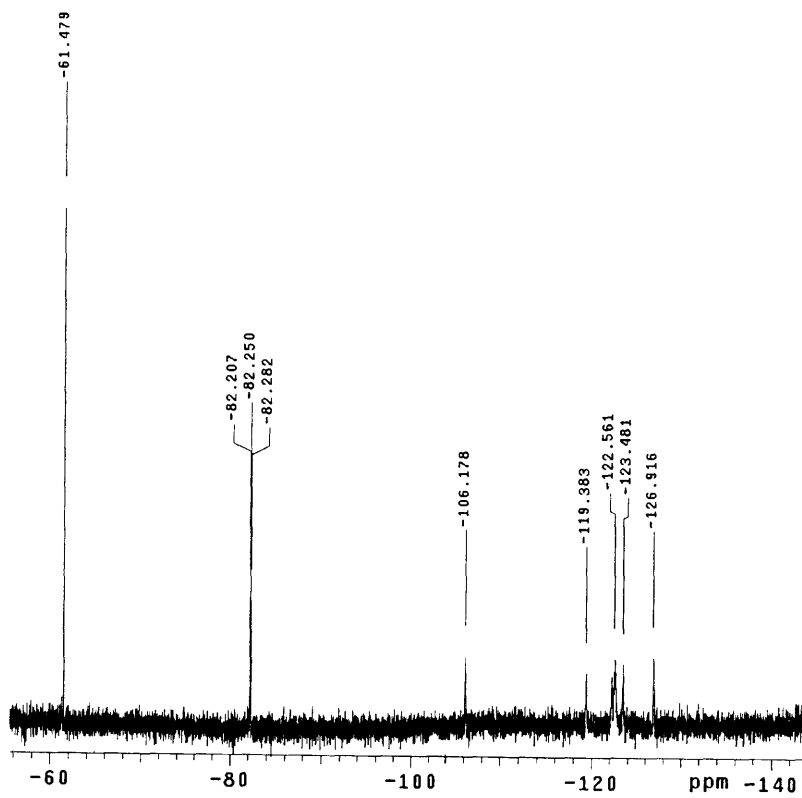
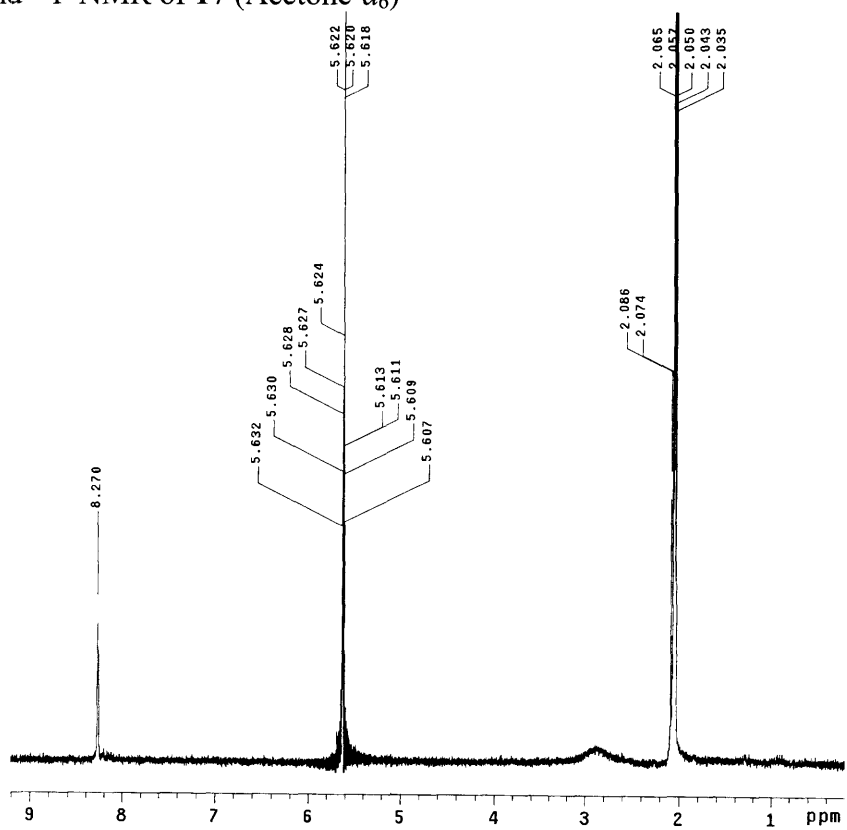
^1H NMR and ^{19}F NMR of **13** (CDCl_3)



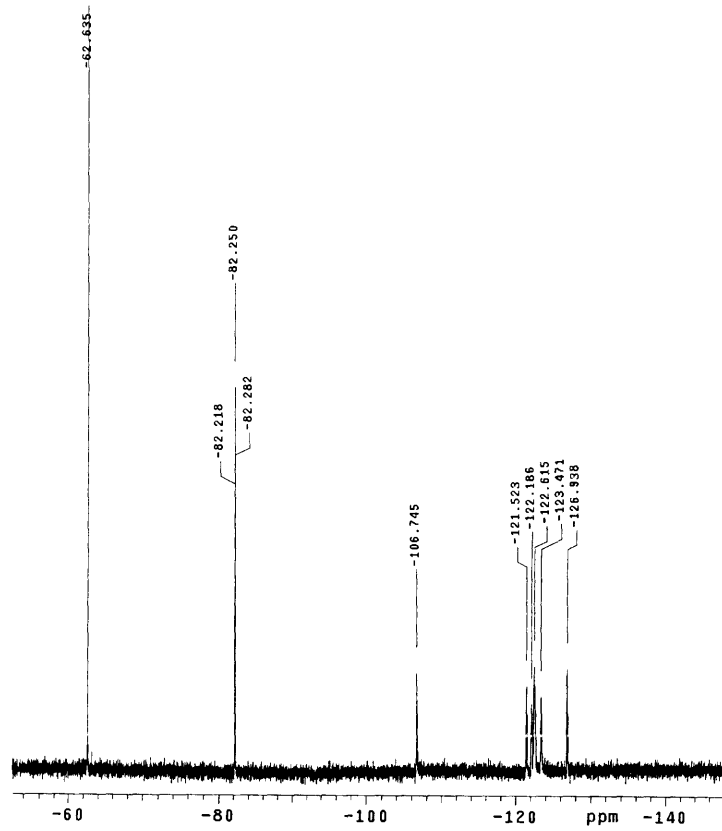
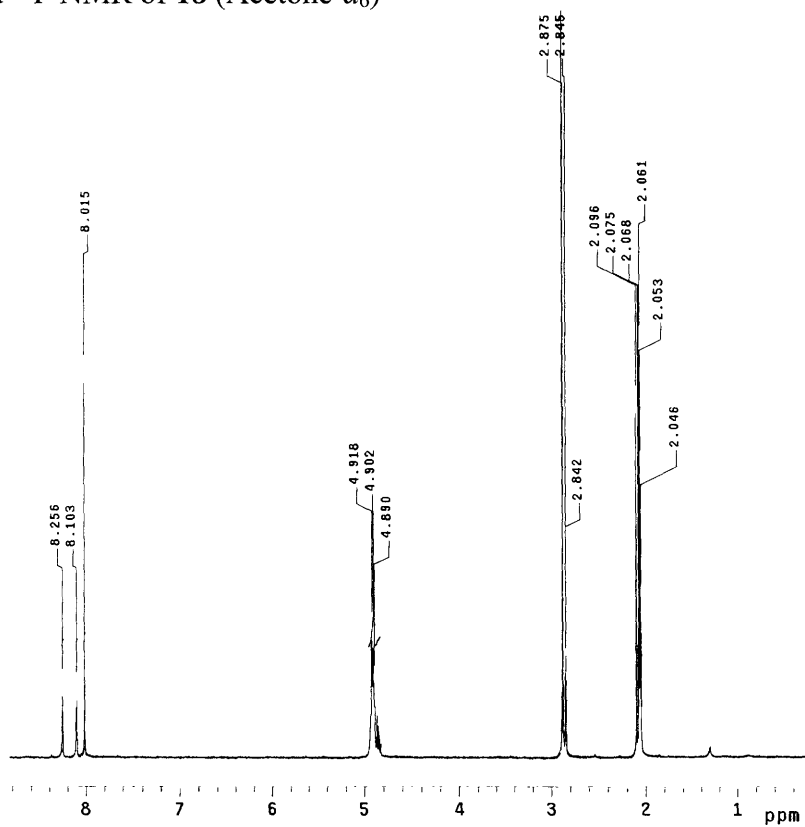
^1H NMR and ^{19}F NMR of **14** (CDCl_3)



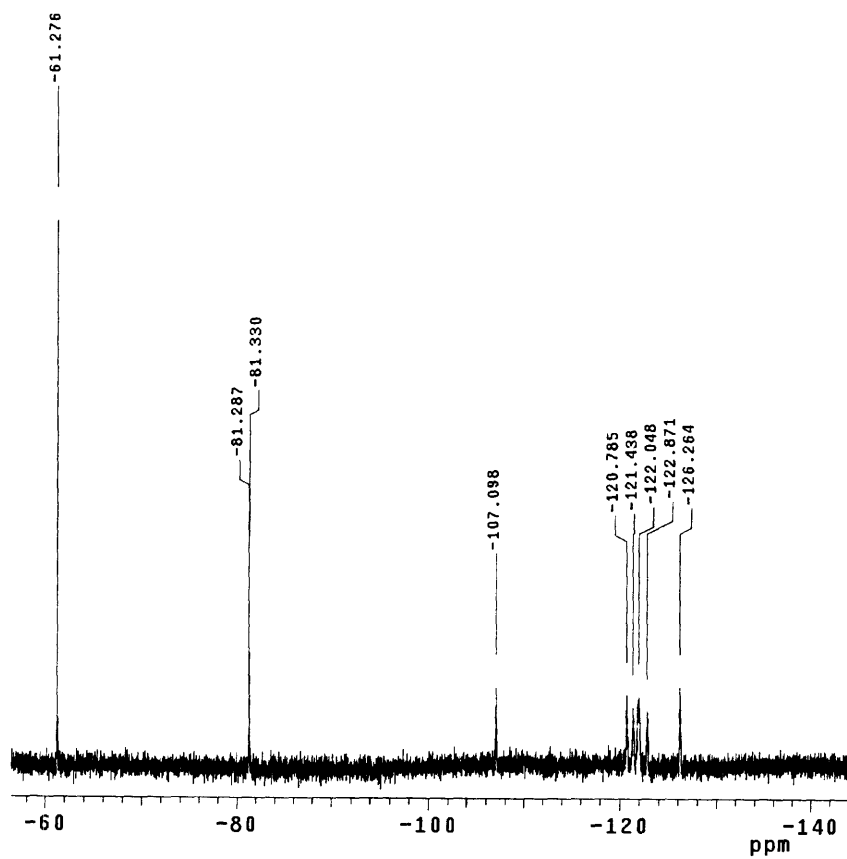
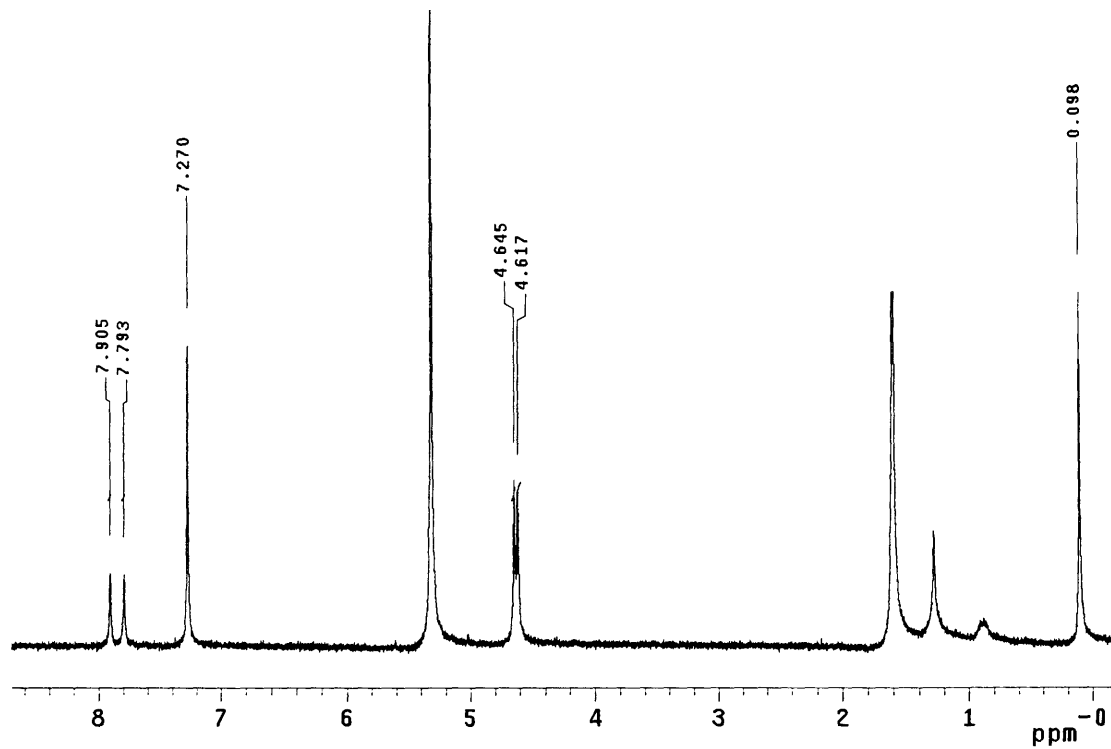
^1H NMR and ^{19}F NMR of 17 (Acetone- d_6)



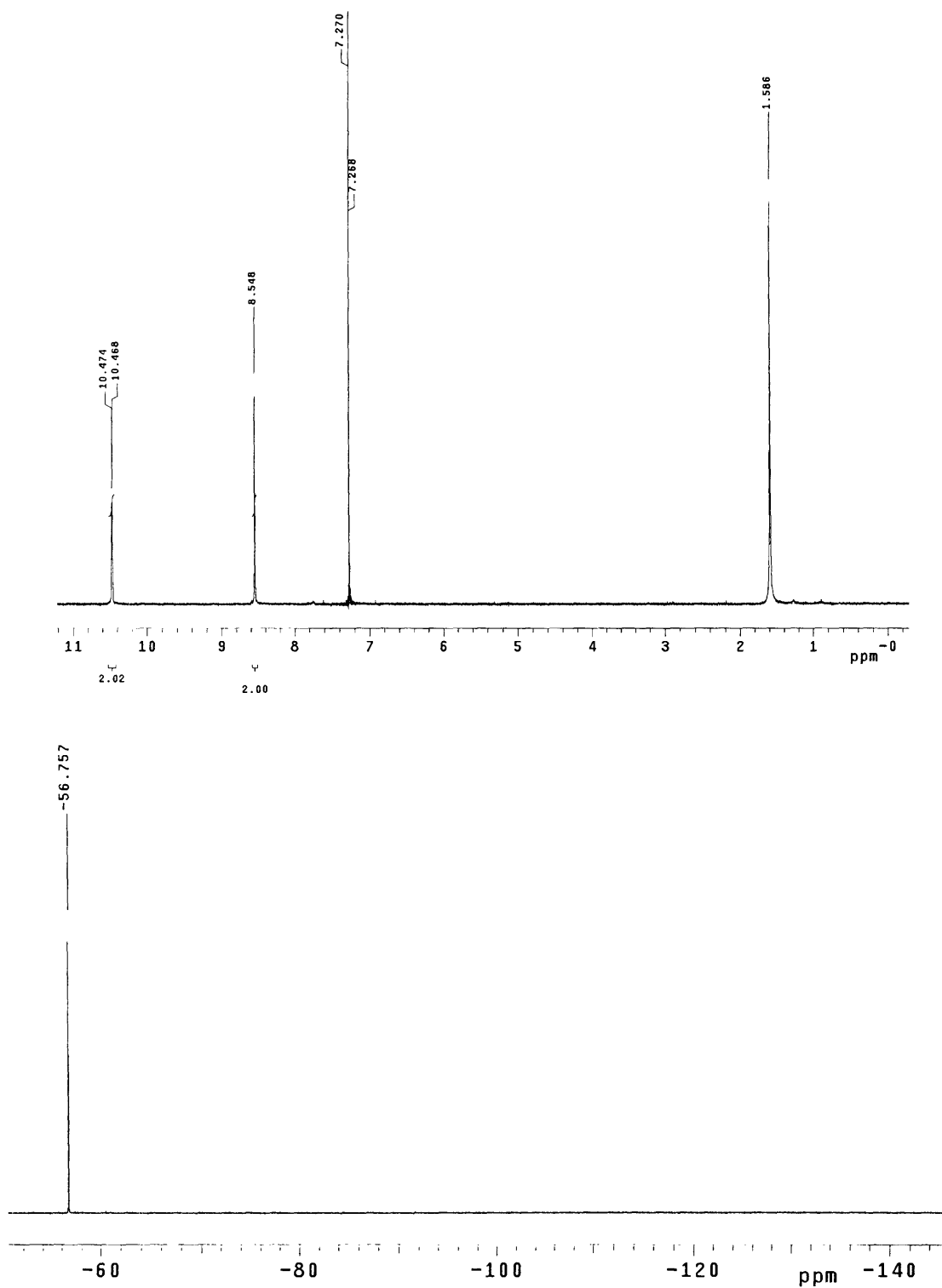
^1H NMR and ^{19}F NMR of **18** (Acetone- d_6)



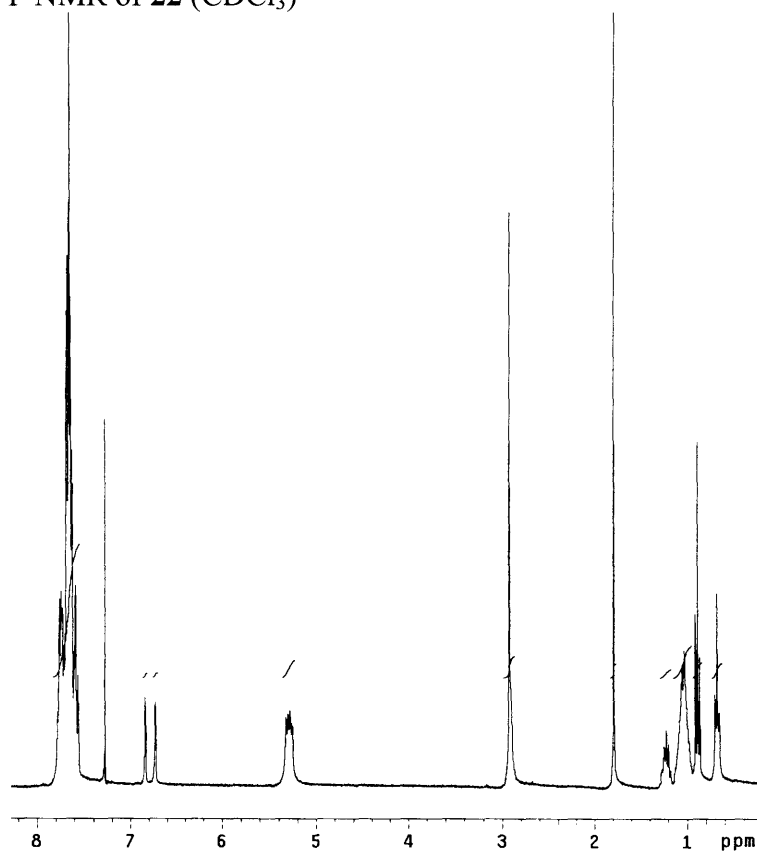
^1H NMR and ^{19}F NMR of **19** (CDCl_3)



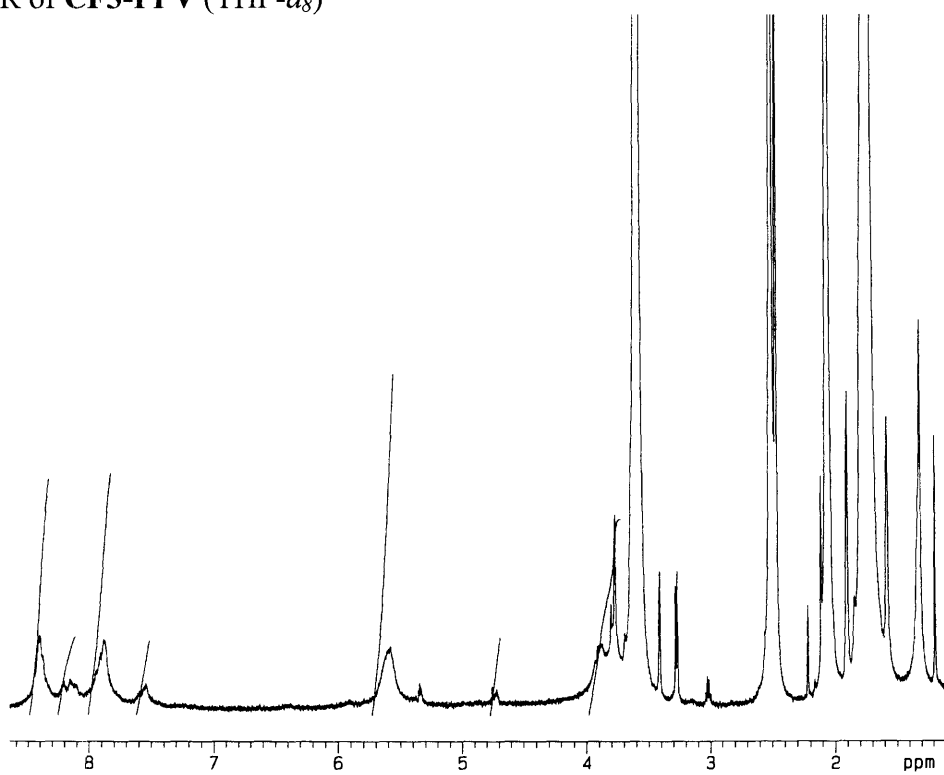
^1H NMR and ^{19}F NMR of **20** (CDCl_3)



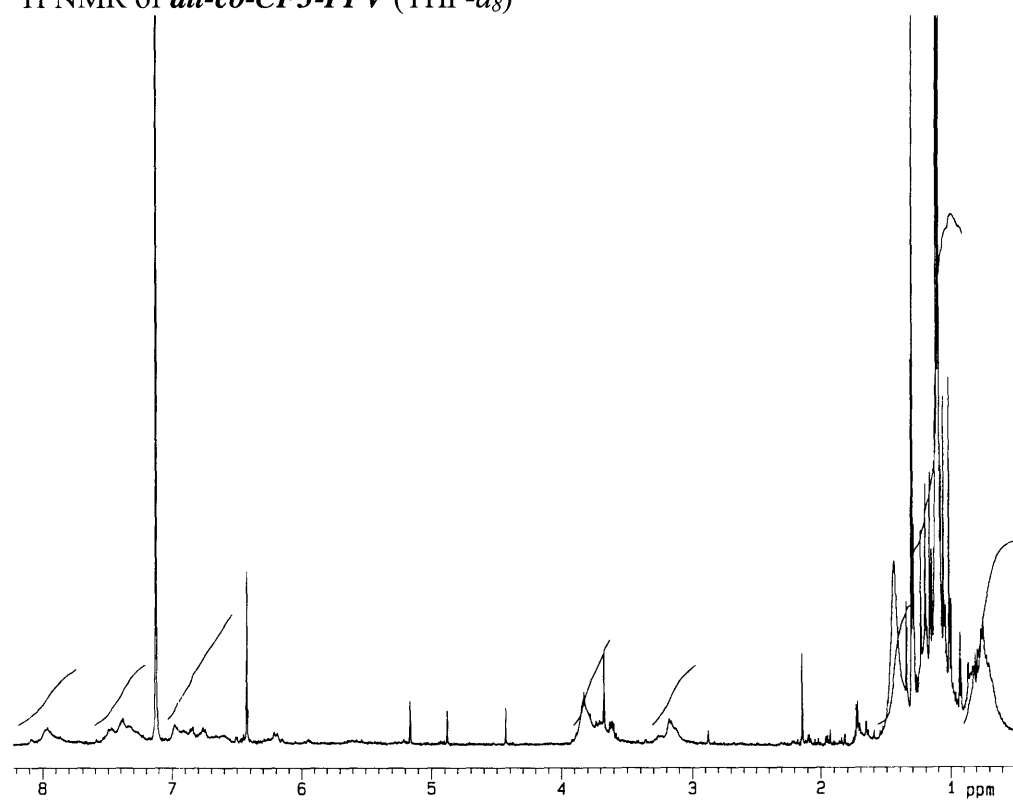
^1H NMR and ^{19}F NMR of **22** (CDCl_3)



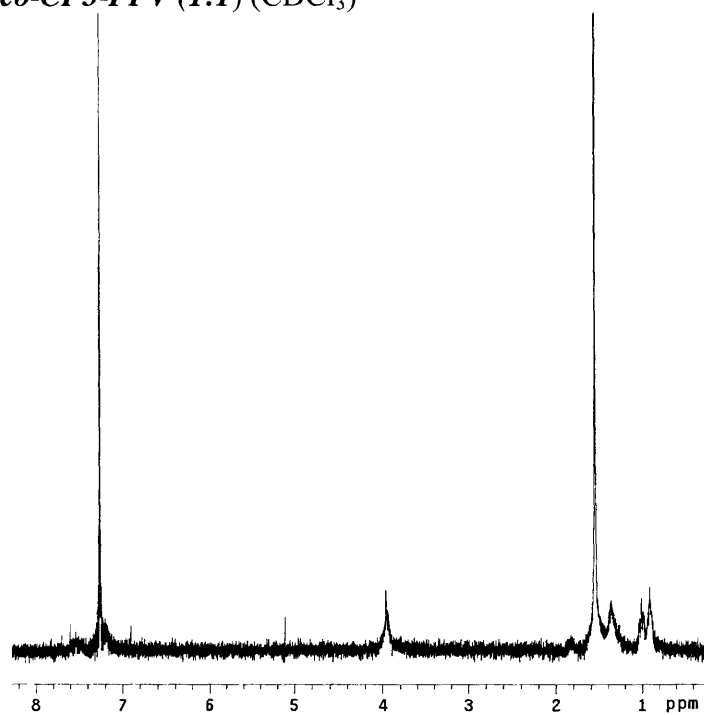
^1H NMR of **CF3-PPV** ($\text{THF-}d_8$)



^1H NMR of *alt-co-CF3-PPV* (THF- d_8)

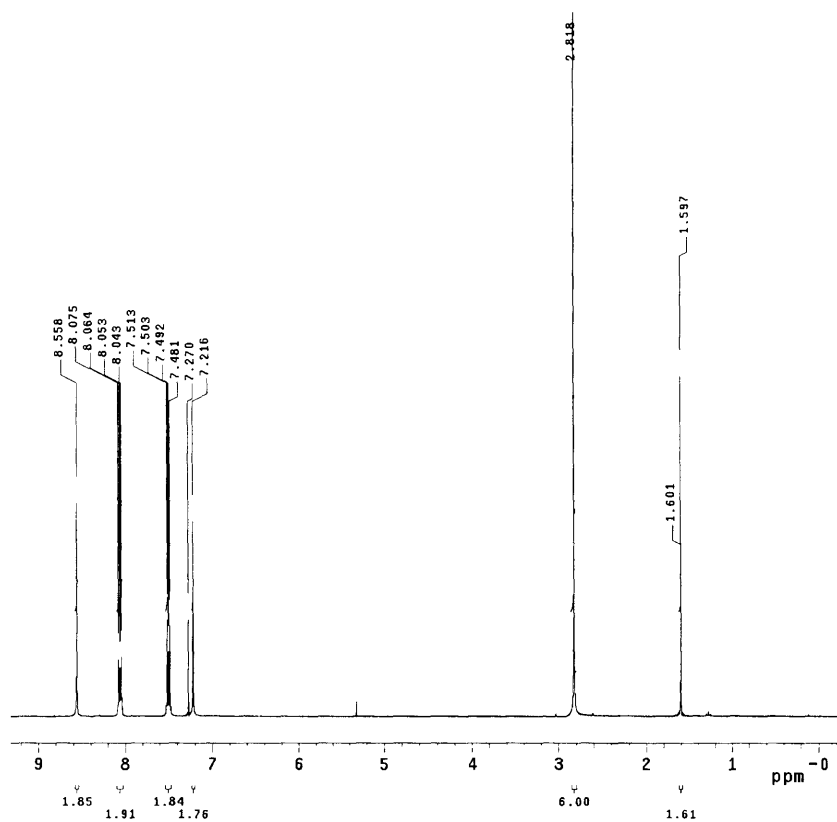


^1H NMR of *ran-co-CF3-PPV (1:1)* (CDCl_3)

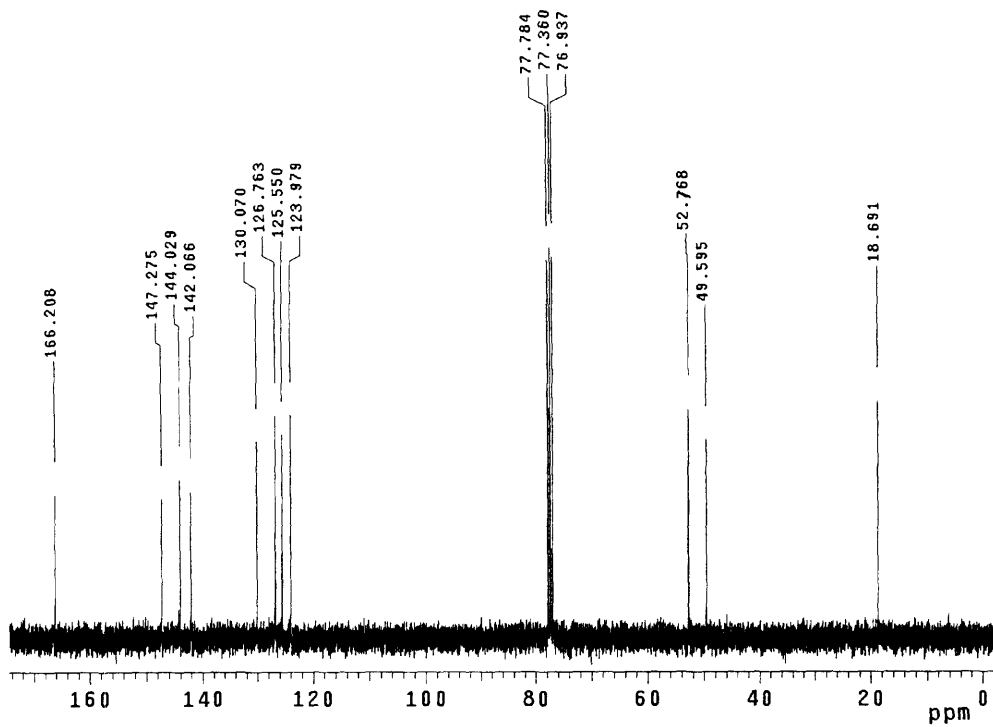
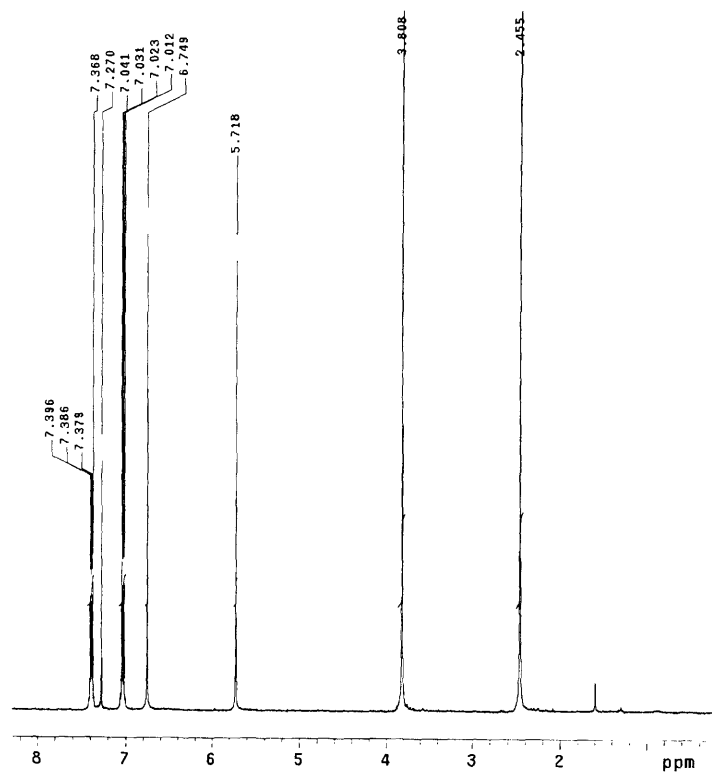


Appendix B:
NMR Spectra of Chapter 3

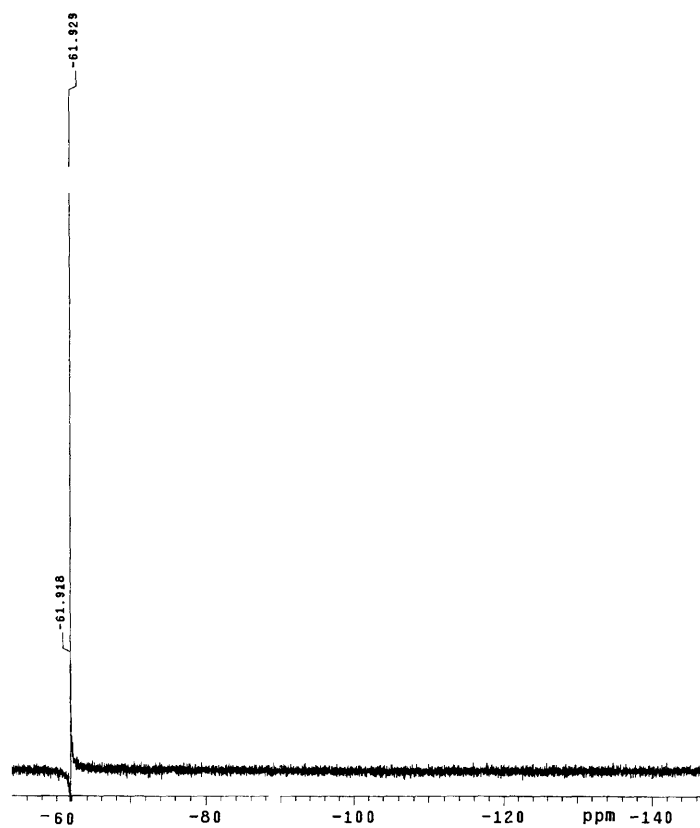
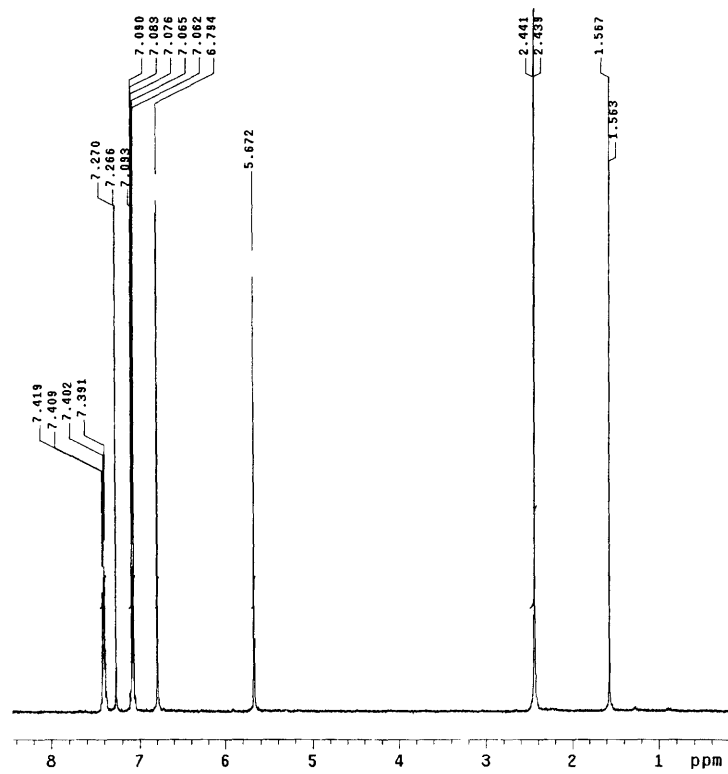
^1H NMR and ^{13}C NMR of **1** (CDCl_3)



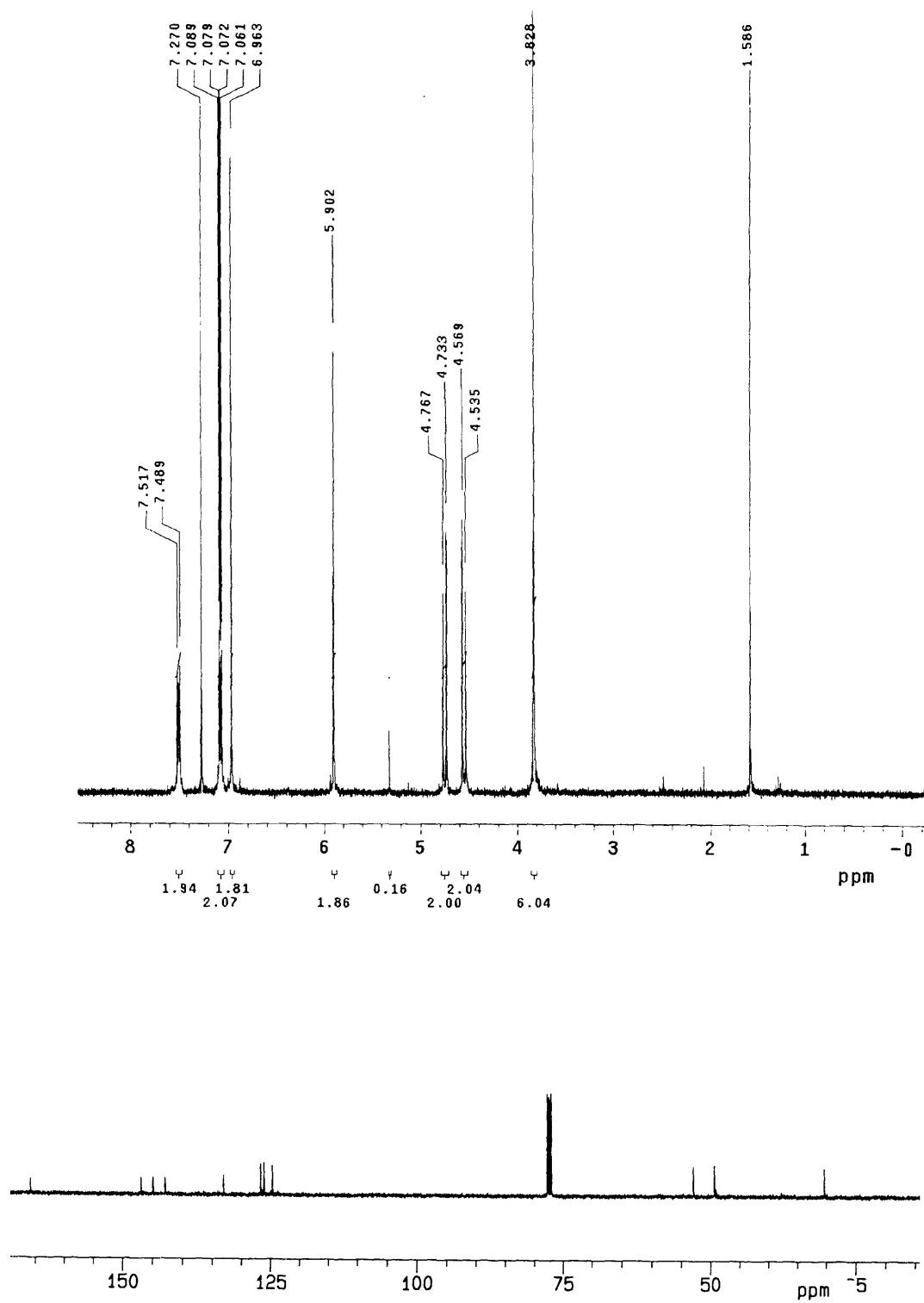
^1H NMR and ^{13}C NMR of **2a** (CDCl_3)



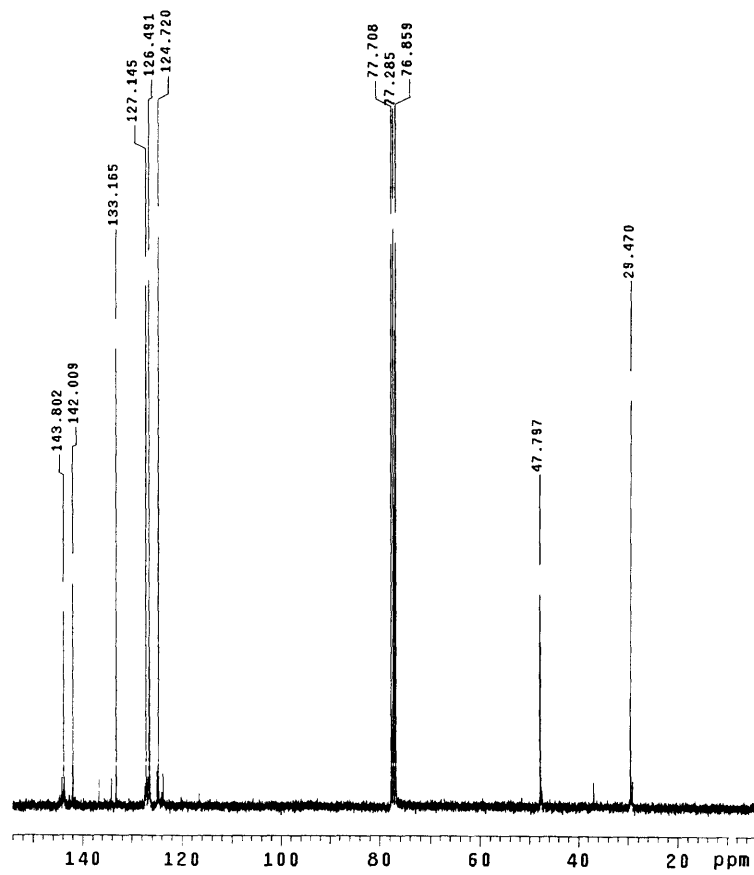
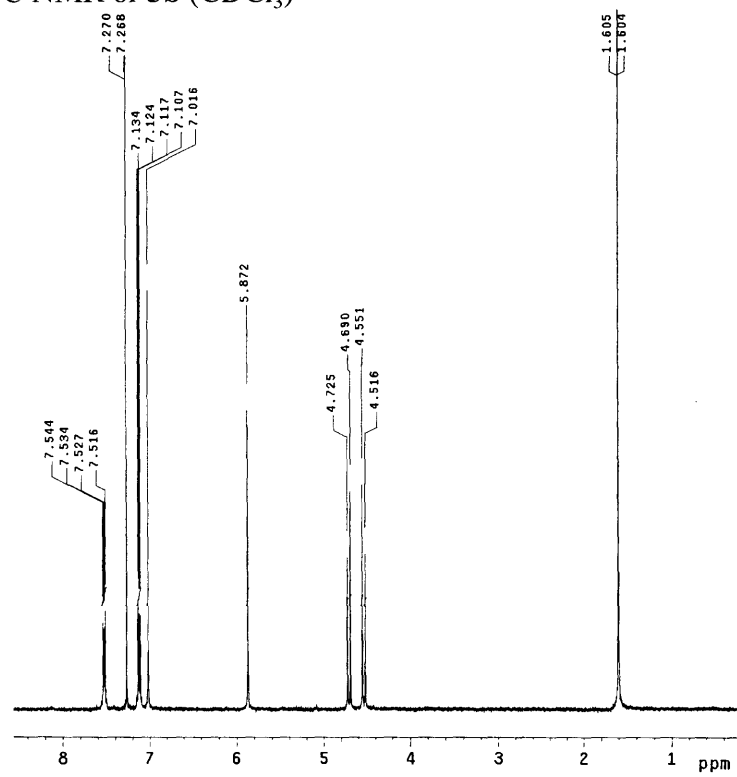
^1H NMR and ^{19}F NMR of **2b** (CDCl_3)



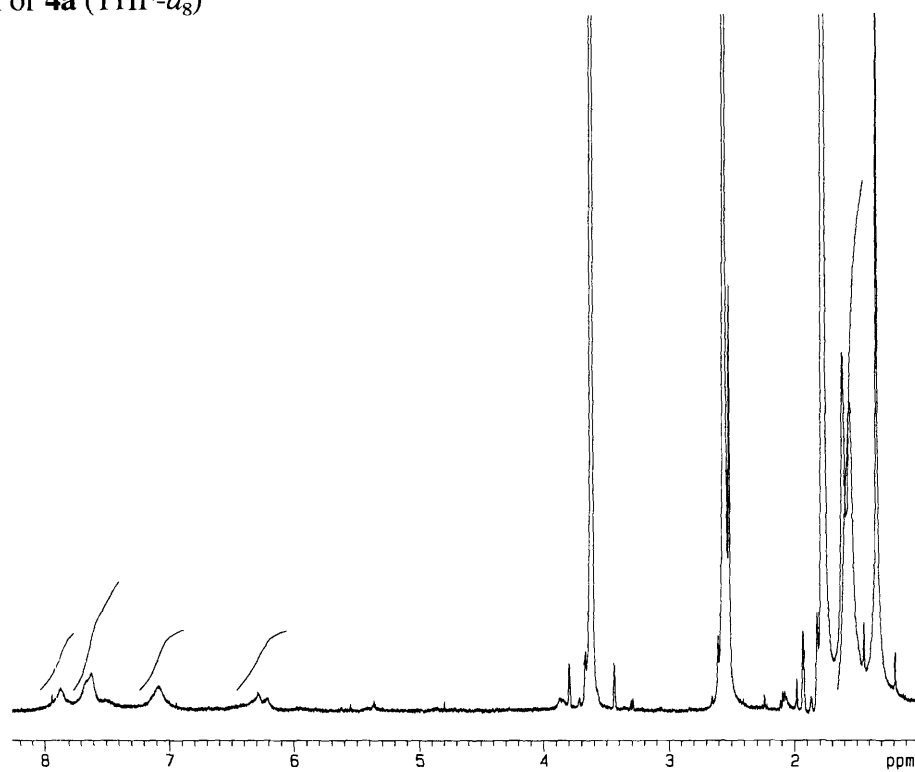
^1H NMR and ^{13}C NMR of **3a** (CDCl_3)



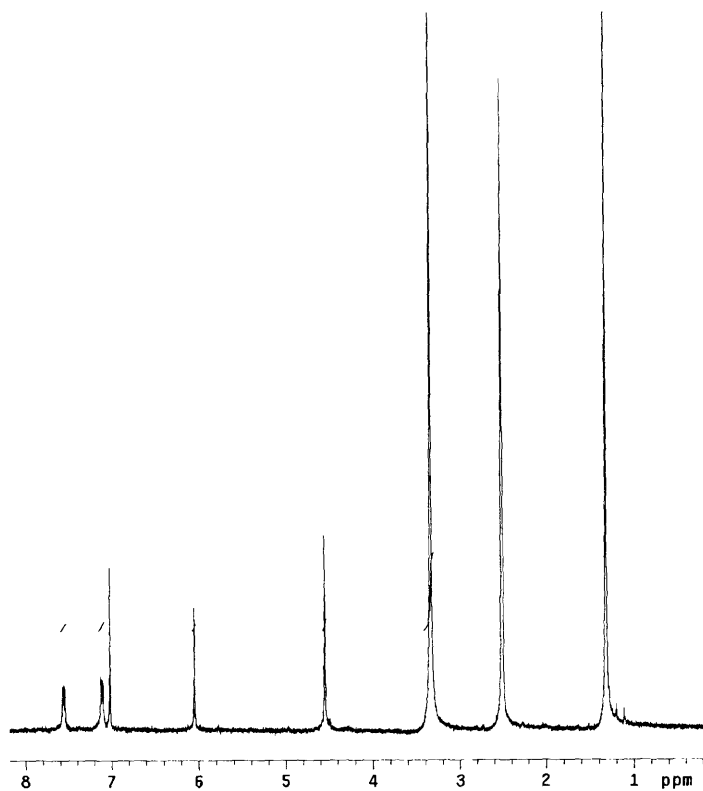
^1H NMR and ^{13}C NMR of **3b** (CDCl_3)



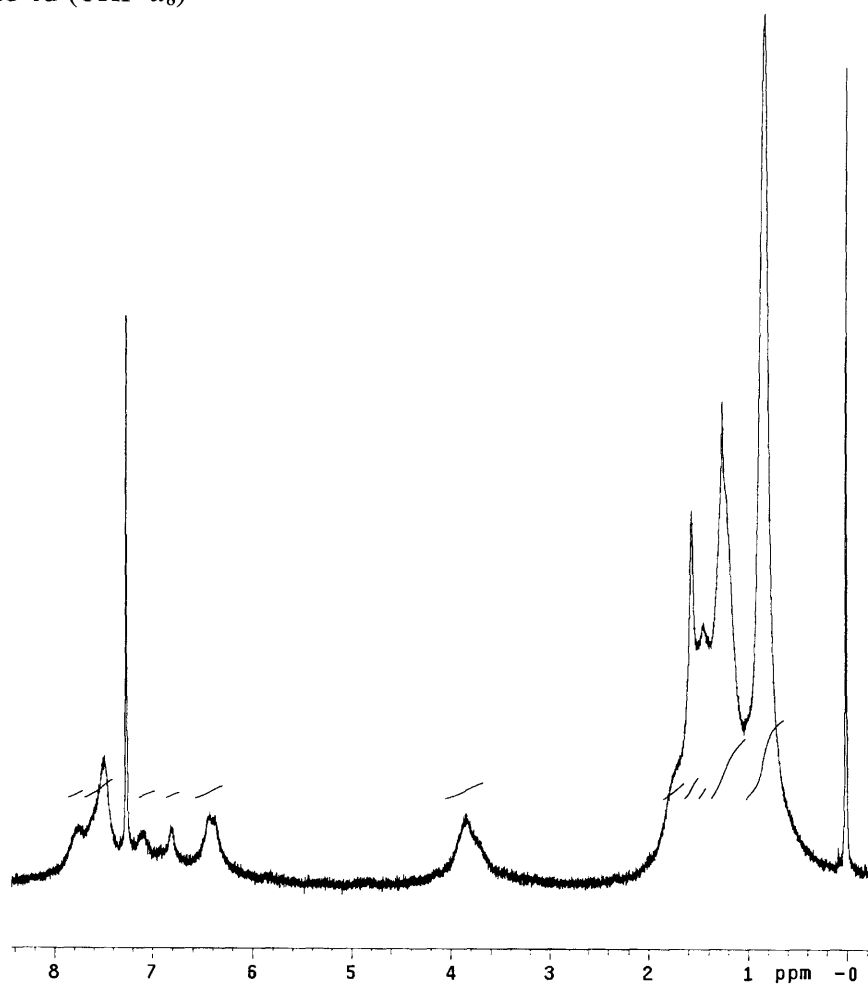
^1H NMR of **4a** ($\text{THF-}d_8$)



^1H NMR of **4b** ($\text{DMSO-}d_6$)

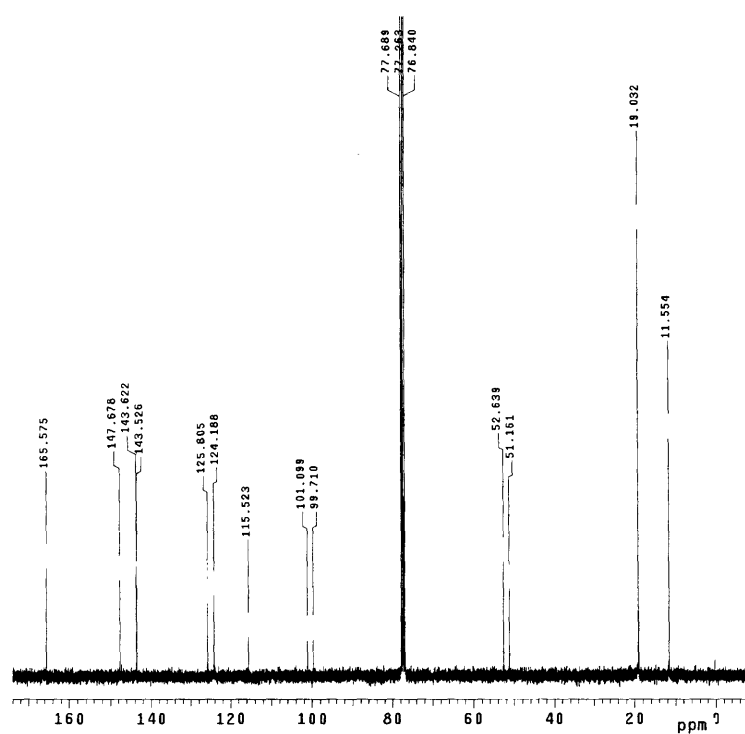
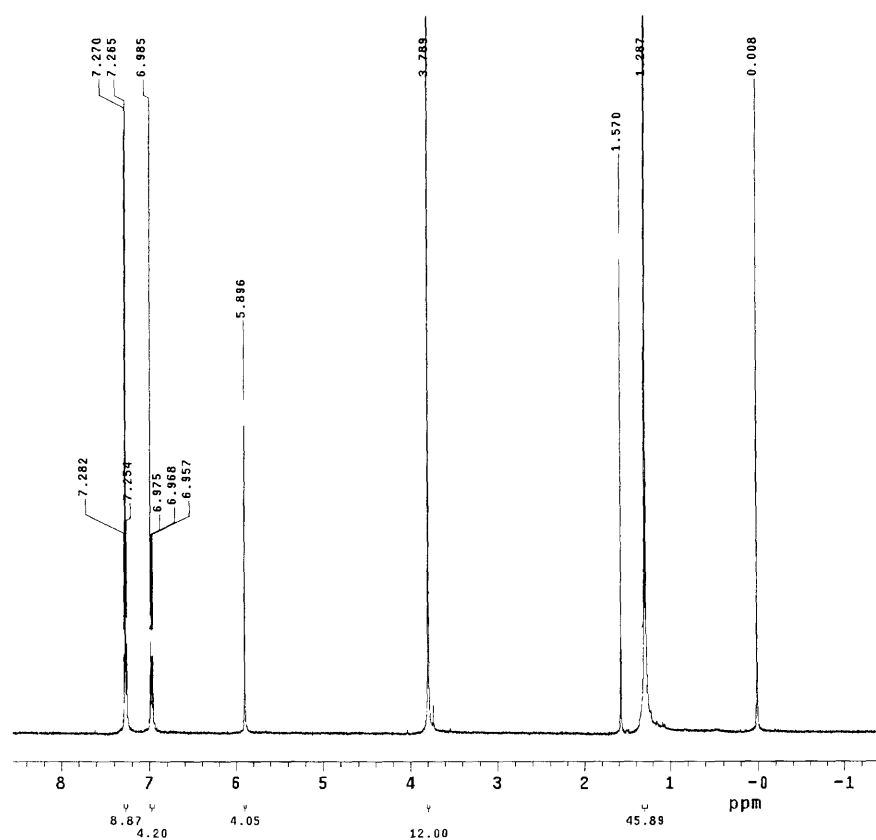


^1H NMR of **4d** ($\text{THF-}d_8$)

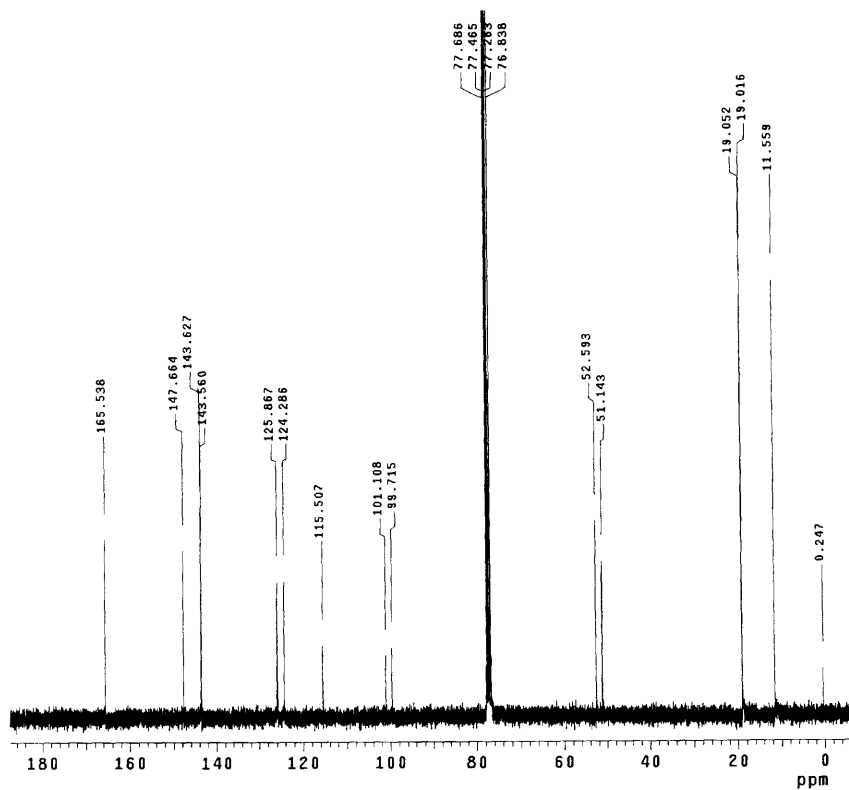
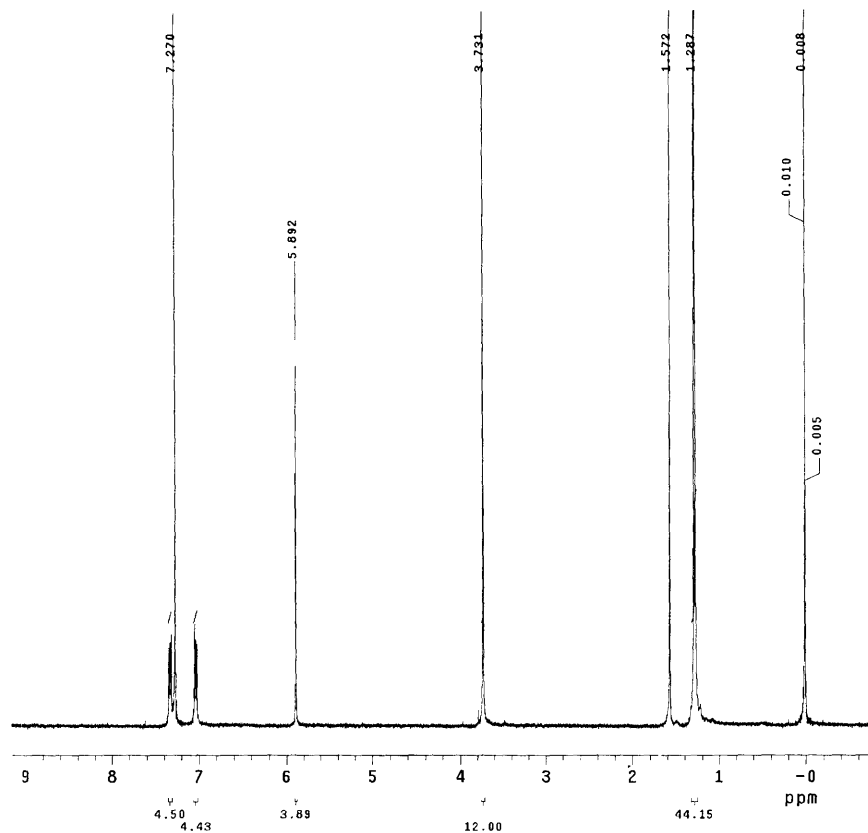


Appendix C:
NMR Spectra of Chapter 4

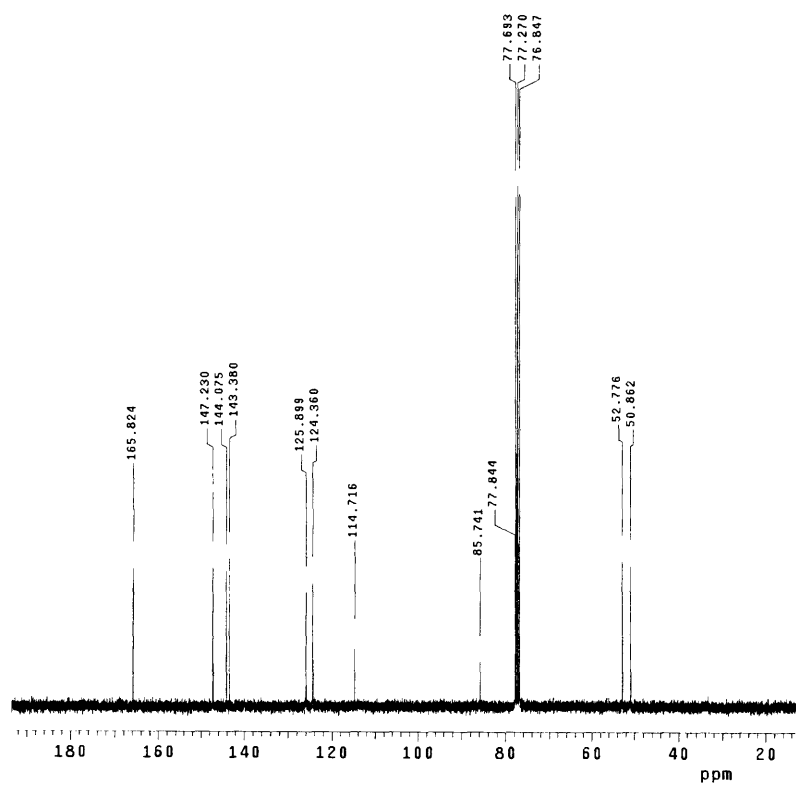
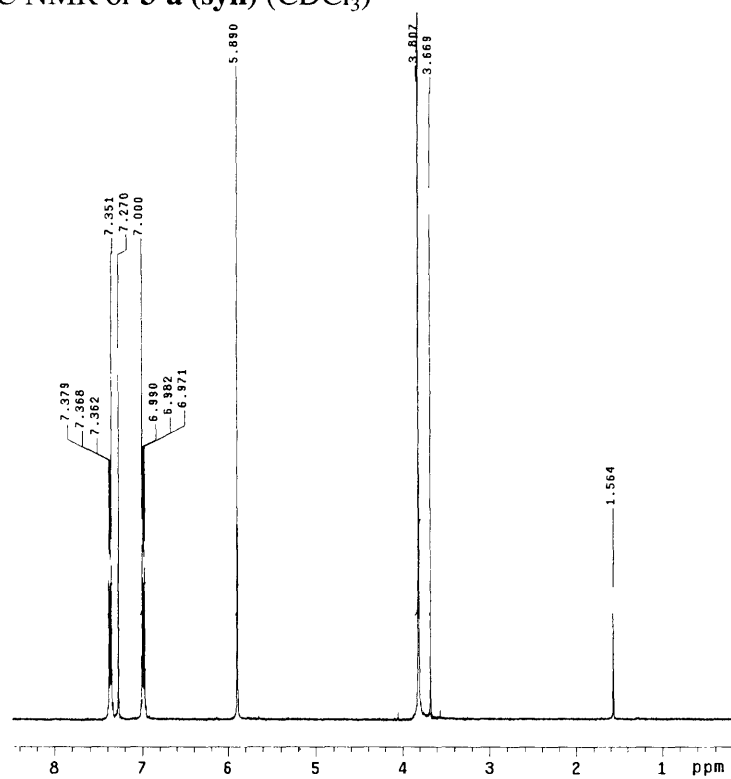
^1H NMR and ^{13}C NMR of **2-a (syn)** (CDCl_3)



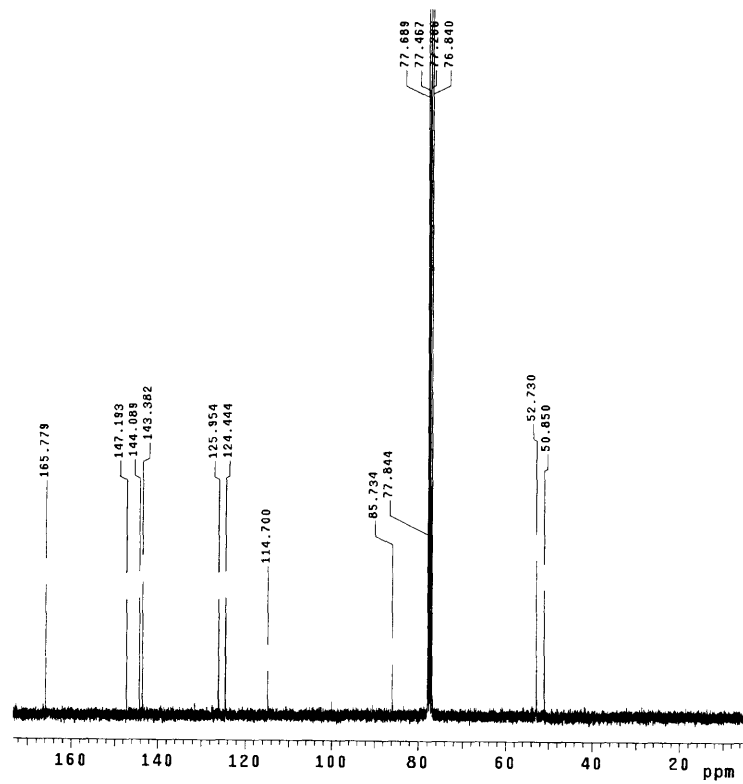
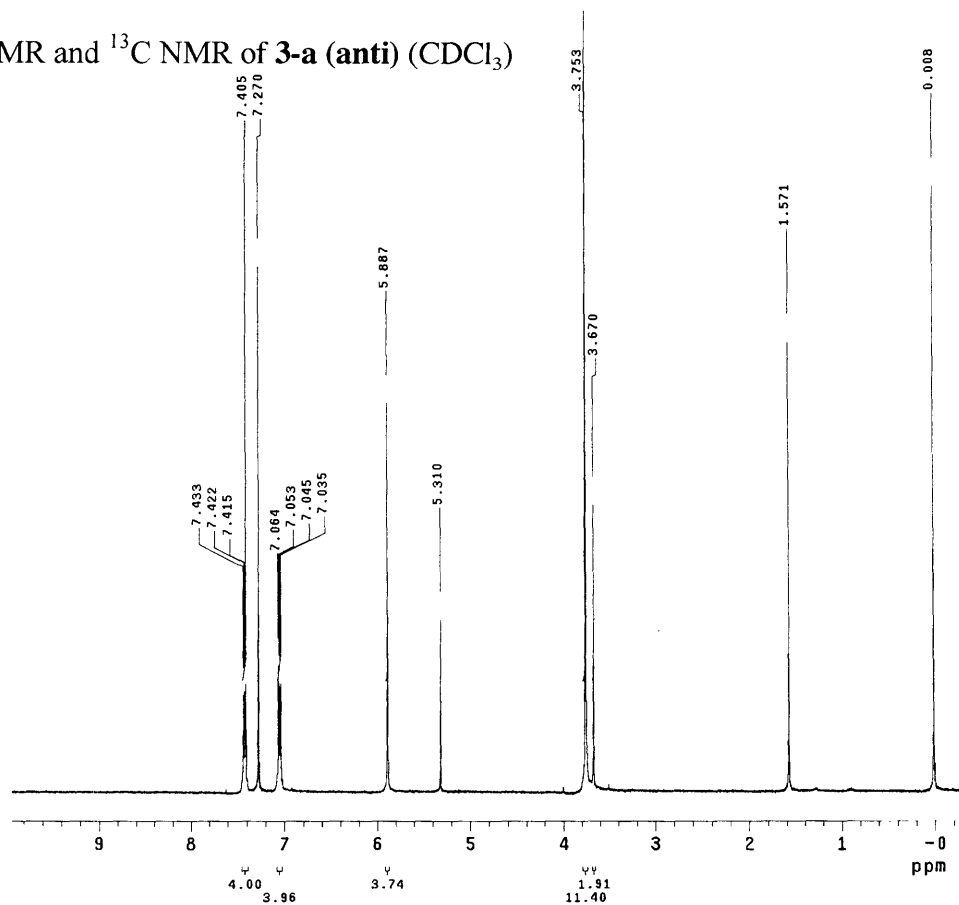
^1H NMR and ^{13}C NMR of **2-a (anti)** (CDCl_3)



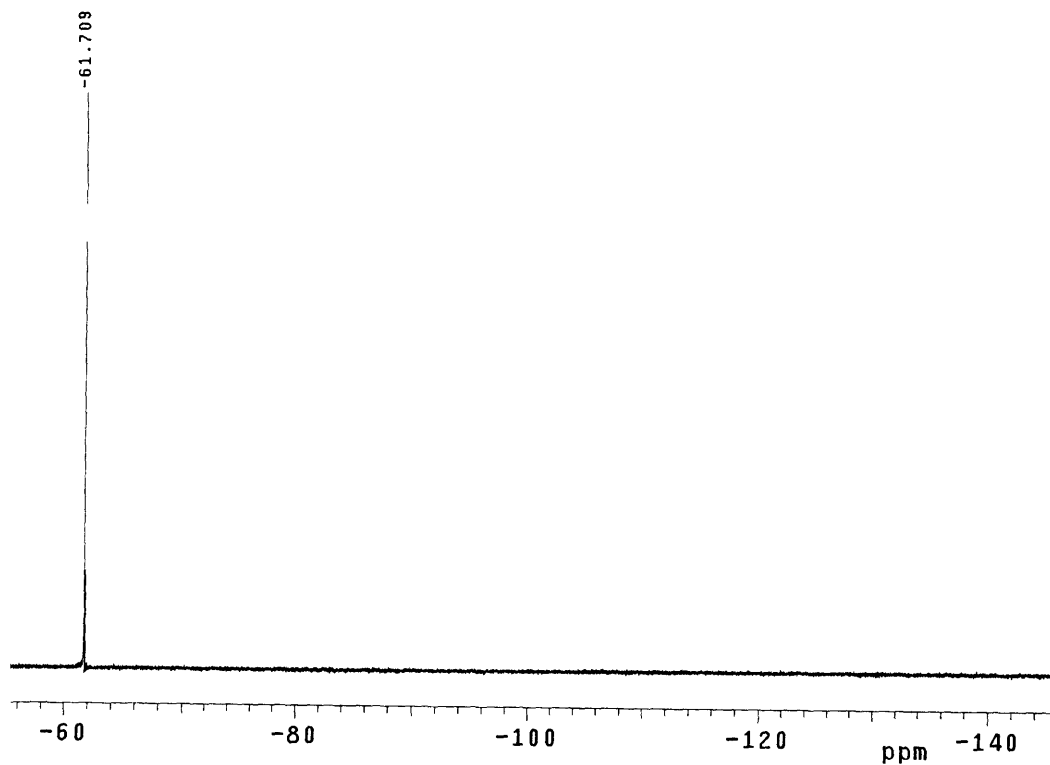
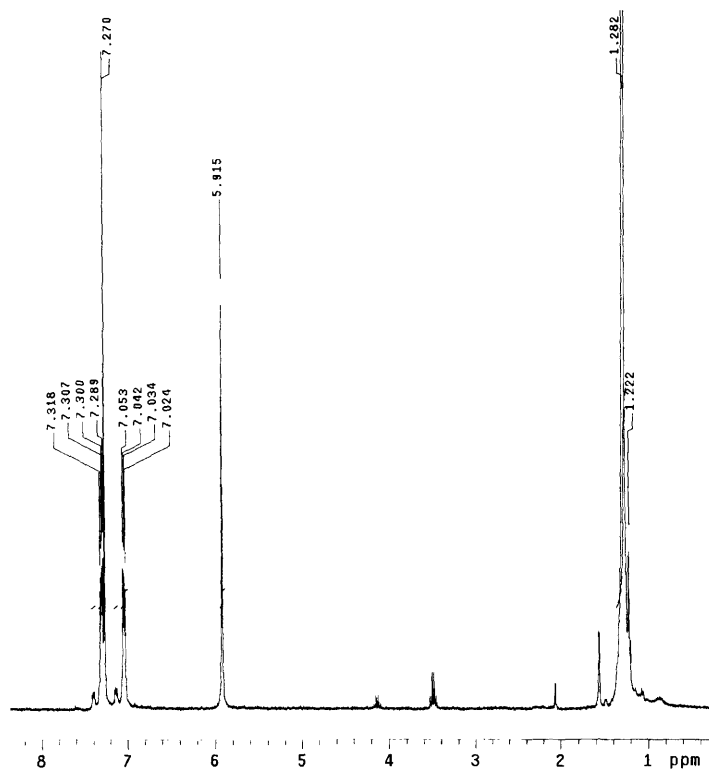
^1H NMR and ^{13}C NMR of **3-a** (syn) (CDCl_3)



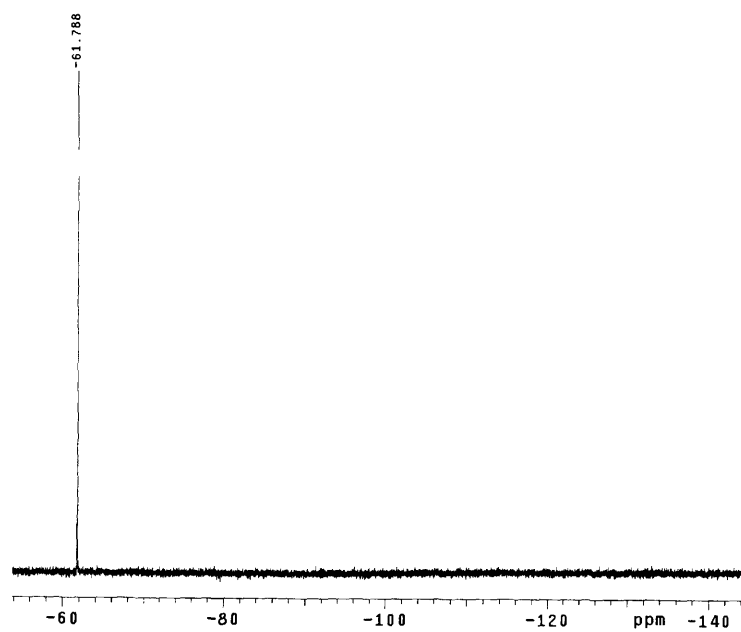
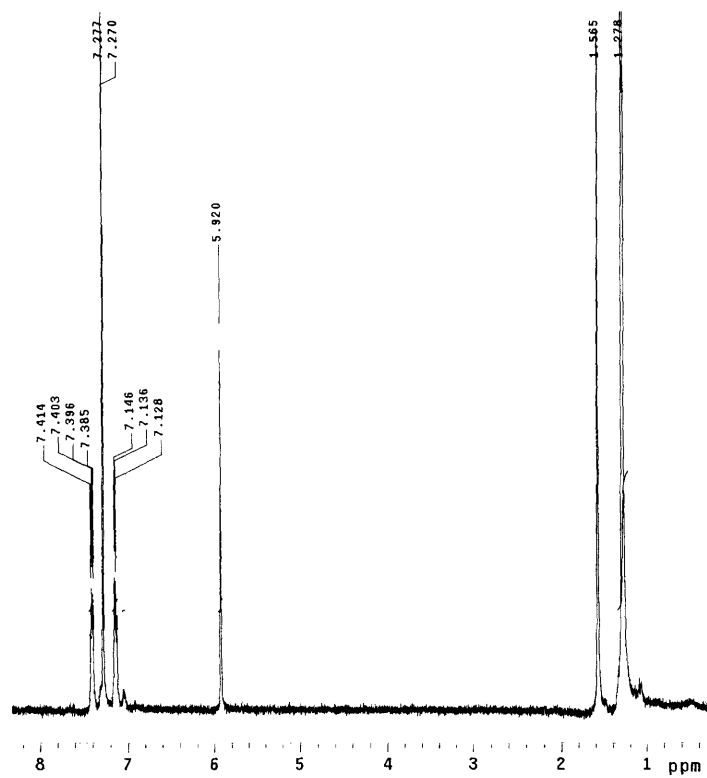
^1H NMR and ^{13}C NMR of **3-a** (anti) (CDCl_3)



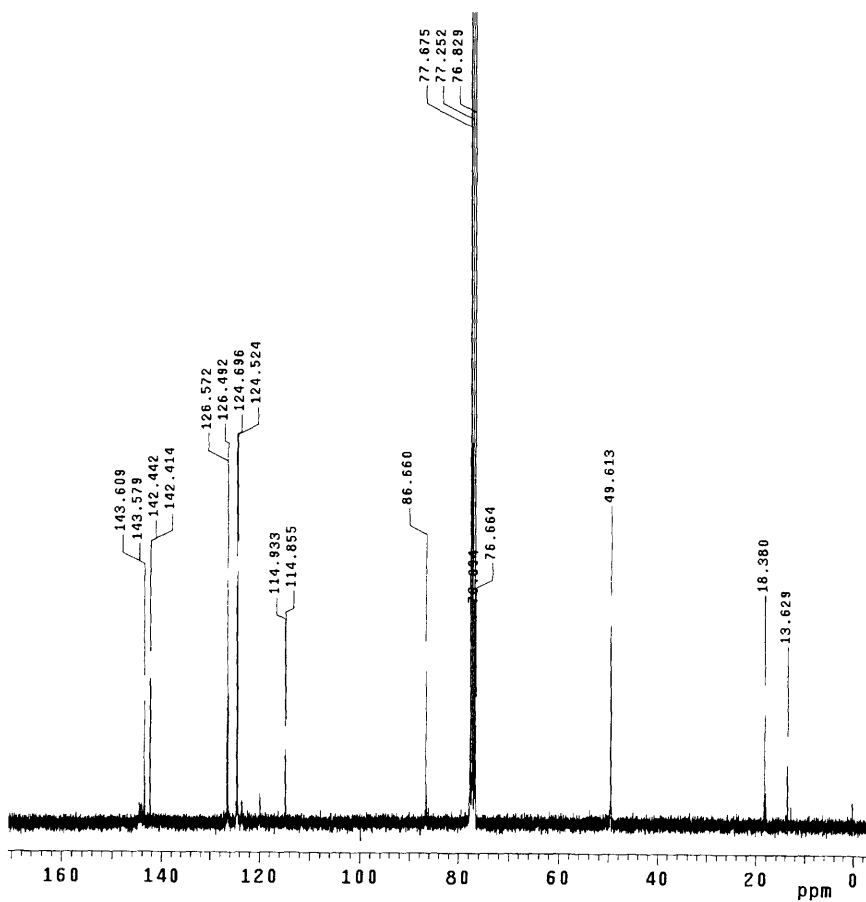
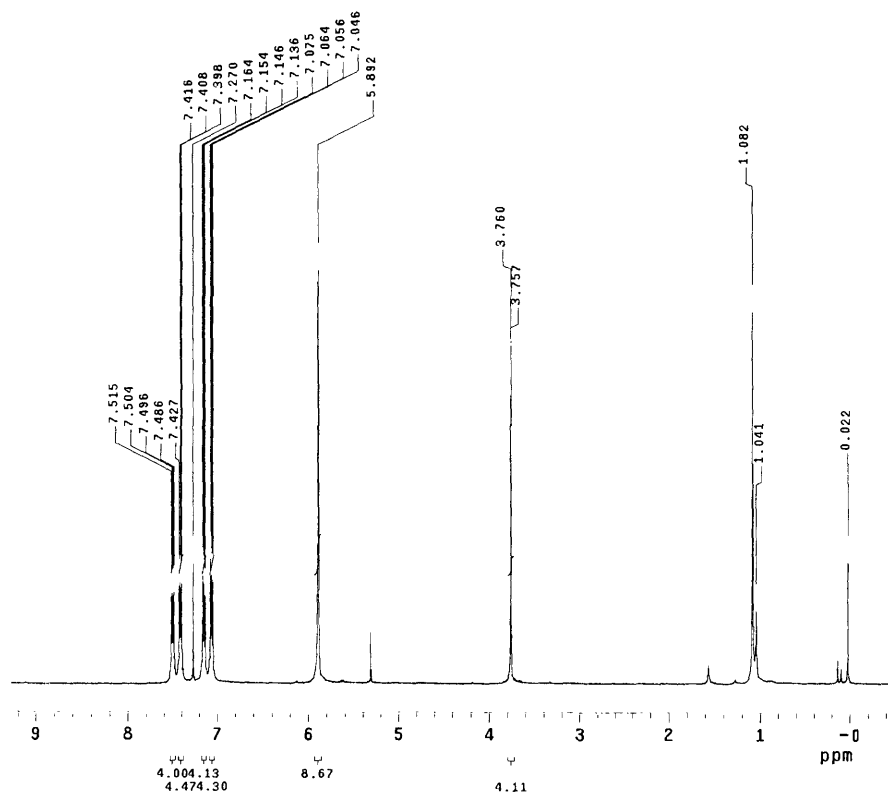
^1H NMR and ^{19}F NMR of **2-b (syn)** (CDCl_3)



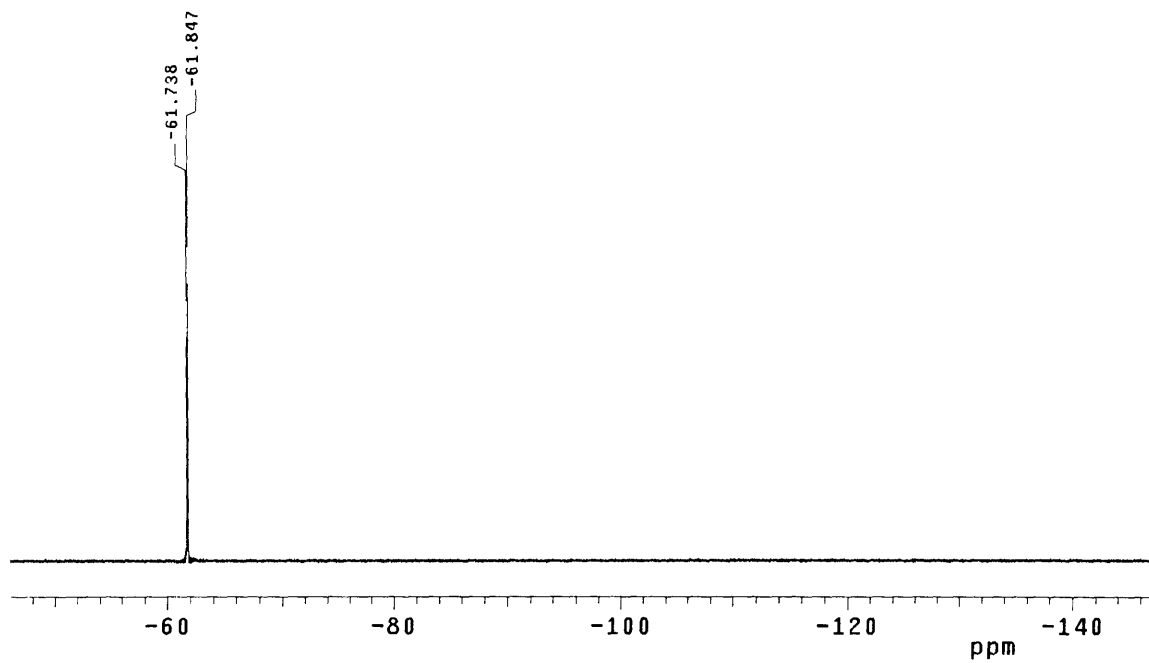
^1H NMR and ^{19}F NMR of **2-b (anti)** (CDCl_3)



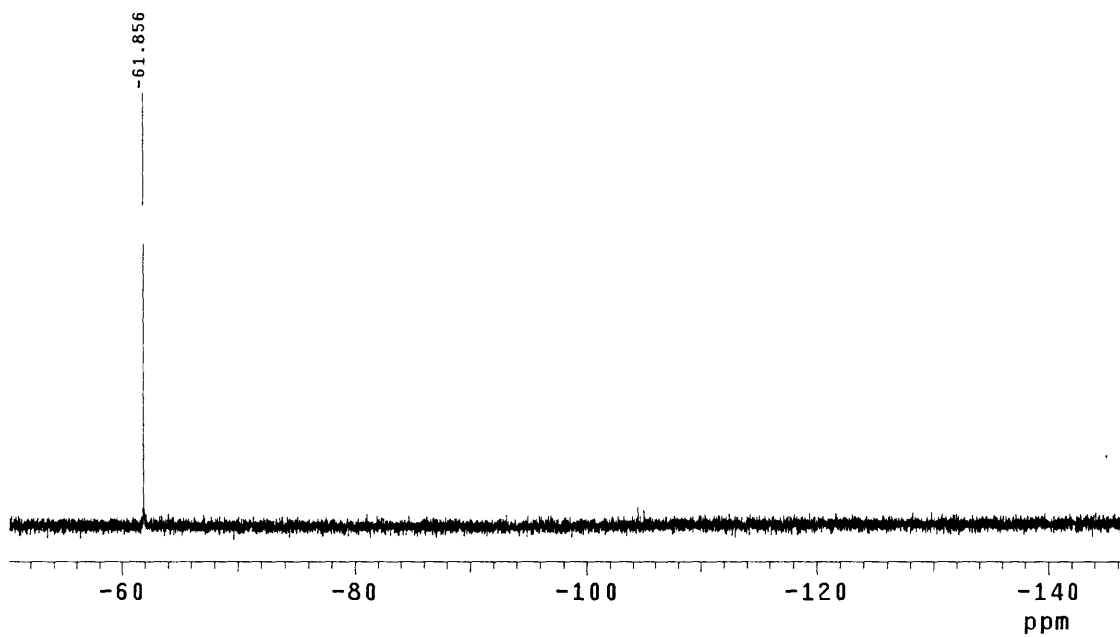
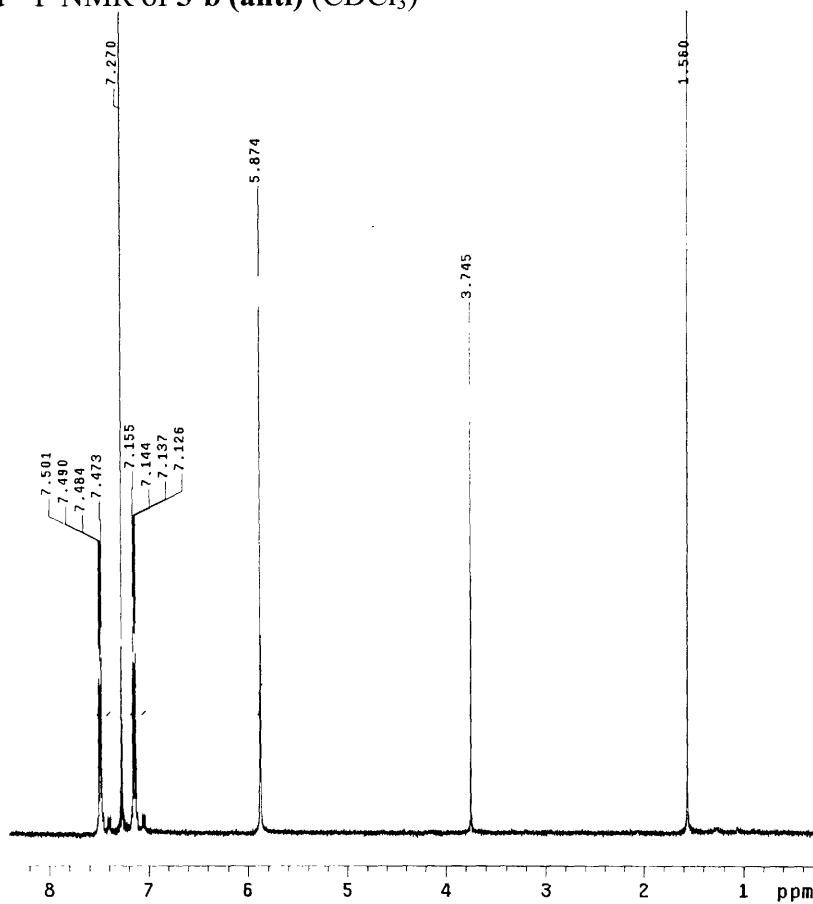
^1H NMR and ^{13}C NMR of **3-b (Mixture)** (CDCl_3)



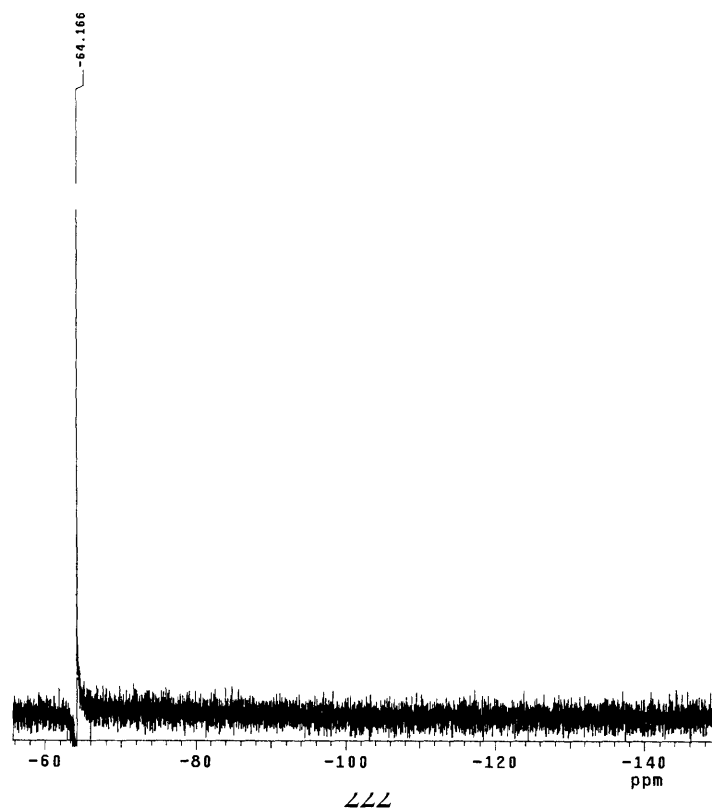
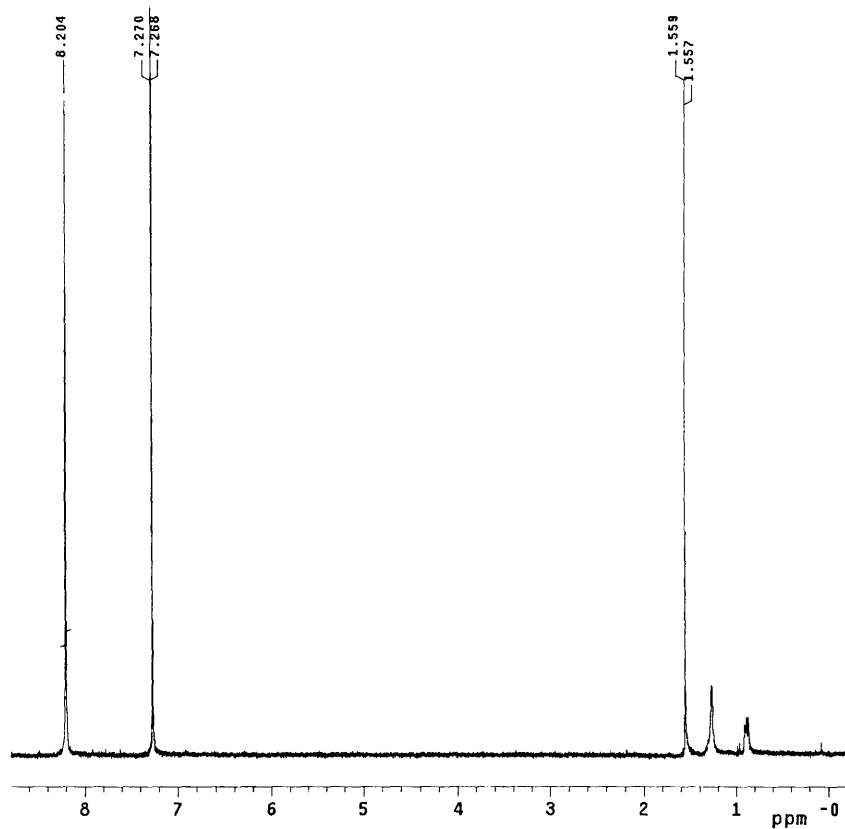
^{19}F NMR of **3-b** (Mixture) (CDCl_3)



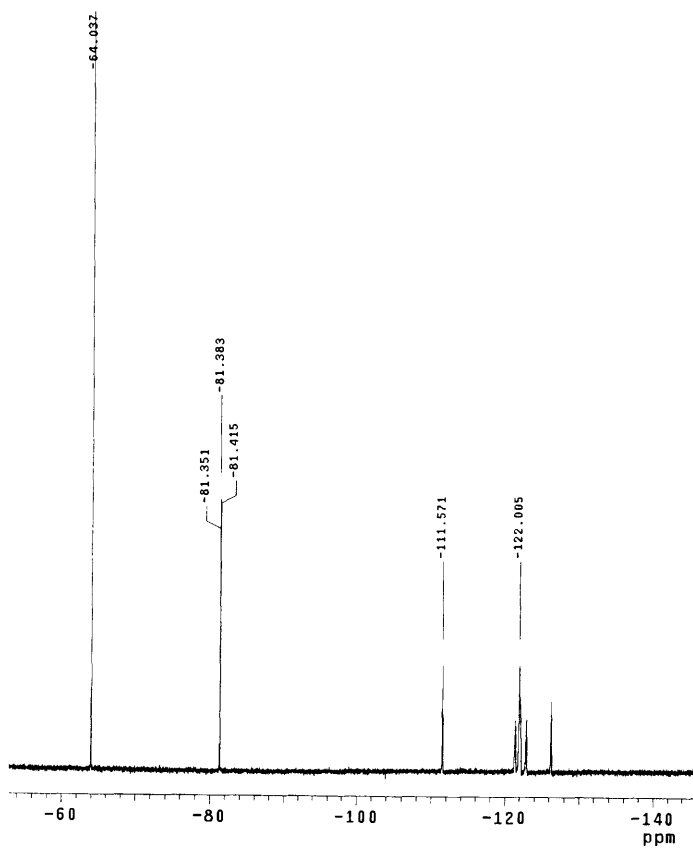
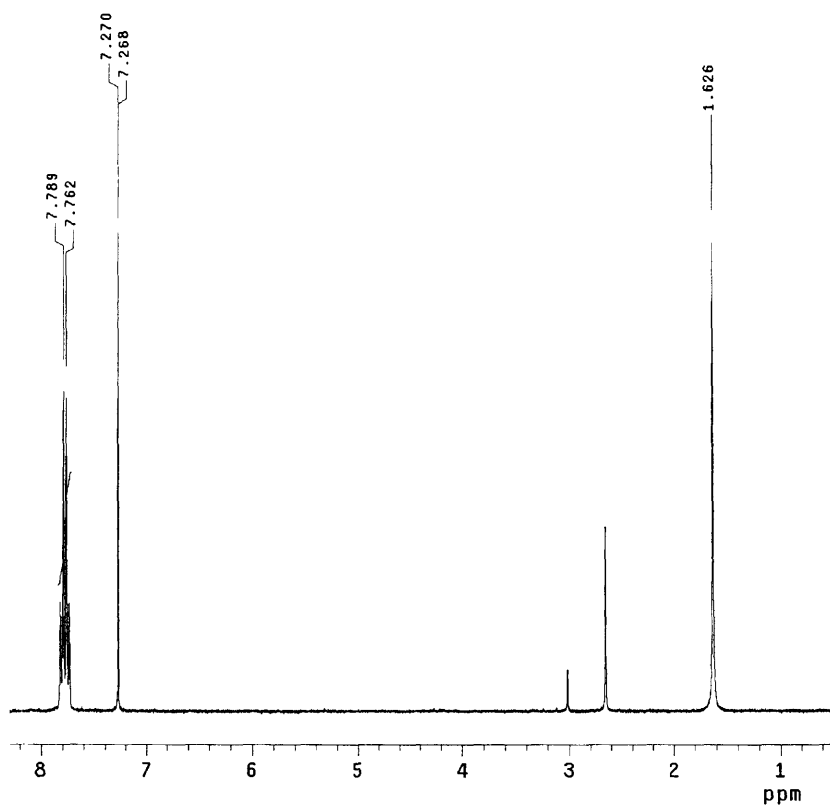
^1H NMR and ^{19}F NMR of **3-b (anti)** (CDCl_3)



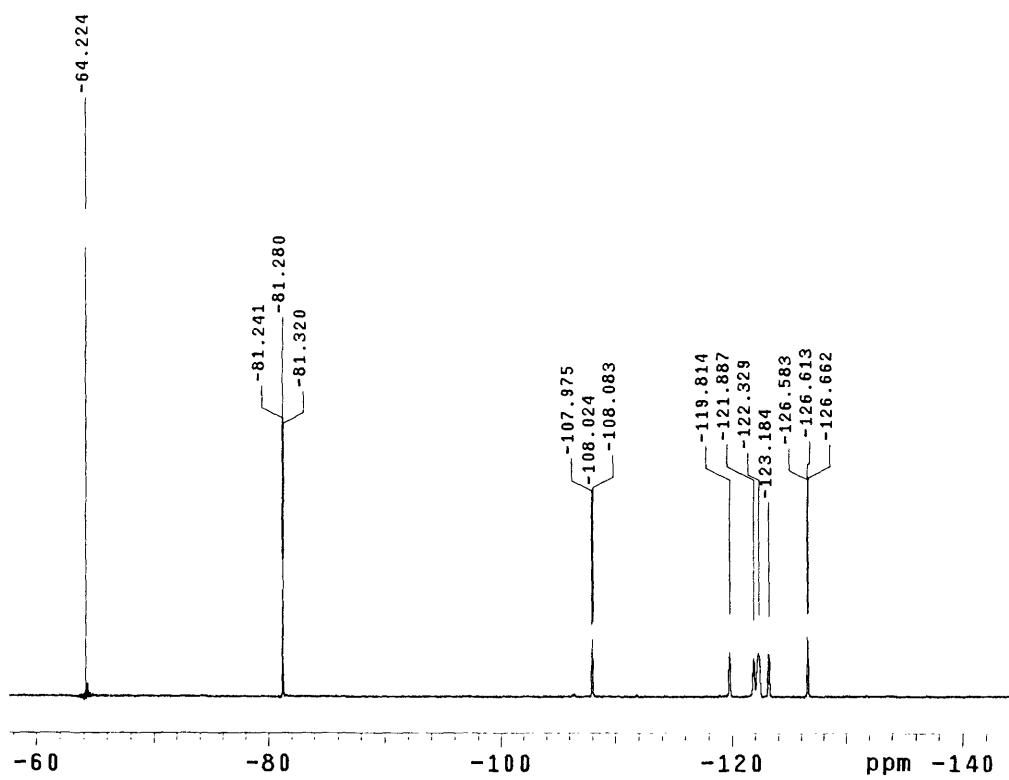
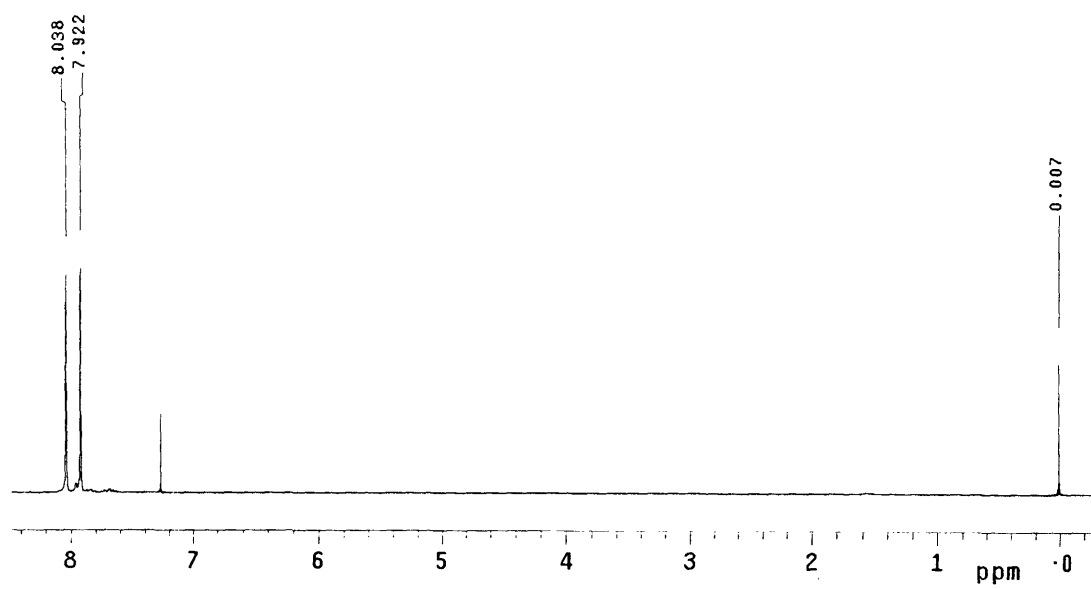
^1H NMR and ^{19}F NMR of **4** (CDCl_3)



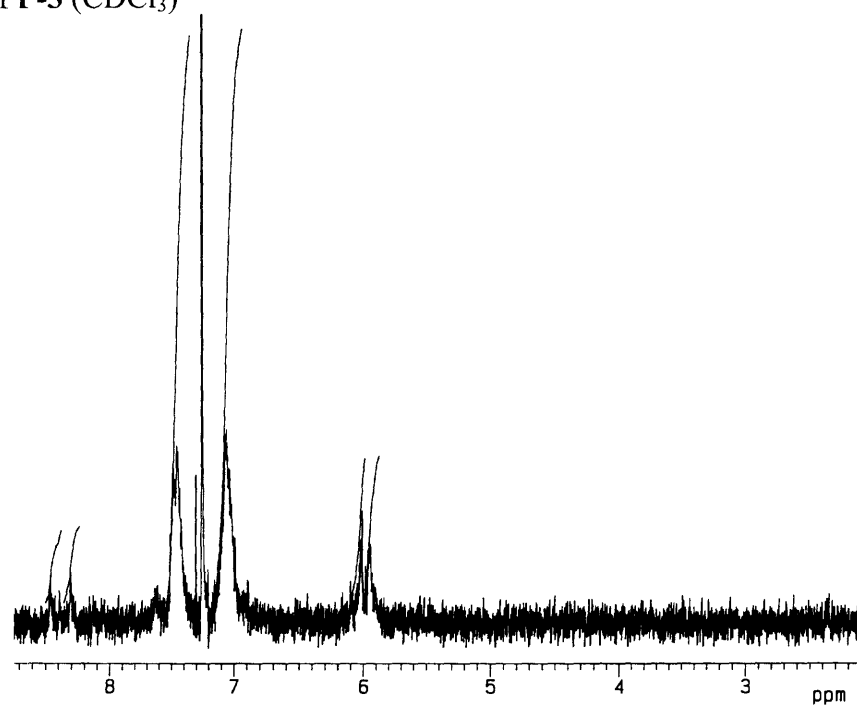
^1H NMR and ^{19}F NMR of **5** (CDCl_3)



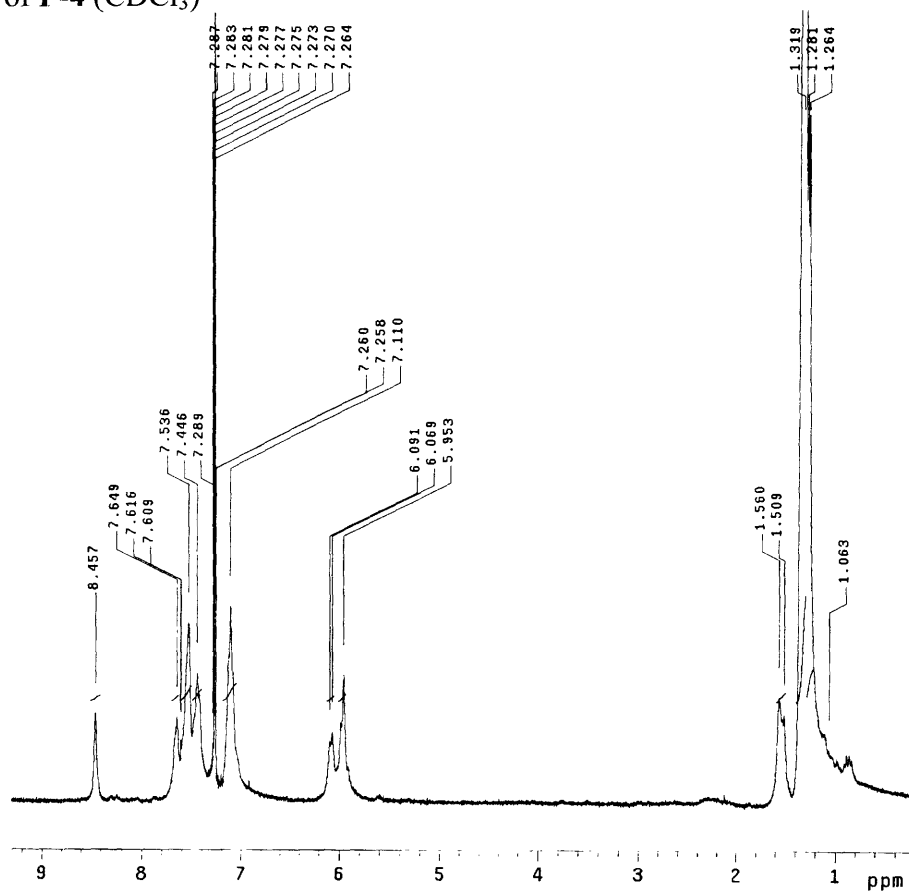
^1H NMR and ^{19}F NMR of **6** (CDCl_3)



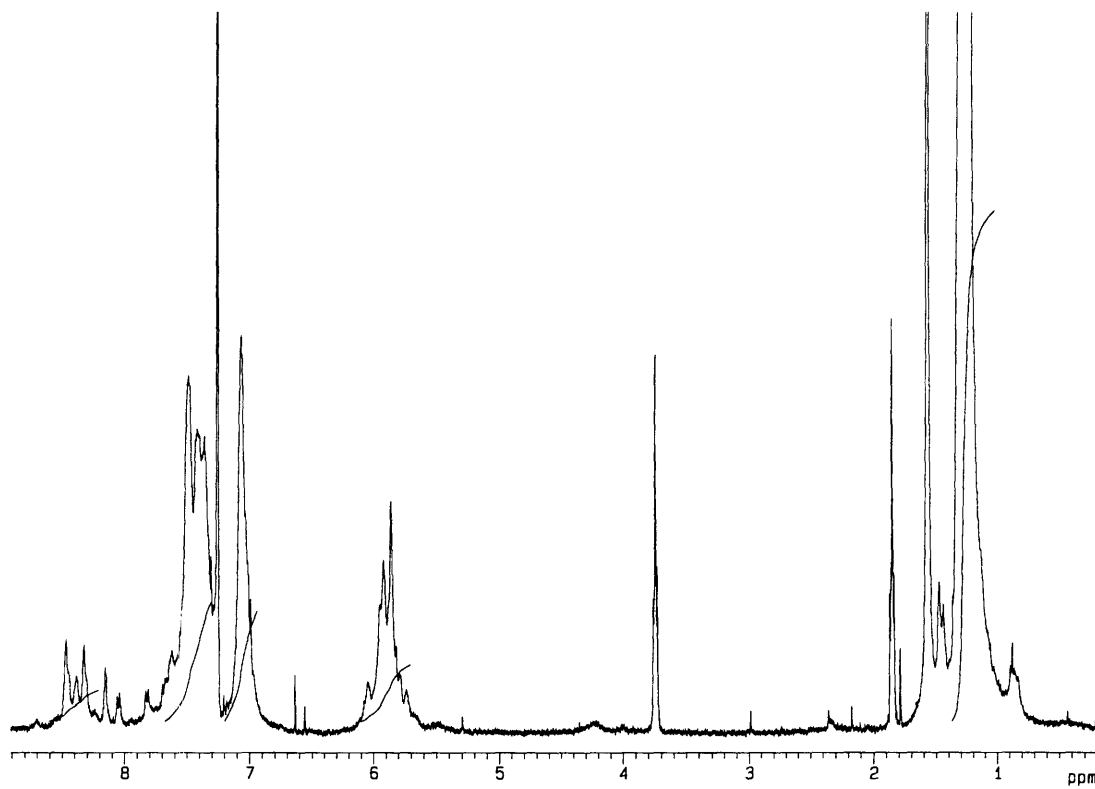
^1H NMR of **P-3** (CDCl_3)



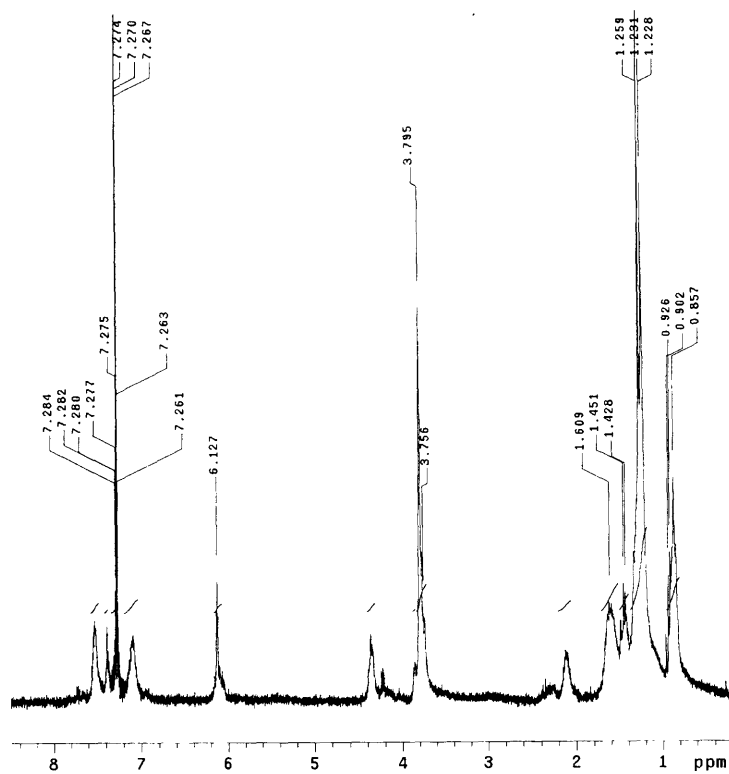
^1H NMR of **P-4** (CDCl_3)



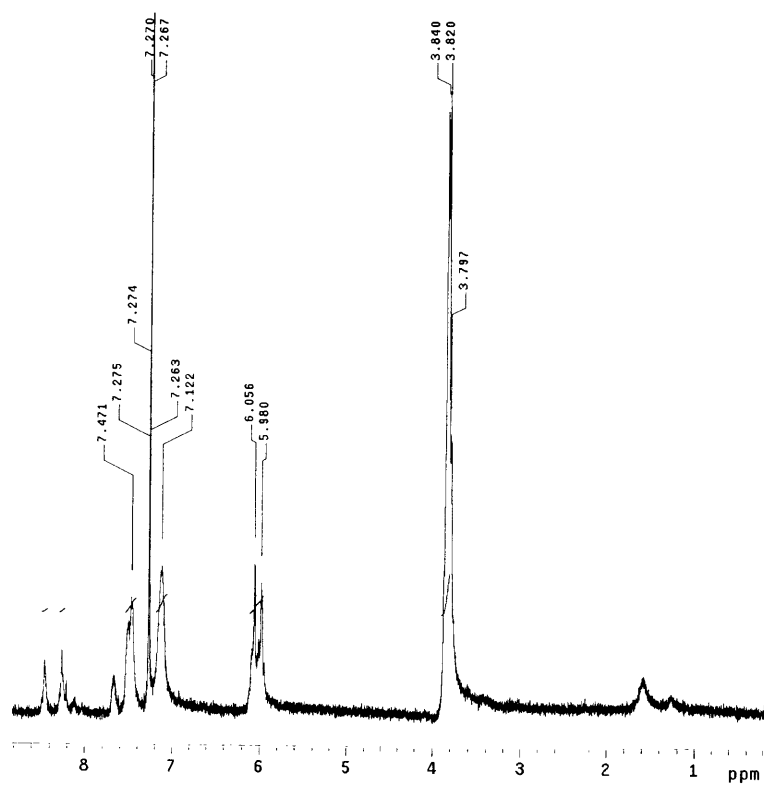
^1H NMR of **P-5** (CDCl_3)



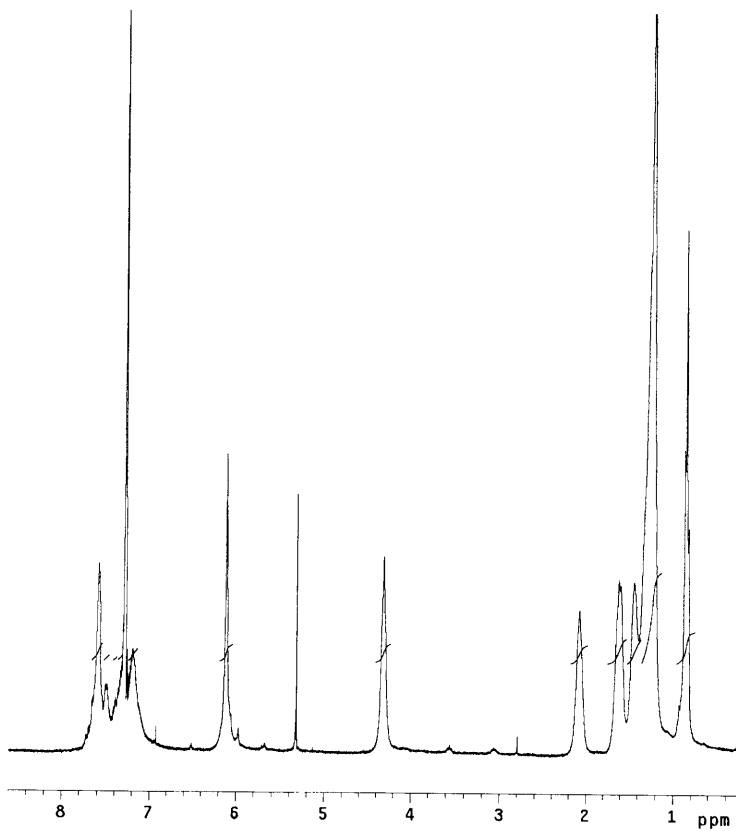
^1H NMR of **P-6** (CDCl_3)



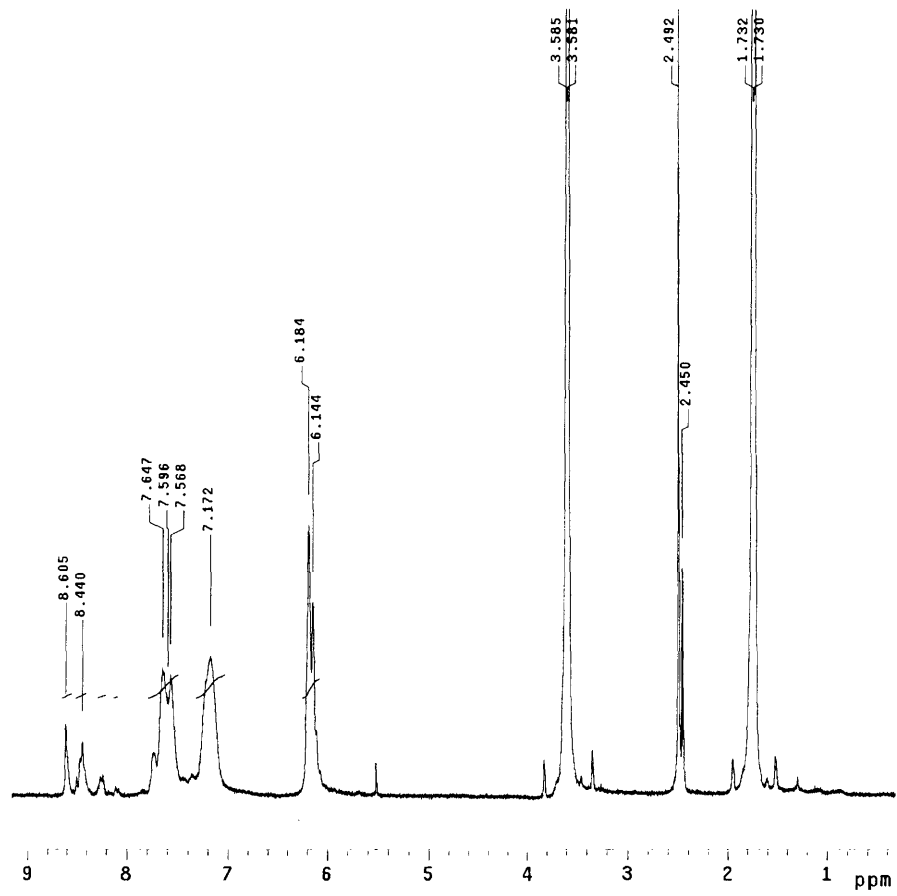
^1H NMR of P-7 (CDCl_3)



^1H NMR of P-8 (CDCl_3)

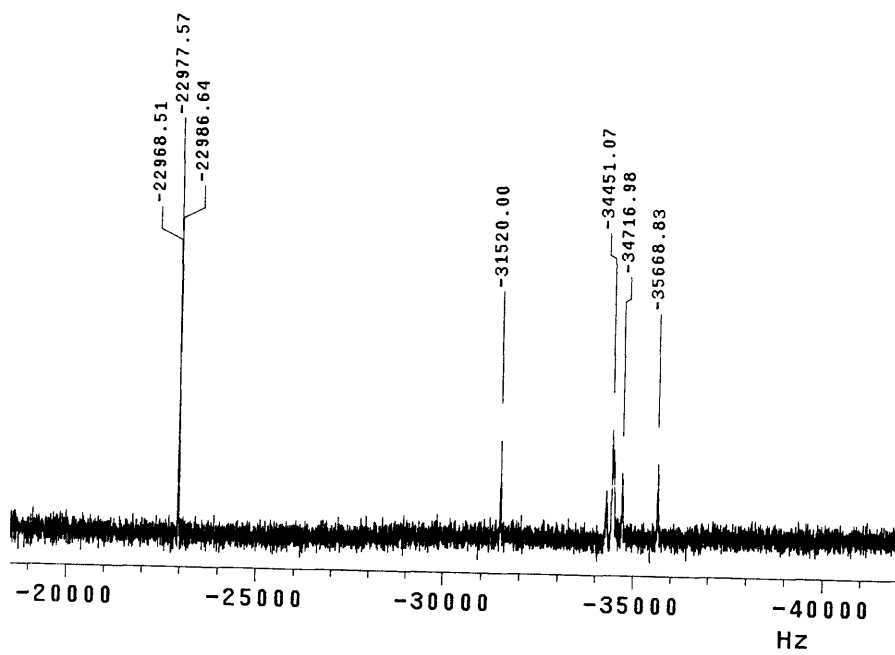
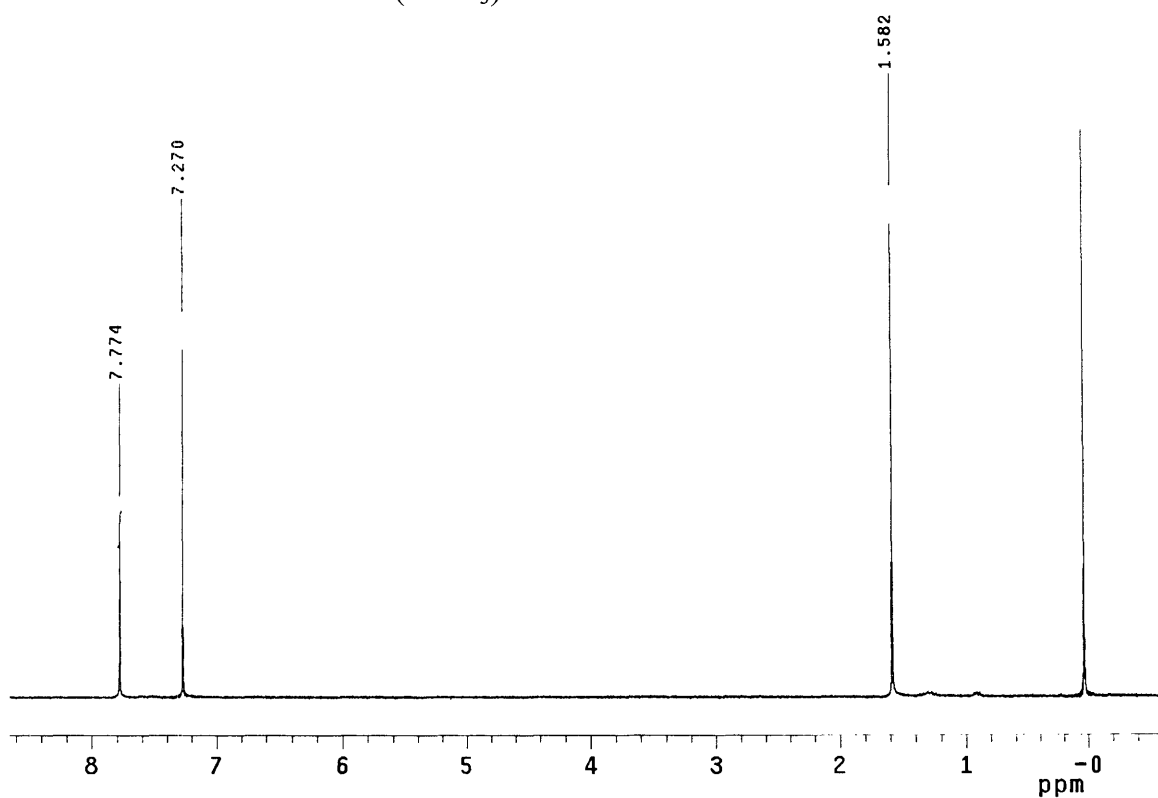


^1H NMR of P-10 (THF- d_8)

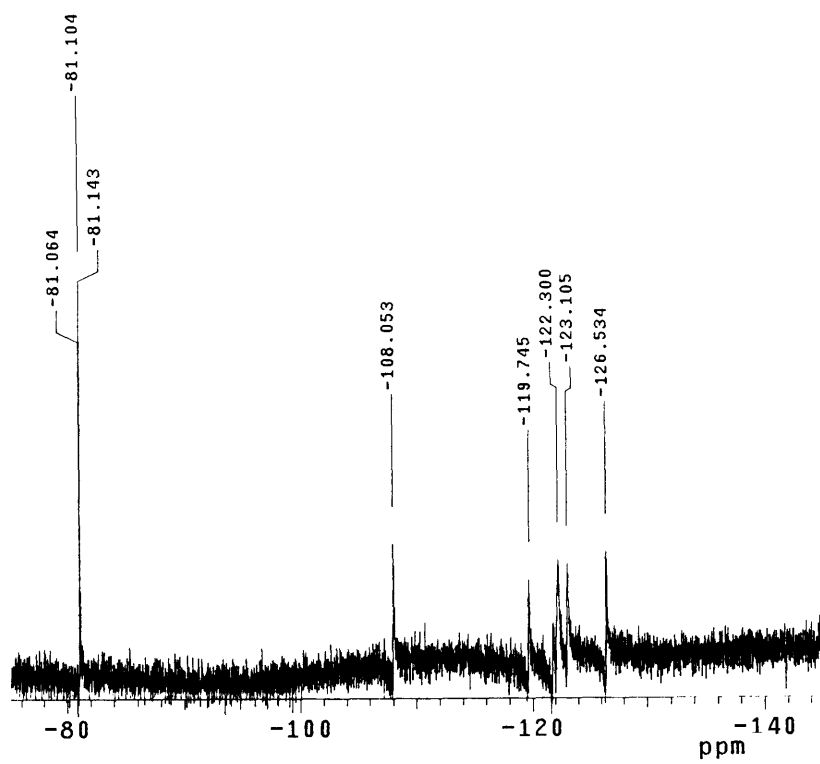
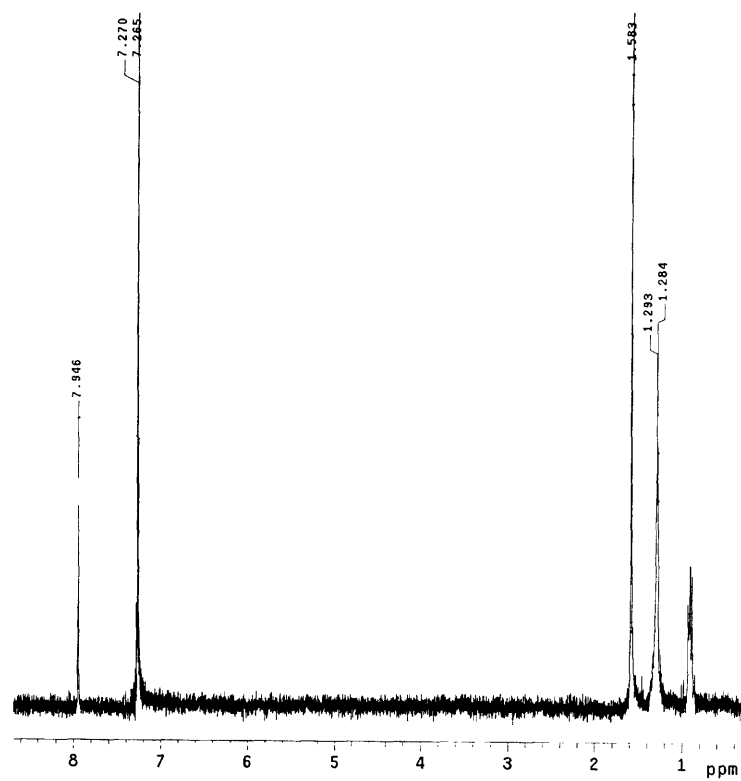


Appendix D:
NMR Spectra of Chapter 5

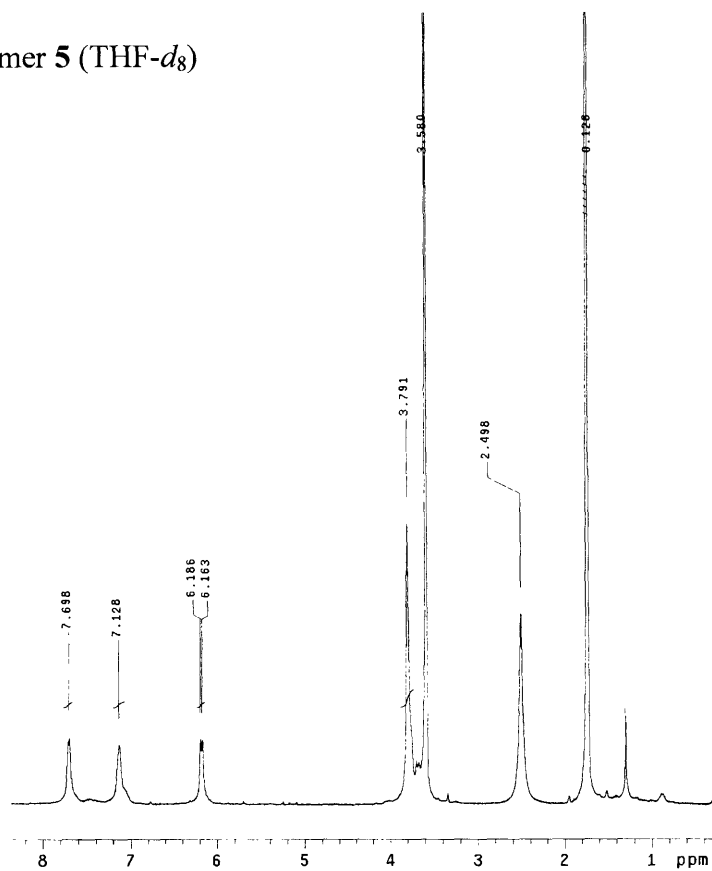
^1H NMR and ^{19}F NMR of **10** (CDCl_3)



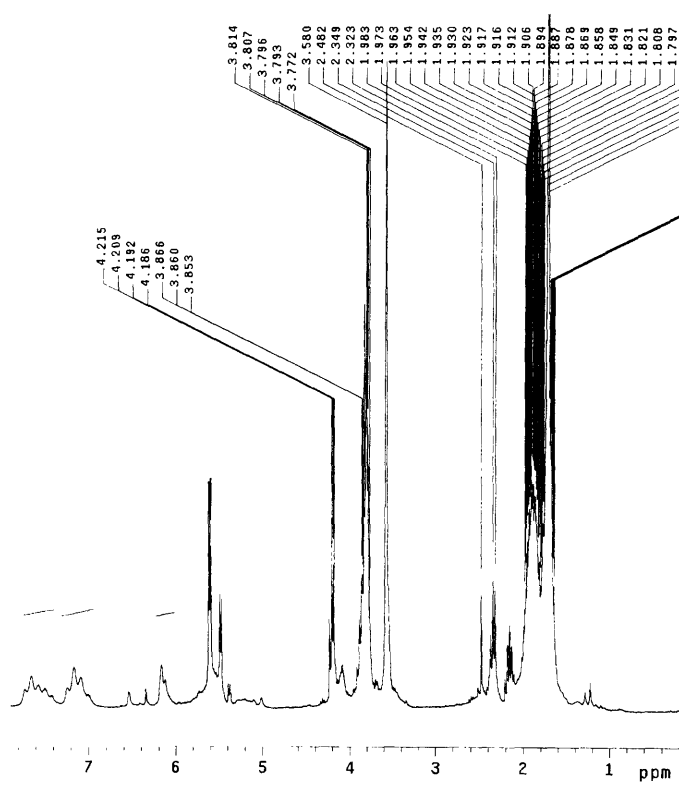
^1H NMR and ^{19}F NMR of **11** (CDCl_3)



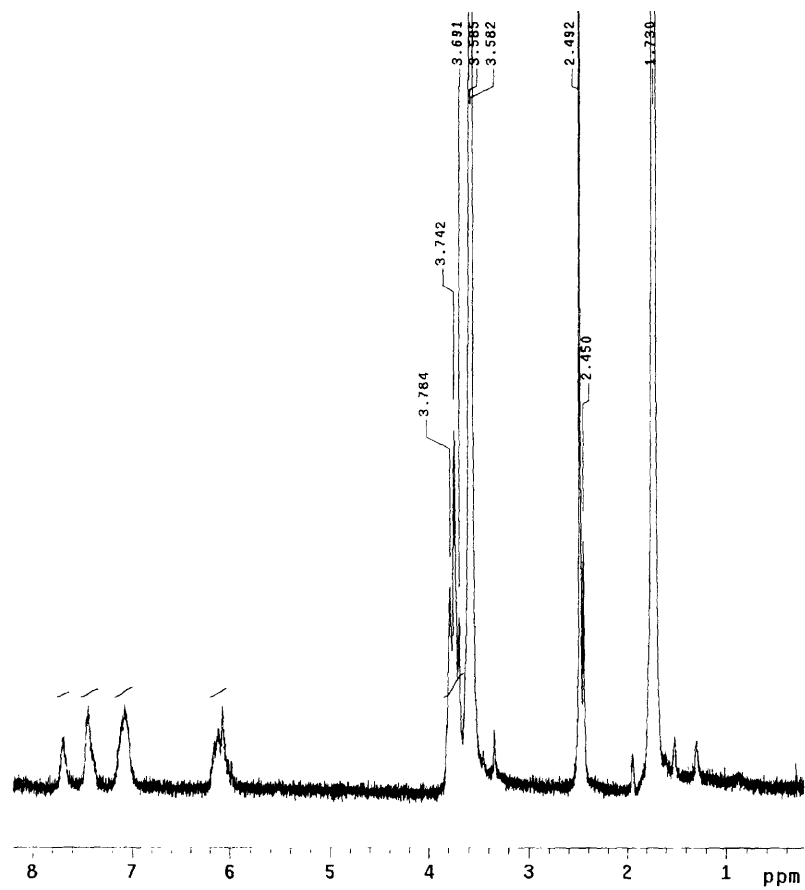
^1H NMR of polymer **5** (THF- d_8)



^1H NMR of polymer **6** (THF- d_8)



^1H NMR of polymer **7** ($\text{THF-}d_8$)



Appendix E:
NMR Spectra of Chapter 6

^1H NMR and ^{19}F NMR of polymer A (THF- d_8)

